



PHD

Benign metal Initiators for the production of biopolymers and their subsequent depolymerisation

Stewart, Jack

Award date:
2022

Awarding institution:
University of Bath

[Link to publication](#)

Alternative formats

If you require this document in an alternative format, please contact:
openaccess@bath.ac.uk

Copyright of this thesis rests with the author. Access is subject to the above licence, if given. If no licence is specified above, original content in this thesis is licensed under the terms of the Creative Commons Attribution-NonCommercial 4.0 International (CC BY-NC-ND 4.0) Licence (<https://creativecommons.org/licenses/by-nc-nd/4.0/>). Any third-party copyright material present remains the property of its respective owner(s) and is licensed under its existing terms.

Take down policy

If you consider content within Bath's Research Portal to be in breach of UK law, please contact: openaccess@bath.ac.uk with the details. Your claim will be investigated and, where appropriate, the item will be removed from public view as soon as possible.



PHD

Benign metal Initiators for the production of biopolymers and their subsequent depolymerisation

Stewart, Jack

Award date:
2022

Awarding institution:
University of Bath

[Link to publication](#)

Alternative formats

If you require this document in an alternative format, please contact:
openaccess@bath.ac.uk

Copyright of this thesis rests with the author. Access is subject to the above licence, if given. If no licence is specified above, original content in this thesis is licensed under the terms of the Creative Commons Attribution-NonCommercial 4.0 International (CC BY-NC-ND 4.0) Licence (<https://creativecommons.org/licenses/by-nc-nd/4.0/>). Any third-party copyright material present remains the property of its respective owner(s) and is licensed under its existing terms.

Take down policy

If you consider content within Bath's Research Portal to be in breach of UK law, please contact: openaccess@bath.ac.uk with the details. Your claim will be investigated and, where appropriate, the item will be removed from public view as soon as possible.



**Benign metal Initiators for the production of biopolymers
and their subsequent depolymerisation**

Jack A. Stewart

A thesis submitted for the degree of Doctor of Philosophy

Department of Chemistry

University of Bath

July 2022

COPYRIGHT

Attention is drawn to the fact that copyright of this thesis rests with the author. A copy of this thesis has been supplied on condition that anyone who consults it is understood to recognise that its copyright rests with the author and that they must not copy it or use material from it except as permitted by law or with the consent of the author.

i Contents

i Contents	1
ii Dedication and acknowledgements	4
iii Abstract	6
iv Abbreviations and notes	8
v Publications	10
Chapter 1: Introduction	15
1.1 Polymers and bio-renewable polymers	16
1.2 Lactic acid, lactide and PLA	20
1.2.1 PLA – Properties and applications	20
1.2.2 Monomer preparation	22
1.2.3 Tacticity	23
1.2.4 Characterisation	25
1.2.5 Degradation	28
1.3 Ring opening polymerisation	30
1.3.1 Anionic and cationic ROP	30
1.3.2 Coordination insertion	32
1.3.3 Activated monomer	33
1.3.4 Side reactions	34
1.3.5 Metal initiators for lactide polymerisation	34
1.4 Research aims	41
1.5 References	42
Chapter 2: Thiolen complexes of iron and aluminium for <i>rac</i> -lactide polymerisation and CO ₂ /epoxide coupling	46
2.1 Introduction	47
2.1.1 Bisphenolate ligands	47
2.1.2 Thiolen ligands	48
2.1.3 Iron complexes for lactide polymerisation	50
2.2 Iron (III) thiolen complexes for <i>rac</i> -lactide polymerisation	55
2.2.1 Synthesis and characterisation of thiolen ligands	55
2.2.2 Synthesis and characterisation of iron (III) thiolen complexes	58
2.2.3 <i>Rac</i> -lactide polymerisation with Fe(A)Cl	63
2.2.4 Isotactic PLA characterisation	68

2.2.5 <i>Rac</i> -lactide polymerisation with Fe(B-E)Cl	70
2.2.6 Polymerisation kinetics with Fe(A - E)Cl.....	72
2.3 CO ₂ /epoxide coupling with iron (III) thioen complexes	75
2.3.1 Introduction – iron complexes for CO ₂ /epoxide coupling	75
2.3.2 Synthesis and characterisation of Fe(A)OAc.....	83
2.3.3 CO ₂ /CHO coupling with Fe(A-E)Cl and Fe(A)OAc	84
2.3.4 Further study of CO ₂ /epoxide coupling with Fe(E)Cl	89
2.4 Aluminium (III) thioen complexes	91
2.4.1 Introduction – aluminium complexes for lactide polymerisation	91
2.4.2 Synthesis and characterisation of aluminium (III) thioen complexes	98
2.4.3 <i>Rac</i> -lactide polymerisation with Al(A-E)Me.....	102
2.4.4 Polymerisation kinetics with Al(B)Me.....	104
2.4.5 Coordination study with Al(A)Cl	105
2.5 Summary and conclusions	106
2.6 References	109
Chapter 3: Zinc ONS complexes for the production and degradation of polyesters.....	115
3.1 Introduction – zinc complexes for lactide polymerisation.....	116
3.2 Zinc {ONS} complexes for lactide polymerisation.....	128
3.2.1 Synthesis and characterisation of {ONS} monophenolate ligands	128
3.2.2 Synthesis and characterisation of zinc {ONS} complexes	129
3.2.3 Lactide polymerisation with Zn(F-N) ₂	137
3.2.4 Reactivity trends and mechanistic considerations	141
3.2.5 Kinetic study of <i>rac</i> -lactide polymerisation with Zn(J) ₂ and Zn(L) ₂	146
3.3 Introduction – Catalytic PLA degradation	150
3.3.1 Chemical recycling	150
3.3.2 PLA degradation – hydrolysis.....	151
3.3.3 PLA degradation – ionic liquids and organocatalysis.....	151
3.3.4 PLA degradation – zinc catalysis	153
3.3.5 PLA degradation – mechanism and characterisation	157
3.4 Polyester degradation with {ONS} zinc complexes	159
3.4.1 PLA degradation with Zn(F-N) ₂	159
3.4.2 Kinetics of PLA degradation with Zn(G) ₂ and Zn(N) ₂	161
3.4.3 PET degradation with Zn(F-N) ₂	163
3.5 Aluminium {ONS} complexes for lactide polymerisation.....	167
3.5.1 Synthesis and characterisation of aluminium {ONS} complexes	167
3.5.2 <i>Rac</i> -lactide polymerisation with Al(K,L,M) ₂ Me and Al(I)Me ₂	171

3.5.3 Polymerisation kinetics with Al(M) ₂ Me	173
3.6 Summary and conclusions	174
3.7 References	176
Chapter 4: Redox switchable initiators for co-polymerisation	180
4.1 Copolymers and redox-switchable initiators	181
4.2 Redox behaviour of iron (III) bisphenolate complexes	188
4.2.1 Identification of redox active iron (III) complexes	188
4.2.2 Electrochemical characterisation of Fe (III) salalen complexes	191
4.3 Redox switching with iron (II) {NNNN} complexes.....	194
4.3.1 Synthesis and characterisation of iron (II) {NNNN} complexes	194
4.3.2 Electrochemical characterisation of Fe(O-Q)Cl ₂	195
4.3.3 Lactide polymerisation with Fe(O-Q)Cl ₂	198
4.4 Summary and conclusion.....	201
4.5 References	202
Chapter 5: Experimental	204
5.1 General experimental methods	205
5.2 Thiolen complexes of iron and aluminium for <i>rac</i> -lactide polymerisation.....	212
5.2.1 Ligand synthesis and characterisation	212
5.2.2 Synthesis and characterisation of iron thiolen complexes	222
5.2.3 MALDI-ToF spectra examples	224
5.2.4 Example GPC spectra	226
5.2.5 Example ¹ H{ ¹ H} NMR spectra	227
5.2.6 Synthesis and characterisation of aluminium thiolen complexes	229
5.2.7 Crystallographic data	240
5.3 Zinc and aluminium {ONS} complexes for polyester production and degradation ...	241
5.3.1 Synthesis and characterisation of {ONS} monophenolate ligands	241
5.3.2 Synthesis and characterisation of zinc {ONS} complexes	259
5.3.3 Example GPC spectra	272
5.3.4 Example ¹ H{ ¹ H} NMR spectra.....	274
5.3.5 Characterisation of aluminium {ONS} complexes.....	275
5.4 Electrochemically switchable initiators	281
5.4.1 Synthesis and characterisation of neutral {NNNN} ligands	281
5.5 References	284

ii Dedication and acknowledgements

This thesis is dedicated to my mum, Dikka Cram, who passed away during my final year. She was an unwavering support to me, and I loved chatting to her about science and my research.

I would like to thank Prof. Matthew Jones for his excellent supervision, guidance and support throughout my PhD and for going above and beyond for my family and I during the highs and lows of new parenthood, COVID-19 and bereavement. Prof. Matthew Jones must also be acknowledged for his endless delight in crystallography and for running many of my samples. I would also like to thank Dr. Ben Ward for his enthusiasm, advice and ideas that have contributed to my research. I would like to thank the CDT Catalysis and the EPSRC for funding and the opportunity to study for my PhD at the University of Bath.

I must also acknowledge Prof. Frank Marken for passing on a small amount of his vast knowledge of electrochemistry and for lending me a trolley-load of equipment.

The first two years of my PhD would have been much harder without the guidance, teachings and friendship of Dr. Paul McKeown who somehow managed to complete his own research whilst running the lab and supporting several grateful PhD students.

I would like to acknowledge the expertise and helpfulness of the members of MC² who have assisted me over the past three years. Particularly: Dr. Tim Woodman, Dr. Catherine Lyall and Dr. John Lowe for NMR support; Dr. Rémi Castaing and Dr. Martin Levere for help with material characterisation; and Dr. Mary Mahon and Dr Gabrielle Kociok-Köhn for assistance with X-ray crystallography.

I am also grateful to the other members of the Jones group and wider shared labs and offices who have made this PhD such an enjoyable experience. Particularly, Jack Payne, Sandeep Kaler, and Dr. Oliver Driscoll for the collaborations and salty banter. I would also like to thank the 2018 cohort of the CDT Catalysis for a brilliant MRes year and many enjoyable events and meet-ups. Particular thanks go to Rob

Amesbury, Ben Howchen and Sam Bates for their valuable friendship and emergency chemistry advice.

Finally, I would like to thank my incredible family. My wife, Natalie Stewart, has been amazing throughout my PhD and her love, support and proofreading have been invaluable to me. Also, thanks go to our son, Rowan, and Dumble the dog for bringing joyful chaos and being an unruly audience for practising my presentations. I am also extremely grateful for the support of my dad, Donald Stewart, and the rest of the Stewart, Cram, Loosley and Martin families.

iii Abstract

Our modern society has been built on the exploitation of fossil resources for fuels, materials and chemicals. However, it has long been apparent that there are serious and potentially existential issues associated with our continued reliance on these finite resources. Innovative, green chemistry is a crucial component in solving these issues and moving towards a more sustainable society. One important example is the use of hydrocarbon polymers that are made from fossil resources and have a devastating impact on ecosystems when released into the environment. **Chapter 1** gives an introduction to the issues associated with plastic production and waste and to the use of poly(lactic acid) (PLA) as an established and viable alternative to these unsustainable materials.

In **Chapter 2**, five tetradentate {ONSO} 'thiolen' ligands were synthesised and complexed with iron (III) chloride. The resulting complexes were applied to the ring opening polymerisation (ROP) of *rac*-lactide, and Fe(**A**)Cl gave highly isotactic PLA with an elevated melting temperature. The kinetics and mechanism of the reaction were studied and competition between activated monomer and coordination insertion mechanisms was identified at low temperature.

Iron (III) thiolen complexes were further applied to the coupling of CO₂ and epoxides in a comparative study with analogous iron (III) salalen complexes. The five ligands were also coordinated to aluminium and applied to *rac*-lactide ROP.

In **Chapter 3**, a series of nine, monophenolate {ONS} ligands were prepared with a range of phenolate, amine and thioether substituents. All ligands were successfully coordinated with diethyl zinc to give homoleptic complexes of the form Zn(Lig)₂. The activity of the initiators for lactide ROP varied significantly, which was rationalised through considering the Zn – S bond lengths and the geometrical preference for tetrahedral geometry (τ_4). Zn(**J**)₂ produced PLA rapidly with a turn over frequency (TOF) around 250,000 h⁻¹. The kinetics of the two most active initiators were studied with *in-situ* Raman spectroscopy. Unfortunately, the high activities seen in small scale reactions could not be replicated but some valuable kinetic insights were obtained.

Five {ONS} ligands were coordinated to aluminium and applied to lactide ROP. Relatively high activity was observed in the melt, and Al(**M**)₂Me was active up to ratios of [LA]/[Al]/[BnOH] = 10000 : 1 : 1.

The chemistry of catalytic PLA degradation was discussed, and all zinc complexes were able to degrade PLA to methyl lactate (Me-LA) in varying amounts over eight hours. Results were consistent with literature values and the degradation of PET was also demonstrated.

In **Chapter 4**, a series of iron complexes were characterised through cyclic voltammetry (CV) towards the goal of achieving electrochemically switchable co-polymerisation. Iron (III) thiolen and salalen complexes were initially tested and the salalen analogues showed quasi-reversible redox peaks, suggesting the potential to switch from Fe^{3+} to Fe^{2+} . The redox potential of the peaks was shown to correlate with polymerisation activity.

Three iron (II) {NNNN} complexes were prepared, analysed by CV and applied to lactide polymerisation. $\text{Fe}(\mathbf{O})\text{Cl}_2$ showed reversible redox behaviour and good activity for lactide ROP. The activity of $\text{Fe}(\mathbf{O})\text{Cl}_2$ was significantly reduced upon the addition of a chemical oxidant and so it was identified as a good candidate for switchable polymerisation.

iv Abbreviations and notes

AGE – Allyl glycidyl ether

Bio-HDPE – Bio-derived high density polyethylene

Bio-PET – Bio-derived polyethylene terephthalic acid

C₆D₆ – Deuterated benzene

CDCl₃ – Deuterated chloroform

CO₂ – Carbon dioxide

CV – Cyclic voltammetry/cyclic voltammogram

DSC – Differential scanning calorimetry

(ϵ -CL) – ϵ -caprolactone

\overline{M}_w – Dispersity (molecular weight distribution)

DCM – Dichloromethane

DMAP – Dimethylamino pyridine

EA – Elemental analysis

ECH – Epichlorohydrin

Et₃N – Triethylamine

Fc – Ferrocene

ΔG_p – Gibbs free energy of polymerisation

GPC – Gel permeation chromatography

HDPE – High density polyethylene

¹H{¹H} NMR – Homonuclear decoupled NMR

HR-MS – High resolution Mass Spectrometry

I – Initiator

LA – lactide

LCA – Life-cycle assessment

LDPE – Low density polyethylene

K_{app} – Observed rate constant

M – metal centre

MALDI-ToF – Matrix assisted laser desorption/ionisation in time-of-flight

Me-LA – Methyl lactate

M_n – Number average molecular weight

M_w – Weight average molecular weight

NMR – Nuclear magnetic resonance

PE - Polyethylene
PEG – polyethylene glycol
PET – Polyethylene terephthalate
PGE – Phenyl glycidyl ether
PDLA – Poly(*D*-lactic acid)
PLA – Poly(lactic acid)
PLLA – Poly(*L*-lactic acid)
PLGA – poly(lactic-co-glycolic) acid
 P_m – Probability of meso/isotactic enchainment
PO – Propylene oxide
PP – Polypropylene
PS – Polystyrene
 P_r – Probability of racemic enchainment
PET – Poly(ethylene terephthalate)
PU - Polyurethane
PVC – Poly(vinyl chloride)
pXRD – Powder X-ray diffraction
ROCOP – Ring-opening copolymerisation
ROP – Ring opening polymerisation
SO – Styrene oxide
SEC – Size exclusion chromatography
 τ_4' – Structural parameter for a four-coordinate complex
 τ_5 – Structural parameter for a five-coordinate complex
TBAPF₆ – Tetrabutylammonium hexafluorophosphate
 T_g – Glass transition temperature
TGA – Thermal gravimetric analysis
THF – Tetrahydrofuran
 T_m – Melting temperature
TOF – Turnover frequency
XRD – X-ray diffraction

Notes:

The term 'ligand' will be used to describe pro-ligands and ligands.

The term 'initiator' will be used to describe pre-initiators and initiators.

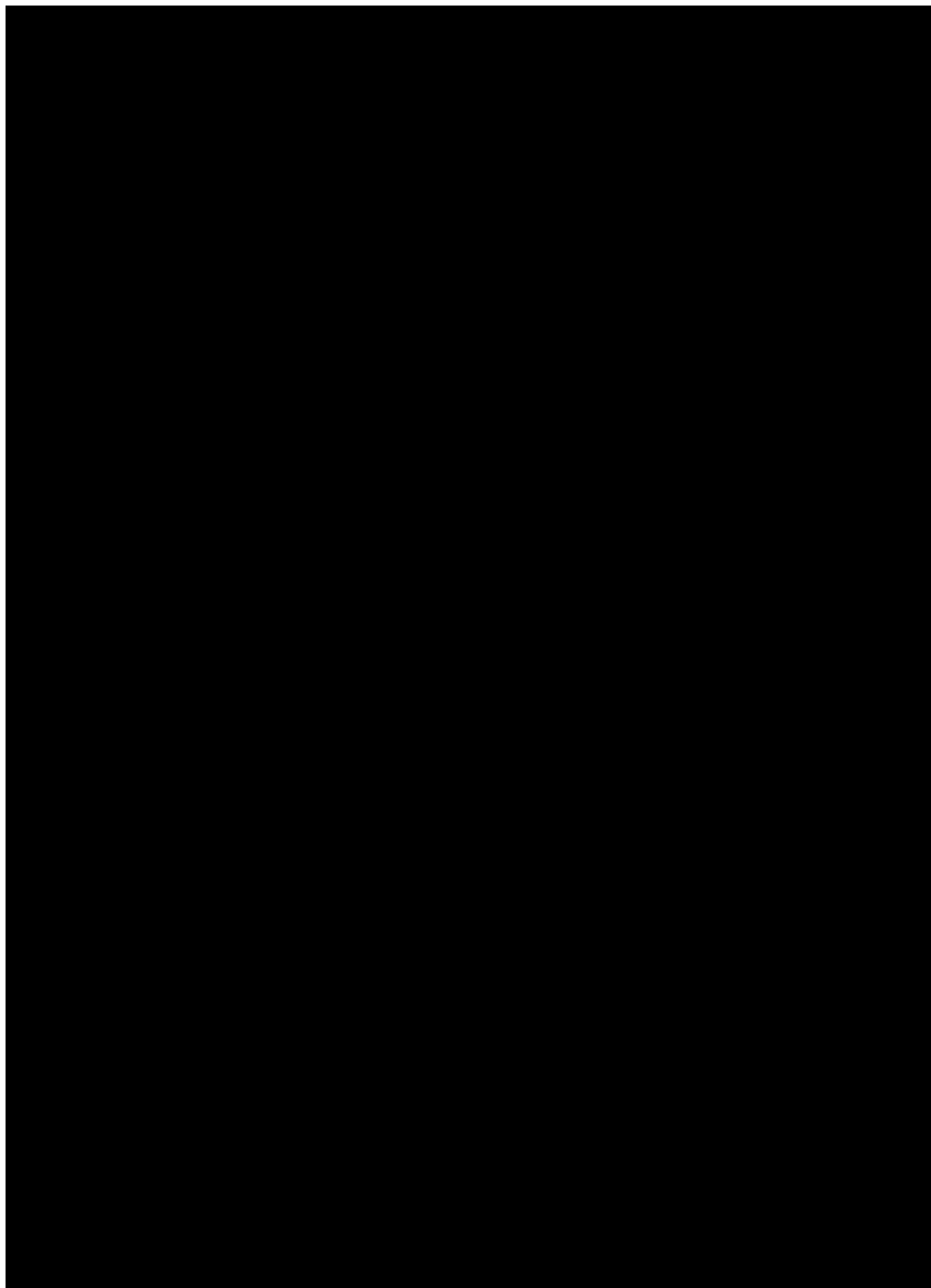
The term 'catalyst' will be used to describe pre-catalysts and catalysts.

v Publications

Publications covered in **Chapter 2**.


Tuning the Thiolen: Al(III) and Fe(III) Thiolen Complexes for the Isolelective ROP of rac-Lactide. J. A. Stewart, P. McKeown, O. J. Driscoll, M. F. Mahon, B. D. Ward, and M. D. Jones. *Macromolecules*, 2019, 52, 5977-5984.

Downloaded via UNIV OF BATH on May 16, 2022 at 07:49:20 (UTC).
See <https://pubs.aos.org/sharingguidelines> for options on how to legitimately share published articles.





Salalen vs. thioen: in the ring(-opening of epoxide and cyclic carbonate formation)†

Oliver J. Driscoll, Jack A. Stewart, Paul McKeown  and Matthew D. Jones *

Cite this: *New J. Chem.*, 2020, 44, 6063

Received 11th February 2020,
Accepted 29th March 2020

DOI: 10.1039/d0nj00725k

rsc.li/njc

A range of Fe(II)-salalen and -thioen-chloride complexes have been prepared and are shown to be active catalysts for the selective coupling of CO₂ and cyclohexene oxide (CHO). The first Fe(II)-thioen-acetate complex is also reported. The effect of the structure of the complex on activity is explored. An epoxide substrate scope is also provided, using the most active catalyst, as well as a study into the effect of co-catalyst equivalents on activity and selectivity.

Introduction

Two contemporary, rapidly growing areas of green chemistry involve the use of sustainable metal complexes, such as iron, for catalysis and catalytic transformations involving CO₂, ideally utilising a waste stream as part of a 'circular economy' approach.^{1–12} The coupling of CO₂, a renewable, abundant, cheap, non-toxic, 'waste' material, with reactive epoxides enables the formation of cyclic organic carbonates (COCs) and/or aliphatic polycarbonates (APCs).^{3,4,7–9,13–20} COCs are used in a range of applications including: high boiling, polar aprotic solvents; lithium-ion battery electrolytes; plasticisers; anti-foam additives; intermediates in both organic synthesis and industry and as monomers for copolymerisation with cyclic esters.^{7,8,14,15,21–23} This is a more sustainable method compared to the use of highly toxic phosgene employed in the traditional synthesis.^{8,14,16,17} Examples for the selective and effective Fe-mediated CO₂/epoxide coupling reaction remain less prevalent than complexes containing metals such as Mg, Cr, Co, Zn and Al.^{15,22–33} This is despite the numerous benefits associated with iron such as high abundance, low toxicity and low commercial and industrial cost.^{1,2,5}

Della Monica *et al.* recently reviewed a variety of ligand classes complexed to iron such as salalen {ONNO} and phenoxy-thioether {OSSO}.⁷ Lamberti and co-workers reported the first example of a Fe(II)-salalen-chloride complex, together with Fe-salen and -salan complexes, for CO₂/epoxide coupling.²⁸ More recently, we reported examples of air-stable Fe(II)-acetate complexes with salalen, salan and salen ligands for the selective coupling of CO₂ with a series of epoxides, predominantly

cyclohexene oxide (CHO).³⁴ *cis*-Cyclohexene carbonate (*cis*-CHC) was formed as the exclusive product under mild, solvent-free conditions (80 °C, 10 bar CO₂, 0.08 mol% metal loading). This is rare in the literature due to the bicyclic ring strain of CHC and the challenging nature of the internal CHO epoxide which imparts steric hindrance and regioselectivity issues associated with the possibility of four different products.

Della Monica, Capacchione and co-workers have reported a variety of mononuclear and dinuclear Fe(II/III)-bis(thioether)-phenolate {OSSO} complexes with two hemilabile sulfur donor atoms.^{7,21,35,36} Indeed, the application of the mononuclear Fe(III)-bis(thioether)-diphenolate complexes with an onium salt co-catalyst achieved very high TOFs and selectivity under mild conditions at 1 bar CO₂ for a large range of internal and terminal epoxide substrates.²¹ For example, the conversion of propylene oxide (PO) to propylene carbonate (PC) achieved a TOF of 290 h⁻¹ at 35 °C and 1 bar CO₂. However, the *cis*-CHC product was not observed with CHO and a TBAC co-catalyst, instead polycyclohexene carbonate (PCHC) was selectively formed.²¹

We recently reported the synthesis of a range of Fe(II)-salalen-chloride {ONNO} and Fe(II)-thioen-chloride {ONSO} complexes and their application to the isoselective ring-opening polymerisation (ROP) of *rac*-lactide.^{37,38} In particular, there are scarce examples of the 'thioen', imine-thiois(phenolate), family of ligands,^{39,40} and they have not been applied to CO₂/epoxide coupling despite the similarities to Della Monica's bis(thioether)-phenolate {OSSO} complexes.

Herein, this work represents the application of previously synthesised Fe(II)-salalen-chloride and Fe(II)-thioen-chloride complexes (Scheme 1) to the selective coupling of CO₂ and epoxides. Furthermore, a new Fe(II)-thioen-acetate complex is reported, applied and fully characterised through High-Resolution Mass Spectrometry (HR-MS) and single crystal XRD. The most effective catalyst was tested with a range of epoxide substrates and co-catalyst

Department of Chemistry, University of Bath, Claverton Down, Bath, BA2 7AY, UK
E-mail: mj205@bath.ac.uk

† Electronic supplementary information (ESI) available. CCDC 1980459. For ESI and crystallographic data in CIF or other electronic format see DOI: 10.1039/d0nj00725k



Cite this: *RSC Adv.*, 2022, **12**, 1416

Received 15th December 2021

Accepted 17th December 2021

DOI: 10.1039/d1ra09087a

rsc.li/rsc-advances

Simple Zn(II) complexes for the production and degradation of polyesters†

 Jack Stewart,^a Martin Fuchs,^b Jack Payne,^a Oliver Driscoll,^a Gabrielle Kociok-Köhn,^{id}^a Benjamin D. Ward,^{id}^c Sonja Herres-Pawlis^{id}^b and Matthew D. Jones^{id}^{*a}

Nine new complexes based on thioether appended iminophenolate (ONS) ligands have been prepared and fully characterized in solution by NMR spectroscopy. Solid-state structures were also obtained for seven complexes. In solution, all complexes were monomeric. The complexes were highly active for the polymerization of purified *rac*-lactide ([M] : [Zn] : [BnOH] = 10 000 : 1 : 30 at 180 °C) reaching TOF values up to 250 000 h⁻¹. The kinetics of the polymerization have been probed by *in situ* Raman spectroscopy. The rate of reaction was dramatically reduced using technical grade *rac*-lactide with increased initiator loading. To move towards a circular economy, it is vital that catalysts are developed to facilitate chemical recycling of commodity and emerging polymeric materials. In this vein, the complexes have been assessed for their ability to break down poly(lactic acid) and poly(ethylene terephthalate). The results from both the polymerization and degradation reactions are discussed in terms of ligand functionality.

Introduction

The widespread use of polymers has revolutionised almost every aspect of modern life. However, the proliferation of these materials has come with serious ecological implications.¹⁻³ Reducing our reliance on the fossil fuel feedstocks which are necessary for producing nearly all commercial plastics is imperative due to the catastrophic environmental impact of extracting and processing these finite resources.⁴ The use of renewable feedstocks to create new polymers or to replace hydrocarbon components of existing products is therefore one of the most important scientific challenges of the 21st century.³⁻⁶

Poly(lactic acid) (PLA) is an important bio-renewable polymer that is sourced from starch-rich materials and is amenable to enzymatic degradation or chemical recycling.^{6,8} It is established as a packaging material and has also found use in the agricultural industry and the bio-medical industry where biocompatible materials are required.⁹⁻¹¹ PLA is typically produced through the ring-opening polymerization (ROP) of lactide initiated by a metal complex. Industrially, Sn(Oct)₂ is used but there are toxicity issues associated with tin residues and so the current focus is to achieve industrially relevant

activity with environmentally benign metal initiators. Poly(*l*-lactide) dominates the PLA market due to the ease of *l*-lactide acid biosynthesis. However, the stereoselective ROP of *rac*-lactide can improve the material properties of the polymer and thus it is often studied in academic research. A diverse range of metals has been applied to lactide ROP including Mg(n),^{12,16} group IV,¹⁷⁻²⁴ Fe(n/m),²⁵⁻³² Al(m),³³⁻⁴⁹ and In(m).⁵⁰⁻⁵²

Initiators based on zinc(n) have consistently shown high activity under solvent-free conditions and, in some cases, stereocontrol is observed. Coates and co-workers published a β -diiminate zinc complex that produced heterotactic PLA (*P_r* = 0.94) at ambient conditions.⁵³ The most isoselective zinc initiator was reported by Ma and co-workers (*P_r* = 0.08) using an aminophenolate complex in toluene at -20 °C.⁵⁴ However, the low temperature required for high selectivity reduced the activity (TOF = 117 h⁻¹) and high stereoselectivity was not maintained under solvent-free conditions (*P_r* = 0.19–0.20). A dizinc bis(imino)diphenylamido initiator reported by Williams and co-workers remains the most active solution-based zinc initiator for lactide ROP (TOF = 60 000 h⁻¹). Using high temperature (130–180 °C), solvent-free, industrial conditions, Jones *et al.* reported simple ethylenediamine monophenolate complexes that polymerised *l*-lactide with TOF values in excess of 100 000 h⁻¹.⁵⁵ Further work by the same group demonstrated the introduction of a propyl linker which increased the activity at 180 °C with *l*-lactide giving high conversion after just 1 minute at low initiator loading (10 000 : 1 : 33).⁵⁶ The most active zinc initiator to date for lactide ROP was reported by Herres-Pawlis and co-workers using a bisguanidine complex which significantly outperformed Sn(Oct)₂ and gave highly

^aDepartment of Chemistry, University of Bath, Claverton Down, Bath BA27AY, UK. E-mail: mj205@bath.ac.uk

^bLehrstuhl für Bioanorganische Chemie, Institut für Anorganische Chemie, RWTH Aachen University, Landoltweg 1, 52074 Aachen, Germany

^cDepartment of Chemistry, Cardiff University, Park Place, Cardiff, CF10 3AT, UK

† Electronic supplementary information (ESI) available. CCDC 2121321–2121327. For ESI and crystallographic data in CIF or other electronic format see DOI: 10.1039/d1ra09087a



Cite this: *Dalton Trans.*, 2019, **48**, 15049

The synthesis, characterisation and application of iron(III)–acetate complexes for cyclic carbonate formation and the polymerisation of lactide†

Oliver J. Driscoll, Claudia H. Hafford-Tear, Paul McKeown, Jack A. Stewart, Gabriele Kociok-Köhn, Mary F. Mahon and Matthew D. Jones^{✉*}

Herein, we report the preparation, characterisation and catalytic applications of air-stable Fe(III)–acetate complexes consisting of *salan*, *salen* and *salalen* ligand frameworks. Owing to the simple synthetic protocol employed, a wide range of complexes have been prepared and structure–activity–relationships investigated. X-ray diffraction confirmed the solid-state structures for eight of the complexes. These represent the first Fe(III)–acetate complexes applied for the selective coupling of CO₂/epoxide and lactide polymerisation. The coupling of CO₂ and challenging cyclohexene oxide substrate was performed under mild, solvent-free conditions (80 °C, 10 bar CO₂) to selectively form the *cis*-cyclohexene carbonate as the exclusive product (selectivity >99%) with a metal loading of 0.08 mol%. A reduced aminopiperidine ligand backbone was found as the most active catalyst, and after investigating four co-catalysts, showed high functional group tolerance and robustness when applied to a broad, commercially available, terminal epoxide substrate scope with high conversions observed. The ring-opening polymerisation of *rac*-lactide was achieved using the Fe(III)OAc complexes using triethylamine and benzyl alcohol for initiation, interestingly isoselectivity was observed in some cases.

Received 15th August 2019,
Accepted 6th September 2019
DOI: 10.1039/c9dt03327k

rsc.li/dalton

Introduction

With global population, energy and material demands increasing, sustainability in chemical processes is critical to address these issues.^{1,2} This has catalysed an impetus to explore Earth-abundant metal systems as catalysts, for example, iron.^{1–4} Recently, iron has re-attracted increasing attention due to its high abundance (4th most abundant element in the Earth's crust), low toxicity, low cost (both at commercial and industrial scale) and potential air-stability. A resurgence of iron catalysed reactions has been seen in the ring-opening polymerisation (ROP) of cyclic esters, such as lactide, and the catalytic transformation of CO₂, such as with the coupling of epoxides.^{5–12}

Poly(lactic acid) (PLA) is a more sustainable, renewable, biodegradable and biocompatible alternative plastic compared to those derived from crude oil, with the potential for a 'closed-loop' lifecycle.^{13,14} PLA can be used in food packaging, drug delivery systems and biomedical applications.^{15–17} Industrially,

PLA is formed *via* the ROP of lactide using Sn(*n*)–octanoate.^{14,18–20} With *rac*-LA, the stereoselectivity of the polymer tacticity is uncontrolled and causes diminished thermal properties. This can be solved by the use of metal initiators able to stereoselectively differentiate between the two enantiomers of a racemic mixture of lactide monomers (*D/L*).^{14,18} Control of the stereochemistry and tacticity enables control of the polymer microstructure and therefore the polymers' bulk physical properties, such as flexibility, durability, thermal properties, crystallinity and biodegradability.²¹

Examples of Fe-mediated ROP in the literature are less prevalent despite the numerous benefits.^{22–27} Recently Duan *et al.* synthesised and applied air-stable Fe(*m*)–*salen*–chloride complexes to the ROP of caprolactone and lactide.¹² Using propylene oxide (PO), as both the solvent and co-initiator, the postulated *in situ* generated Fe(*m*)–alkoxide species, formed *via* opening of PO by insertion of the Fe(*m*)–Cl bond, resulted in isotactic PLA ($P_m = 0.53–0.78$) with broad dispersities ($D = 1.38–2.36$). We recently reported a variety of Fe(*m*)–*salalen* complexes that followed this mechanism.¹⁰ Moderate isotacticity ($P_m = 0.75–0.80$) and good molecular weight control in PO were observed ($D = 1.02–1.18$). Batch kinetics using an Fe(*m*)–*salalen* complex indicated there was an induction period within the six hours, likely relating to the *in situ* generation of the Fe(*m*)–alkoxide species. Shaver and co-workers attempted to decrease

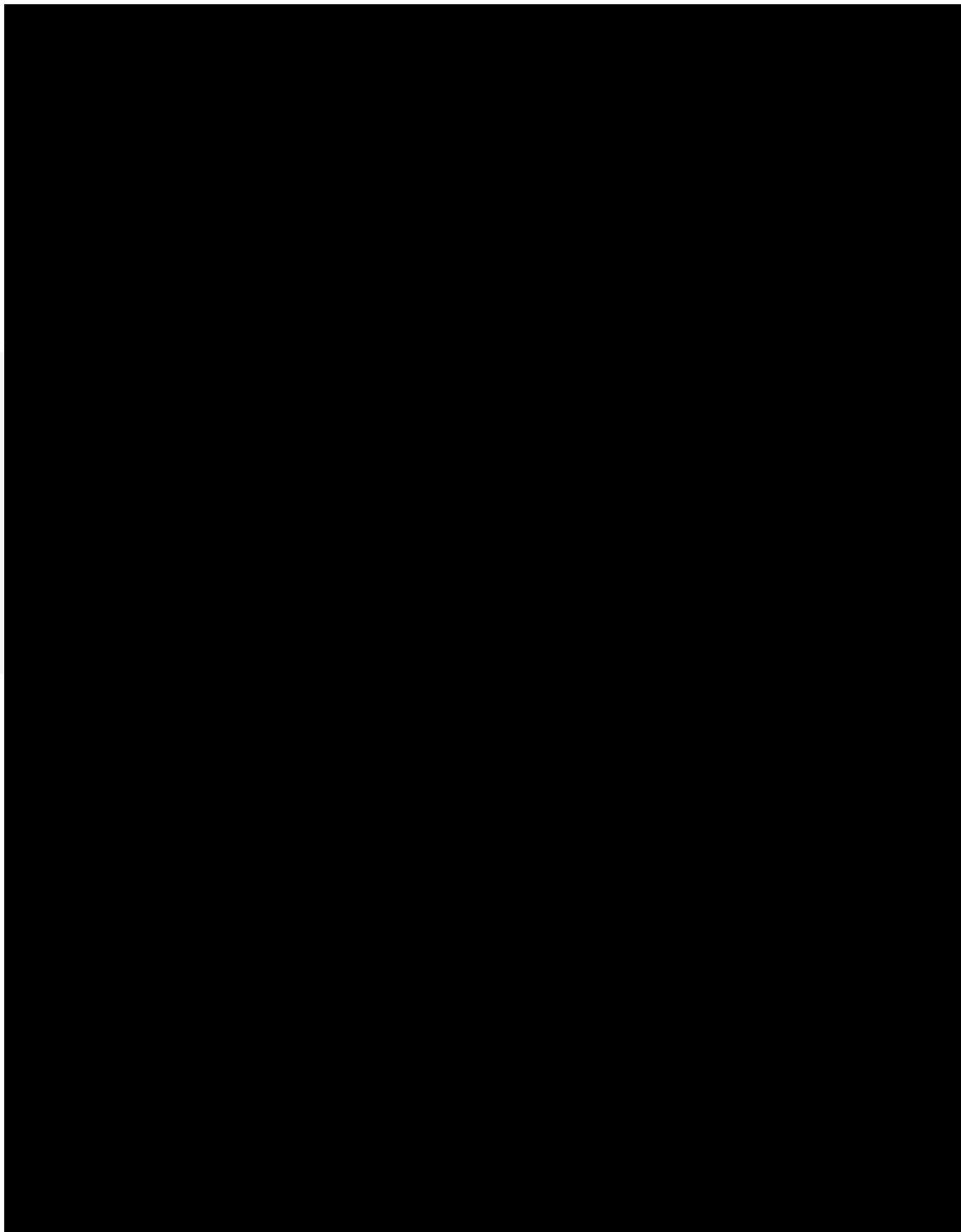
Department of Chemistry, University of Bath, Claverton Down, Bath, BA2 7AY, UK.
E-mail: mj205@bath.ac.uk

† Electronic supplementary information (ESI) available: Complex characterisation and representative spectra for catalysis. CCDC 1940647–1940654. For ESI and crystallographic data in CIF or other electronic format see DOI: 10.1039/c9dt03327k



Ring-Opening Copolymerization Using Simple Fe(III) Complexes and Metal- and Halide-Free Organic Catalysts.
O. J. Driscoll, J. A. Stewart, P. McKeown, and M. D. Jones. *Macromolecules* 2021, 54, 8443-8452.

Downloaded via UNIV OF BATH on May 16, 2022 at 08:01:26 (UTC).
See <https://pubs.acs.org/sharingguidelines> for options on how to legitimately share published articles.



Chapter 1: Introduction

1.1 Polymers and bio-renewable polymers

Humans have been exploiting polymeric materials for at least 3,500 years but it is the invention of synthetic plastics that has profoundly changed the world we live in and revolutionised modern life.^[1] The key reason for the success of plastic materials is the vast range of different properties that can be accessed. This includes: thermal, chemical or light resistance; toughness; flexibility; processability at high temperatures; optical clarity; conductivity, and durability. The range of available synthetic polymers can cover almost any set of properties for a given application and thus modern plastics have become ubiquitous in society. The most prevalent commodity thermoplastics are typically polyolefins such as polypropylene (PP), high-density polyethylene (HDPE), low-density polyethylene (LDPE), polystyrene (PS) and poly(vinyl chloride) (PVC) in addition to Polyurethanes (PU) and poly(ethylene terephthalate) (PET) (**Figure 1.01**). In aggregate, these materials account for 92% of all plastic ever made.^[2] In 2017, Geyer and co-workers estimated that 30% of plastics produced after 1950 were in use and that 6,300 Mt of plastic waste had been generated. Of this total, only 9% had been recycled with the rest either being incinerated or discarded.

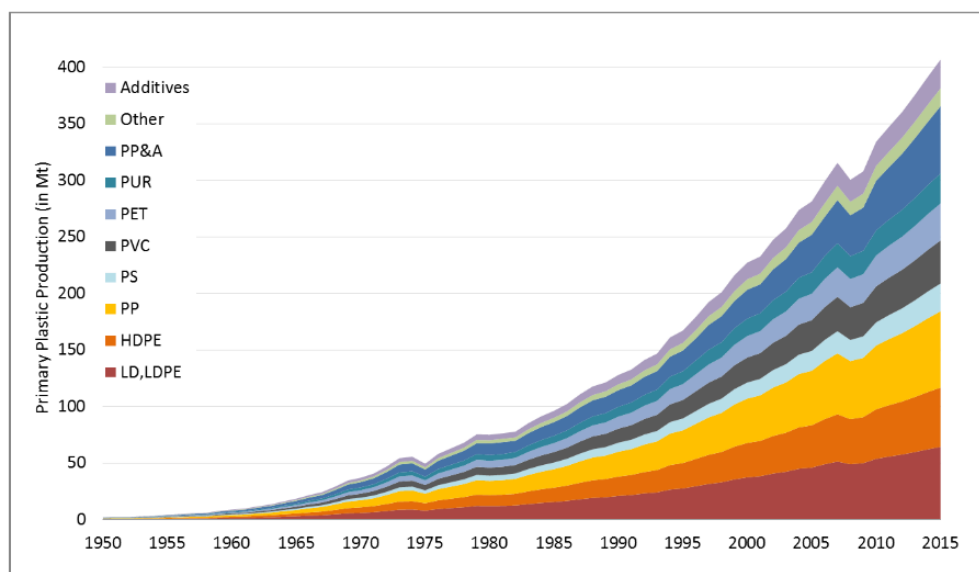


Figure 1.01: Global production of plastic by type. Taken from Law 2017.^[2]

The realisation of the profound ecological harm caused by processing hydrocarbon resources and plastic pollution has rendered it imperative to rethink our relationship with plastics. This need arises both from the environmental impact of extracting and processing crude oil as well as the sheer volume of waste that has accumulated in landfill and in the environment. In 2015 it was calculated that 275m tonnes of plastic waste per year had been generated with between 4.8 – 12.3m tonnes entering the ocean, causing unknown damage to marine ecosystems.^[3] Plastic waste has also been found in almost all terrestrial ecosystems including some of the most remote, such as Antarctica.^[4] **Figure 1.02** shows that cumulative plastic production is predicted to reach 25,000 million metric tons by 2050. There are signs that plastic disposal is reducing relative to production and this is a crucial aspect of the sustainable use of polymers.^[2]

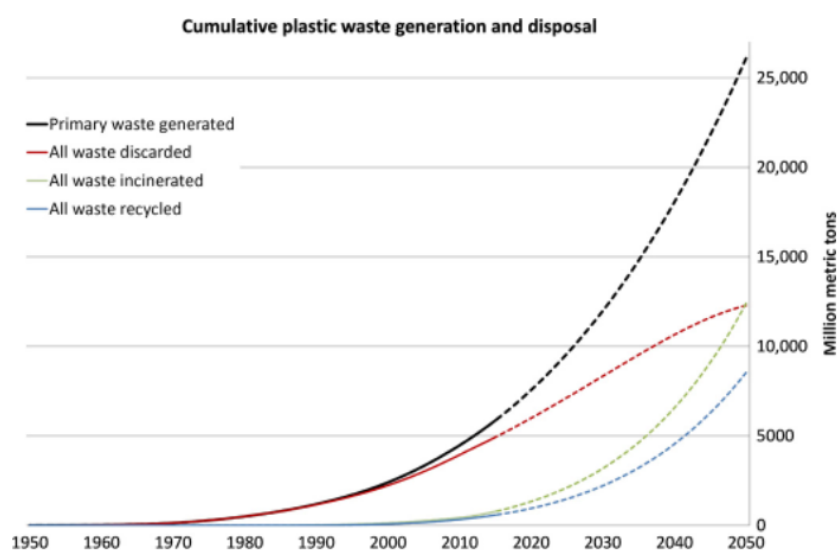


Figure 1.02: Cumulative plastic waste generation and disposal (in million metric tons). Taken from Law 2017.^[2]

In addition to the enormous volume of plastic waste, the nature of the plastics is also an important issue. Petrochemical polymers are typically long, aliphatic hydrocarbon chains. This makes them very inert with no obvious chemical handle for facile degradation. Moreover, when degradation does occur, it is often to micro- or nano-plastic particles which have been shown to bioaccumulate in many organisms and

are often toxic.^[5] A recent publication has even reported the presence of plastic nanoparticles in the human bloodstream.^[6] Issues regarding direct toxicity are particularly prevalent for polymer additives which have been shown to be especially toxic to both wildlife and humans.^[7] The authors also identify the issue of using pure polymers for toxicological studies which ignores the impact of additive migration.

One aspect of tackling this issue comes from legislating for the reduction of unnecessary and single-use plastic materials such as plastic bags, straws, plates/cutlery and cotton swabs. The EU approved a directive in 2019 to limit the use of these products as well as committing to recycle 90% of plastic bottles.^[8] Furthermore, this legislation introduced a responsibility for manufacturers to consider the full lifecycle of their products and the possibility of fines related to pollution. Another ambitious international project is the G7 “Ocean Plastic Charter”, which aims to implement 100% plastic recovery by 2040.^[8] These are in addition to unilateral regulation by individual countries on various aspects of plastic waste and recycling, and international bans on certain materials such as plastic microbeads for cosmetics.

Another crucial route towards mitigating the destructive potential of plastic waste is the production of bio-renewable polymers that can compete with traditional plastics for key applications. Typically, this involves the use of a renewable feedstock that can be processed into a monomer through chemical or biochemical means. The result can be either to create a new fully bio-based polymer, or to produce existing polymers from renewable sources. Progress in the latter scenario has led to the development of polymers such as HDPE and PET with high renewable content. Bio-HDPE can be produced from the fermentation of crops such as wheat or sugar beet to bio-ethanol, which is subsequently dehydrated to give bio-ethylene.^[9] A recent life-cycle assessment (LCA) compared bio-HDPE to fossil-fuel produced HDPE (**Figure 1.03**).^[9] Traditionally produced HDPE was significantly worse when considering climate change and fossil depletion but was favourable for the other measured outcomes, including acidification, particulate matter, land use and ozone depletion. This underlines the importance of conducting a thorough LCA when considering polymer alternatives.

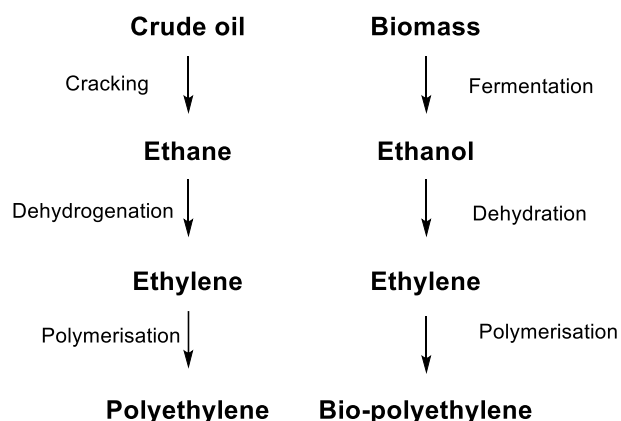


Figure 1.03: Comparison of synthetic routes to fossil-based PE and bio-based PE.

When considering new bio-based polymers, it is important to consider the full lifecycle of the product, ideally applying a “circular economy” approach. This must include an effective end-of-life strategy for new polymers. One option is biodegradability - where the polymer is broken down into harmless by-products in a compost heap or similar environment. Recycling is a favourable option as it retains some of the value of the original product. The current standard of mechanical recycling is insufficient and there is great interest in chemically recycling polymers back to their original components or to value-added chemicals, thus retaining or increasing the value of the original product.^[10] This will be covered in detail in **Section 3.3.1**.

Commercially available bio-based polymers must also be able to compete with petrochemical plastics both materially and economically. The material properties of successful new polymers must be at least as effective as their established counterparts to be attractive to consumers.^[11] Depending on the application, these could include durability, flexibility, heat-resistance or one of the many other properties that make synthetic polymers such useful materials.^[12] Petrochemical plastics are very cheap and there is a well-established infrastructure in place for their production and distribution. Therefore, the economics of bio-based polymer production must be considered at all stages to ensure that they are competitive.

1.2 Lactic acid, lactide and PLA

1.2.1 PLA – Properties and applications

PLA is a thermoplastic, aliphatic polyester that was first synthesised by Carothers in 1932 but was not commercialised until many decades later.^[13] PLA is among the most prevalent bio-renewable polymers and has properties allowing it to compete with some petrochemical polymers for certain applications. PLA can be amorphous or semi-crystalline depending on the microstructure of the polymer (**Section 1.2.3**). The glass transition temperature (T_g) of PLA is usually in the range of 55 – 65 °C and for semi-crystalline samples, a melting point between 160 – 230 °C can be observed. These parameters can be affected by the stereochemistry of the polymer, thermal history and molecular weight.^[14] A comparison of key mechanical properties between PLA and common commodity polymers is shown in **Figure 1.04**.^[15] Favourable comparisons can be made for the Young's modulus and tensile strength but PLA is a brittle polymer and therefore the elongation at break is comparatively low.

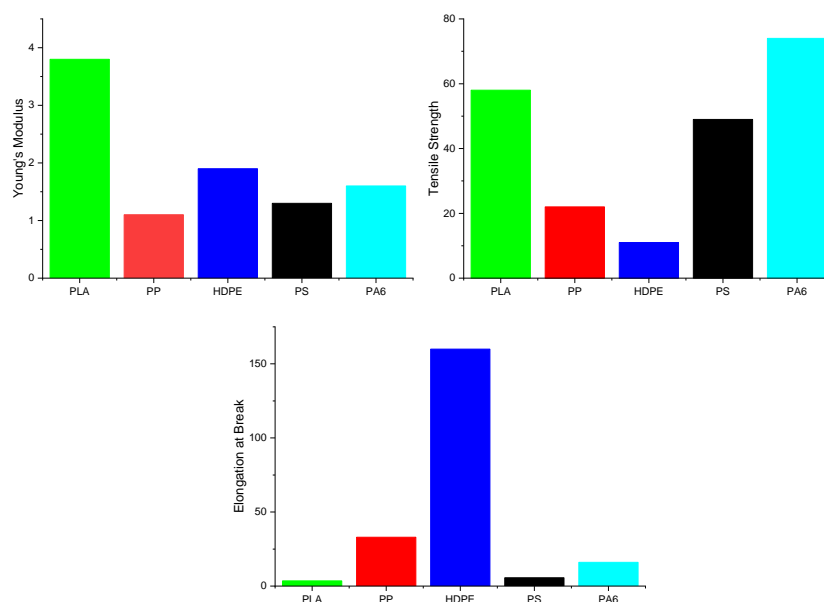


Figure 1.04: Comparison of Young's modulus, tensile strength and elongation at break for PLA, PP, HDPE, PS and PA6. Adapted from Balakrishnan 2012.^[15]

Although sometimes limited by relatively poor thermal properties, PLA has mechanical and chemical properties that make it suitable for many applications. This includes crease-retention; resistance to grease, oil and gasses; relatively low processing temperatures and scalability; and good retention of flavour and aroma.^[16] In some respects, PLA can be compared with PS; both polymers have high modulus and tensile strength with low toughness.^[17] The rheological properties of PLA, particularly sensitivity to shear forces and strength of melt, are suitable for certain forms of processing such as fibre spinning, sheet extrusion and film blowing. Where other processing methods are required, branching is often employed through either post-modification with H₂O₂ or the introduction of co-monomers or multifunctional initiators.

PLA has become widely used in the packaging industry as it has properties that are comparable to established polymers such as PS, HDPE and PET in some cases.^[18–20] The drawbacks of PLA usage as a packaging material come mainly from its brittle nature, which can be addressed using plasticisers such as glycerol, and issues surrounding gas diffusion. The latter is extremely important for maintaining the quality of food and can be achieved through structural alteration of the pure polymer or through additives in the form of layers or composites.^[20]

PLA is also a key biocompatible/bioabsorbable polymer and has thus found extensive application in the biomedical industry.^[21] This includes *in vivo* screws, tacks and pins for bone breakages and reconstructive surgery; spinal cages; tissue engineering implants and scaffolds; drug delivery and plastic surgery.^[14] PLA is often co-polymerised with glycolic acid to give poly(lactic-co-glycolic) acid (PLGA) and this has also been approved for use in medical devices. Furthermore, PLA is a common material used for additive manufacturing and this has been employed to make specialised medical equipment.

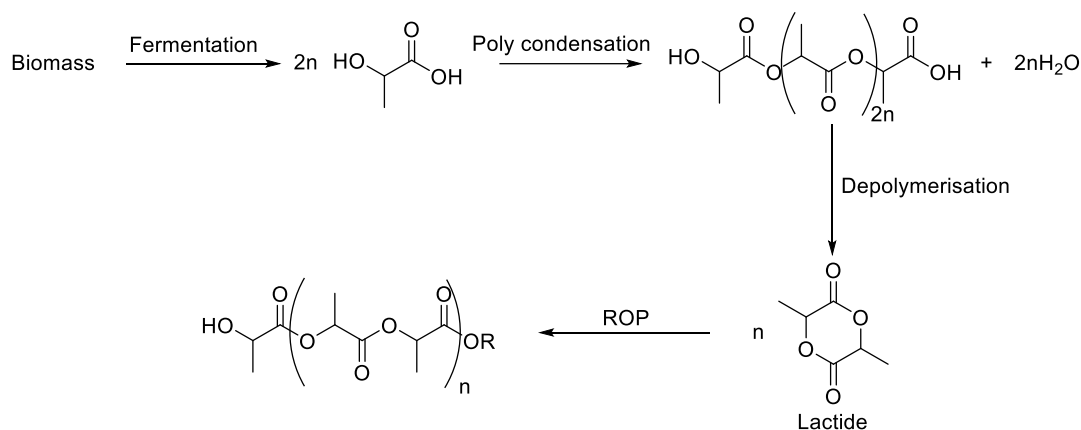
There is increasing interest in PLA fibres being used in the textiles industry.^[22] It is competitive with other common polyesters such as PET and nylon in terms of flammability, dyeability, hydrophilicity and resistance to weather and UV light.^[23] Interestingly, PLA fibres also have antibacterial properties, which are hypothesised

to arise from the migration of lactic acid units through the polymer.^[24] Thus, PLA is a promising candidate for hygienic products such as towels and wipes.

1.2.2 Monomer preparation

Lactic acid is found widely in nature and is typically produced from the fermentation of sugars, such as glucose and fructose, by the bacteria *Lactobacillus*. This process has been widely commercialised and bacteria can be selected to give either *L*-, *D*- or racemic lactic acid with productivities of up to $5.41 \text{ g L}^{-1} \text{ h}^{-1}$.^[25] Starchy materials, such as corn, are typically used as they are cheaper than pure sugars and also avoid glucose repression of the bacteria.^[26] However, with global lactic acid production reaching 1220 kilotons in 2016 and predicted to grow another 16.2% by 2025,^[27] there is now a focus on utilising waste streams from the food and agricultural industries so as to reduce costs and avoid competition with global food production. Lignocellulosic biomass is an attractive renewable resource that does not compete with food supply and which can be converted to LA through a variety of chemical and biochemical processes.^[28] Another example of this approach is the conversion of glycerol, a by-product of biodiesel production, into lactic acid through a bio-/chemocatalytic route.^[29]

The most direct way to synthesise PLA is through the poly-condensation of lactic acid (**Scheme 1.01**), however, in practice there are numerous problems with this approach.^[30] The most fundamental of these issues is that one molecule of water is released with every addition of a monomer unit. This water can act as a chain transfer agent which disrupts the propagation and reduces M_n . Furthermore, the removal of water requires energy intensive processes to be added downstream. For these reasons, a further step is added wherein low-molecular weight PLA obtained from polycondensation is depolymerised over a catalyst to give lactide, the cyclic dimer of lactic acid.^[31] Lactide can then undergo ring-opening polymerisation (ROP) in the presence of a suitable initiator to give a more controlled polymer with access to far higher molecular weights.



Scheme 1.01: PLA production from lactic acid and lactide.

1.2.3 Tacticity

The lactide molecule contains two stereocentres and can therefore exist in three stereochemical forms: *D*- lactide, *L*- lactide or *meso*- lactide (**Figure 1.05**). PLA made from enantiomerically pure *L*- or *D*- lactide (PLLA/PDLA) should be perfectly isotactic, with all lactic acid units having the same stereochemistry (**Figure 1.06**). If the racemic mixture, *rac*-lactide, is used, then there are three possible microstructures available. Heterotactic PLA is formed from the alternating insertion of *L*- and *D*- stereoisomers to give doubly alternating -RRSS- blocks. Although scientifically interesting, heterotactic PLA has thermal properties that are inferior to PLLA and is therefore not useful from a commercial standpoint.^[32] The same can be said for atactic PLA which is formed from a random insertion of monomers. Isotactic PLA can also be formed from *rac*-lactide with blocks of *D*- and *L*- stereoisomers along the polymer chain.

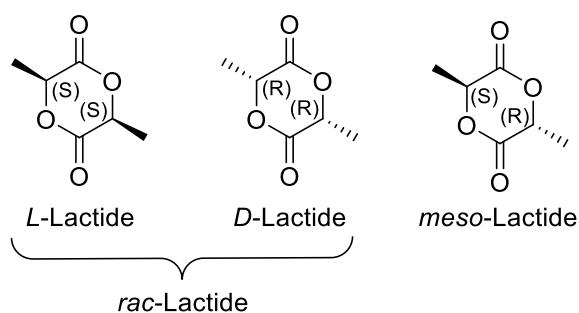


Figure 1.05: The three stereoisomers of lactide.

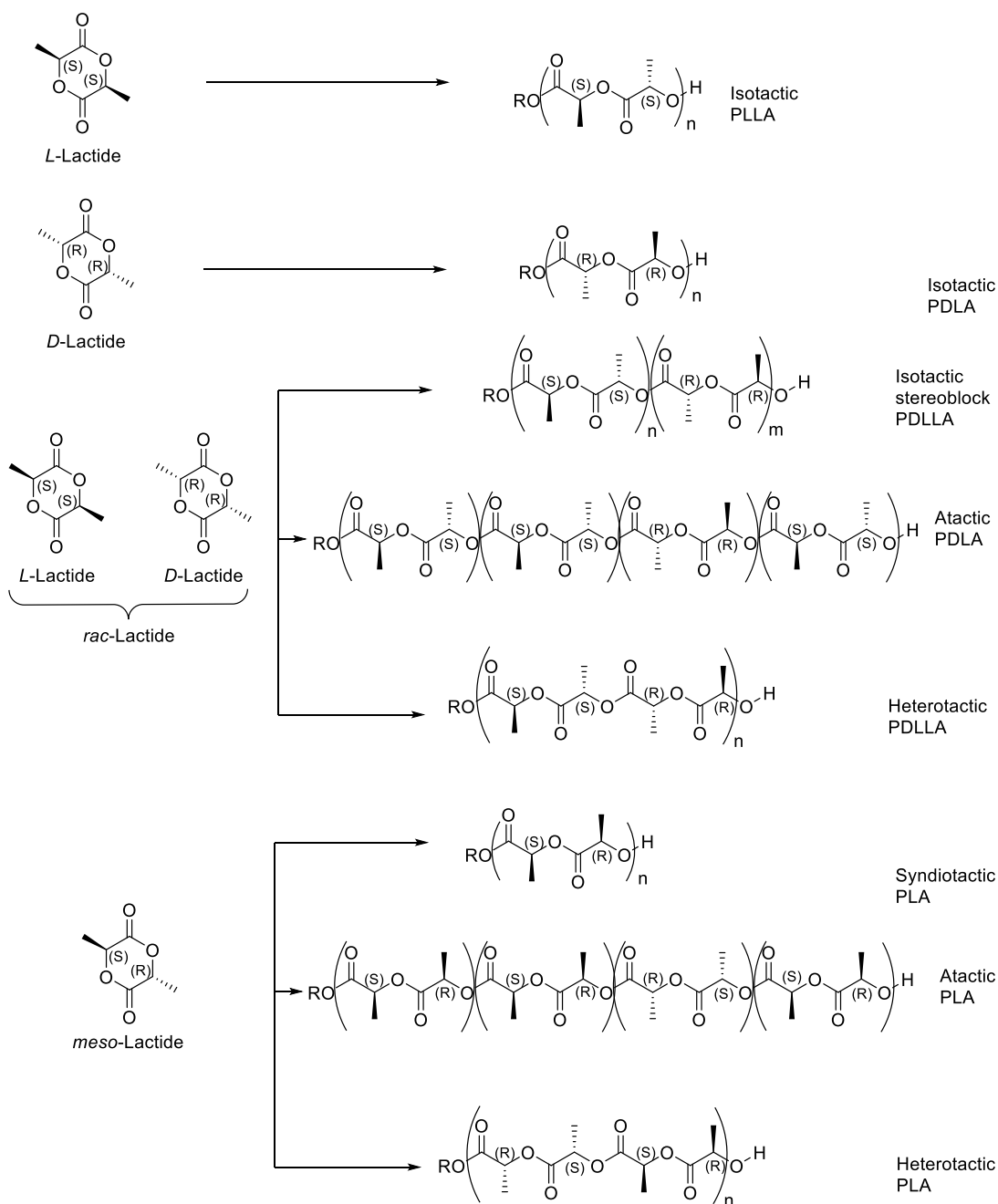


Figure 1.06: Possible lactide polymerisation pathways.

PLLA is the industrial standard due to the ease of biosynthesis of *L*-lactic acid. It has a melting temperature (T_m) of around 175 °C and a glass transition temperature (T_g) of 55 °C. These properties can be improved through the physical blending of PLLA and PDLA chains which creates a stereocomplex interaction and can improve the T_m by up to 50 °C. However, this approach is limited by the high cost of PDLA. As a result of this, there has been a great deal of research into finding initiators that are able to

produce highly isotactic PLA from *rac*-lactide.^[33] With an isoselective, achiral initiator, a chain-end control mechanism can operate whereby a monomer of a certain stereochemistry will be polymerised preferentially until an error is made.^[34] As the growing polymer chain dictates the order of insertion, the error will propagate, ultimately giving long isotactic blocks within the polymer. The stereocomplex interaction can then occur leading to an improvement in thermal and mechanical properties. With the racemic mixture of a chiral initiator, it is possible for each stereoisomer to favour a specific lactide stereoisomer through an enantiomorphic site control mechanism wherein the chirality of the initiator controls the order of insertion.^[35] In this case, errors do not propagate but chain transfer events mean that block stereopolymers are still formed in favour of a PLLA/PDLA blend.

1.2.4 Characterisation

There are a range of characterisation techniques relevant to the study of PLA. These can be used in conjunction with each other to assess properties such as the structure and size of the polymers, the microstructure, stereochemistry and thermal properties such as T_g and T_m .

Gel Permeation Chromatography (GPC), also known as Size Exclusion Chromatography (SEC), is a fundamental technique used to assess the average molecular weight and the dispersity of a given polymer sample. The sample is typically eluted through a column packed with porous gel particles. Larger particles are unable to pass through the pores and so elute before the smaller particles which can diffuse through the porous structure. Upon detection at the end of the column, the retention time is referenced against well-defined polystyrene standards. Another option is to use a combination of light scattering and refractive index detection to give “absolute” size data for a polymer, although this technique is highly sensitive to concentration and impurities.

GPC analysis of polymers gives a range of data of which three are commonly reported (**Figure 1.07**). The number average molecular weight (M_n) is commonly given as the molecular weight of the polymer and is the statistical average of all chains in the

sample. The weight average molecular weight (M_w) takes into account the added contribution of longer chains in the sample. The dispersity (\mathfrak{D}) is the ratio of M_w and M_n and gives a measure of how broad the molecular weight distribution is. As a result of the inherent differences between PLA and polystyrene, the M_n values obtained from GPC analysis tend to be overstated. It has therefore become common practice to apply a correction factor of 0.58 as initially proposed by Kowalski *et al.*^[36] This is tailored towards PLLA but is often applied to PLA formed from *rac*-lactide.

$$M_w = \frac{\sum M_i^2 N_i}{\sum M_i N_i}; \quad M_n = \frac{\sum M_i N_i}{\sum N_i}; \quad \mathfrak{D} = \frac{M_w}{M_n}$$

Figure 1.07: Equations for molecular weight and dispersity.

Similar, yet complimentary, information can be gained through Matrix assisted laser desorption/ionisation in time-of-flight (MALDI-ToF) mass-spectrometry. For this technique, the sample is ionised with a laser upon a suitable matrix. The result is a polymer mass-spectrum where each signal represents a chain length. It is possible to ascertain the molecular weight (M_p) that can be compared with M_n and M_w . The peak separation of a MALDI-ToF spectrum gives the repeat unit of the polymer. In the case of PLA, 144 g mol⁻¹ is favourable as it shows a repeat unit of lactide. A series separated by 72 g mol⁻¹ indicates that transesterification has taken place and that the repeat unit is lactic acid. From the MALDI-ToF spectrum, it is also possible to ascertain the molecular weight of the end groups, particularly useful if the nature of the active species is not clear.

When analysing polymers made from *rac*-lactide, it is useful to assess the tacticity of the sample through ¹H{¹H} NMR. For every four units of monomer, there will be three stereochemical relationships which can be designated as syndiotactic (*s*), where neighbouring units have opposite stereochemistry, or isotactic (*i*), where neighbouring units have identical stereochemistry (**Figure 1.08**).^[37] In the methine region of the ¹H NMR spectrum, each set of three relationships gives a distinct quartet, that can be turned into a singlet through decoupling from the methyl

protons. The probability of racemic enchainment (P_r) can be calculated from the normalised intensity of the *sis* tetrad; this represents the tetrad LDDL as would be expected for heterotactic PLA and therefore $P_r = 1$ is perfectly heterotactic.^[37] The probability of *meso*-enchainment is given by $P_m = 1 - P_r$ and gives the probability of LLLL or DDDD tetrads being formed i.e. a low fraction of *sis* relationships. Atacticity can be attributed when both P_r and P_m are approximately equal to 0.5. Although less quantitative, these tetrads can also be found in the methine region of the $^{13}\text{C}\{^1\text{H}\}$ NMR spectrum.

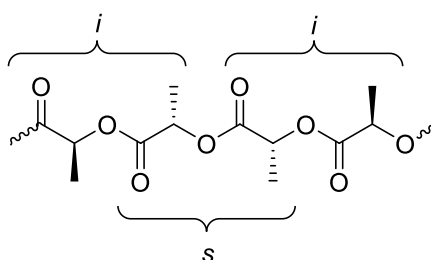


Figure 1.08: An *isi* PLA tetrad, indicative of heterotactic PLA.

When characterising polymers, it is also of key importance to assess their thermal properties. Thermal Gravimetric Analysis (TGA) can be used to assess the thermal decomposition of a polymer through carefully weighing a small sample whilst heating in air or under an inert atmosphere. The resulting curve shows the temperature at which degradation begins and when full decomposition is reached. This can be useful to assess maximum operating conditions and to set the parameters for other thermal techniques.

Differential Scanning Calorimetry (DSC) is another important thermal analysis technique that is commonly used for PLA. During a DSC run, the sample is heated past its melting temperature and then cooled down to a crystallisation temperature before another heating cycle. During the process, the specific heat capacity is measured against a control giving values for T_g and T_m as well as thermodynamic parameters. This technique is particularly useful for isotactic stereocomplex PLA

where elevated melting temperatures are expected; DSC analysis is often related to P_m and crystallinity of the sample.

Some insight into the crystallinity of the polymer can be gained from powder X-Ray Diffraction (pXRD). This is not necessarily a quantitative technique, but sharp signals generally indicate a degree of crystallinity.

1.2.5 Degradation

Considering the recent emphasis on plastic waste and pollution, it is vital that all plastic products have a clear end-of-use strategy, ideally looking towards a “circular economy” approach.^[38] As of 2015, it was estimated that 6,300 Mtonnes of plastic waste had been disposed of and 79% has ended up either in landfill or accumulating in the environment.^[2] The incineration of plastic waste has some benefits over landfill as some energy can be recovered and it reduces the volume of waste to be disposed. It does, however, result in increased GHG emissions and it destroys the value inherent in the polymers. It is therefore crucial to research and implement alternative recycling, reuse and degradation strategies.

When considering the disposal of PLA products, there are several options that are favourable to traditional disposal methods (**Figure 1.09**). Although it is not entirely biodegradable, PLA can be composted, under the right conditions, into harmless by-products.^[39] This is a useful approach, however it is a slow process and is sensitive to other polymers in the waste stream. Furthermore, efforts to improve the material properties of PLA often render composting more difficult.^[38] LCA studies suggest that composting is not desirable from an environmental standpoint, giving similar results to landfill disposal.^[40] Other common polyesters, such as PET, are widely recycled mechanically into lower grade materials.^[41] This is an important process but does not recapture the value or quality of the original product and is therefore limited in its long-term usefulness.

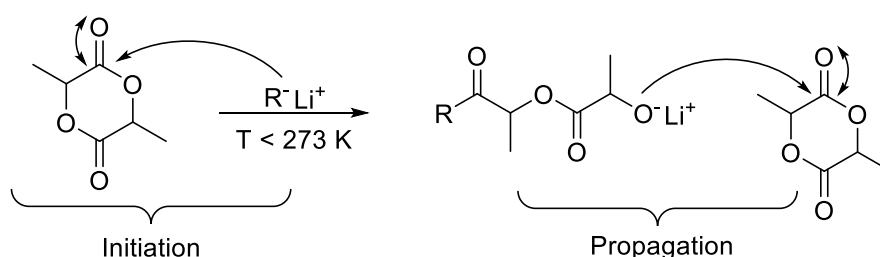
The most promising route for recovering the value of used PLA products is through chemical recycling. This falls into two main categories: depolymerisation and degradation.^[38] Depolymerisation occurs when the monomer (lactide or lactic acid)

1.3 Ring opening polymerisation

Ring opening polymerisation (ROP) refers to the reaction in which a cyclic monomer is ring opened by an initiating group, or the end of a polymer chain, to give a linear polymer. In the case of cyclic esters, such as lactide, this is achieved through cleavage of acyl oxygen bonds to form aliphatic ester linkages. For lactide, and other cyclic esters, ring strain provides the thermodynamic driving force towards propagation for four, six and seven membered rings; five membered rings are less favourable due to low ring strain and a corresponding positive Gibbs free energy of polymerisation (ΔG_p).^[46]

1.3.1 Anionic and cationic ROP

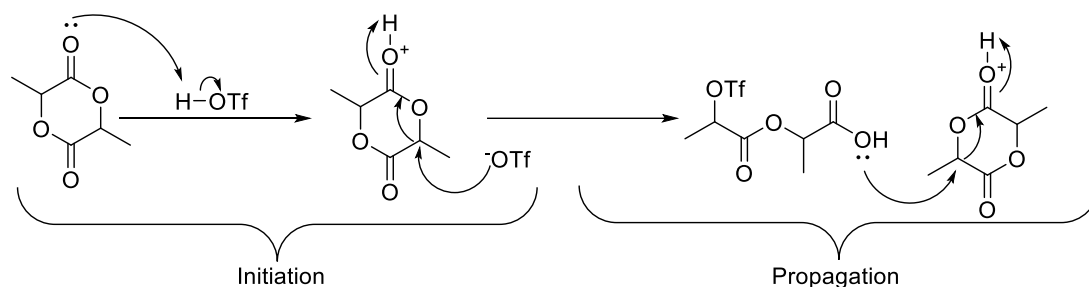
There are various pathways towards initiating the ring-opening step, the simplest of which are anionic and cationic ROP. During anionic ROP (**Scheme 1.02**), a nucleophile is used to cleave the acyl oxygen bond and initiate propagation. Alkyl lithium reagents are often employed for this reaction and early work by Kasperczyk demonstrated a heterotactic preference ($P_r = 0.76$) using *t*-butyl lithium as an initiator.^[47] Further work from the same group continued to demonstrate heterotacticity, however, a significant degree of intramolecular transesterification and epimerisation were also observed, leading to poor control in polymerisation.^[48,49]



Scheme 1.02: General mechanism for anionic ROP with lithium alkyls. R = *t*-BuO, Bu.

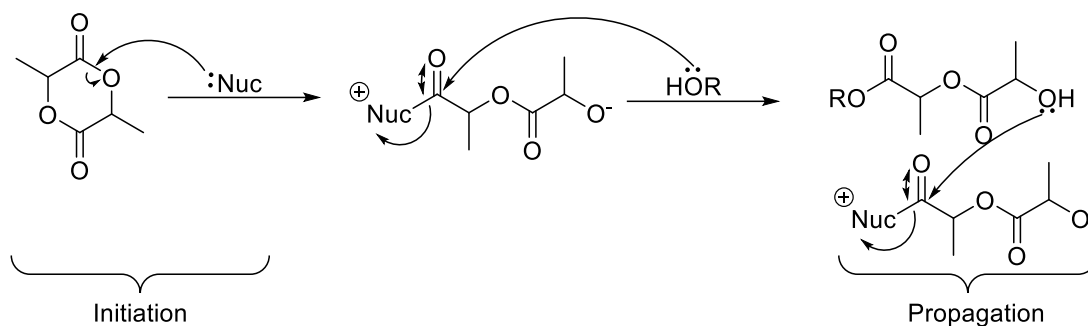
Cationic ROP (**Scheme 1.03**) proceeds through an electrophilic activated monomer mechanism, wherein the lactide carbonyl is protonated to give an effective leaving group, thus facilitating attack at the carbon centre. This has been achieved using

triflates with some success, although there remain control issues and no tacticity has been observed with *rac*-lactide.^[50]



Scheme 1.03: General mechanism for cationic ROP with triflic acid.

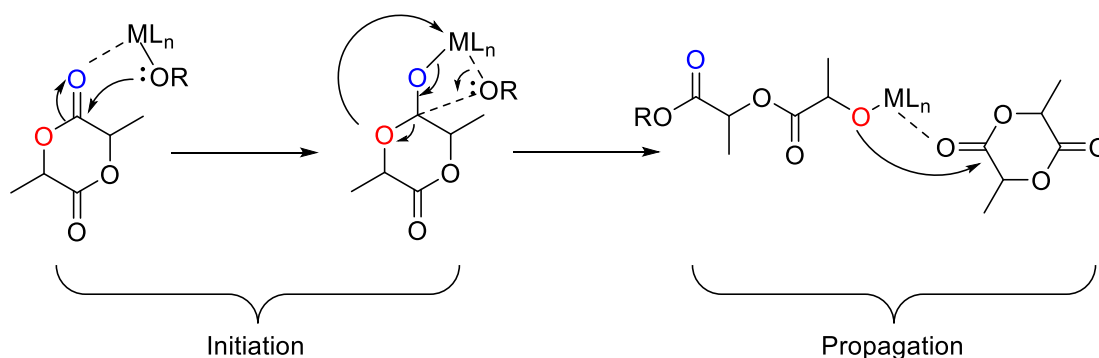
Another strategy towards lactide ROP is the use of nucleophilic organocatalysts; the chief benefit of which is the lack of potentially toxic metals in the final polymer. The first example of this approach was reported by Nederberg and co-workers who employed dimethyl amino pyridine (DMAP), with various alcohol co-initiators, in both the melt and solution phase. They postulated a mechanism wherein the monomer is activated by DMAP before reacting with an initiating alcohol (**Scheme 1.04**).^[51] Organocatalysts typically require high loadings or long reaction times and it is also often difficult to impart stereochemical control over the polymer. There are, however, some examples of isoselective organocatalysts for lactide ROP,^[52–57] including work by Taton *et al.* who achieved highly isotactic PLA ($P_m = 0.96$) with a bulky, chiral amino acid organocatalyst at room temperature ($[LA]/[BnOH]/[cat] = 50:1:1$). To achieve this selectivity, a single enantiomer of initiator was employed with a strong preference for *L*-LA, hence the conversion was limited to 50%. When a racemic mixture of initiator was used, the stereoselectivity was lost ($P_m = 0.60$).



Scheme 1.04: General mechanism for organocatalysed ROP.

1.3.2 Coordination insertion

Coordination insertion is the most common and well-studied mechanism for initiating ROP of lactide. The mechanism (**Scheme 1.05**) proceeds through the coordination of one lactide molecule to a metal centre through a carbonyl oxygen. This activates the associated carbonyl carbon to attack from a nucleophile, typically a labile group on the metal centre such as an alkoxide ligand. The coordinated polymer chain then becomes the nucleophile and opens successive monomers upon coordination.



Scheme 1.05: General mechanism for coordination insertion ROP.

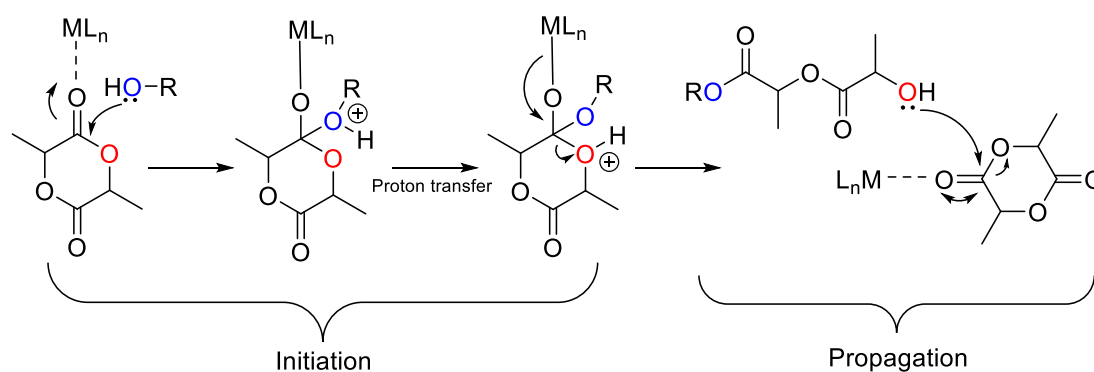
Depending on the nature of the initiating coordination complex, there are two possible mechanisms that can impart tacticity onto the polymer. Sterically bulky, achiral ligands can instigate a chain end control mechanism wherein the lactide stereoisomer that is coordinated controls the nature of the following monomer unit.

Alternatively, it is possible for chiral initiators to control stereoselectivity through favouring one lactide stereoisomer over the other.

In an industrial setting, it is preferable to conduct the ROP of lactide “in the melt” where the temperature is set higher than the melting point of lactide ($\geq 130\text{ }^{\circ}\text{C}$) allowing the reaction to be carried out without a solvent. At industrial scale, the reaction is usually carried out at a temperature of $180\text{ }^{\circ}\text{C}$ or higher so that the polymer is also in the melt phase and can be easily processed. Avoiding the use of a solvent has benefits both in terms of cost, potential toxicity and downstream processing. There is, however, a loss of stereocontrol often associated with high temperatures and so most small-scale investigations of new initiators are carried out in a solvent such as toluene or DCM.

1.3.3 Activated monomer

When a lactide molecule coordinates to a metal centre but there is no labile, nucleophilic ligand, ROP can proceed through an attack by an exogenous nucleophile, usually an alcohol (**Scheme 1.06**). In some cases, there can be competition between activated monomer and coordination insertion, particularly at low temperatures.^[58,59]



Scheme 1.06: Activated monomer ROP.

1.3.4 Side reactions

Epimerisation and transesterification are the two main deleterious side reactions that can occur during lactide ROP. Epimerisation occurs where there is some inversion of stereochemistry of the monomer units. This is particularly a problem for PLLA as a loss of isotacticity can drastically reduce the thermal properties of the polymer. It is however possible to exploit epimerisation at the monomer stage to produce *rac*-lactide from *meso*-lactide.^[60]

Transesterification is a result of an activated polymer attacking an established polymeric chain through a carbonyl oxygen instead of a lactide monomer. This can lead to a broadening in molecular weight distributions, a decrease in chain lengths and the scrambling of stereocentres. Transesterification can proceed through an intermolecular pathway or as an intramolecular reaction where cyclic PLA is the product. In some cases, the latter reaction can be useful where cyclic PLA is the target.^[61]

1.3.5 Metal initiators for lactide polymerisation

Tin octanoate

There is a wide range of metal complexes that can promote lactide ROP. The classic example from industry is tin octanoate [Sn(Oct)₂] (**Figure 1.10**). This initiator is highly active, giving very high molecular weight after 30 minutes with loading as low as 7.2×10^{-5} mol%.^[62] The levels of tin initiator remaining in the final polymer has been deemed safe for food packaging. However, tin residues can be toxic and can accumulate in waste streams. Therefore, there is significant research into more benign metal initiators. Although being ideal for the industrial synthesis of PLLA, tin octanoate is unable to stereoselectively polymerise *rac*-lactide, giving completely atactic PLA. It does, however, set a benchmark in terms of availability and performance that must be matched by a stereoselective alternative if it is going to be commercially competitive.

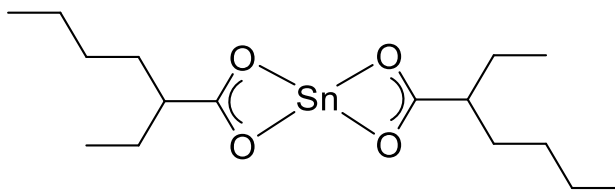


Figure 1.10: Structure of tin(II)bis(2-ethylhexanoate).

The most active research area in this field is the hunt for isoselective initiators for lactide ROP to gain reliable and economical access to stereocomplexed PLA with improved thermal properties. There is also a need for highly active initiators that can compete with tin octanoate on an industrial scale, but without using a toxic, heavy metal. Examples of lactide polymerisation initiators can be found across the periodic table and are typically based on Lewis acidic metal complexes. Selected examples of metal initiators are herein explored to demonstrate the scope and variation of active metal complexes. The metals relevant to this thesis, iron, aluminium and zinc, are discussed in detail in sections **2.1.3**, **2.4.1** and **3.1** respectively.

Group I metals

There are many examples of group I alkali metals being reported for lactide polymerisation, many of which show excellent activity or stereocontrol.^[63] A recent report from Garden *et al.* described lithium half-salen complexes for room temperature polymerisation of *rac*-lactide.^[64] Complex aggregation was noted and could be related to the activity of the initiators. The most active examples reached high conversion in under a minute at ambient temperatures although molecular weights were low and wide dispersities were observed ($\bar{D} = 1.31 - 3.27$).

Lai *et al.* tested a series of amidate ligands with sodium, which were expected to take a cubic form with the vertices consisting of four oxygen and four sodium atoms (**Figure 1.11**).^[65] The complex formed from ligand **1** achieved essentially quantitative lactide conversion in one minute at 0 °C with a relatively high ratio of initiator to lactide ($[LA]/[I]/[ROH] = 2400 : 1 : 80$). Good control of molecular weight and dispersity was also noted under these conditions ($M_{n, \text{theo.}} = 8700 \text{ gmol}^{-1}$, $M_{n, \text{GPC}} = 9500 \text{ gmol}^{-1}$, $\bar{D} = 1.14$).

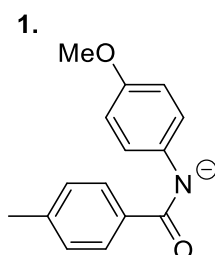


Figure 1.11: Carbamate ligand reported by Lai with Sodium for lactide polymerisation.^[65]

Simple sodium and potassium phenolate complexes reported by Wu and co-workers were able to polymerise lactide with high isoselectivities (**Figure 1.12**).^[66,67] The alkali metal centres were coordinated to a large crown-ether ligand and a series of bulky phenolates. The complex formed from the coordination of **2** to potassium with dibenzo-18-crown-6 ether could reach high conversion after one minute at room temperature giving well-controlled PLA with an isotactic bias ($P_m = 0.77$).^[66] The isotacticity of the complex could be improved to 0.89 however this required cooling to $-60\text{ }^\circ\text{C}$ and a ten hour reaction time. Further work from the same group used anthryl substituted phenols to achieve higher isoselectivities.^[67] The origin of the stereospecificity arose from the sandwich effect of the bulky crown ether and the planar anthryl- group. Ligand **3** gave the most isotactic product ($P_m = 0.94$) with an elevated melting temperature ($T_m = 192.5\text{ }^\circ\text{C}$). In all cases, potassium was shown to be superior to sodium for these complexes.

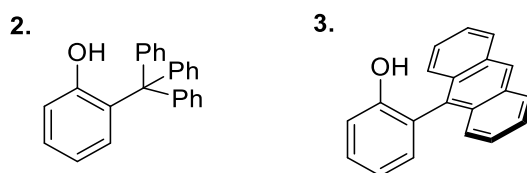


Figure 1.12: Bulky phenolate ligands for lactide polymerisation with sodium and potassium.^[66,67]

Group II metals

Simple magnesium salts were first applied to lactide polymerisation by Kricheldorf and magnesium oxide gave high conversion in the melt after 72 h at 150 °C.^[68] Coates *et al.* introduced β -diiminate ligated magnesium complexes which were active at room temperature (**Figure 1.13**).^[69] At a ratio of $[LA]/[I]/[iPrOH] = 500 : 1 : 1$, up to 96% of lactide could be converted to PLA after five minutes. However, no stereocontrol was observed unlike the zinc equivalents. More recently, Kol and co-workers reported a series of {ONNN} magnesium complexes that were capable of high activity and excellent stereoselectivity at room temperature.^[70] Complex **4** reached full conversion after five minutes with low initiator loading ($[LA]/[I]/[BnOH] = 5000 : 1 : 50$). A chain-end control mechanism led to isotactic PLA being formed ($P_m \leq 0.92$).

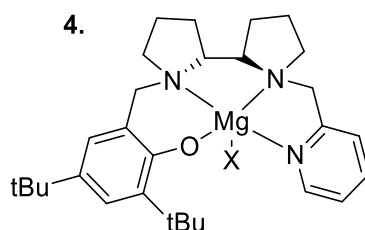


Figure 1.13: {ONNN} magnesium complex reported by Kol for stereoselective lactide ROP.^[70]

There are fewer reports of calcium complexes for lactide polymerisation, in part due to a rapid Schlenk-equilibrium which tends to see calcium forming inactive homoleptic complexes. Cui recently reported Zwitterionic heteroscorpionate calcium complexes.^[71] Rapid room-temperature polymerisation was reported and cooling to -78 °C afforded heterotactic ($P_r = 0.84$) or isotactic PLA ($P_m = 0.74$), dependent on ligand structure.

Group IV metals

Group IV metal complexes have been applied extensively to lactide polymerisation (**Figure 1.15**). Titanium salen complexes published by Gibson and co-workers reached high conversion in 8 – 24 h under solvent-free conditions.^[72] Interestingly, electron withdrawing substituents reduced the rate of reaction whereas electron-donating groups were beneficial. This contradicts the trends seen with many other metals. Walter and co-workers prepared a series of chiral, pincer NHC ligands coordinated to group IV metals.^[73] Titanium complex **5** polymerised 70% of *rac*-lactide after 30 minutes at 70 °C in toluene giving moderately heterotactic PLA ($P_m = 0.72$). The larger group IV metal complexes, **6** and **7**, were more active, both giving 100% conversion under the same conditions with lower stereoselectivity. The authors attributed the activity differences to the small ionic radius of Ti^{4+} . Wong and co-workers noted a similar stereoselectivity trend with aminobisphenolate complexes of titanium, zirconium and hafnium although titanium complex **8** was marginally more active than its heavier counterparts.^[74] Complexes of zirconium, **9**, and hafnium, **10**, gave PLA with a moderate isotactic bias ($P_m = 0.60 - 0.75$) whereas all titanium complexes gave atactic PLA. Jones *et al.* produced PLA with a strong isotactic bias ($P_m = 0.85$) with zirconium salalen complex **11** in toluene at 50 °C.^[75] Some selectivity was retained in the melt ($P_m = 0.74$) and the reaction reached high conversion in two hours at a ratio of $[LA]/[I] = 300 : 1$. The hafnium equivalent (**12**) was similarly active in solution, but less selective ($P_m = 0.77$).

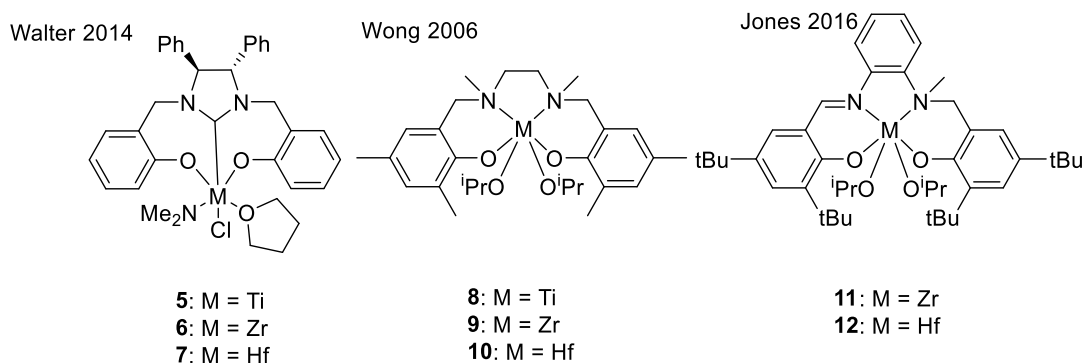


Figure 1.14: Group IV complexes for lactide polymerisation.^[73,74]

Rare earth metals

There are many examples of rare-earth metal complexes that show activity for lactide polymerisation (**Figure 1.15**).^[76–78] Ma and Okuda presented {OSSO} complexes of yttrium (**13**) and lutetium (**14**) capable of room-temperature lactide polymerisation at ratios up to $[LA]/[I] = 1500 : 1$.^[79] The effect of the labile initiating group was explored. The silylamido group gave rapid but poorly controlled polymerisation, whereas the addition of an exogenous alcohol slowed the reaction considerably but improved control. Lui and Shi recently reported phosphasalalen complexes of scandium, yttrium and lutetium.^[80] Scandium complex **15** was the least active initiator but gave excellent control of the reaction at room temperature ($M_{n, calc} = 20,800 \text{ gmol}^{-1}$, $M_{n, GPC} = 22,600 \text{ gmol}^{-1}$, $\bar{D} = 1.03$). Yttrium complex **16** was active at room temperature for monomer to initiator ratios up to 2000 : 1 giving molecular weights in excess of $100,000 \text{ gmol}^{-1}$. The addition of a bulky cumyl- substituent (**17**) gave PLA with a moderate heterotactic bias ($P_r = 0.75$).

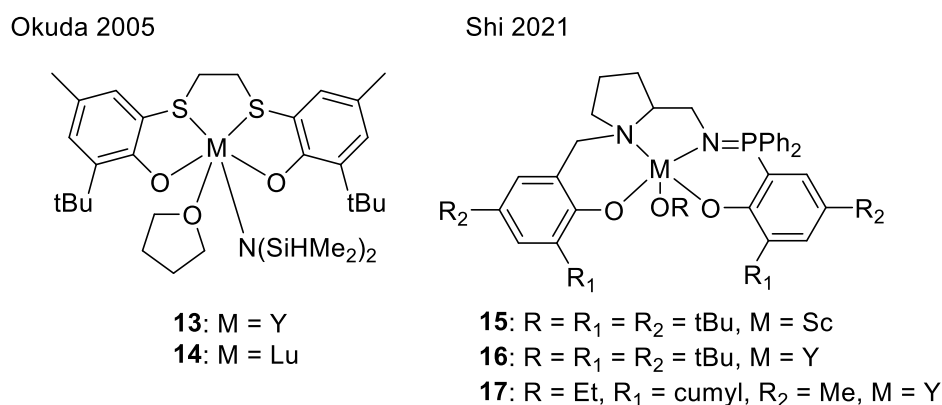


Figure 1.15: Selected examples of rare-earth initiators for lactide polymerisation.^[79,80]

Group XIII metals

Aluminium complexes have been dominant in PLA research in recent years. However the heavier elements in group XIII, gallium and indium, have also been successfully applied to lactide ROP (**Figure 1.16**).^[59,81] Sarazin *et al.* developed a series of aluminium, gallium and indium complexes with enantiopure, chiral salen ligands

based on (*R,R*)-1,2-diphenyl ethylenediamine.^[82] Indium complex **18** polymerised *rac*-lactide in toluene at 95% conversion (80 °C, [LA]/[I]/[BnOH] = 100 : 1 : 1) giving atactic PLA. The authors attributed the change in selectivity between aluminium and indium to a change in mechanism from coordination-insertion for aluminium to activated monomer for indium. The synthesis of analogous gallium complexes was unsuccessful but bimetallic complex **19** was active at room temperature after 100 minutes producing atactic PLA. By contrast, the aluminium complexes were much more stereoselective but took up to 10 days to reach high conversion.

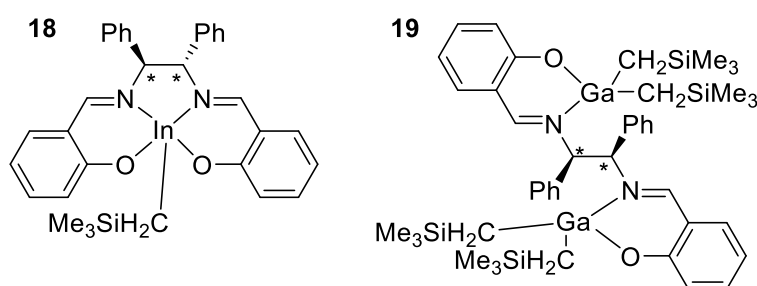


Figure 1.16: Group XIII complexes for lactide polymerisation from Sarazin *et al.*^[82]

Williams and co-workers presented highly isoselective indium initiators supported by phosphasalen ligands (**Figure 1.17**).^[83] Complex **20** was active at room temperature with relatively low initiator loading ([LA]/[I] = 500 : 1) and gave PLA with a strong isotactic bias ($P_m = 0.87$). This could be improved to $P_m = 0.92$ by adding sequential portions of *rac*-lactide when conversion had reached 80%. This method exploited the effect of re-initiation upon monomer addition and allowed high molecular weights to be obtained in a relatively controlled manner ($M_{n\text{ calc.}} = 136,200\text{ gmol}^{-1}$, $M_{n\text{ GPC}} = 157,800\text{ gmol}^{-1}$, $\bar{D} = 1.25$).

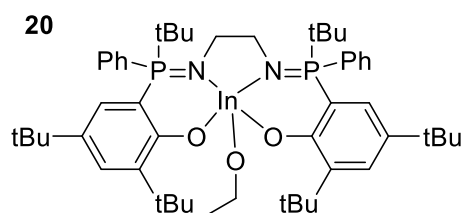


Figure 1.17: Indium phosphasalen initiator for isoselective lactide polymerisation.^[83]

1.4 Research aims

With the drive towards a more sustainable future, many of the issues addressed in **Chapter 1** require innovative technological solutions and sustainable chemistry is at the core of this. One aspect of this is sustainable catalysis, which avoids the use of toxic, heavy metals that are expensive and relatively rare in nature. Another important challenge is the development and application of bio-renewable plastics to replace the ecologically damaging hydrocarbon polymers that are so widespread in society.

Iron, aluminium and zinc are classified as benign and abundant metals and form the basis of this research. Mono- and bis-phenolate complexes of these three metals were applied to lactide polymerisation. Iron complexes gave high selectivity (**Chapter 2**) and zinc complexes polymerised lactide with high activity at very low initiator loading whilst also being capable of polyester degradation to discrete products (**Chapter 3**). Aluminium analogues provided valuable comparative insight whilst showing modest activity. The electrochemical behaviour of iron complexes was assessed in **Chapter 4** as an initial step towards electrochemically switchable copolymerisation.

1.5 References

- [1] D. Hosler, S. L. Burkett, M. J. Tarkanian, *Science* **1999**, *284*, 1988–1991.
- [2] R. Geyer, J. R. Jambeck, K. L. Law, *Sci. Adv.* **2017**, *3*, e1700782.
- [3] J. R. Jambeck, R. Geyer, C. Wilcox, T. R. Siegler, M. Perryman, A. Andrady, R. Narayan, K. L. Law, *Science* **2015**, *347*, 768–771.
- [4] G. Anfuso, H. J. Bolívar-Anillo, F. Asensio-Montesinos, R. Portantiolo Manzolli, L. Portz, D. A. Villate Daza, *Mar. Pollut. Bull.* **2020**, *160*, 111657.
- [5] K. L. Law, R. C. Thompson, *Science* **2014**, *345*, 144–145.
- [6] H. A. Leslie, M. J. M. van Velzen, S. H. Brandsma, A. D. Vethaak, J. J. Garcia-Vallejo, M. H. Lamoree, *Environ. Int.* **2022**, 107119.
- [7] M. O. Rodrigues, N. Abrantes, F. J. M. Gonçalves, H. Nogueira, J. C. Marques, A. M. M. Gonçalves, *Environ. Toxicol. Pharmacol.* **2019**, *72*, 103239.
- [8] I. Conti, C. Simioni, G. Varano, C. Brenna, E. Costanzi, L. M. Neri, *Environ. Pollut.* **2021**, *288*, 117708.
- [9] S. Belboom, A. Léonard, *Biomass and Bioenergy* **2016**, *85*, 159–167.
- [10] K. Ragaert, L. Delva, K. Van Geem, *Waste Manag.* **2017**, *69*, 24–58.
- [11] X. Zhang, M. Fevre, G. O. Jones, R. M. Waymouth, *Chem. Rev.* **2018**, *118*, 839–885.
- [12] J. Mark, K. Ngai, W. Graessley, L. Mandelkern, E. Samulski, G. Wignall, J. Koenig, *Physical Properties of Polymers*, Cambridge University Press, **2004**.
- [13] J. E. Mark, *Polymer Data Handbook*, Oxford University Press, **2009**.
- [14] F. Ebrahimi, H. Ramezani Dana, *Int. J. Polym. Mater. Polym. Biomater.* **2021**, 1–14.
- [15] H. Balakrishnan, A. Hassan, M. Imran, M. U. Wahit, *Polym. Plast. Technol. Eng.* **2012**, *51*, 175–192.
- [16] R. E. Drumright, P. R. Gruber, D. E. Henton, *Adv. Mater.* **2000**, *12*, 1841–1846.
- [17] D. L. Kaplan, in (Ed.: D.L. Kaplan), Springer Berlin Heidelberg, Berlin, Heidelberg, **1998**, pp. 1–29.
- [18] E. Castro-Aguirre, F. Iñiguez-Franco, H. Samsudin, X. Fang, R. Auras, *Adv. Drug Deliv. Rev.* **2016**, *107*, 333–366.
- [19] R. Auras, B. Harte, S. Selke, *Macromol. Biosci.* **2004**, *4*, 835–864.
- [20] S. Marano, E. Laudadio, C. Minnelli, P. Stipa, *Polym.* **2022**, *14(8)*, 1626.
- [21] R. P. Pawar, S. U. Tekale, S. U. Shisodia, J. T. Totre, A. J. Domb, *Rec. Pat. Regen. Med.* **2014**, *4*, 40–51.
- [22] Y. Chen, L. M. Geever, J. A. Killion, J. G. Lyons, C. L. Higginbotham, D. M. Devine, *Polym. Plast. Technol. Eng.* **2016**, *55*, 1057–1075.

- [23] M. Mochizuki, in Woodhead Publ. Ser. Text. (Eds.: S.J. Eichhorn, J.W.S. Hearle, M. Jaffe, T.B.T.-H. of T.F.S. Kikutani), Woodhead Publishing, **2009**, pp. 257–275.
- [24] M. Mutsuga, Y. Kawamura, K. Tanamoto, *Food Addit. Contam. Part A* **2008**, *25*, 1283–1290.
- [25] A. Komesu, J. Allan, R. De Oliveira, S. Martins, *BioRes.* **2020**, *12(2)*, 4364–4383.
- [26] S. Nakano, C. U. Ugwu, Y. Tokiwa, *Bioresour. Technol.* **2012**, *104*, 791–794.
- [27] M. A. Abdel-Rahman, K. Sonomoto, *J. Biotechnol.* **2016**, *236*, 176–192.
- [28] D. A. Esquivel-Hernández, J. S. García-Pérez, I. Y. López-Pacheco, H. M. N. Iqbal, R. Parra-Saldívar, *J. Environ. Manage.* **2022**, *301*, 113925.
- [29] M. Morales, P. Y. Dapsens, I. Giovinazzo, J. Witte, C. Mondelli, S. Papadokostantakis, K. Hungerbühler, J. Pérez-Ramírez, *Energy Environ. Sci.* **2015**, *8*, 558–567.
- [30] H. R. Kricheldorf, *Chemosphere* **2001**, *43*, 49–54.
- [31] H. Tsuji, I. Fukui, H. Daimon, K. Fujie, *Polym. Degrad. Stab.* **2003**, *81*, 501–509.
- [32] L.-E. Chile, P. Mehrkhodavandi, S. G. Hatzikiriakos, *Macromolecules* **2016**, *49*, 909–919.
- [33] C. K. Williams, M. A. Hillmyer, *Polym. Rev.* **2008**, *48*, 1–10.
- [34] M. Wisniewski, A. Le Borgne, N. Spassky, *Macromol. Chem. Phys.* **1997**, *198*, 1227–1238.
- [35] N. Spassky, M. Wisniewski, C. Pluta, A. L. Borgne, *Macromol. Chem. Phys.* **1996**, *197*, 2627–2637.
- [36] A. Kowalski, A. Duda, S. Penczek, *Macromolecules* **1998**, *9297*, 2114–2122.
- [37] M. T. Zell, B. E. Padden, A. J. Paterick, K. A. M. Thakur, R. T. Kean, M. A. Hillmyer, E. J. Munson, *Macromolecules* **2002**, *35*, 7700–7707.
- [38] J. Payne, P. McKeown, M. D. Jones, *Polym. Degrad. Stab.* **2019**, *165*, 170–181.
- [39] K. Fukushima, C. Abbate, D. Tabuani, M. Gennari, G. Camino, *Polym. Degrad. Stab.* **2009**, *94*, 1646–1655.
- [40] M. F. Cosate de Andrade, P. M. S. Souza, O. Cavalett, A. R. Morales, *J. Polym. Environ.* **2016**, *24*, 372–384.
- [41] N. Malik, P. Kumar, S. Shrivastava, S. B. Ghosh, *Int. J. Plast. Technol.* **2017**, *21*, 1–24.
- [42] E. T. H. Vink, K. R. Rábago, D. A. Glassner, B. Springs, R. P. O’Connor, J. Kolstad, P. R. Gruber, *Macromol. Biosci.* **2004**, *4*, 551–564.
- [43] C. Vogel, H. W. Siesler, *Macromol. Symp.* **2008**, *265*, 183–194.
- [44] H. Tsuji, *Macromol. Biosci.* **2005**, *5*, 569–597.
- [45] L. A. Román-Ramírez, P. Mckeown, M. D. Jones, J. Wood, *ACS Catal.* **2019**, *9*, 409–416.

- [46] P. Olsén, K. Odelius, A.-C. Albertsson, *Biomacromolecules* **2016**, *17*, 699–709.
- [47] J. E. Kasperczyk, *Macromolecules* **1995**, *28*, 3937–3939.
- [48] M. Bero, P. Dobrzyński, J. Kasperczyk, *J. Polym. Sci. Part A Polym. Chem.* **1999**, *37*, 4038–4042.
- [49] J. Kasperczyk, M. Bero, *Polymer (Guildf)*. **2000**, *41*, 391–395.
- [50] D. Bourissou, B. Martin-Vaca, A. Dumitrescu, M. Graullier, F. Lacombe, *Macromolecules* **2005**, *38*, 9993–9998.
- [51] F. Nederberg, E. F. Connor, M. Möller, T. Glauser, J. L. Hedrick, *Angew. Chemie Int. Ed.* **2001**, *40*, 2712–2715.
- [52] B. G. G. Lohmeijer, R. C. Pratt, F. Leibfarth, J. W. Logan, D. A. Long, A. P. Dove, F. Nederberg, J. Choi, C. Wade, R. M. Waymouth, J. L. Hedrick, *Macromolecules* **2006**, *39*, 8574–8583.
- [53] A. P. Dove, H. Li, R. C. Pratt, B. G. G. Lohmeijer, D. A. Culkin, R. M. Waymouth, J. L. Hedrick, *Chem. Commun.* **2006**, 2881–2883.
- [54] L. Zhang, F. Nederberg, J. M. Messman, R. C. Pratt, J. L. Hedrick, C. G. Wade, *J. Am. Chem. Soc.* **2007**, *129*, 12610–12611.
- [55] S. Liu, H. Li, N. Zhao, Z. Li, *ACS Macro Lett.* **2018**, *7*, 624–628.
- [56] A. Sanchez-Sanchez, I. Rivilla, M. Agirre, A. Basterretxea, A. Etxeberria, A. Veloso, H. Sardon, D. Mecerreyes, F. P. Cossío, *J. Am. Chem. Soc.* **2017**, *139*, 4805–4814.
- [57] B. Orhan, M. J.-L. Tschan, A.-L. Wirotius, A. P. Dove, O. Coulembier, D. Taton, *ACS Macro Lett.* **2018**, *7*, 1413–1419.
- [58] Y. Sun, Y. Cui, J. Xiong, Z. Dai, N. Tang, J. Wu, *Dalt. Trans.* **2015**, *44*, 16383–16391.
- [59] D. A. Atwood, M. J. Harvey, *Chem. Rev.* **2001**, *101*, 37–52.
- [60] J.-B. Zhu, E. Y.-X. Chen, *J. Am. Chem. Soc.* **2015**, *137*, 12506–12509.
- [61] P. Piromjitpong, P. Ratanapanee, W. Thumrongpatanaraks, P. Kongsaree, K. Phomphrai, *Dalton. Trans.* **2012**, *41*, 12704–12710.
- [62] X. Zhang, D. A. MacDonald, M. F. A. Goosen, K. B. McAuley, *J. Polym. Sci. Part A Polym. Chem.* **1994**, *32*, 2965–2970.
- [63] J. Bhattacharjee, A. Sarkar, T. K. Panda, *Curr. Opin. Green Sustain. Chem.* **2021**, *31*, 100545.
- [64] Y. Zhou, G. S. Nichol, J. A. Garden, *European J. Org. Chem.* **2021**, 5557–5568.
- [65] F.-J. Lai, C.-H. Lee, K.-H. Wu, Y.-L. Chang, Y.-C. Lai, H.-Y. Chen, S. Ding, C.-H. Lai, *Polym. Bull.* **2021**, *78*, 2813–2827.
- [66] Z. Dai, Y. Sun, J. Xiong, X. Pan, N. Tang, J. Wu, *Catal. Sci. Technol.* **2016**, *6*, 515–520.
- [67] Y. Sun, J. Xiong, Z. Dai, X. Pan, N. Tang, J. Wu, *Inorg. Chem.* **2016**, *55*, 136–143.
- [68] R. Dunsing, H. R. Kricheldorf, *Polym. Bull.* **1985**, *14*, 491–495.

- [69] B. M. Chamberlain, M. Cheng, D. R. Moore, T. M. Ovitt, E. B. Lobkovsky, G. W. Coates, *J. Am. Chem. Soc.* **2001**, *123*, 3229–3238.
- [70] T. Rosen, J. Rajpurohit, S. Lipstman, V. Venditto, M. Kol, *Chem. - A Eur. J.* **2020**, *26*, 17183–17189.
- [71] N. Liu, D. Liu, B. Liu, H. Zhang, D. Cui, *Polym. Chem.* **2021**, *12*, 1518–1525.
- [72] C. K. A. Gregson, I. J. Blackmore, V. C. Gibson, N. J. Long, E. L. Marshall, A. J. P. White, *Dalton Trans.* **2006**, 3134–3140.
- [73] N. Zhao, G. Hou, X. Deng, G. Zi, M. D. Walter, *Dalton Trans.* **2014**, *43*, 8261–8272.
- [74] A. J. Chmura, M. G. Davidson, M. D. Jones, M. D. Lunn, M. F. Mahon, A. F. Johnson, P. Khunkamchoo, S. L. Roberts, S. S. F. Wong, *Macromolecules* **2006**, *39*, 7250–7257.
- [75] S. M. Kirk, G. Kociok-Köhn, M. D. Jones, *Organometallics* **2016**, *35*, 3837–3843.
- [76] H. Yasuda, E. Ihara, *Adv. Polym. Sci.* **1997**, *133*, 52–101.
- [77] U. Bayer, R. Anwander, *Dalton Trans.* **2020**, *49*, 17472–17493.
- [78] D. M. Lyubov, A. O. Tolpygin, A. A. Trifonov, *Coord. Chem. Rev.* **2019**, *392*, 83–145.
- [79] H. Ma, J. Okuda, *Macromolecules* **2005**, *38*, 2665–2673.
- [80] H. Liu, X. Shi, *Inorg. Chem.* **2021**, *60*, 705–717.
- [81] S. Dagorne, M. Normand, E. Kirillov, J.-F. Carpentier, *Coord. Chem. Rev.* **2013**, *257*, 1869–1886.
- [82] N. Maudoux, T. Roisnel, V. Dorcet, J.-F. Carpentier, Y. Sarazin, *Chem. – A Eur. J.* **2014**, *20*, 6131–6147.
- [83] N. Yuntawattana, T. M. McGuire, C. B. Durr, A. Buchard, C. K. Williams, *Catal. Sci. Technol.* **2020**, *10*, 7226–7239.

Chapter 2: Thiolen complexes of iron and aluminium for *rac*-lactide polymerisation and CO₂/epoxide coupling

2.1 Introduction

2.1.1 Bisphenolate ligands

Tetradentate bisphenolate ligands are among the most common supporting ligands for lactide ROP and are also employed for a range of other catalytic reactions. Typically, these complexes have an {ONNO} coordination motif such as the classic salen ligand which is formed from a 2:1 mixture of salicylaldehyde and ethylene diamine to give dianionic Schiff base ligand (**Figure 2.01**). A wide range of salen derivatives have been applied to lactide polymerisation with aluminium salen complexes constituting the first examples of isoselective *rac*-lactide ROP. [1–8] Replacing both imine functionalities with amine groups, either through reduction or altered synthesis, gives salan ligands that can also be coordinated to a metal centre and applied to lactide ROP.[84–89] The intermediate, salalen, ligand, with one imine and one amine donor, has also been applied to the ROP of lactide showing some interesting reactivity compared with its symmetrical counterparts. [8,9,13–18]

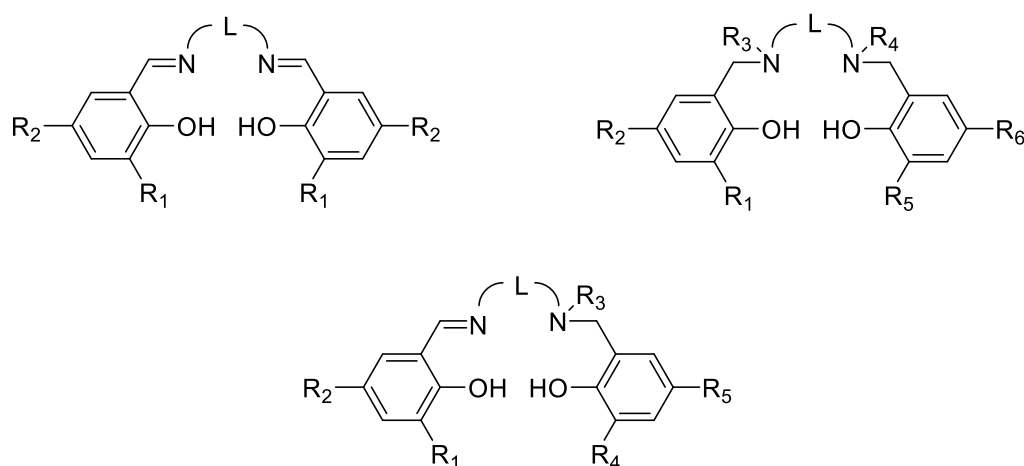


Figure 2.01: General formula for salen (top left), salan (top right) and salalen (bottom).

Despite the ubiquity of the {ONNO} structure, the introduction of a soft, second row donor has been shown to regulate Lewis acidity and improve the activity of some complexes.^[19] There is also a drastic difference in the flexibility of thioether and imine bonds potentially allowing a greater variety of coordination geometries.

2.1.2 Thiolen ligands

Imine(thiobis) phenolate (thiolen) ligands are tetradentate ligands with an {ONSO} coordination motif. They share a similar structure to the classic salen ligand but with a thioether donor in place of the typical imine functionality (**Figure 2.02**). The structure is therefore analogous to the semi-rigid salalen family of ligands which contain a flexible amine donor atom as well as a more rigid imine functionality. This family of ligands was first introduced by Kol and co-workers in an attempt to synthesise a semi-rigid ligand where fluxionality was dependant on the phenolate substitution pattern.^[20] Six derivatives were reported, bearing combinations of electron-withdrawing and bulky substituents, and complexed to zirconium (**Figure 2.03**). The resultant complexes were all active for *rac*-lactide polymerisation both in toluene at 70 °C and in the melt at 140 °C. In solution, a range of tacticities were observed with the most fluxional derivative (**21**) giving heterotactically inclined PLA ($P_r \leq 0.72$) whereas the most rigid structure (**22**) produced PLA with an isotactic bias ($P_m \leq 0.67$). Throughout the study, dispersities were relatively broad ($\mathcal{D} = 1.10 - 1.70$) and molecular weights tended to be significantly lower than the expected values.

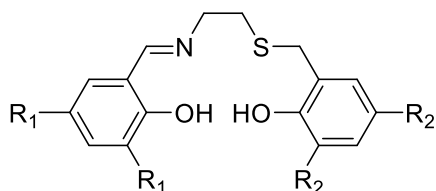


Figure 2.02: General formula of a thiolen ligand.

Further work by the same group looked at phenylene bridged {ONSO} zirconium complexes and the resulting PLA varied from heterotactic to atactic (**23**: $P_r = 0.87$; **24**: $P_r = 0.49$).^[21] In this case, the change in selectivity was attributed to the nature of the substituents, rather than the fluxionality of the complexes. More electron-withdrawing ligands gave higher activity and tended to be heteroselective whereas bulky adamantyl and *tert*-butyl substituents reduced activity and stereoselectivity.

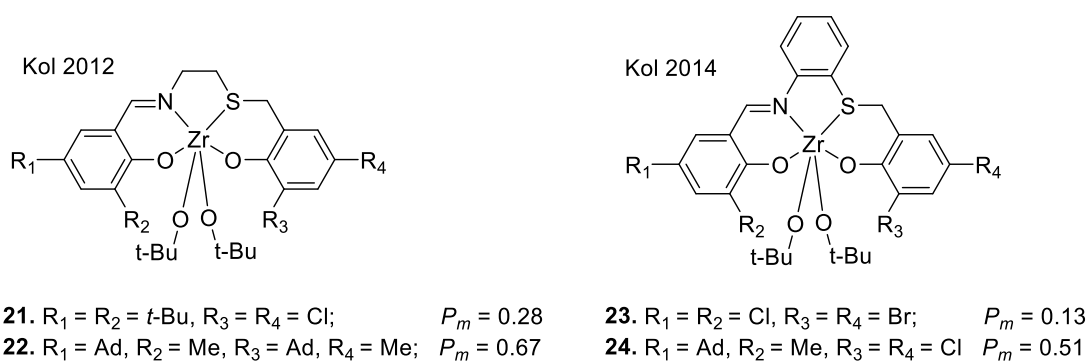


Figure 2.03 Selected literature examples of thioen complexes that are active for lactide ROP.

Chromium thioen complexes have also been reported and shown to be active for the copolymerisation of CO_2 and epoxides,^[22] as well as the copolymerisation of norbornene anhydrides with epoxides.^[23] A dinuclear, chromium bis-{ONSO} complex was reported comprised of two bisphenolate ligand units connected through a piperazine linker.^[24] This complex selectively produced polyether from a mixture of phthalic anhydride and cyclohexene oxide (97% ether linkage). This is in contrast to the aforementioned mononuclear complex which gave 83% ester linkages under identical conditions, although with different anhydride monomers.^[23] Two examples of titanium-thioen-chloride complexes have also been reported and applied to the syndiospecific polymerisation of styrene.^[25]

Despite these promising studies, there remains relatively few examples of the application of complexes bearing imine thiobis(phenolate) ligands. The ease of synthesis means that there are many derivatives, in addition to those previously reported, that could be targeted using commercially available or easily synthesised

starting materials. Furthermore, only zirconium-thiolen complexes have been applied to lactide polymerisation and so there is scope to explore more active and more abundant metals.

2.1.3 Iron complexes for lactide polymerisation

There are numerous benefits to using iron-based initiators for the ROP of lactide. Iron is the second most abundant metal and is therefore cheap and readily available. It is also non-toxic and biocompatible making it especially useful for biomedical applications of PLA.^[26] Furthermore, iron (III) complexes are often air-stable, making them easier to handle and potentially more industrially viable. Despite these clear benefits, there are limited reports of iron (III) complexes being applied to lactide polymerisation. An early study by Tolman applied well-defined ferric alkoxide clusters to the ROP of *L*-lactide in toluene at 70 °C.^[27] A conversion of 97% was achieved in 21 mins ($M_n = 34,000 \text{ gmol}^{-1}$) with good molecular weight control maintained throughout the study ($\bar{D} = 1.11 - 1.28$). Further work by the same group introduced mononuclear iron(III) complexes which were active towards lactide and ϵ -CL polymerisation maintaining good control throughout.^[28] Stolt *et al.* reported iron complexes with simple carboxylic acids giving high molecular weight in the melt ($M_n > 150,000 \text{ gmol}^{-1}$).^[29] Mononuclear ferric alkoxides were applied to the ROP of *rac*-lactide and *L*-lactide in the melt giving 90% conversion after 36 h.^[30] NMR analysis of the PLA microstructure demonstrated an isotactic bias, however a significant degree of intramolecular transesterification was observed.

More recent studies have applied discrete iron (III) chloride complexes bearing tetradentate bisphenolate ligands to lactide polymerisation (**Figure 2.04**).^[2,4,8,31] Duan and co-workers have reported a series of iron salen complexes that are all active for ROP of *rac*-lactide in toluene, **25 – 32**.^[4] The complexes tended to produce moderately isotactic PLA with **25**, bearing a cyclohexyl backbone and *t*-butyl phenolate substituents, being the most isoselective at 60 °C after 24 h ($P_m = 0.78$) at a ratio of $[LA]/[I] = 100 : 1$. As the steric bulk of either the linker, **27 – 32**, or the phenolate groups (**28, 31, 32**) was reduced, the isoselectivity was diminished and

heterotactically-inclined PLA was observed with electron-withdrawing chloride substituents, **31** – **32**. These were also shown to be the most active initiators. Broad dispersities were observed throughout the study and measured molecular weights tended to be lower than expected.

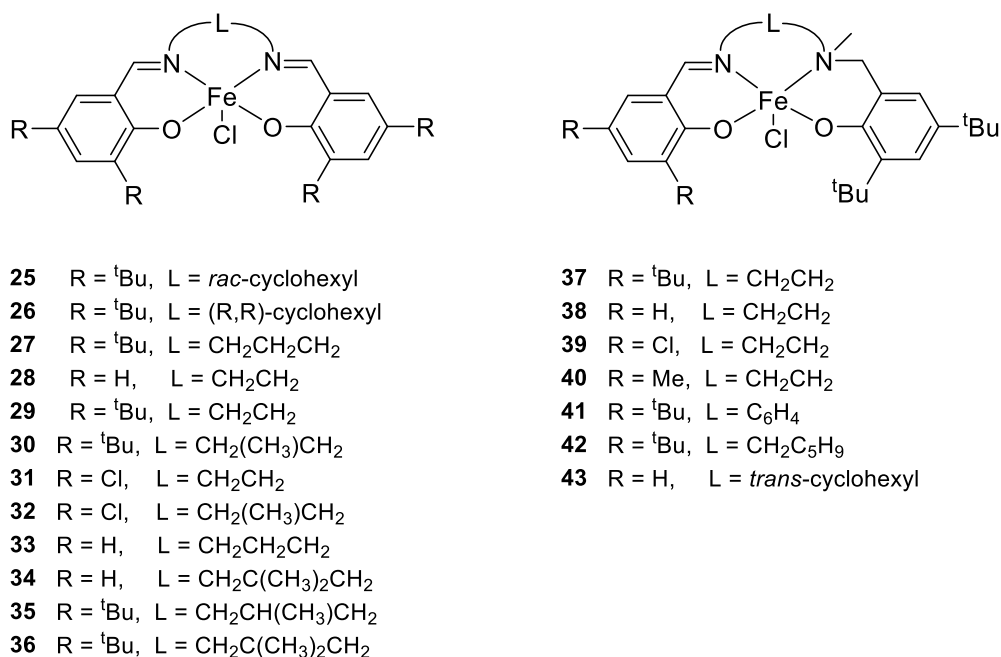
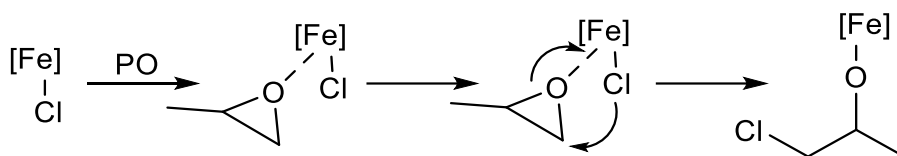


Figure 2.04 Literature examples of salen and salalen ligands that have been applied to lactide ROP with iron (III).^[2,4,8,31]

A publication from the same group tested propylene-backbone salen complexes with various methylation at the central carbon, **33** – **36**.^[2] Although the selectivity was lower than with **25**, these initiators tended to be more active, and **36** gave well-controlled ROP ($\bar{D} = 1.06$). One feature of these studies is the use of propylene oxide (PO) as both a solvent and co-initiator. It is proposed that one molecule of PO is ring-opened and inserts into the Fe – Cl bond, thus generating a classical alkoxide initiating group (**Scheme 2.01**). Through a combination of MALDI-ToF and 2D-NMR spectroscopy, the polymer was shown to have a repeat unit of 144 g mol⁻¹ with the expected chloropropoxide end group. These data indicate a single ring-opening event with PO, followed by ROP of lactide with no polyether being formed.



Scheme 2.01 Generation of alkoxide with PO and an iron (III) chloride complex.

The first examples of iron(III) chloride complexes bearing salan and salalen ligands were published by Lamberti and co-workers who observed no activity towards lactide ROP after four hours.^[8] Our group subsequently reported a series of salalen complexes, **37** – **43**, that were active towards lactide polymerisation in the presence of PO.^[31] Although being less active than the equivalent salen complexes under the same conditions, (**29**: 95% conversion after 12.6 hours, **37**: 72% conversion after 24 hours) the salalen complexes were superior in terms of dispersity ($\mathcal{D} = 1.06 - 1.30$) and isoselectivity ($P_m \leq 0.80$). As expected, reducing the steric bulk and adding electron-withdrawing groups to the phenolate moieties increased the activity at the expense of stereocontrol. Alteration of the backbone reduced both the selectivity and activity of the complexes. For **37**, batch kinetics showed lactide being consumed with a first order dependence after an initiation period, in keeping with the findings of Lamberti.^[8]

Further work investigated the lactide ROP activity of a broad range of salen, salan and salalen iron(III) acetate complexes.^[32] All complexes were active for lactide ROP at 100 °C in toluene with catalytic amounts of BnOH and Et₃N ([LA]/[Fe]/[BnOH]/[Et₃N] = 100 : 1 : 1 : 1). The salalen-acetate complexes were less active and selective than the chloride equivalents taking 24 hours to reach moderate conversion (5 – 60%) and producing atactic PLA. Salen and salan iron acetate complexes tended to be more active achieving 21 – 95% conversion in 24 h and the salen complexes showed some isoselectivity ($P_m = 0.56 - 0.71$). The most active complexes, **44** – **47**, (**Figure 2.05**) were tested at 80 °C for 24 h showing minimal reduction in activity and an improvement in molecular weight control and dispersity ($\mathcal{D}_{100\text{ °C}} = 1.09 - 1.65$, $\mathcal{D}_{80\text{ °C}} = 1.07 - 1.49$).

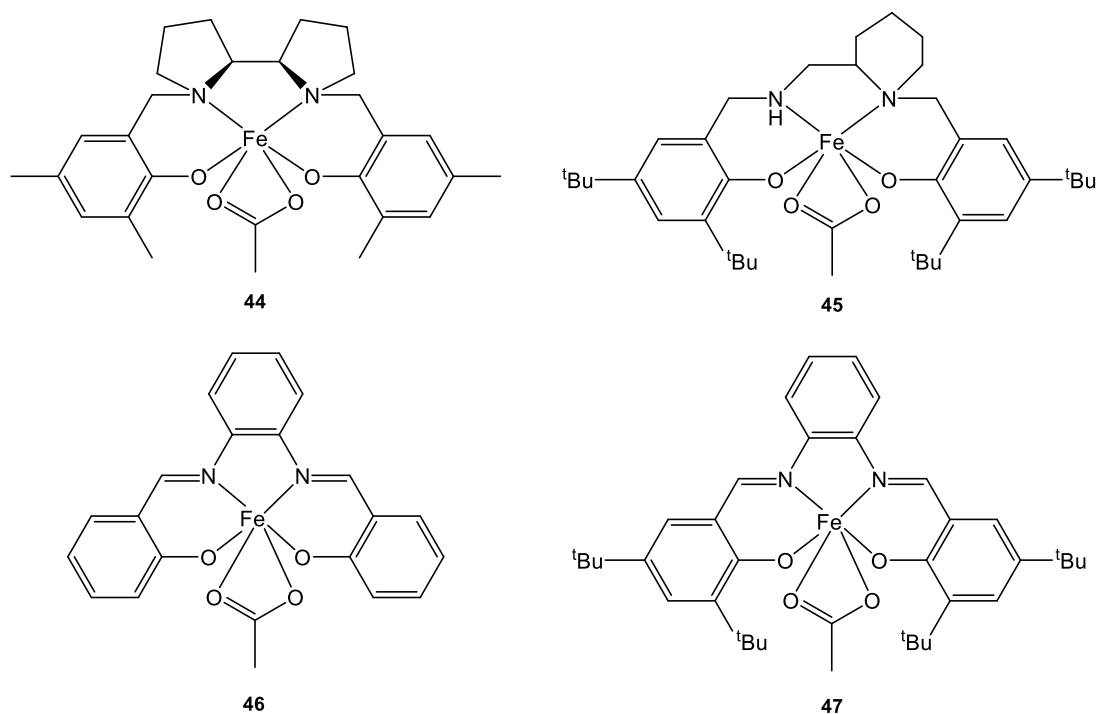
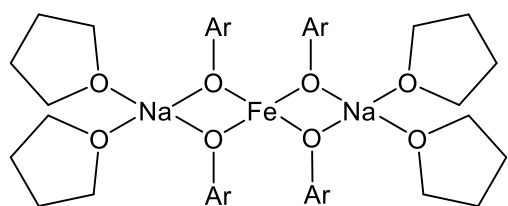


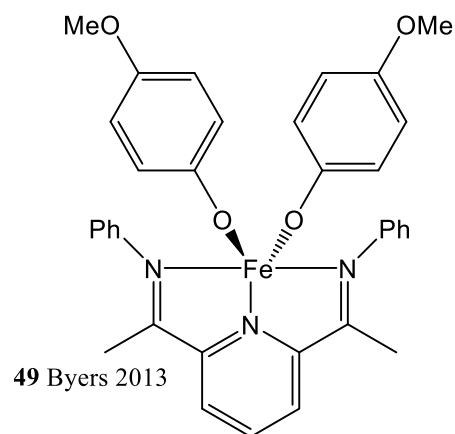
Figure 2.05 Selected literature examples of iron (III) acetate complexes for lactide ROP.^[32]

Iron (II) complexes with varying ligand frameworks have also been reported for the ROP of lactide (**Figure 2.06**). McGuinness *et al.* reported anionic heterobimetallic iron (II) alkoxide complexes that polymerised lactide in a controlled manner achieving high conversion in 60 – 420 min.^[34] Room-temperature polymerisation was achieved by Byers and co-workers using a bis(imino)pyridine iron initiator (**49**), albeit at relatively high initiator loading (50 – 200 : 1).^[35] Further work using this complex demonstrated an ability to switch oxidation state using chemical or electrochemical means and to selectively polymerise a mixture of monomers to make block copolymers.^[35–37] A series of tetradentate iron (II) bis(pyrazolyl)methane complexes with {NNNN} coordination motifs were developed by Herres-Pawlis and co-workers.^[38] The most active complex produced PLA from technical-grade *rac*-lactide with molecular weights up to 30,000 gmol⁻¹ in 30 h at 150 °C. More recent work from the same group introduced a series of three iron (II) guanidine complexes. The most active complex (**30**) was capable of outperforming Sn(Oct)₂ under industrially relevant conditions with technical-grade *rac*-lactide.^[39] Marin *et al.* achieved remarkable stereoselectivity at mild conditions using achiral iron (II) initiators with

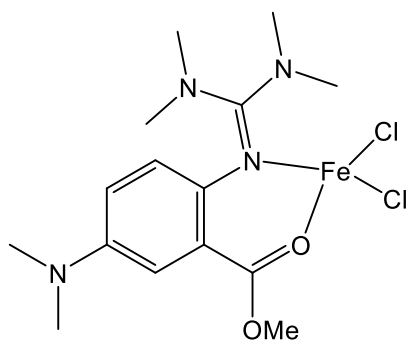
simple, tripodal ligands.^[40] When the temperature was reduced to -10 °C, complex **51** produced isotactic, stereocomplexed PLA from *rac*-lactide with an elevated melting temperature ($P_m = 0.92$, $T_m = 195$ °C).



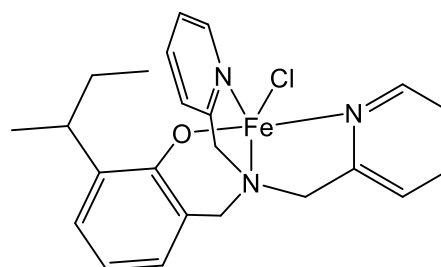
48 Steed, 2003



49 Byers 2013



50 Herres-Pawlis 2019



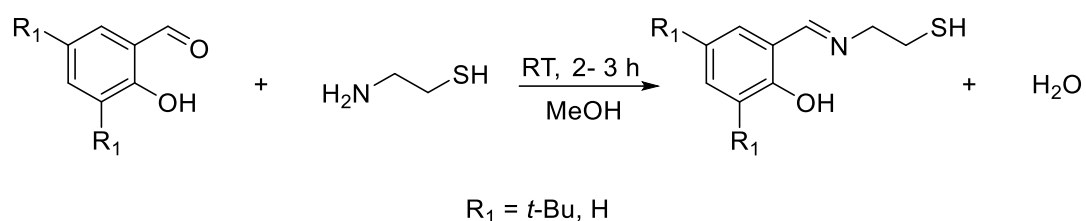
51 Thomas 2019

Figure 2.06 Selected iron(II) initiators for lactide ROP. ^[34,35,39,40]

2.2 Iron (III) thiolen complexes for *rac*-lactide polymerisation

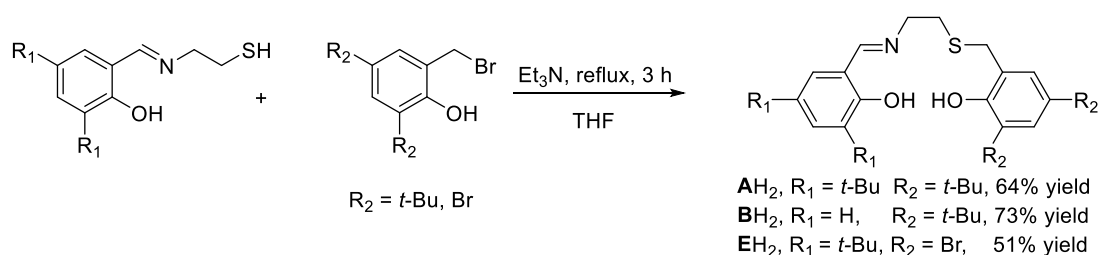
2.2.1 Synthesis and characterisation of thiolen ligands

Thiolen ligands were prepared using a method similar to that employed by Kol and co-workers.^[90] For ligands **AH₂**, **BH₂** and **EH₂**, the relevant salicylaldehyde derivative was initially reacted with one equivalent of cysteamine to give the imine condensation product with a free thiol group (**Scheme 2.02**). The reaction mixture was stirred in methanol until the product precipitated out of solution. After filtration, a pale-yellow solid was collected and used for the next reaction without further purification.



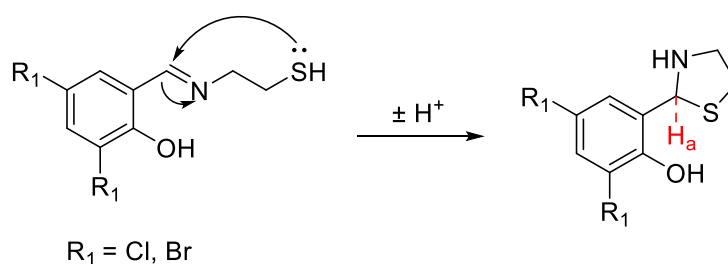
Scheme 2.02: First step of sequential synthesis of thiolen ligands.

The imine condensation product was subsequently dissolved in THF with one equivalent of Et₃N. The relevant benzyl bromide derivative was dissolved in THF and added dropwise to the reaction mixture (**Scheme 2.03**). After reflux for 3 hours, a white precipitate of Et₃N.HBr was observed and removed by filtration. Upon removal of the solvent, a yellow oil remained which could be recrystallised from methanol to give ligands **AH₂**, **BH₂** and **EH₂** as yellow crystalline solids.



Scheme 2.03: Second step of sequential synthesis of thiolen ligands, showing ligand scope.

During the attempted synthesis of ligands (C–D)H₂, following the aforementioned procedure, a deleterious side reaction led to a high proportion of a cyclised side-product during the initial imine condensation step (**Scheme 2.04**). This product was presumably formed via nucleophilic attack of the thiol group on the imine carbon and subsequent proton transfer to form a thiazolidine heterocycle. These products could be identified and quantified through a characteristic ¹H NMR resonance at approximately $\delta = 5.7$ ppm, indicative of the methine proton H_a. This can be seen in the ¹H NMR spectrum of the reaction between cysteamine and 3,5-dichlorosalicylaldehyde which shows a 7 : 1 ratio of undesired side product to the imine target compound (**Figure 2.07**). Although these products were consistently observed as a trace impurity after imine condensation, they only became problematic when halide substituents were present. The trend can be rationalised in terms of the electron withdrawing ability of halides reducing the electron density at the imine carbon making it more susceptible to nucleophilic attack by the thiol group.



Scheme 2.04: Mechanism for the formation of thiazolidine by-product.

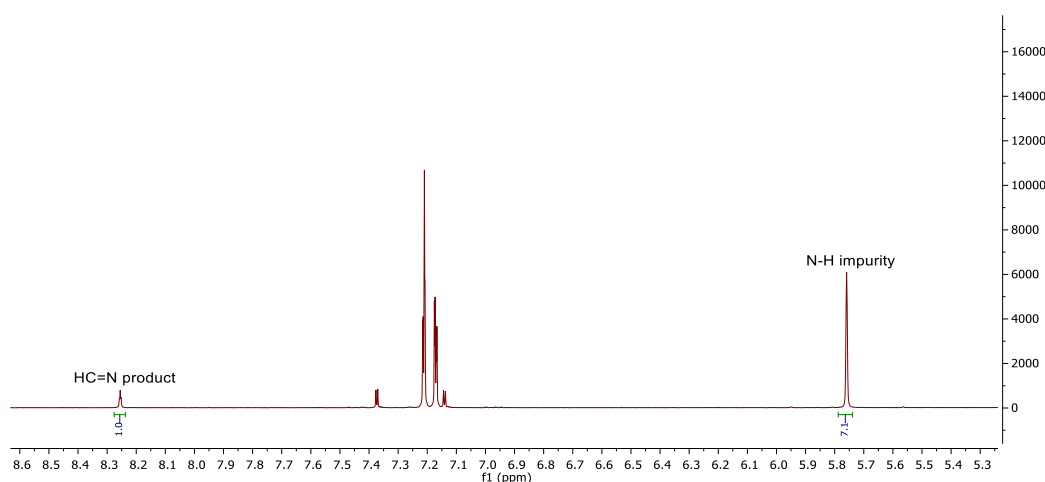
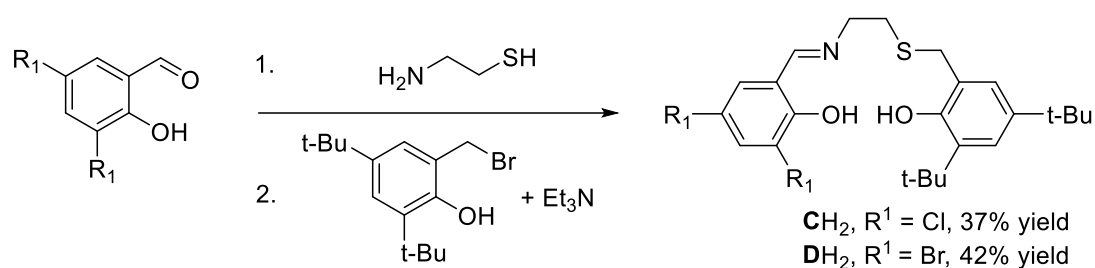


Figure 2.07 ¹H NMR (400 MHz, CDCl₃, 298K) spectrum of the product mixture from the reaction of cysteamine and 3,5-dichlorosalicylaldehyde.

In order to avoid the aforementioned side reaction, a new synthetic protocol was devised with the aim of minimising the time spent during the imine condensation step. To this end, the whole reaction was performed in THF, with no intermediate purification, in a “one-pot” process (**Scheme 2.05**). After stirring the relevant salicylaldehyde derivative with cysteamine for 2 h in THF, 100% yield was assumed, and the process detailed in **Scheme 2.03** was followed. This allowed the synthesis of halogenated thioen derivatives **CH₂** and **DH₂**.



Scheme 2.05: "One-pot" synthesis of halogenated thioen ligands, **CH₂** and **DH₂**. Conditions:
 1. THF, RT, 2 h; 2. THF, 80 °C, 3 h.

Ligands were synthesised in reasonable yields (37% - 73%) and fully characterised through ¹H NMR, ¹³C{¹H} NMR and HR-MS; in all cases a single, pure product was observed after recrystallisation. An example ¹H NMR spectrum is shown in **Figure 2.08** where the identity and purity of ligand **AH₂** can be observed.

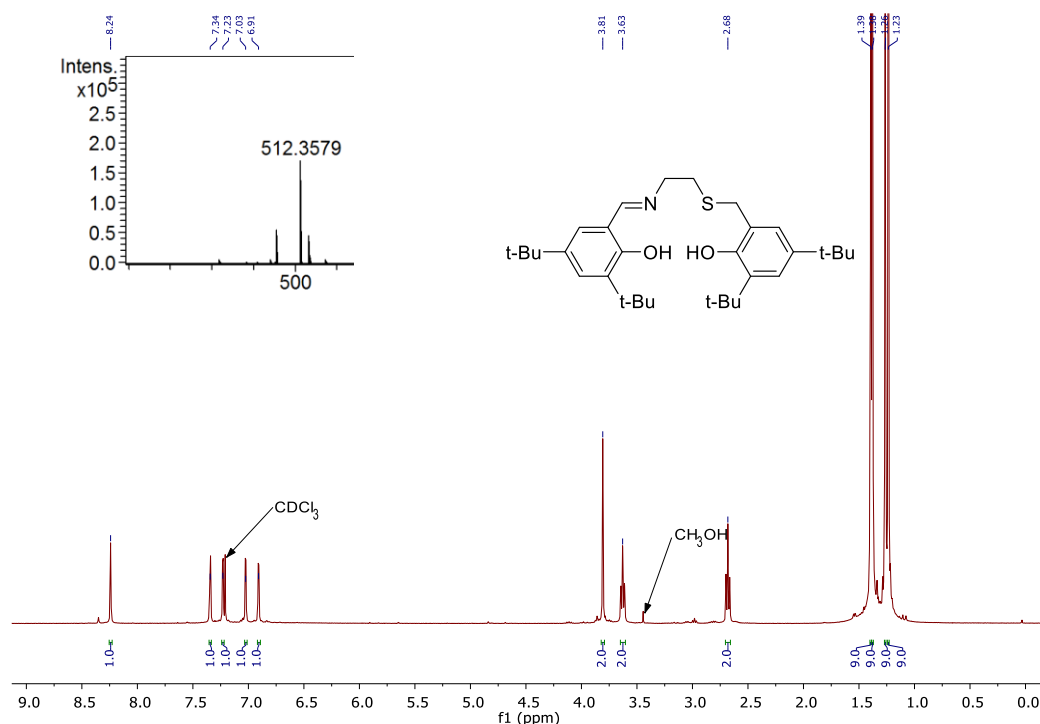


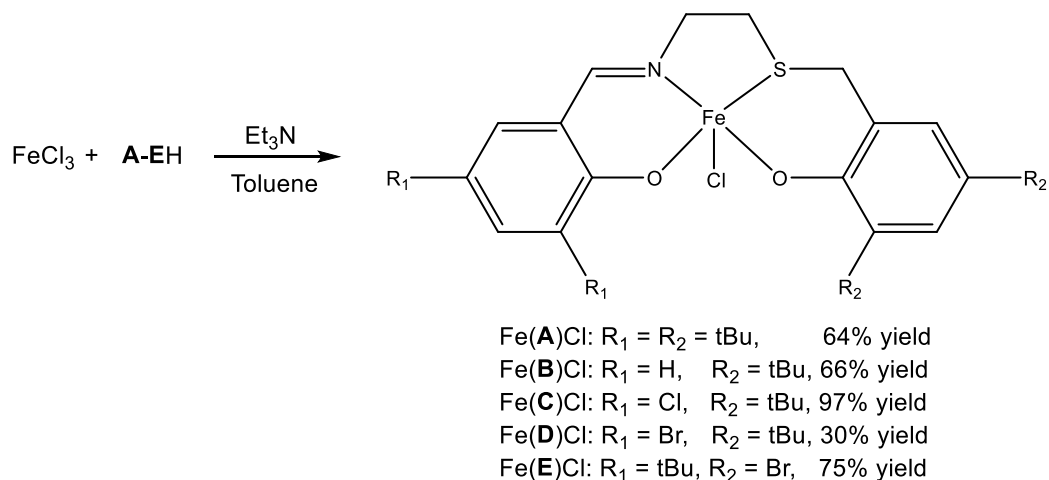
Figure 2.08: ^1H NMR (400 MHz, CDCl_3 , 298K) spectrum of AH_2 . Inset: ESI mass spectrum of AH_2 .

The five thioen ligands that have been detailed comprise a range of steric and electronic profiles designed to allow the study of structure activity relationships. Several comparisons are available, for example: complexes formed from AH_2 ($\text{R}_1 = \text{R}_2 = t\text{-Bu}$) and BH_2 ($\text{R}_1 = \text{H}$, $\text{R}_2 = t\text{-Bu}$) should offer insight into steric effects; CH_2 ($\text{R}_1 = \text{Cl}$, $\text{R}_2 = t\text{-Bu}$) and DH_2 ($\text{R}_1 = \text{Br}$, $\text{R}_2 = t\text{-Bu}$) offers a comparison between halide groups and DH_2 ($\text{R}_1 = \text{Br}$, $\text{R}_2 = t\text{-Bu}$) and EH_2 ($\text{R}_1 = t\text{-Bu}$, $\text{R}_2 = \text{Br}$) is a comparison between the same modification carried out on both sides of the asymmetric ligand framework.

2.2.2 Synthesis and characterisation of iron (III) thioen complexes

Ligands A-EH_2 were complexed to iron (III) chloride in the presence of two equivalents of triethylamine to facilitate the removal of chloride and hence the coordination of the ligands (**Scheme 2.06**). After removal of the $\text{Et}_3\text{N}\cdot\text{HCl}$ precipitate, the product was extracted into hexane which was removed to give $\text{Fe}(\text{A} - \text{E})\text{Cl}$ in moderate to good yields (30% - 97%). The coordination of ligand to metal was supported by HR-MS which in all cases gave the $[\text{Fe}(\text{A} - \text{E})]^+$ ion. Elemental analysis

(CHN) was carried out for all complexes and was consistent with the desired chloride complex in all cases.



Scheme 2.06: Synthesis of Fe(**A–E**)Cl.

A solid-state structure of Fe(**A**)Cl was obtained after recrystallisation from dry hexane and showed the desired iron (III) chloride complex (**Figure 2.09**, **Table 2.01**). The geometric preference for a five-coordinate complex, τ_5 , was calculated from the two largest coordination angles and a preference for trigonal bipyramidal geometry was observed ($\tau_5 = 0.78$).^[91] The axial positions are occupied by O(2) and S(1) and the bond angle (O(2)-Fe(1)-S(1) = 166.82(7)°) differs from the ideal, as would be expected from the geometric preference. The largest equatorial angle is between Fe-O(1) and Fe-N(1) and is very close to the ideal value (120.24(10)°).

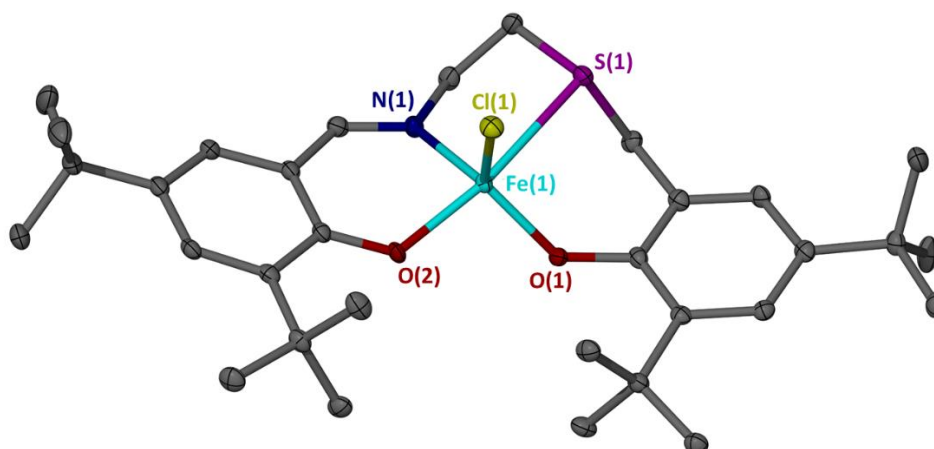


Figure 2.09: Solid state structure of Fe(**A**)Cl. Ellipsoids are shown at the 30% probability level. Hydrogen atoms have been removed for clarity.

In comparison to the analogous salalen complex, the main point of difference is that the Fe–S(1) bond in Fe(A)Cl is considerably longer (2.6220(8) Å) compared to the Fe–N(1) (2.300(2) Å) bond in the respective salalen. The increased flexibility of the Fe–S bond could account for the increased bond length and the increased geometric preference, which is lower with the salalen complex ($\tau_5 = 0.66$).

After complexation of CH₂ to Fe(III) and subsequent recrystallisation from methanol, a dimeric solid-state structure was obtained featuring two bridging methoxy groups (Figure 2.10). Elemental analysis was consistent with the iron chloride species suggesting that the structure was based on an impurity produced by extended exposure to the recrystallisation solvent.

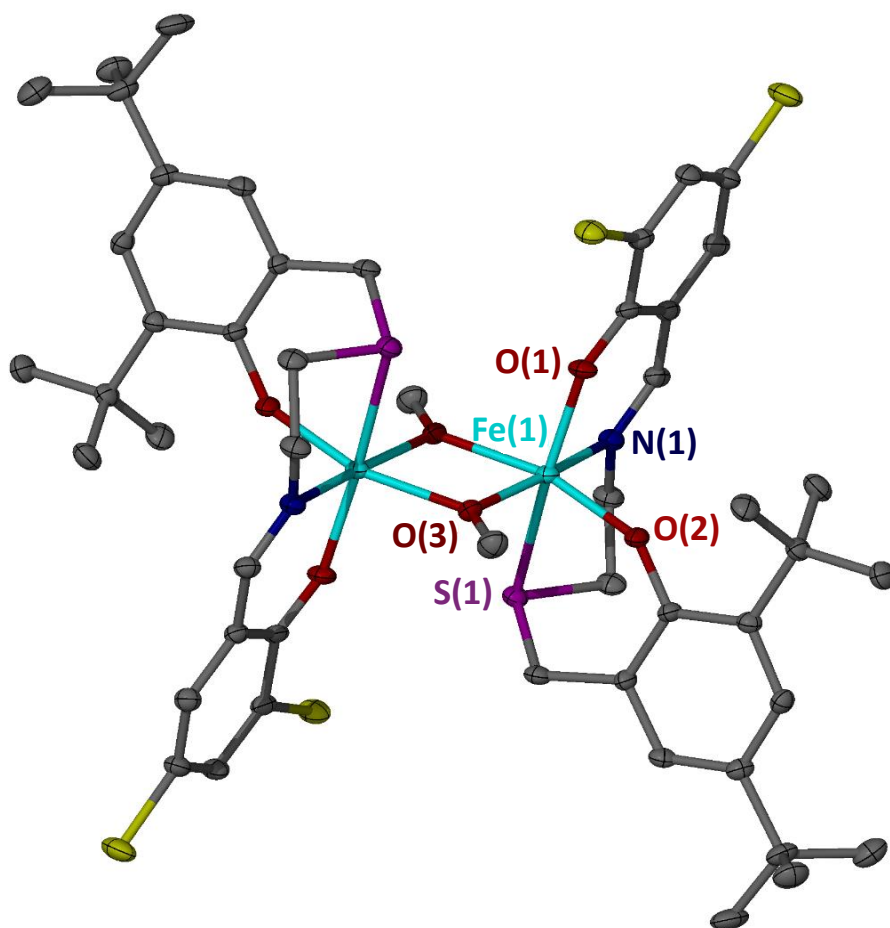
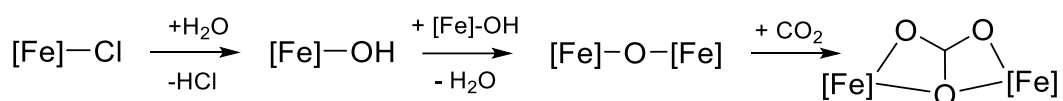


Figure 2.10: Solid state structure of [Fe(C)(μ -OMe)]₂. Ellipsoids are shown at the 30% probability level. Hydrogens have been removed for clarity.

Whilst attempting to recrystallise Fe(A)Cl, structures of two dimeric species were obtained showing a μ -oxo bridged complex [Fe(A)]₂O (**Figure 2.11**) and a carbonato bridge complex [Fe(A)]₂ μ ₂-CO₃ (**Figure 2.12**). The proposed reaction scheme for the formation of [Fe(A)]₂ μ ₂-CO₃ is shown in **Scheme 2.07** wherein H₂O from the atmosphere or recrystallisation solvent displaces the chloride ligand to give Fe(A)OH. This is followed by dehydration to give [Fe(A)]₂O. Subsequent activation of atmospheric CO₂ gives [Fe(A)]₂ μ ₂-CO₃ which represents rare solid-state evidence of CO₂ insertion into an M-O-M bond within a salen type complex. This is comparable to the iron (III) carbonato complexes reported by Hoffman *et al.*^[42]



Scheme 2.07: Proposed reaction scheme for the production of [Fe(A)]₂ μ ₂-CO₃.

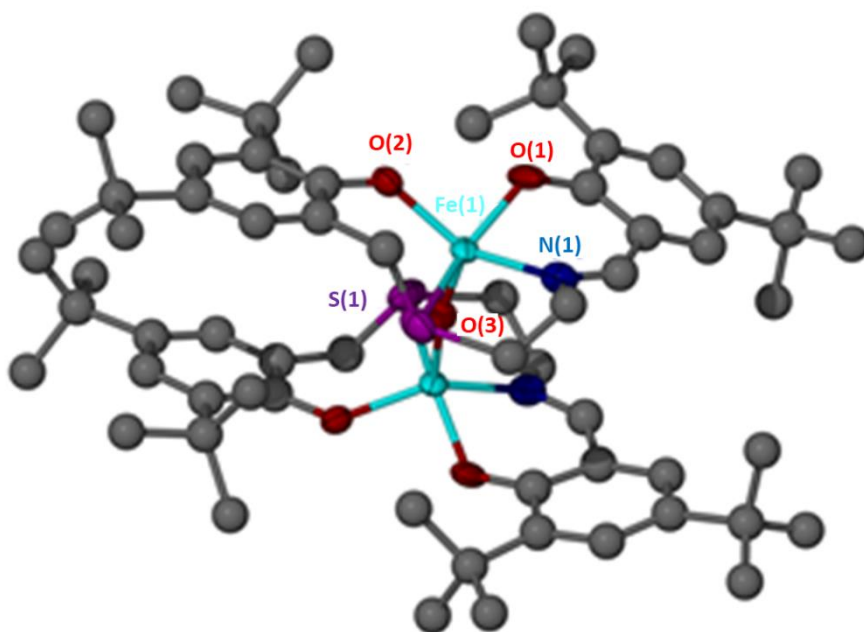


Figure 2.11: Solid state structure of [Fe(A)]₂O. The data quality is poor and therefore the central atoms only are shown as ellipsoids at the 30% probability level. Despite the poor-quality data, the coordination motif around Fe(III) is unambiguous.

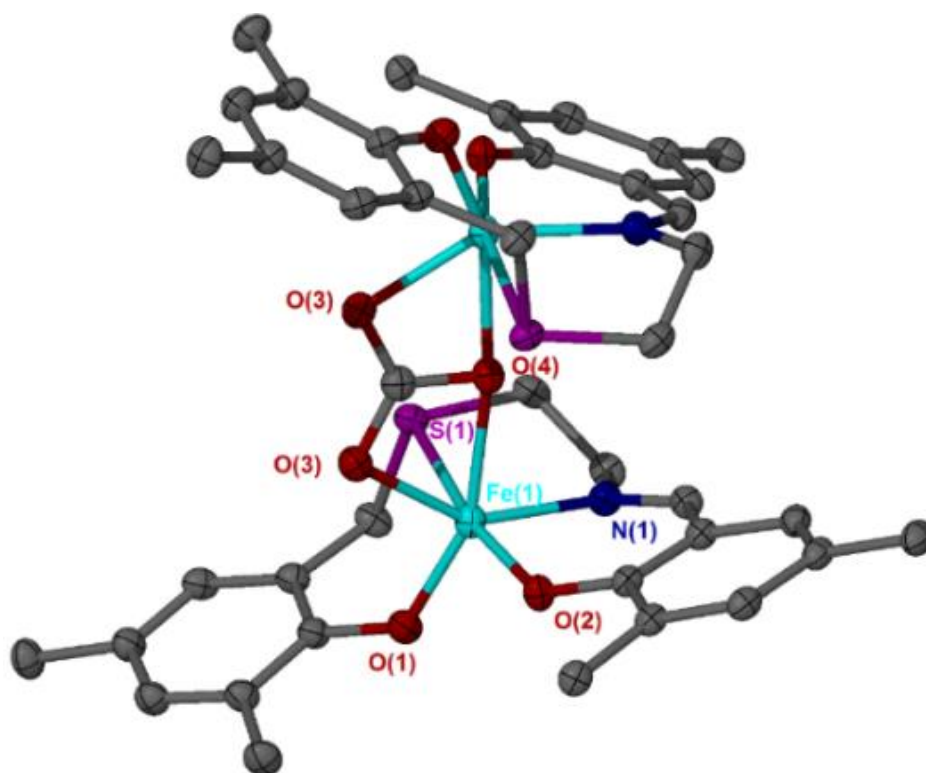


Figure 2.12: Solid state structure of $[\text{Fe}(\mathbf{A})_2\mu_2\text{-CO}_3]$. Ellipsoids are shown at the 30% probability level. Hydrogen atoms and t-Bu carbon atoms have been removed for clarity.

Table 2.01: Selected bond lengths (\AA) and angles ($^\circ$) for $\text{Fe}(\mathbf{A})\text{Cl}$, $[\text{Fe}(\mathbf{A})_2\mu_2\text{-CO}_3]$ and $[\text{Fe}(\mathbf{C})(\mu\text{-OMe})_2]$.

	$\text{Fe}(\mathbf{A})\text{Cl}$	$[\text{Fe}(\mathbf{A})_2\mu_2\text{-CO}_3]$	$[\text{Fe}(\mathbf{C})(\mu\text{-OMe})_2]$
τ_5	0.77	-	-
Fe–O(1)	1.851(2)	1.881(2)	1.9387(15)
Fe–O(2)	1.9065(18)	1.8908(18)	1.8741(15)
Fe–N(1)	2.065(3)	1.094(2)	2.184(2)
Fe–S(1)	2.6220(8)	2.5907(7)	2.5803(6)
Fe–Cl(1)	2.2367(9)	-	-
O(1)–Fe–O(2)	99.12(9)	97.55(8)	98.88(7)
O(2)–Fe–S(1)	166.82(7)	168.10(6)	85.19(5)
O(1)–Fe–Cl(1)	120.36	-	-

2.2.3 *Rac*-lactide polymerisation with Fe(A)Cl

When applying metal chloride initiators to lactide polymerisation, PO is commonly used as a solvent and co-initiator which undergoes a single ring opening event to form an alkoxide initiating group.^[88,92–94] Initiator Fe(A)Cl was initially tested using this system with 2 mL of purified PO and a ratio of [LA]/[I] = 100 : 1 (**Table 2.02**). A reasonable conversion was obtained after 24 h which is comparable to the correspondingly substituted salalen complex^[92] but slower than the respective salen.^[94] However, the resulting polymer was more isotactic than the previously reported analogues ($P_m = 0.81$). After 6 h, no conversion of lactide was observed, which is consistent with an initiation period as previously observed.^[88,92] Lowering the temperature to 60 °C improved the isotactic bias ($P_m = 0.85$) and reduced the conversion to 51%; these results were not improved at 40 °C even after a 240 h reaction time.

Table 2.02: ROP of *rac*-lactide with Fe(A)Cl in PO.

Entry	Init.	T/ °C	Time /hours	Conv. % ^a	P_m ^b	M_n Calc. ^c	M_n ^d	\bar{D} ^d
1	Fe(A)Cl	80	24	76	0.81	11050	15550	1.31
2	Fe(A)Cl	80	6	0	-	-	-	-
3	Fe(A)Cl	60	72	51	0.85	7450	17100	1.27
4	Fe(A)Cl	40	240	50	0.85	7300	21100	1.19

Conditions: *rac*-LA (0.4 g), [LA]/[Fe] = 100 : 1 in PO (2 mL); ^a Determined by ¹H NMR spectroscopy; ^b Probability of isotactic enchainment, determined by ¹H{¹H} NMR spectroscopy; ^c Theoretical molecular weight calculated from conversion (rounded to the nearest 50): {[LA]/[I] × (Conversion × 144.13) / BnOH equiv. + M_n (BnOH)}; ^d Determined from GPC (in THF) referenced against polystyrene standards, × 0.58.

GPC analysis of the PLA samples from PO initiation showed relatively broad dispersities with some bimodality. This is likely a result of diol impurities that were present in the solvent, as has previously been reported.^[31] The molecular weights are also higher than would be expected from the conversion values. The elevated molecular weights imply that there is, on average, less than one polymer chain per

metal centre. This can be linked to incomplete conversion of the complex to the active alkoxide species, resulting in fewer active centres.

As a result of the lack of control observed in PO, it was decided to perform subsequent reactions in toluene (**Table 2.03**). To generate the alkoxide initiating group, one equivalent of Et₃N was added to remove the chloride along with BnOH to form the active benzoxy complex ([LA]/[I]/[BnOH]/[Et₃N] = 100: 1 : 1 : 1). As a comparison to the PO system, an initial experiment with Fe(**A**)Cl was carried out for 24 h at 80 °C (**Table 2.03**, entry 1). Some improvement in molecular weight control was observed ($\bar{D} = 1.15$) along with a significant increase in conversion. When the reaction time was reduced to four hours, reasonable conversion was attained and a significant increase in control was observed in terms of dispersity (**Figure 2.13**, $\bar{D} = 1.04$) and molecular weight control ($M_{n, \text{Calc.}} = 11,500 \text{ gmol}^{-1}$, $M_{n, \text{GPC}} = 10,500 \text{ gmol}^{-1}$). This suggests that over a 24 h reaction time there was some decomposition of the polymer taking place. To test the necessity of Et₃N addition, an experiment was carried out in its absence ([LA]/[Fe]/[BnOH] = 100:1:1), 80% conversion was achieved after 3 hours at 80 °C but P_m was reduced 0.76 from 0.79 with Et₃N, suggesting that Et₃N promotes a more controlled coordination-insertion mechanism.

Table 2.03: ROP of *rac*-lactide with Fe(**A**)Cl in toluene.

Entry	Init.	T/°C	Time /hours	Conv. /% ^a	P_m^b	M_n Calc. ^c	M_n^d	\bar{D}^d	T_m /°C
1	Fe(A)Cl	80	24	96	0.79	13950	9400	1.15	- ^f
2	Fe(A)Cl	80	4	79	0.79	11500	10500	1.04	170
3	Fe(A)Cl	50	48	95	0.84	13800	13500	1.04	174
4	Fe(A)Cl	40	96	96	0.85	13950	11350	1.51	177
5	Fe(A)Cl	40	48	82	0.84	11900	14300	1.44	174
6	Fe(A)Cl ^e	40	48	88	0.89	12800	16500	1.19	181

Conditions: *rac*-LA (0.4 g), [LA]/[Fe]/[BnOH]/[Et₃N] = 100 : 1 : 1 : 1 unless otherwise stated; ^a Determined by ¹H NMR spectroscopy; ^b Probability of isotactic enchainment, determined by ¹H{¹H} NMR spectroscopy; ^c Theoretical molecular weight calculated from conversion (rounded to the nearest 50): $\{[LA]/[I] \times (\text{Conversion} \times 144.13) / \text{BnOH equiv.}\} + M_n(\text{BnOH})$; ^d Determined from GPC (in THF) referenced against polystyrene standards, x 0.58; ^e stirred at 80 °C for 4 hours prior to addition of *rac*-LA. ^f Not determined.

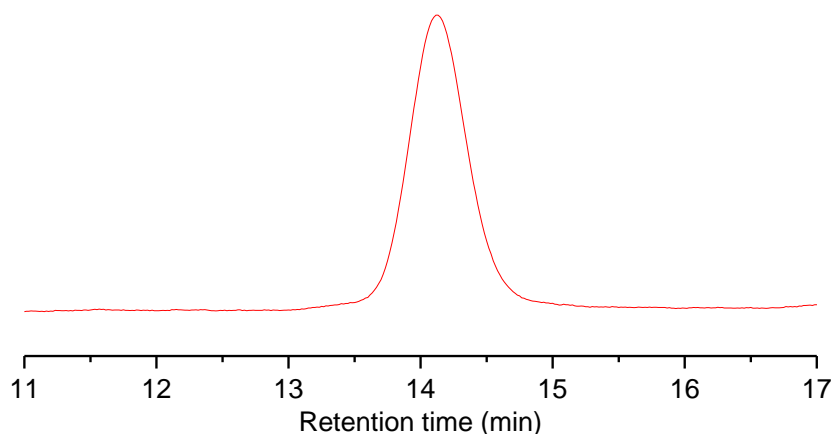


Figure 2.13: GPC trace of PLA initiated by Fe(A)Cl (80 °C, 4 hours) at a ratio of 100 : 1 : 1 : 1 ([LA]/[I]/[BnOH]/[Et₃N]) in toluene. $M_{n, \text{GPC, corr.}} = 9,850 \text{ gmol}^{-1}$, $\bar{D} = 1.06$, $M_{n, \text{theo.}} = 11,750 \text{ gmol}^{-1}$.

MALDI-ToF analysis of the polymer (**Figure 2.14**) showed a symmetrical distribution with the expected BnO- + H- end groups and a repeat unit of 144 gmol^{-1} . This supports the GPC data and shows that there is no undesired transesterification taking place. At 50 °C, the polymerisation control was maintained and an increase in the isotactic bias was observed ($P_m = 0.84$). When the reaction was carried out at 40 °C for 96 hours, a further increase in selectivity was observed ($P_m = 0.85$). However, the GPC trace was bimodal and showed a broad dispersity ($\bar{D} = 1.51$).

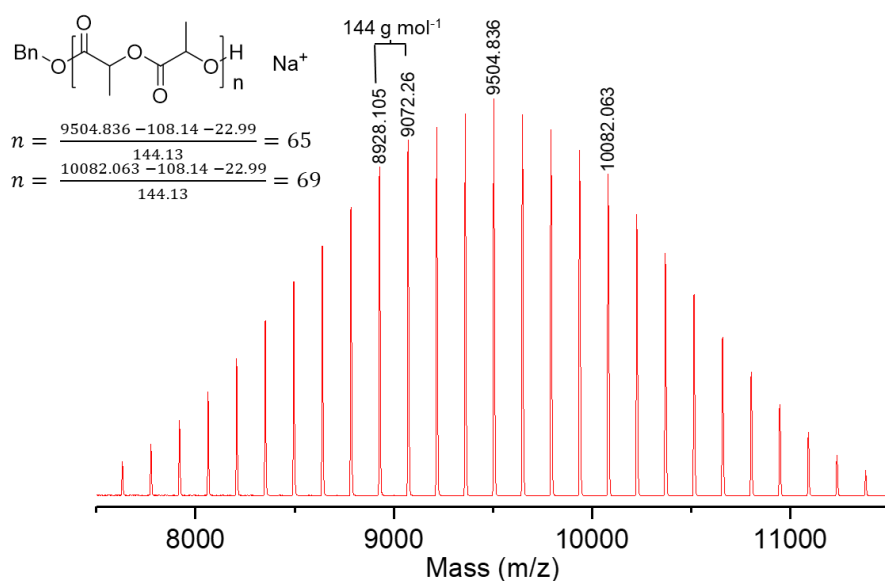
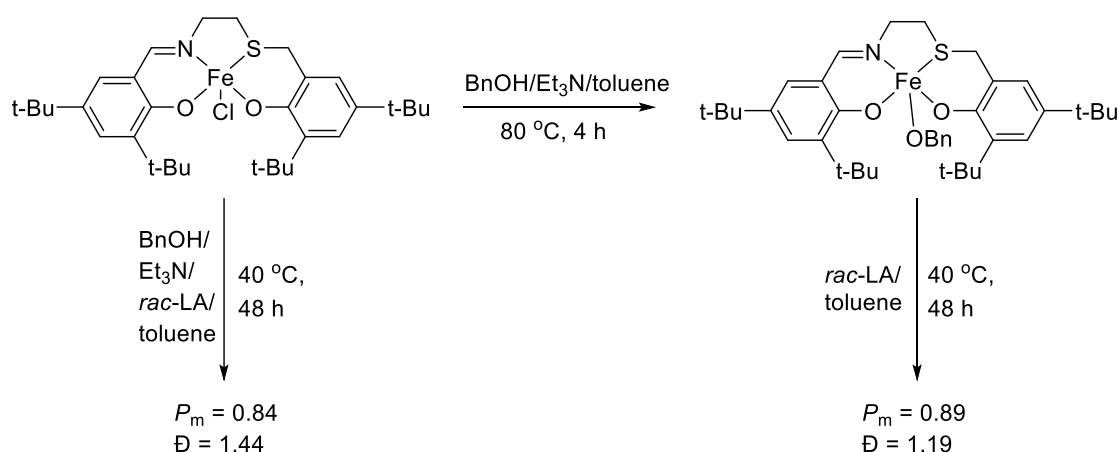


Figure 2.14: MALDI – ToF spectrum of PLA derived from Fe(A)Cl (80 °C, 4 hours) at a ratio of 100 : 1 : 1 : 1 ([LA]/[I]/[BnOH]/[Et₃N]) in toluene. $M_{n, \text{(GPC, corr.)}} = 9850 \text{ gmol}^{-1}$, $M_{n, \text{(Theo.)}} = 11750 \text{ gmol}^{-1}$. Linear polymer with BnO + H end groups.

To ascertain the origin of the bimodality observed at low temperature, the reaction time was shortened to 48 h. The dispersity narrowed slightly ($\mathcal{D} = 1.44$) but not enough to explain the bimodality through polymer degradation at extended reaction times. Another explanation could be a different mechanism, such as activated-monomer, competing at low temperatures with a typical coordination-insertion pathway, as has been previously reported with binuclear magnesium and zinc alkoxides.^[58] At 40 °C, it is suggested that the chloride is not fully displaced, allowing activated monomer to compete with coordination insertion and thus producing a bimodal GPC trace with a broad dispersity. To test this, the reaction mixture was “preactivated” at 80 °C for 4 h before the addition of lactide (**Scheme 2.08**). Based on previous results, this was deemed sufficient to form the alkoxide complex required for coordination insertion.



Scheme 2.08: Pre-activation experiment with Fe(A)Cl.

This experiment resulted in a significant narrowing of the dispersity ($\mathcal{D} = 1.19$) alongside improved isoselectivity (**Figure 2.15**, $P_m = 0.89$). This is consistent with a suppression of activated monomer in favour of coordination-insertion. From the deconvoluted GPC traces, with and without preactivation (**Figure 2.16**), there are two contributing peaks for each trace. The peak at lower molecular weight is significantly reduced after preactivation suggesting that it represents the polymer formed through activated monomer reactivity. This is corroborated by MALDI-ToF analysis of

the non-preactivated polymer which shows a low molecular weight series ($M_p = 5032 \text{ g mol}^{-1}$), which would be more readily ionised than the high M_n fraction and corresponds to the low M_n GPC signal.

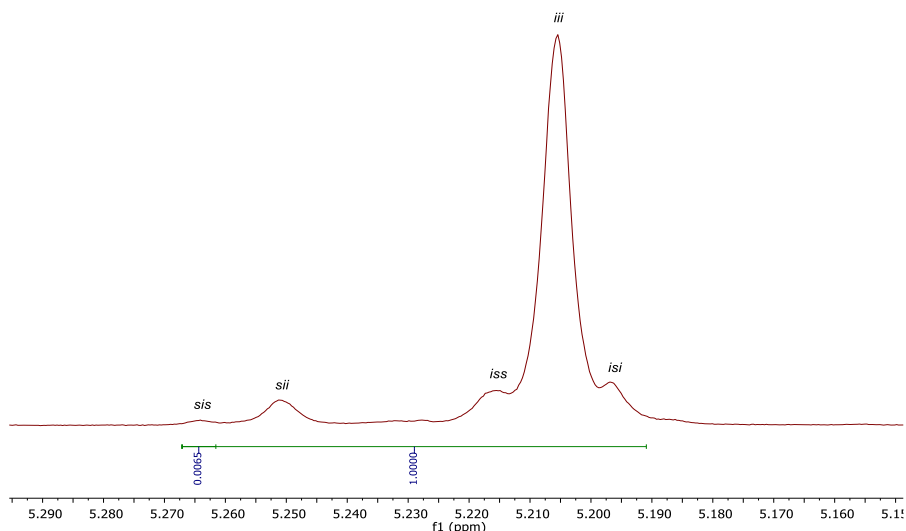


Figure 2.15: $^1\text{H}\{^1\text{H}\}$ NMR spectrum of isotactically enriched PLA from $\text{Fe}(\text{A})\text{Cl}$. $P_m = 0.89$.

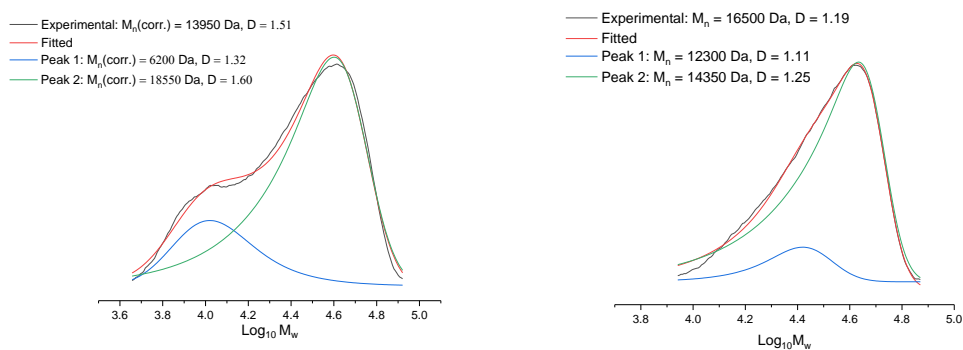


Figure 2.16: Deconvoluted GPC trace of PLA initiated by $\text{Fe}(\text{A})\text{Cl}$ ($40 \text{ }^\circ\text{C}$, 96 hours) at a ratio of 100 : 1 : 1 : 1 ($[\text{LA}]/[\text{I}]/[\text{BnOH}]/[\text{Et}_3\text{N}]$) in toluene (left) and GPC trace of PLA initiated by $\text{Fe}(\text{A})\text{Cl}$ with pre-activation ($80 \text{ }^\circ\text{C}$, 4 hours) prior to addition of lactide.

2.2.4 Isotactic PLA characterisation

Further characterisation was carried out for samples of the most isotactic polymers to assess their crystallinity and thermal properties. Two PLA samples were analysed using $^{13}\text{C}\{^1\text{H}\}$ NMR wherein a very small *sis* tetrad was observed, thus supporting the isotacticity implied by $^1\text{H}\{^1\text{H}\}$ NMR. pXRD analysis (**Figure 2.17**) of a polymer sample (**Table 2.03**, entry 4) displayed sharp peaks, indicating a degree of crystallinity. The lack of peaks above $2\theta = 40^\circ$, indicates a lack of long-range order, as would be expected of a semi-crystalline polymer.

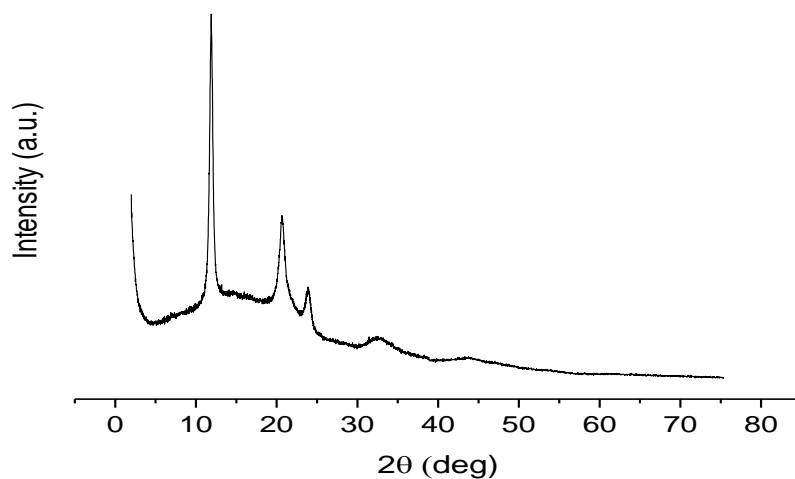


Figure 2.17: pXRD pattern for **Table 2.03**, entry 4. $P_m = 0.85$.

The same sample was subject to TGA (**Figure 2.18**) and a decomposition profile was obtained with degradation onset at 215 °C and full decomposition at 308 °C. These data are consistent with values reported by Marin and co-workers for isotactic stereocomplex PLA.^[40] The decomposition profile was also used to set the maximum temperature for DSC to avoid decomposition during the first heating cycle.

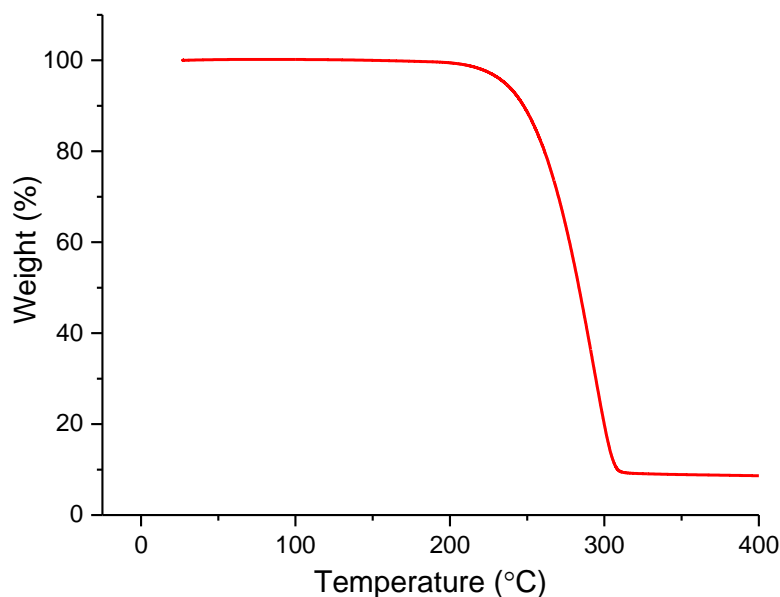


Figure 2.18: TGA degradation curve for **Table 2.03**, entry 4. M_n (GPC, corr.) = 11350, P_m = 0.85.

Six of the most isotactic polymer samples were analysed through DSC to find melting temperatures and other thermal properties (**Table 2.04**, **Figure 2.19**). Well-defined melting temperatures were obtained for all six polymer samples, with the highest (T_m = 181 °C) corresponding to the most isotactic polymer as measured by $^1\text{H}\{^1\text{H}\}$ NMR (P_m = 0.89). This is good evidence of a stereocomplexed polymer, and this conclusion is supported by the other samples' melting temperature increasing with isotacticity. The exception to this is the polymer initiated with PO (**Table 2.02** entry 1), which has a significantly lower melting temperature than would be expected (P_m = 0.81, T_m = 154 °C). The enthalpies of melting (ΔH_m) for PLA samples ranged from 3 – 45 J g⁻¹ and consistently increased with P_m and T_m . The polymer samples had melting enthalpies lower than that of PLLA/PDLA blends reported by Chen *et al.* (ΔH_m = 50 – 70 J g⁻¹),^[44] but greater than that of amorphous PLA.^[45] The glass transition temperatures were less consistent but broadly followed the same trend, giving values between 52 °C and 65 °C.

Table 2.04: T_m , T_g and ΔH_m values from selected polymer samples. Taken from DSC 2nd heating cycle.

Reference	P_m	$T_g/^\circ\text{C}$	$T_m/^\circ\text{C}$	$\Delta H_m/\text{J g}^{-1}$
Table 2.03, entry 1	0.79	55	170	3
Table 2.02, entry 2	0.81	52	154	13
Table 2.03, entry 3	0.84	65	174	29
Table 2.03, entry 4	0.85	61	177	39
Table 2.03, entry 5	0.84	65	174	25
Table 2.03, entry 6	0.89	62	181	45

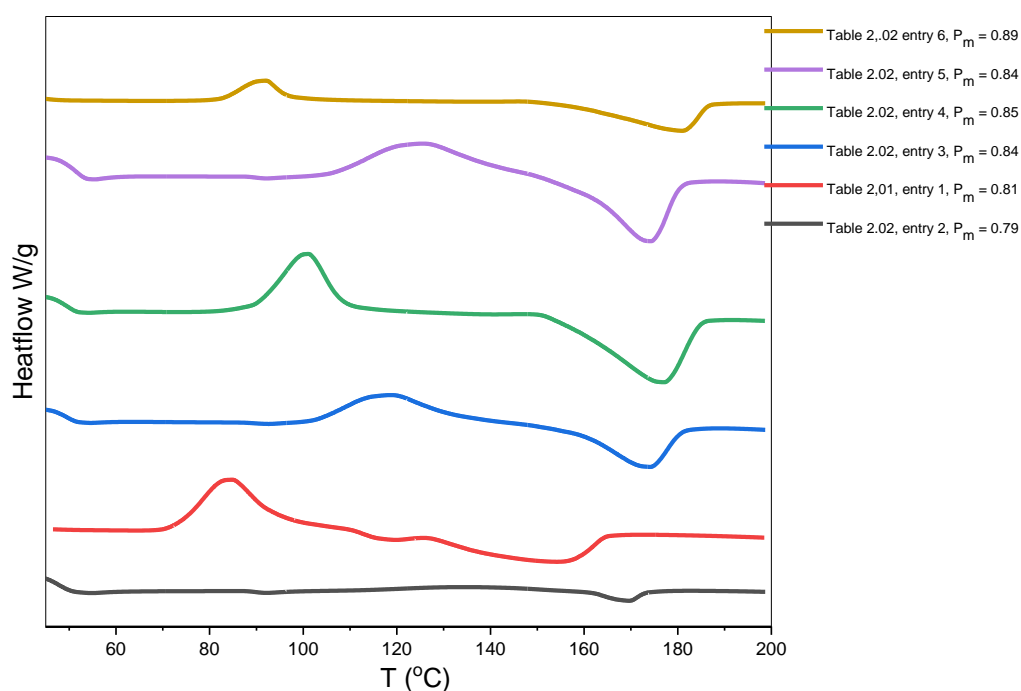


Figure 2.19: DSC analysis of selected polymers.

2.2.5 *Rac*-lactide polymerisation with Fe(**B-E**)Cl

Complex Fe(**B**)Cl ($R_1 = \text{H}$, $R_2 = t\text{-Bu}$) was synthesised to provide a less sterically hindered analogue to Fe(**A**)Cl (**Scheme 2.06**). This resulted in an initiator that was more active, giving high conversion after 2 h (**Table 2.05**, entry 1). However, the stereocontrol was significantly reduced and the resulting polymer was close to atactic ($P_m = 0.57$). The activity could be increased further by adding electron-withdrawing halide substituents to the phenolate groups (Fe(**C**)Cl: $R_1 = \text{Cl}$, $R_2 = t\text{-Bu}$; Fe(**24**)Cl: $R_1 = \text{Br}$, $R_2 = t\text{-Bu}$). Fe(**C**)Cl gave high conversion after 1 h with a moderate

isotactic bias ($P_m = 0.61$) whereas Fe(**D**)Cl unexpectedly achieved an even higher conversion after 0.5 h. For initiators Fe(**A** – **D**)Cl, the stereoselectivity increased with steric bulk ($R_1 = H < Cl < Br < t\text{-Bu}$), whereas the most dramatic increase in activity comes from an electronic effect. The polymerisations carried out with Fe(**B**–**D**)Cl were well-controlled with narrow dispersities maintained throughout ($\mathcal{D} = 1.04 - 1.11$) although the molecular weights were consistently below the theoretical values, suggesting greater than one chain per metal centre or significant chain transfer events. MALDI – ToF analysis of the PLA produced from Fe(**B**–**D**)Cl all showed symmetrical distributions with no evidence of tails or bimodality, in keeping with the narrow dispersities measured by GPC. Furthermore, only one series can be observed with a repeat unit of 144 g mol^{-1} throughout, indicating a lack of transesterification or other side-reactions. The expected BnO- + H- end groups were observed throughout.

Table 2.05: ROP of *rac*-lactide with Fe(**B**–**E**)Cl.

Entry	Init.	T/°C	Time /hours	Conv. % ^a	P_m ^b	M_n Calc. ^c	M_n ^d	\mathcal{D} ^d
1	Fe(B)Cl	80	2	88	0.57	12800	9500	1.11
2	Fe(C)Cl	80	1	79	0.61	11500	7600	1.04
3	Fe(D)Cl	80	0.5	93	0.62	13500	5750	1.08
4	Fe(E)Cl	80	3	83	0.71	12050	7950	1.04

Conditions: *rac*-LA (0.4 g), [LA]/[Fe]/[BnOH]/[Et₃N] = 100 : 1 : 1 : 1 unless otherwise stated; ^a Determined by ¹H NMR spectroscopy; ^b Probability of isotactic enchainment, determined by ¹H{¹H} NMR spectroscopy; ^c Theoretical molecular weight calculated from conversion (rounded to the nearest 50): $\{[LA]/[I] \times (\text{Conversion} \times 144.13) / \text{BnOH equiv.}\} + M_n(\text{BnOH})$; ^d Determined from GPC (in THF) referenced against polystyrene standards, $\times 0.58$.

Due to the asymmetric nature of the ligand, the effect of altering the imino-phenolate and thio-phenolate substituents was investigated through the synthesis of the isomeric pair Fe(**D**)Cl ($R_1 = Br, R_2 = t\text{-Bu}$) and Fe(**E**)Cl ($R_1 = t\text{-Bu}, R_2 = Br$). Fe(**E**)Cl was less active towards lactide ROP taking 3 h to achieve high conversion. However, Fe(**E**)Cl did produce a slightly more controlled polymer with a narrower dispersity

(Fe(**D**)Cl: $\bar{D} = 1.08$, Fe(**E**)Cl: $\bar{D} = 1.04$) and a closer agreement between measured and theoretical molecular weights. Stereocontrol was also increased when altering the thio-phenolate (Fe(**E**)Cl: $P_m = 0.71$) rather than the imino phenolate (Fe(**D**)Cl: $P_m = 0.62$). The lack of control associated with Fe(**D**)Cl could be somewhat explained by polymer degradation at high conversion. When compared with the tetrakis-*tert*-butyl initiator Fe(**A**)Cl, altering either of the phenolate groups results in a significant drop in isoselectivity, most prominent with the imino phenolate modification. The activity also significantly increased with this change, whereas halogenating the thio-phenolate moiety had a minimal effect on lactide conversion. The molecular weight control for both was reduced compared to Fe(**A**)Cl suggesting that sterics are the main driver for control and selectivity.

2.2.6 Polymerisation kinetics with Fe(**A** – **E**)Cl

Batch kinetics were carried out for initiators Fe(**A,B,C,E**)Cl (**Figure 2.20, Table 2.06**). As a result of the rapid conversion achieved with Fe(**D**)Cl, it was deemed too active to produce comparable kinetics. The fitted lines intercept close to zero, suggesting that there is no induction period with the toluene system, unlike with PO as the solvent. Lactide is consumed with a first order dependence in all cases. Fe(**C**)Cl gave the highest rate ($k_{app} = 0.025 \text{ min}^{-1}$, $R^2 = 0.97$) as may be expected from the incorporation of electron-withdrawing phenolate substituents. This also explains the high activity of Fe(**D**)Cl. The reduced steric bulk of Fe(**B**)Cl resulted in the second highest rate ($k_{app} = 0.017 \text{ min}^{-1}$, $R^2 = 0.99$). The observed rate constant for Fe(**A**)Cl ($k_{app} = 0.009 \text{ min}^{-1}$, $R^2 = 0.97$) is higher than that of the analogous salalen complex^[31] and is approximately the same as with Fe(**E**)Cl, supporting the observation that altering the thio-phenolate has little effect on activity.

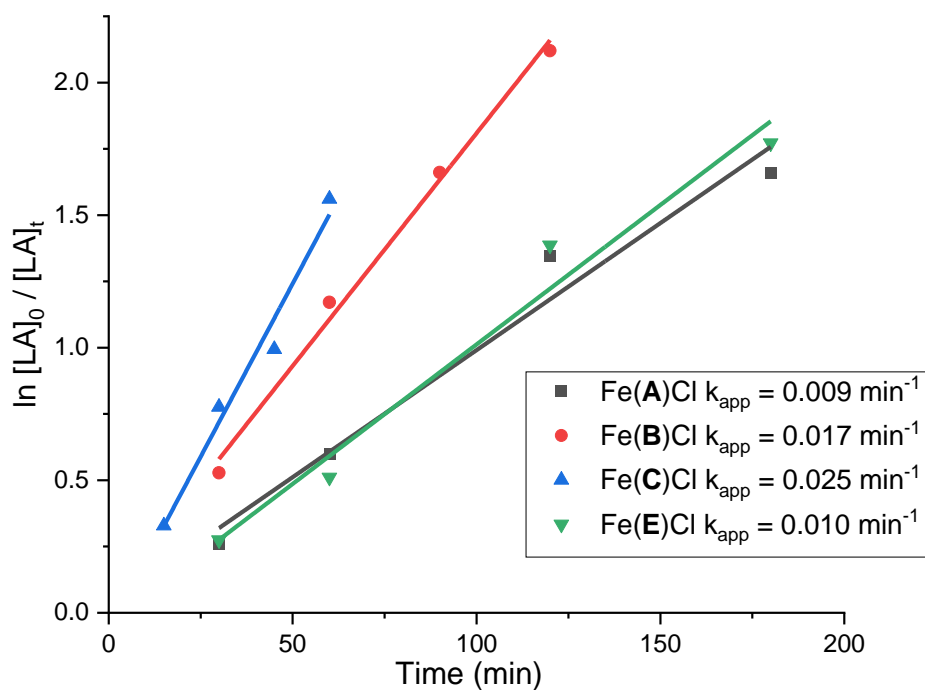


Figure 2.20: Semi-logarithmic plot of ROP of rac-LA with Fe(A,B,C,E)Cl.

Table 2.06: Kinetic data for Fe(A,B,C,E)Cl.

	Fe(A)Cl	Fe(B)Cl	Fe(C)Cl	Fe(E)Cl
Intercept	0.031	0.053	-0.063	-0.030
Slope / min^{-1}	0.0093	0.016	0.025	0.010
R-Square (COD)	0.97	0.99	0.97	0.97

The molecular weight vs. conversion plot shown in **Figure 2.21** shows a linear relationship between the two variables, good evidence of controlled polymerisation. The plot also shows that a narrow dispersity is maintained across all time points and that P_m is consistent after the first point. A trendline gradient around the molecular weight of lactide ($144.13 \text{ g mol}^{-1}$) would indicate one polymer chain growing per metal centre whereas a gradient closer to 72 would indicate two polymer chains. In this case, the gradient of the trendline is around 105, which suggests an average of 1.5 chains per metal centre.

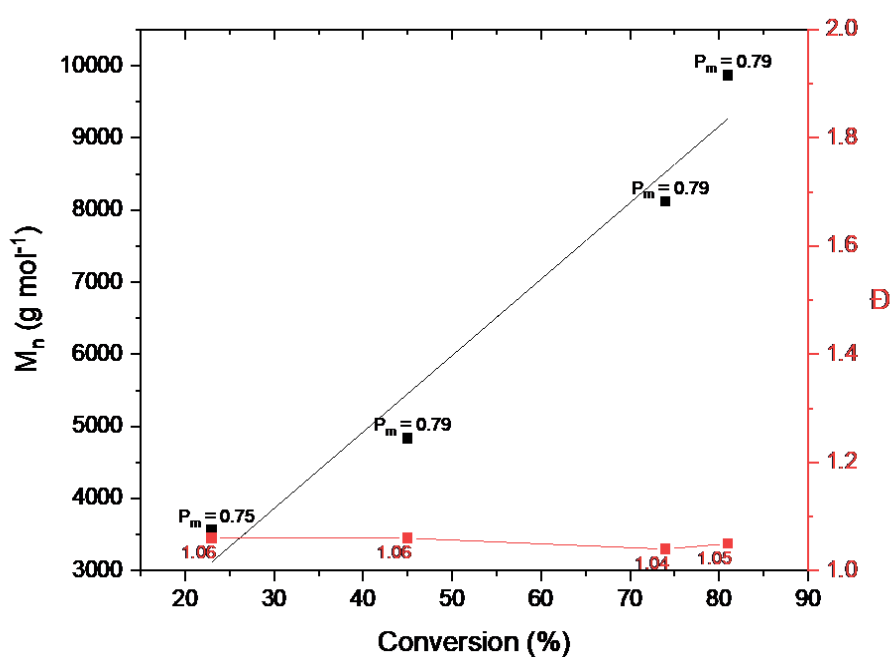


Figure 2.21: M_n vs. conversion plot for $\text{Fe}(\text{A})\text{Cl}$, $T = 80 \text{ }^\circ\text{C}$.

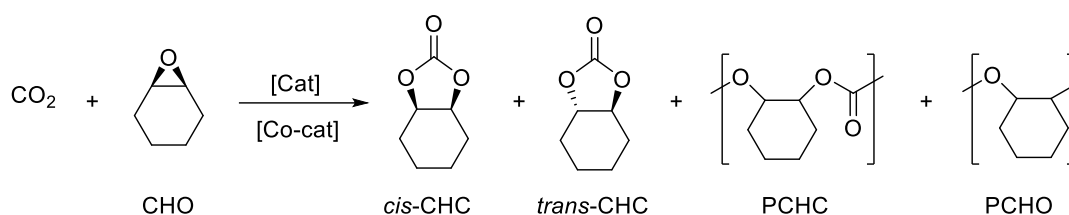
2.3 CO₂/epoxide coupling with iron (III) thiolen complexes

2.3.1 Introduction – iron complexes for CO₂/epoxide coupling

The work detailed in this section was produced in collaboration with Dr. Oliver Driscoll.

The transformation of CO₂ into useful chemicals is one of the most significant challenges faced by modern chemists.^[46–51] As the thermodynamic endpoint of combustion, almost all our industrial processes release CO₂ into the atmosphere and this, coupled with strong atmospheric persistence, means that the reduction of atmospheric CO₂ is an extremely important goal. From a different perspective, CO₂ can be viewed as a cheap and abundant C1 building block from which a wide range of useful chemicals could be produced; this is particularly desirable if industrial waste streams can be harnessed.^[52–54] However, due to the challenges associated with the activation of such an inert molecule, there are only a few examples of established chemical processes involving CO₂.^[55,56]

One example of such a process is the reaction between CO₂ and epoxides. The reaction is usually carried out in the presence of a Lewis-acidic metal complex and a nucleophilic co-catalyst such as phosphonium or tetrabutylammonium salts.^[56–62] Depending on the nature of the catalyst, the ratio of co-catalyst and the conditions used, the product of CO₂/epoxide coupling can be either cyclic organic carbonates (COCs), aliphatic polycarbonates (APCs) or a combination of both. In some cases, CO₂ is not incorporated into the polymer and polyether is formed. Furthermore, if cyclohexene oxide (CHO) is used, there are two COC product isomers available: *cis*-cyclohexene carbonate (*cis*-CHC) and *trans*-cyclohexene carbonate (*trans*-CHC). The reaction scheme with all possible products is shown in **Scheme 2.09** and highlights the importance of selective catalysis when targeting a specific product.

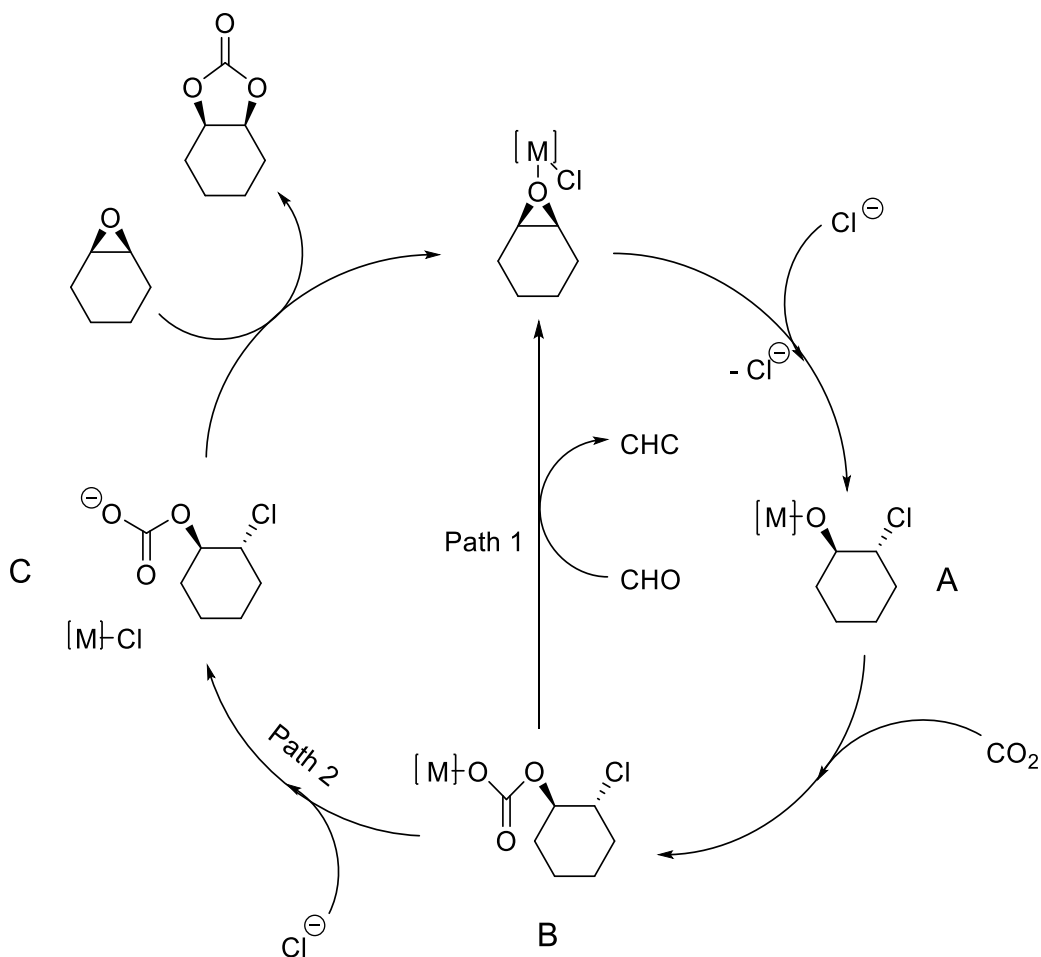


Scheme 2.09: Reaction scheme for CO₂/CHO coupling showing all possible product.

There are several important applications of COCs both in industrial and academic settings.^[63] One example is the use of COCs as “green” solvents.^[64] Examples such as ethylene carbonate and propylene carbonate are high-boiling, aprotic and highly polar; these properties allow for replacement of undesirable solvents, such as DMF, for certain reactions.^[65] The high dielectric constant of COCs has also led to their use as an electrolyte in lithium batteries.^[66,67] COCs can also be employed as additives in many industrial products, such as paints, plasticisers and anti-foam agents. Furthermore, COCs are important reagents in organic synthesis and can be copolymerised with cyclic esters.^[68–70] The traditional synthesis of COCs relies on highly toxic reagents, such as phosgene, and so there is significant interest in developing more sustainable synthetic protocols.^[64]

The catalytic cycle shown in **Scheme 2.10** was proposed by Lamberti and co-workers using aluminium salen complexes following an NMR spectroscopic study and the isolation of intermediate B.^[71] The epoxide is initially activated through coordination to the pre-catalyst before being ring-opened by the chloride ion, which is provided by the co-catalyst. Following this, a molecule of CO₂ inserts into the [M]-O bond to give the metal carbonate adduct, B. There are two paths the reaction can follow from this point to produce the cyclic carbonate product from intermediate B. Path one is followed when the alkoxide oxygen attacks the chlorine-bearing carbon to form the cyclic carbonate product which is replaced by a molecule of CHO to reform the active metal-epoxy species. Alternatively, another chloride ion can displace from the metal centre to give carbonate anion C alongside the original metal chloride precatalyst. Compound C can then undergo S_N2 ring-closure to form *cis*-CHC.

APCs are thought to form when another molecule of epoxide inserts into the metal – carbonate bond of intermediate B, allowing propagation of a polymer chain.^[72] In order to avoid co-polymerisation when targeting COCs, an excess of co-catalyst can be used to promote the exchange reaction between chloride and the carbonate anion in intermediate B to favour the production of C.^[73] The catalytic cycle shows the formation of *cis*-CHC, however it has been reported that *trans*-CHC is the thermodynamic product and is formed through backbiting reactions occurring along a polymer chain; thus catalysts that produce exclusively *cis*-CHC are relatively rare in the literature.^[56,74] The use of excess co-catalyst should therefore reduce the amount of polymer that is available for the formation of *trans*-CHC, further improving the selectivity.^[73]



Scheme 2.10: Proposed catalytic cycle for the formation of cyclic carbonates from CO₂ and CHO using aluminium salen complexes. Adapted from Lamberti (2017).^[71]

Despite the numerous benefits associated with iron catalysis, there are relatively few literature examples for CO₂/epoxide coupling when compared to other metals such as Mg, Cr, Co, Zn and Al. Della Monica and, more recently, Kerton have reviewed a range of iron complexes encompassing several ligand classes including bisphenolates such as salen, salan, salalen and phenoxy-thioether.^[75,76] The first iron catalyst for this reaction was a bimetallic iron (III) complex (**52**) bearing a macrocyclic bisphenolate {NONNON} ligand (**Figure 2.22**).^[73] Selectivity could be switched between PCHC and *cis*-CHC with the latter being promoted by increased co-catalyst concentration. Complex **52** selectively converted CO₂/CHO to *cis*-CHC at 1 bar CO₂ in 24 hours. High conversion was attained at 1% catalyst loading and 2% [PPN]Cl, however a relatively low TOF was recorded (TOF = 4 h⁻¹). TOF could be increased to 9 h⁻¹ by decreasing the catalyst and [PPN]Cl loading ([**52**] = 0.1%, [PPN]Cl = 0.4%) but activity was decreased. Complex **52** was also able to convert PO and styrene oxide (SO) into their respective APCs under mild conditions (1 bar CO₂, 25 – 80°C).

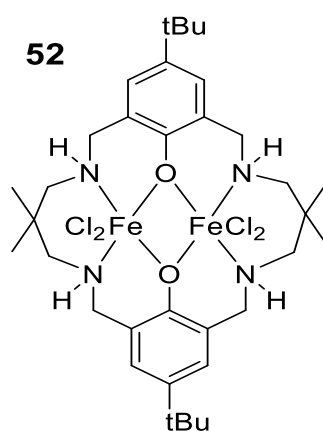


Figure 2.22: First reported iron catalyst for CO₂/epoxide coupling.^[73]

Kerton and co-workers reported the first iron (III) {ONNO} bisphenolate catalysts for CO₂/epoxide coupling with a series of iron salan chloride complexes with a homopiperazine backbone (**Figure 2.23**).^[77] Complex **53** converted PO to PC in moderate to high yields at 100°C. TBAB was found to be the optimal co-catalyst and the system achieved 84% conversion after 22 hours at a ratio of [PO]:[**33**]:[TBAB] = 4000 : 1 : 4. The TOF value of 153 h⁻¹ could be improved to 173 h⁻¹ when t-Bu groups

were replaced with electron withdrawing halide substituents (complex **54**). A further study by the same group looked at a range of bisphenolate ligands, mostly bearing pendant donors.^[78] Complex **55** was shown to be the most active giving a TOF value of 180 h^{-1} under the same conditions as with **53**. The versatility of **55** was established through substrate screening and all epoxides were converted to cyclic carbonates in 4 h with moderate to high yields.

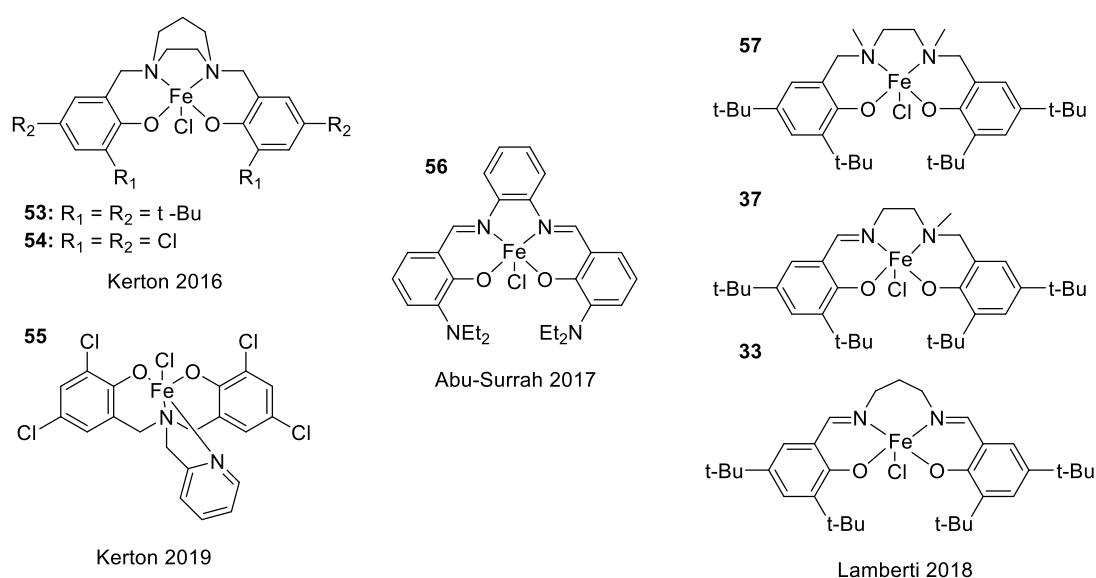


Figure 2.23: Selected examples of iron (III) {ONNO} chloride complexes for CO_2 /epoxide coupling.^[8,77–79]

A series of phenylene backbone salen iron (III) chloride complexes for CO_2 /SO coupling have also been reported and complex **56** achieved a relatively high TOF value of 289 h^{-1} , albeit at elevated temperature (130°C , 6 bar CO_2), in 6 h.^[79] Iron complexes in this study were also shown to be more active than equivalent cobalt catalysts.

The first active example of an iron salen chloride complex was reported by Lamberti alongside two salen and one salan examples (**Figure 2.23**).^[8] Using the same conditions reported by Kerton ($[\text{PO}]:[\text{Cat}]:[\text{TBAB}] = 4000 : 1 : 4$), salen complex **57** converted 85% PO to PC in 16 h at $\text{TOF} = 213 \text{ h}^{-1}$. Salalen complex **37** was the least active catalyst for CO_2 coupling with PO, SO and CHO. Complex **33**, bearing a propyl

backbone and a salen framework, was equal in reactivity to **37** for SO and CHO conversion, although only low conversions of the latter were reported, presumably due to the steric bulk of the substrate (13 – 19%). In all cases, COCs were the exclusive product and *cis*-CHC was selectively produced from CHO.

There are also some examples of iron (III) {ONNO} complexes without an auxiliary chloride ligand. Kerton and co-workers took a series of homopiperazine-bridged salan iron (III) chloride complexes (including **53** & **54**) and exposed them to air in the presence of NaOH.^[80] This generated five μ -oxo bridged complexes. They proposed that epoxide deoxygenation lead to the formation of oxo-bridge complexes over the course of the reaction, as evidenced by a colour change to red-brown and supporting UV-vis spectrophotometry data. However, the oxo-bridge intermediate does not constitute the active catalyst.

Driscoll *et al.* reported a series of air-stable iron (III) acetate complexes with salen, salan and salalen ligands (**Figure 2.24**).^[32] When applied to CO₂/CHO coupling, *cis*-CHC was formed as the major product for all complexes; in most cases it was seen as the exclusive product. Complex **58**, bearing an aminopiperidine backbone and secondary amine donor, was most active for CO₂/CHO coupling at mild conditions (80°C, 10 bar CO₂) giving 66% conversion in 24 h (TOF = 34 h⁻¹) at 0.08 mol% Fe and eight equivalents of TBAC. Using complex **58**, a range of co-catalysts and epoxide substrates were explored. TBAC was confirmed as the most active and selective co-catalyst in this case and activity was confirmed for a range of epoxides with differing steric and electronic profiles.

A small study on the effect of chirality was also carried out with **59_{RR}**, **59_{SS}** and **59_{meso}** (**Figure 2.24**). The reaction using **59_{RR}** gave the highest conversion whereas the conversion recorded for **59_{meso}** was significantly lower than with the chiral counterparts, with some polyether also being formed (**59_{RR}** = 60%, **59_{SS}** = 47, **59_{meso}** = 30%). This is attributed to changes in coordination geometry rather than any inherent chiral effects. A UV-vis study confirmed the presence of μ -oxo bridged complex in the final reaction mixture in keeping with the findings of Kerton.^[80]

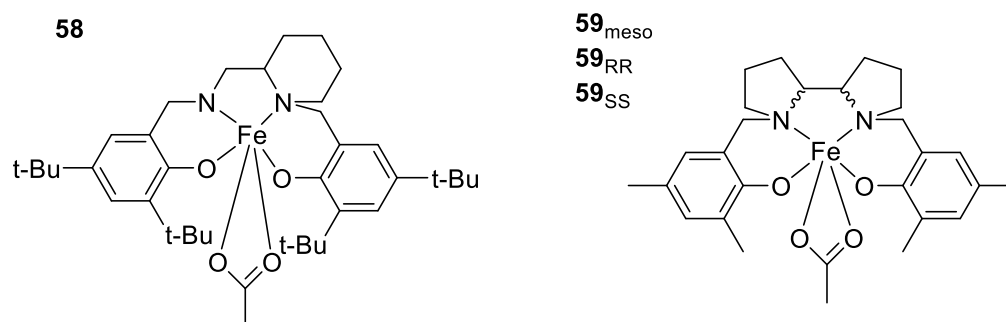


Figure 2.24: Selected examples of iron (III) acetate complexes for CO₂/epoxide coupling.^[32]

There are also several reported examples of iron (III) complexes with ligands that contain thioether donors.^[81] A dimeric {OSOSO} di-iron complex (**60**) was reported by Rieger and co-workers.^[82] Using **60** and TBAB, PO was converted to PC with >99% selectivity under a range of conditions. A maximum TOF value of 580 h⁻¹ was achieved, albeit employing relatively forcing conditions (100°C, 20 bar CO₂). Three mono-nuclear {SOS} iron (III) (**61**) and iron (II) (**62**) complexes were reported by Capacchione and could convert 2-butyl oxirane to the respective cyclic carbonate with TBAB co-catalyst (**Figure 2.25**).^[83] For the iron (III) complexes, modification of the ligand substituents had little effect on activity (conversion = 76 – 77%, TOF = 31 – 32 h⁻¹) and the iron (III) complexes were generally more active than their iron (II) equivalents.

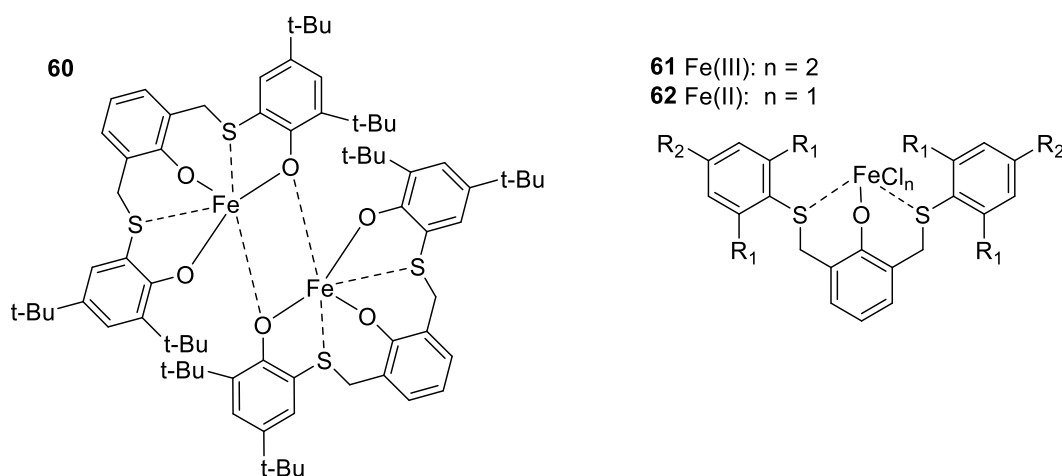


Figure 2.25: Selected iron (III) complexes with thioether donors for CO₂/epoxide coupling.^[82,83]

There are reported examples of {OSSO} iron (III) chloride complexes (**Figure 2.26**). Capacchione tested four derivatives, the most active of which, **63**, converted 2-butyl oxirane with a TOF of 63%, although the reactions were kept to low conversion.^[84] A broad substrate scope was also reported with **63** and TBAB wherein 12 epoxides were selectively converted to the relevant cyclic carbonate. Further work by the same group took complex **63** and converted it to metallate complex **64** through addition of TBAB.^[85] The resultant complex was active as a single-component catalyst for a range of epoxide substrates.

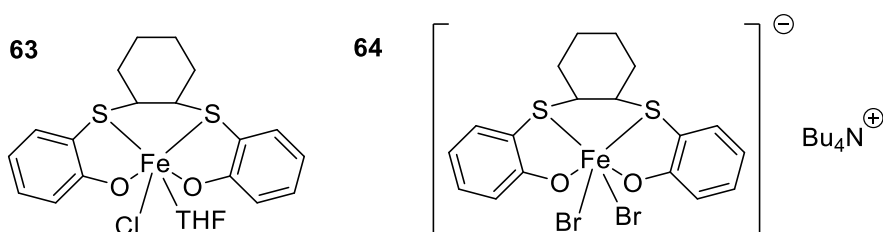


Figure 2.26: Selected examples of iron (III) {OSSO} complexes for CO₂/epoxide coupling.^[84,85]

Based on the above examples, it was decided to attempt the formation of cyclic carbonates using the iron (III) thioen chloride complexes detailed in **Section 2.2**. This includes a study of co-catalyst equivalents and substrate scope, as well as a comparison with a wider range of iron (III) salen chloride complexes than have previously been reported.

2.3.2 Synthesis and characterisation of Fe(A)OAc

One iron (III) thioen acetate complex was synthesised to provide insight into the importance of the auxiliary ligand and to provide a direct comparison with the iron (III) {ONNO} acetate complexes reported by Driscoll *et al.*^[86] The synthetic protocol used for iron (III) {ONNO} acetates was followed. Ligand AH₂ and Fe(OAc)₂ were dissolved in ethanol and refluxed in air for three hours, after which an air-stable black solid was collected through filtration. The identity of [Fe(A)]⁺ was confirmed through HR-MS and the EA values were consistent with a monomeric acetate complex.

A solid-state structure was obtained for Fe(A)OAc (**Figure 2.27**). During the reaction, the acetate group acts as a single donor ligand and, with this assumption, the complex tends towards a trigonal bipyramidal geometry ($\tau_5 = 0.63$, **Table 2.07**) with the acetate group occupying an equatorial site. The direct chloride analogue, Fe(A)Cl, has a stronger preference towards trigonal bipyramidal geometry ($\tau_5 = 0.78$). The chloride ($\tau_5 = 0.66$) and acetate ($\tau_5 = 0.65$) salalen analogues are similar in terms of their geometric preference.

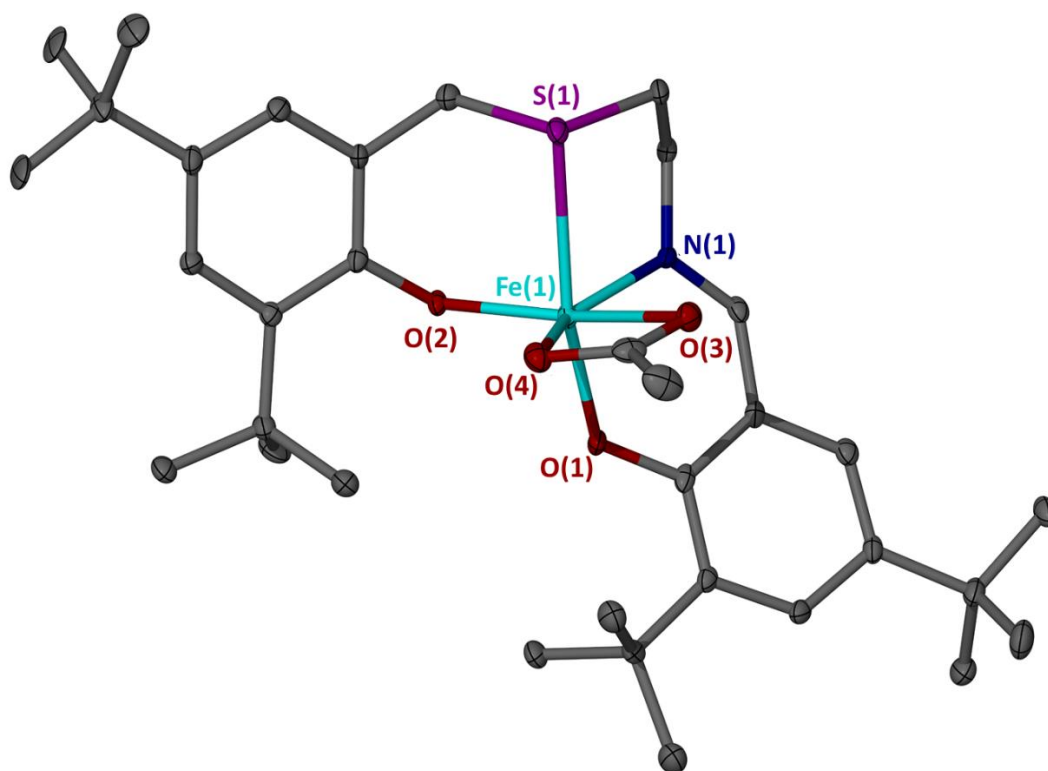


Figure 2.27: Solid state structure of Fe(A)OAc, ellipsoids shown at 30% probability level.

Table 2.07: Selected bond lengths (Å) and angles (°) for Fe(**A**)OAc

	Fe(A)OAc
τ_5	0.63
Fe–O(1)	1.887(3)
Fe–O(2)	1.873(3)
Fe–N(1)	2.077(4)
Fe–S(1)	2.5904(17)
O(1)–Fe–N(1)	87.64(14)
O(2)–Fe–N(1)	109.78(14)
N(1)–Fe–S(1)	81.07(12)
O(1)–Fe–S(1)	168.43(10)
O(2)–Fe–C(acetate)	130.40(17)

2.3.3 CO₂/CHO coupling with Fe(**A-E**)Cl and Fe(**A**)OAc

The complexes, Fe(**A-E**)Cl and Fe(**A**)OAc, were tested for their catalytic activity towards CO₂/CHO coupling (**Table 2.08**). CHO was chosen as it is a “challenging” substrate in terms of sterics and the potential to form four separate products. TBAC was employed as the co-catalyst as it was shown to be most effective when using iron (III) salalen acetate complexes^[32] and it was used at an 8 : 1 ([TBAC] : [Fe]) ratio to promote the formation of carbonate anions and hence favour the *cis*-CHC product. The reaction conditions were based on previous literature, with a small amount of catalyst (0.08 mol% Fe) being employed at relatively mild conditions (10 bar CO₂, 80 °C) for 24 hours.^[8,32]

¹H NMR was used to ascertain the conversion and selectivity through the characteristic methine resonances for each of the four potential products, which were integrated against unreacted CHO in accordance with previously reported literature.^[73] The characteristic resonances of *cis*-CHC and *trans*-CHC are $\delta = 4.66$

ppm and $\delta = 3.99$ ppm respectively and are therefore easily distinguishable; the same can be said for PCHO ($\delta = 3.35$ ppm). However, the methine resonance for PCHC ($\delta = 4.65$) could easily overlap with the desired *cis*-CHC product. To confirm the presence of cyclic carbonate, HR-MS was carried out of the crude reaction mixture, although this cannot distinguish between stereoisomers, and showed the presence of CHC in all cases. GPC analysis confirmed a lack of polymer in the reaction mixture thus confirming the identity of the signal pertaining to *cis*-CHC.

Initially, three control reactions were carried out to ascertain the necessity of the ligand, the metal precursor and the co-catalyst (**Table 2.08**, entry 1 – 3). When FeCl₃ and TBAC were added, moderate conversion was achieved (44%), however the selectivity was poor compared to previously reported iron systems (selectivity of *cis*-CHC = 83%).^[95] When TBAC was added as the sole catalyst, the results were almost identical to those observed with FeCl₃, suggesting that the iron precursor has no activity for this reaction. Finally, the reaction was carried out with Fe(**E**)Cl with no co-catalyst. As may be expected from previously reported data, no cycloaddition was recorded and only a small quantity of PCHO was detected at the end of the reaction.

All complexes showed equal or higher activity than the TBAC control (conversion = 43 – 60%) and were more selective; *cis*-CHC was the exclusive product for all catalysts with the exception of Fe(**D**)Cl where a small amount of *trans*-CHC and PCHO were formed. An example spectrum can be seen in **Figure 2.28** showing the crude reaction mixture of CO₂/CHO coupling with Fe(**E**)Cl giving *cis*-CHC as the exclusive product. The addition of electron withdrawing groups had the biggest impact on activity, whereas sterics seems to have only a small impact. The most sterically hindered complex, Fe(**A**)Cl (R₁ = R₂ = t-Bu), was less active (TOF = 22 h⁻¹) than the relatively unhindered analogue, Fe(**B**)Cl (R₁ = H, R₂ = t-Bu) (TOF = 24 h⁻¹) as you might expect from a more accessible and therefore more active metal centre. Introducing electron withdrawing chlorides at the R₁ position boosted activity as may be expected from an increase in Lewis acidity at the metal centre. Fe(**C**)Cl (R₁ = Cl, R₂ = t-Bu) gave improved activity (TOF = 28 h⁻¹) and maintained *cis*-CHC as the exclusive product.

Table 2.08: CO₂/CHO reaction catalysed by Fe(A-E)Cl and Fe(A)OAc with TBAC.

<div style="display: flex; justify-content: space-around; width: 100%;"> CO₂ + CHO [Cat] → cis-CHC + trans-CHC + PCHC + PCHO </div>					
Entry	Catalyst	Conv./% ^a	Selectivity for cis-CHC /% ^a	cis-CHC : trans-CHC : PCHC : PCHO ratio /% ^a	TOF ^b /h ⁻¹
1	FeCl ₃	44	83	83 : 1 : 0 : 16	23
2	None	43	83	83 : 0 : 0 : 17	22
3	EH ₂	8	0	0 : 0 : 0 : >99	4
4	Fe(A)Cl	43	>99	>99 : 0 : 0 : 0	22
5	Fe(B)Cl	47	>99	>99 : 0 : 0 : 0	24
6	Fe(C)Cl	54	>99	>99 : 0 : 0 : 0	28
7	Fe(D)Cl	51	90	90 : 1 : 0 : 9	27
8	Fe(E)Cl	60	>99	>99 : 0 : 0 : 0	31
9 ^d	Fe(E)Cl	75	94	94 : 1 : 0 : 5	156
10	Fe(A)OAc	44	>99	>99 : 0 : 0 : 0	23

Conditions: [Fe] Catalyst (0.08 mol%, 1 eq.), TBAC (0.64 mol%, 8 eq.), CHO (5.0 mL), 10 bar CO₂, 80 °C, 24 h. ^a Determined *via* ¹H NMR spectroscopy using the methine resonances of *cis*-CHC (δ = 4.66 ppm), *trans*-CHC (δ = 3.99 ppm), PCHC (δ = 4.65) and PCHO (δ = 3.35 ppm). ^b TOF = [(Conv. % / 100) x (100 / 0.08 mol%)] / 24 h = [(Conv. / 100) x 1250] / 24. ^c 0 equivalents of TBAC ^d 120 °C, 6 h.

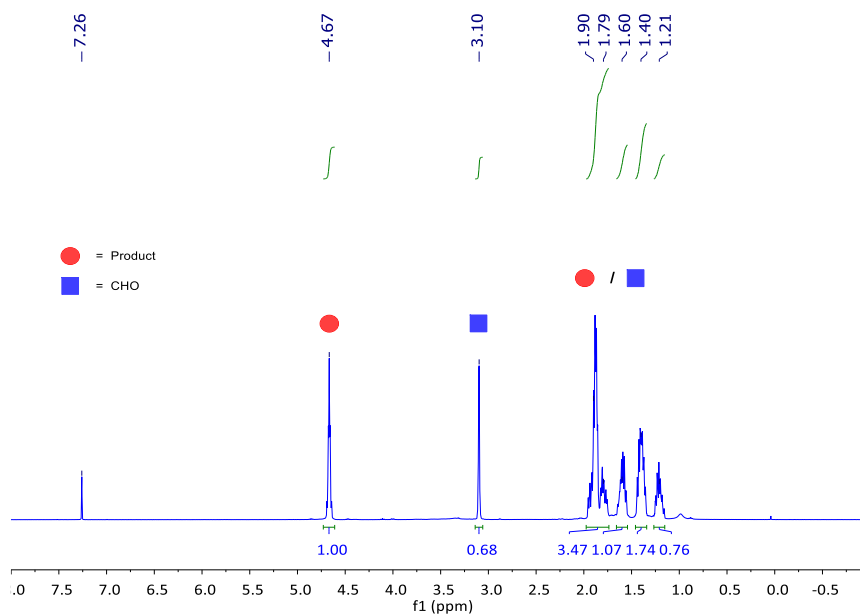
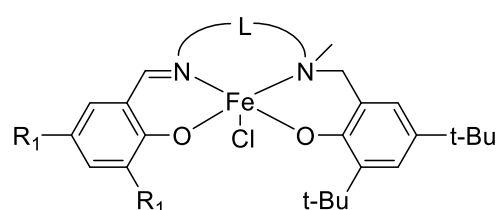


Figure 2.28: ^1H NMR (400 MHz, C_6D_6 , 298K) spectrum of CO_2/CHO coupling with $\text{Fe}(\text{E})\text{Cl}$. (Table 2.08, entry 8).

The combination of $\text{Fe}(\text{D})\text{Cl}$ ($\text{R}_1 = \text{Br}$, $\text{R}_2 = \text{t-Bu}$) and $\text{Fe}(\text{E})\text{Cl}$ ($\text{R}_1 = \text{t-Bu}$, $\text{R}_2 = \text{Br}$) represents an isomeric pair and were included to compare the effect of equivalent substitution on either side of the asymmetric ligand. With bromides at the R_1 position, the activity was similar to that obtained with the chlorinated complex ($\text{TOF} = 27 \text{ h}^{-1}$), however the selectivity was reduced (selectivity for *cis*-CHC = 94%) with some *trans*-CHC and PCHO being recorded. Conversely, adding bromide substituents to the thio-phenolate moiety gave *cis*-CHC as the exclusive product and gave the highest activity that was found in the study ($\text{TOF} = 31 \text{ h}^{-1}$). The TOF could be improved to 156 h^{-1} through increasing the temperature to $120 \text{ }^\circ\text{C}$ and reducing reaction time to 6 h, but this came at the expense of selectivity and a small amount of *trans*-CHC and PCHO was observed.

A direct comparison between $\text{Fe}(\text{A})\text{Cl}$ and $\text{Fe}(\text{A})\text{OAc}$ showed that the auxiliary ligand does not have a significant effect on the activity or selectivity of the complexes, with both producing only *cis*-CHC and giving similar TOF values. This is in contrast to the comparison between iron (III) salen chloride complexes reported by Lamberti, and the iron (III) salen acetate complexes reported by Jones, where the acetate complexes were more active.^[8,32] The apparent unimportance of the auxiliary ligand suggests that it rapidly dissociates under reaction conditions.

Seven iron (III) salalen chloride complexes were applied to CO₂/CHO coupling in this study (**Figure 2.29**). The conditions were identical to those detailed for the thioen complexes and all iron salalen catalysts produced *cis*-CHC as the exclusive product. In keeping with thioen catalysts, increasing the steric bulk of the salalen ligands decreased the activity towards CO₂/CHO coupling, as would be expected. With an unsubstituted imino-phenolate, salalen complex **38** was more active (TOF = 28 h⁻¹) than the equivalent thioen, Fe(**B**)Cl (TOF = 24 h⁻¹). With t-Bu substituents at R₁, the activities were equivalent [Fe(**A**)Cl: TOF = 22 h⁻¹, **37**: TOF = 21h⁻¹].



- 37**: R₁ = t-Bu, L = -CH₂CH₂-, Conversion = 41%, TOF = 21 h⁻¹
38: R₁ = H, L = -CH₂CH₂-, Conversion = 53%, TOF = 28 h⁻¹
39: R₁ = Cl, L = -CH₂CH₂-, Conversion = 44%, TOF = 23 h⁻¹
40: R₁ = Me, L = -CH₂CH₂-, Conversion = 47%, TOF = 24 h⁻¹
41: R₁ = t-Bu, L = -C₆H₄-, Conversion = 46%, TOF = 24 h⁻¹
42: R₁ = t-Bu, L = -CH₂C₅H₉-, Conversion = 48%, TOF = 25 h⁻¹
43: R₁ = t-Bu, L = -C₆H₁₀-, Conversion = 51%, TOF = 27 h⁻¹

Figure 2.29: Iron (III) salalen chloride complexes (**37 – 43**): structure plus conversion and TOF values for CO₂/CHO coupling. Conditions: [Fe] Catalyst (0.08 mol%, 1 eq.), TBAC (0.64 mol%, 8 eq.), CHO (5.0 mL), 10 bar CO₂, 80 °C, 24 h. *cis*-CHC was the exclusive product in all cases.

When chloride substituents were introduced at the R₁ position, thioen complex, Fe(**C**)Cl, gave significantly higher conversion after 24 h (54%) than the equivalent salalen complex, **39** (44%). This suggests that electronic effects are more important with the thioen framework. As previously mentioned, the introduction of bromide substituents to the thioen ligand resulted in the most active catalyst in this study, and it would be interesting to test an equivalent salalen with halide substitution at the amino-phenolate. Interestingly, increasing the steric bulk of the backbone resulted in more active complexes (**41 – 43**) when compared to **37**, which has the same substitution with an ethylene linker. Overall, the improved activity of the

thiolen complexes could be attributed to the softer sulphur donor forming a more labile bond with the metal, allowing for easier binding of the epoxide.

2.3.4 Further study of CO₂/epoxide coupling with Fe(E)Cl

The most active thiolen complex, Fe(E)Cl, was further investigated to ascertain the effect of co-catalyst concentration (**Table 2.09**) and functional group tolerance through the coupling of CO₂ with a range of epoxides (**Table 2.10**). In keeping with the findings of Williams *et al.*, when no co-catalyst was added, only polyether was formed at very low conversion (**Table 2.09**, entry 1).^[73] With two equivalents of TBAC, conversion was still low but there was selectivity towards *cis*-CHC (79%). Ultimately, eight equivalents were necessary to ensure complete selectivity to *cis*-CHC and this is consistent with the idea of promoting carbonate anion formation through excess co-catalyst.

Table 2.09: CO₂/CHO reaction catalysed by Fe(E)Cl and various equivalents of TBAC.

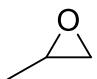
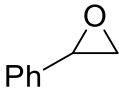
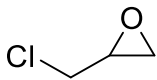
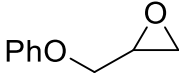
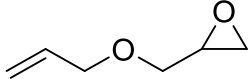
Entry	Eq. of TBAC	Conv. /% ^a	Selectivity for <i>cis</i> -CHC /% ^a	<i>cis</i> -CHC : <i>trans</i> -CHC : PCHC : PCHO ratio /% ^a	TOF ₁ ^b /h ⁻¹
1	0	8	0	0 : 0 : 0 : >99	4
2	2	8	79	79 : 8 : 0 : 13	4
3	4	42	94	94 : 4 : 0 : 2	22
4	8	60	>99	>99 : 0 : 0 : 0	31

Conditions: [Fe] Catalyst (0.08 mol%, 1 eq.), TBAC, CHO (5.0 mL), 10 bar CO₂, 80 °C, 24 h. ^a Determined *via* ¹H NMR spectroscopy using the methine resonances of *cis*-CHC (δ = 4.66 ppm), *trans*-CHC (δ = 3.99 ppm) and PCHO (δ = 3.35 ppm). ^b TOF = [(Conv. % / 100) x (100 / 0.08 mol%)] / 24 h = [(Conv. / 100) x 1250] / 24.

The results of substrate screening with Fe(E)Cl are shown in **Table 2.10**, and all epoxides were converted into their cyclic carbonate equivalents at high yields. Under the same reaction conditions, these epoxides were converted with higher activity than was observed with CHO. This was expected as CHO is an internal epoxide and therefore has a greater steric barrier to activation.^[32] PO and SO gave similar TOF values (PO: TOF = 42 h⁻¹, SO: TOF = 40 h⁻¹) suggesting that the nature of the epoxide,

terminal or internal, is more important than the steric bulk of the substituent. However, the electronics of the substrate do seem to play an important role in activity. Epichlorohydrin (ECH) gave the lowest conversion (73%), apart from CHO, and this could be attributed to the electron withdrawing effects of the chlorinated epoxide. Conversely, phenyl glycidyl ether (PGE) and allyl glycidyl ether (AGE), both bearing electron donating ether groups, were by far the most susceptible substrates to CO₂/epoxide coupling (PGE: TOF = 64 h⁻¹, AGE 48 h⁻¹). However, these are not direct comparisons as the reaction time for PGE had to be shortened to 18 hours due to the solidification of the product.

Table 2.10: CO₂ coupled with various epoxides catalysed by Fe(E) and TBAC.

Entry	Epoxide	Conv. / % ^a	Product selectivity / % ^a	TOF ^b / h ⁻¹	
1		PO	81	>99	42
2		SO	76	>99	40
3		ECH	73	>99	38
4 ^c		AGE	92	>99	64
5		PGE	93	>99	48

Conditions: [Fe] Catalyst (0.08 mol%, 1 eq.), TBAC (0.64 mol%, 8 eq.), CHO (5.0 mL), 10 bar CO₂, 80 °C, 24 h. ^a Determined *via* ¹H NMR Spectroscopy. ^b TOF = [(Conv. % / 100) x (100 / 0.08 mol%)] / 24 h = [(Conv. / 100) x 1250] / 24. ^c Reduced reaction time of 18 h.

2.4 Aluminium (III) thiolen complexes

2.4.1 Introduction – aluminium complexes for lactide polymerisation

Aluminium complexes are among the most common isoselective initiators for PLA synthesis^[88] in conjunction with a range of ligands including salen,^[1,3,5–7,18,89–91] salan,^[9,10,92] half-salan^[93] and salalen.^[15,16,94] Pioneering work from Spassky showed that isotactic stereocomplexed PLA could be formed with the use of a chiral salen complex, **65**, through an enantiomorphic site control mechanism, where each enantiomer of the initiating complex favours the insertion of one lactide stereoisomer. The racemic initiator achieved elevated melting temperatures of up to 187 °C (**Figure 2.30**).^[90] Feijen and co-workers also demonstrated chiral control of ROP achieving isotactic PLA ($P_m = 0.93$) using a racemic Jacobsen's ligand aluminium complex, **66**.^[7] The Spassky complex was subsequently applied to the polymerisation of *meso*-lactide by Ovitt and Coates; this was the first highly syndiospecific polymerisation of *meso*-lactide.^[95]

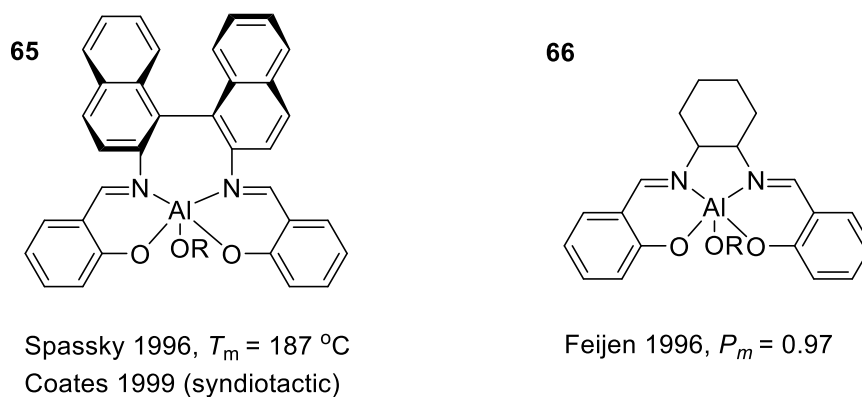
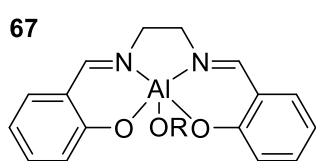


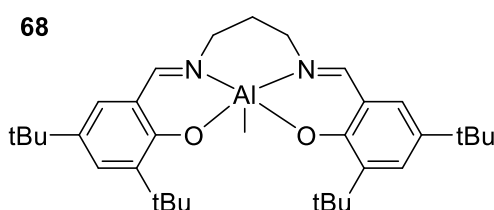
Figure 2.30: Selected early examples of chiral salen aluminium initiators for isotactic PLA production.^[7,90,95]

Further work by Spassky and co-workers achieved isotactic PLA using an achiral aluminium initiator (**67**) with the isotactic microstructure arising from a chain-end control mechanism (**Figure 2.31**).^[91] Hormnirun and co-workers investigated 24 different salen ligands, including several instances of inflexible aromatic

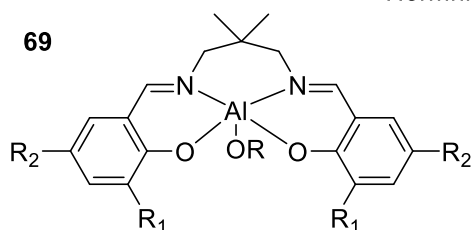
backbones.^[96] The *ortho* position of the phenolate was found to have the most significant impact on stereoselectivity and propylene-bridged complex **68** gave isotactic PLA ($P_m = 0.88$). Highly isotactic stereocomplex PLA ($P_m = 0.98$, $T_m = 210$ °C) was achieved by Nomura using a salen ligand with extremely bulky *t*-BuMe₂Si phenolate substituents (**69**). High initiator loadings ($[LA]/[69] = 50 : 1$) were required to avoid lengthy reaction times in solution (≤ 40 h) whereas ROP was significantly quicker in the melt, with a corresponding decrease in stereoselectivity.^[5]



Spassky 1997, $T_m = 151$ °C



Hormnirun 2006, $P_m = 0.88$



Nomura 2007, $P_m < 0.98$, $T_m < 210$ °C

Figure 2.31: Selected early examples of achiral isoselective aluminium salen complexes for lactide ROP.^[5,91,92]

The range of potential salen linking groups was further increased by Lin *et al.* who employed bulky cumyl groups at the *ortho* and *para* positions of the phenolate (**Figure 2.32**).^[97] At 70 °C, complex **70** gave highly stereocomplexed PLA with an elevated melting temperature ($P_m = 0.97$, $T_m = 205$ °C). Studies with *L*-lactide demonstrated excellent control of the reaction with little transesterification. The chiral initiator, **71**, with a diphenylethylene backbone gave highly isotactic PLA ($P_m = 0.90$), however the steric bulk of the complex meant it required a reaction time of 144 h with a conversion of only 38% to achieve this stereoselectivity.^[98] A more recent example of a bulky, stereoselective aluminium complex was reported by Pang

and co-workers using an adamantyl-bridged salen complex.^[99] Complex **72** gave isotactically enriched PLA ($P_m = 0.87$) but polymerisation remained slow ($t \leq 24$ h).

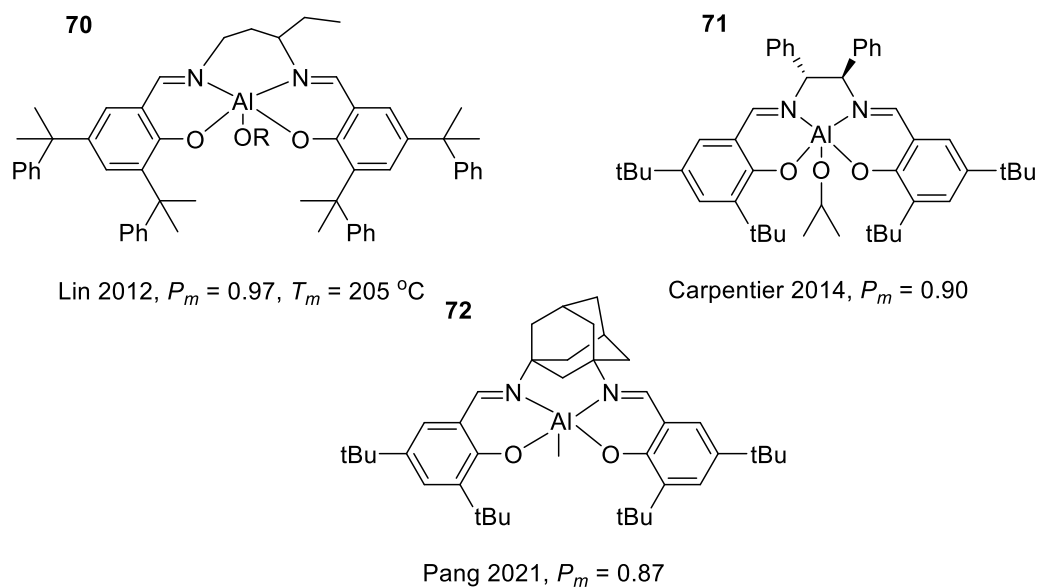


Figure 2.32: Further examples of isoselective aluminium salen initiators.^[98–100]

The salen family of ligands results from either the reduction of the imine groups of a salen ligand or a modified Mannich reaction to give an amino bisphenolate coordination motif. This introduces another point of variation at the amine nitrogen atoms and the lack of conjugation means that the complexes are more likely to be white. The first example of an aluminium salen complex for lactide polymerisation was reported by Gibson *et al.* following the reduction of a simple ethylene-bridged salen with a range of methyl and benzyl amine substituents (**Figure 2.33**).^[92] The backbone substitution had little effect on the stereoselectivity, however, the phenolate substitution could vary the microstructure from heterotactic (**73**: $R_1 = \text{Cl}$, $P_m = 0.04$) to isotactic (**74**: $R_1 = \text{tBu}$, $P_m = 0.79$). Complete reduction of the salen system proposed by Feijen resulted in a series of chiral salen ligands with two methylated amine donors.^[10] Moderate isoselectivity ($R = \text{H}$, $P_m = 0.66$) and moderate heterotacticity ($P_m \geq 0.27$) were observed with **75** dependant on substitution patterns.

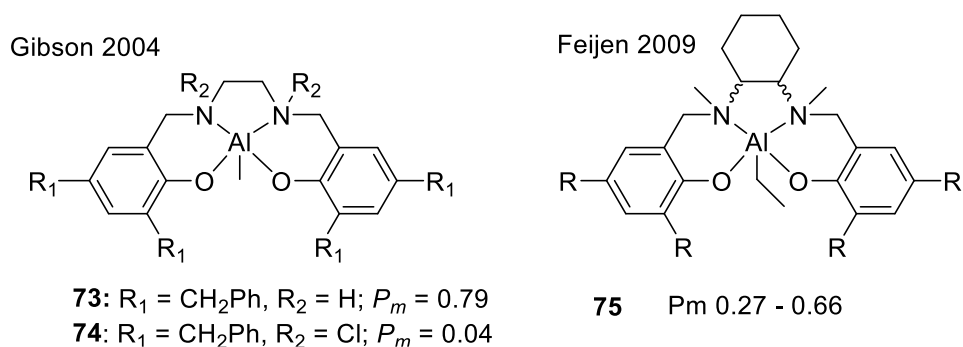


Figure 2.33: Early aluminium salan complexes for lactide ROP.^[10,92]

Jones and co-workers have reported a number of salan aluminium systems with novel backbones based on aminopiperidine,^[9] bipyrrolidine^[11,101] and 3-aminopyrrolidine.^[102] Bipyrrolidine aluminium salan complexes with methyl and tBu substituents produced heterotactic PLA with narrow dispersities (**Figure 2.34**). The stereoselectivity was greatest when the *meso* form of the ligand was used (**76**_{R,R} $P_m = 0.49$, **76**_{meso} $P_m = 0.87$). The range of bipyrrolidine salan ligands was expanded by Kol *et al.* with unsubstituted and chloro phenolate analogues.^[12] Interestingly, the chirality of the complexes had a strong influence on the stereoselectivity. For the unsubstituted complex, isotactic PLA was formed from the enantiomerically pure initiator (**78**_{R,R} $P_m = 0.79$) whereas the racemic mixture produced atactic PLA (**78**_{rac} $P_m = 0.56$). The chloro complex produced almost perfectly heterotactic PLA (**79**_{rac} $P_m = 0.02$) from the racemic initiator with much lower selectivity observed from the single diastereomer (**79**_{R,R} $P_m = 0.36$). Salan ligands based on 3-aminopyrrolidine were formed from the reduction of salalen ligands and their aluminium complexes gave PLA with a moderate isotactic bias ($P_m = 0.44 - 0.72$). These complexes were also active in the melt, with reactions times less than one hour, in some cases.^[102]

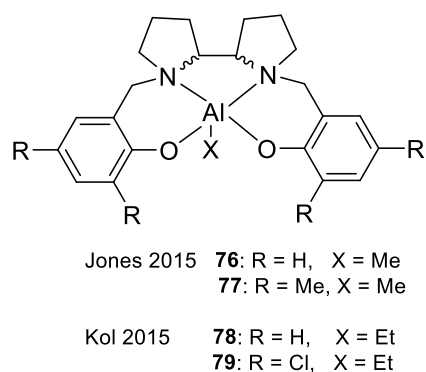


Figure 2.34: Chiral bipyrrolidine-based salen complexes for *rac*-lactide ROP.^[11,12]

The salalen family of ligands was first introduced by Kol and co-workers in 2004.^[103] It is comprised of an imino-phenolate and an amino-phenolate and can be considered a hybrid of the salen and salan ligands (**Figure 2.35**).

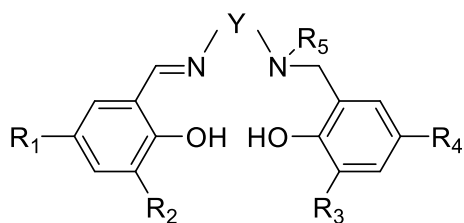
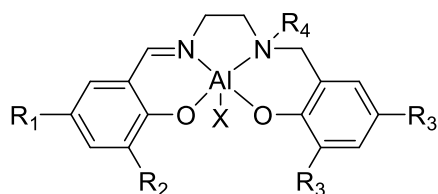


Figure 2.35: General structure of a salalen ligand.

The first application of aluminium salalen complexes to lactide ROP was reported by Whitelaw and co-workers with a series of eight ethylene-bridged ligands (**Figure 2.36**).^[94] Variation was focused on the imino-phenolate and the amine nitrogen. The stereospecificity of the polymerisation was found to be most dependent on the nature of the amine substituent. Methyl substitution gave PLA with a slight isotactic bias (**80** $P_m \leq 0.61$), whereas the bulkier phenyl groups resulted in heterotactically enriched PLA (**81** $P_m \geq 0.25$). Lamberti *et al.* subsequently expanded the scope of ethylene-bridged salalen ligands through the introduction of chloride substituents at the amino-phenolate along with an extremely bulky adamantyl group at the *ortho*-position of the imino-phenolate.^[16] Moderately isotactic PLA was produced from **82** ($P_m \leq 0.71$) and copolymerisation with ϵ -caprolactone was also achieved.



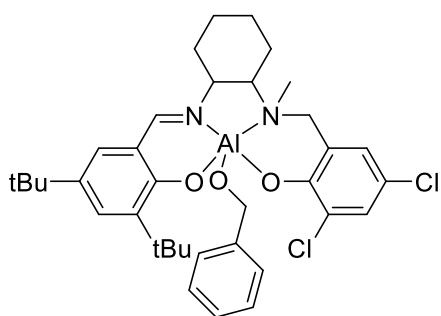
Jones 2011 **80** $R_1=R_2=R_3 = tBu$, $R_4 = Me$, $P_m = 0.61$

81 $R_1 = H$, $R_2 = Me$, $R_3 = tBu$, $R_4 = Ph$ $P_m = 0.25$

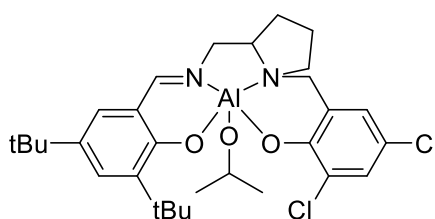
Lamberti 2015 **82** $R_1=R_2 = tBu$, $R_3 = Cl$, $R_4 = Me$ $P_m = 0.71$

Figure 2.36: Selected examples of ethylene-bridged aluminium salen complexes for lactide ROP.^[16,94]

More recently, a diverse range of linking groups have been explored with salen ligands (**Figure 2.37**). Hancock and co-workers reported salen ligands based on 1,2-diaminocyclohexane which were active in solution and in the melt at 130 °C giving atactic to moderately isotactic PLA (**83**) $P_m = 0.69$.^[104] More stereoselective initiators were reported by Kol based on chiral aminomethylpyrrolidine salen ligands.^[105] A novel microstructure of gradient isotactic multiblock PLA was produced from a combination of chain end and enantiomorphous site control from **84**. Jones *et al.* have subsequently reported salen ligands with phenylene and 3-aminopyrrolidine linkers, both of which gave well-controlled initiation with little stereoselectivity.^[18,102]



83 Jones 2011, $P_m = 0.69$



84 Lamberti 2014, $P_m = 0.82$

Figure 2.37: Selected examples of isoselective aluminium Salalen complexes.^[94,105]

The range of bisphenolate aluminium complexes that have been discussed are universally hampered by low activity, with long reaction times typically ranging from one to several days in solution. Recent developments have introduced novel frameworks that result in far more active aluminium species (**Figure 2.38**). Romain *et al.* reported a catam ligand with amine donors directly bonded to the phenolate ring.^[106] Initial studies with an ethylene-bridged analogue (**85**) bearing tBu phenolate substituents achieved high conversion after just 90 minutes at room temperature; an analogous salen complex took 7200 minutes to reach a similar conversion. The introduction of a neopentyl linker (**86**) maintained excellent activity whilst also producing highly heterotactic PLA.^[107] A combination of experimental and theoretical studies indicated that the N-H moieties were perfectly placed to hydrogen bond with the incoming lactide monomers, facilitating rapid rates and stereoselectivity. Payne and co-workers recently introduced the hybrid catalen family of ligands comprised of a rigid iminophenolate and a catam-like *ortho*-aminophenolate.^[108] Aluminium catalen complexes were active in solution taking 0.5 hours to achieve high conversion at 80 °C and 8 hours at room temperature (**87**) with a range of tacticities observed ($P_m = 0.28 - 0.70$). High activity was also observed under melt conditions at 130 °C at low initiator loadings ($[LA]/[I]/[BnOH] = 3000 : 1 : 10$).

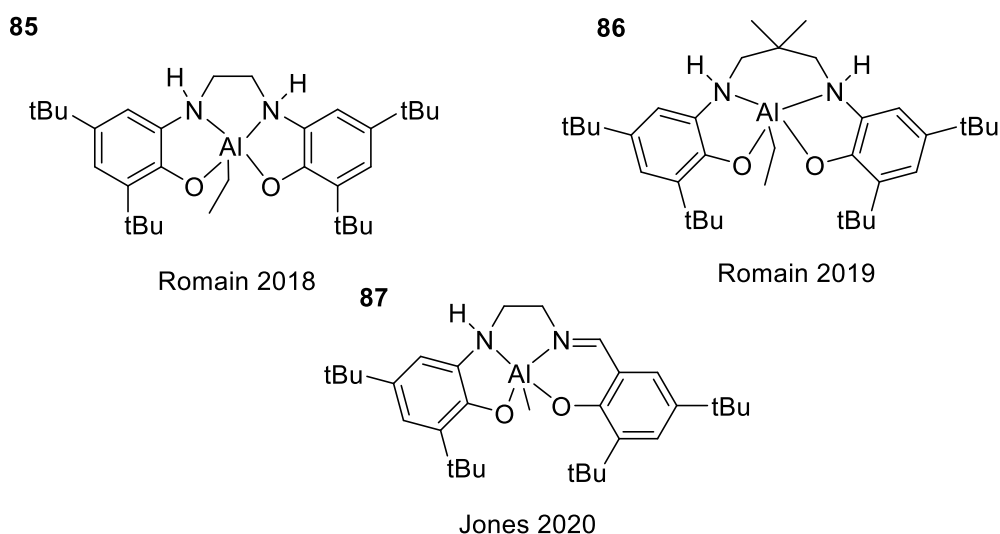


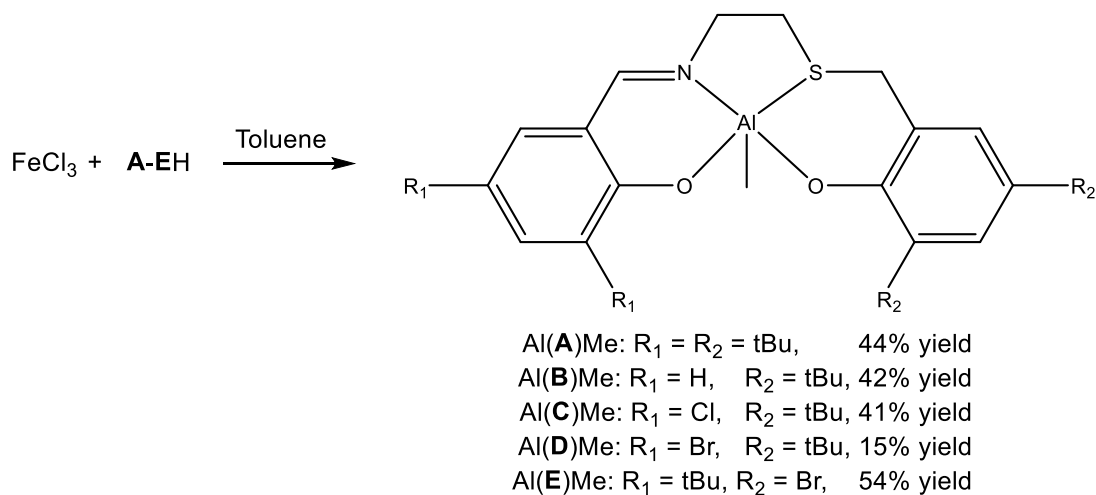
Figure 2.38: Aluminium complexes with Catam moieties for lactide ROP.^[106–108]

Although there are numerous examples of bisphenolate {ONNO} aluminium complexes, the incorporation of a thioether donor has not been reported. There is a potential incompatibility between the small, highly Lewis acidic Al^{3+} cation and the relatively large and polarisable thioether donor and this could lead to hemilability, an effect which has been shown to positively influence the catalytic performance of aluminium complexes applied to isocyanate trimerisation.^[109] Alternatively, the complexation of thioen ligands to aluminium could result in a four coordinate {ONO} methyl complex.

The investigation of aluminium thioen complexes detailed in this section can also be viewed as a comparative study with the aforementioned iron thioen complexes. Both sets of complexes are based on a similar +3 cation, however aluminium complexes are amenable to standard NMR techniques making it far easier to assess purity, coordination and initiation than with their paramagnetic iron counterparts. Furthermore, both metal centres tend to be isoselective and limited by relatively low activity. Thus, both sets of complexes were studied in tandem with the richer data set that could be acquired from aluminium complexes used to rationalise the behaviour of the equivalent iron (III) initiators.

2.4.2 Synthesis and characterisation of aluminium (III) thioen complexes

The complexation of ligands **A** – EH_2 with AlMe_3 was carried out at room temperature in toluene to give the alkyl complexes, $\text{Al}(\mathbf{A-E})\text{Me}$ (**Scheme 2.11**). All complexes crystallised from a mixture of toluene and hexane and were initially characterised through ^1H NMR spectroscopy (example spectrum given in **Figure 2.39**) and displayed a clear resonance at around -0.15 ppm which integrated to 3 against the imine proton; this shows that one equivalent of methyl ligand is retained and is consistent with the targeted monomer product. This was matched in all cases by a $^{13}\text{C}\{^1\text{H}\}$ resonance around -15 ppm for the methyl carbon. Elemental analysis (CHN) was again consistent with monomeric methyl complexes for $\text{Al}(\mathbf{A-E})\text{Me}$.



Scheme 2.11: Synthesis of Al(**A-E**)Me.

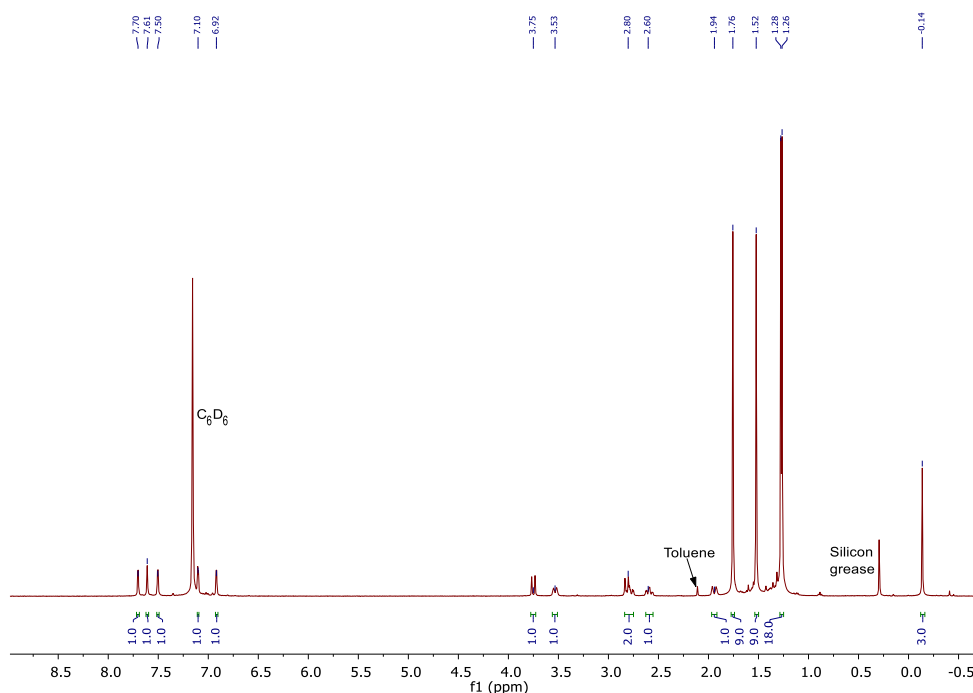


Figure 2.39: ^1H NMR (400 MHz, C_6D_6 , 298K) spectrum of Al(**A**)Me.

For Al(**A,B,E**)Me, the products were recrystallised from a mixture of toluene and hexane and solid-state structures were obtained (**Figure 2.40**). Unlike with iron complex Fe(**A**)Cl, the sulphur atom is uncoordinated in the aluminium analogue and a four-coordinate geometry was observed in all cases. This can be attributed to the disparity between the hard aluminium centre and the soft thioether donor. The geometric preference for a four-coordinate complex, τ_4' , was calculated from the two

largest coordination angles giving a number between 0 (square planar) and 1 (tetrahedral).^[91] All three complexes have a strong preference for tetrahedral geometry ($\tau_4' = 0.90 - 0.94$), with Al(B)Me ($R_1 = \text{H}$, $R_2 = t\text{-Bu}$) having the closest adherence to the ideal geometry ($\tau_4' = 0.94$), presumably as a result of low steric hindrance.

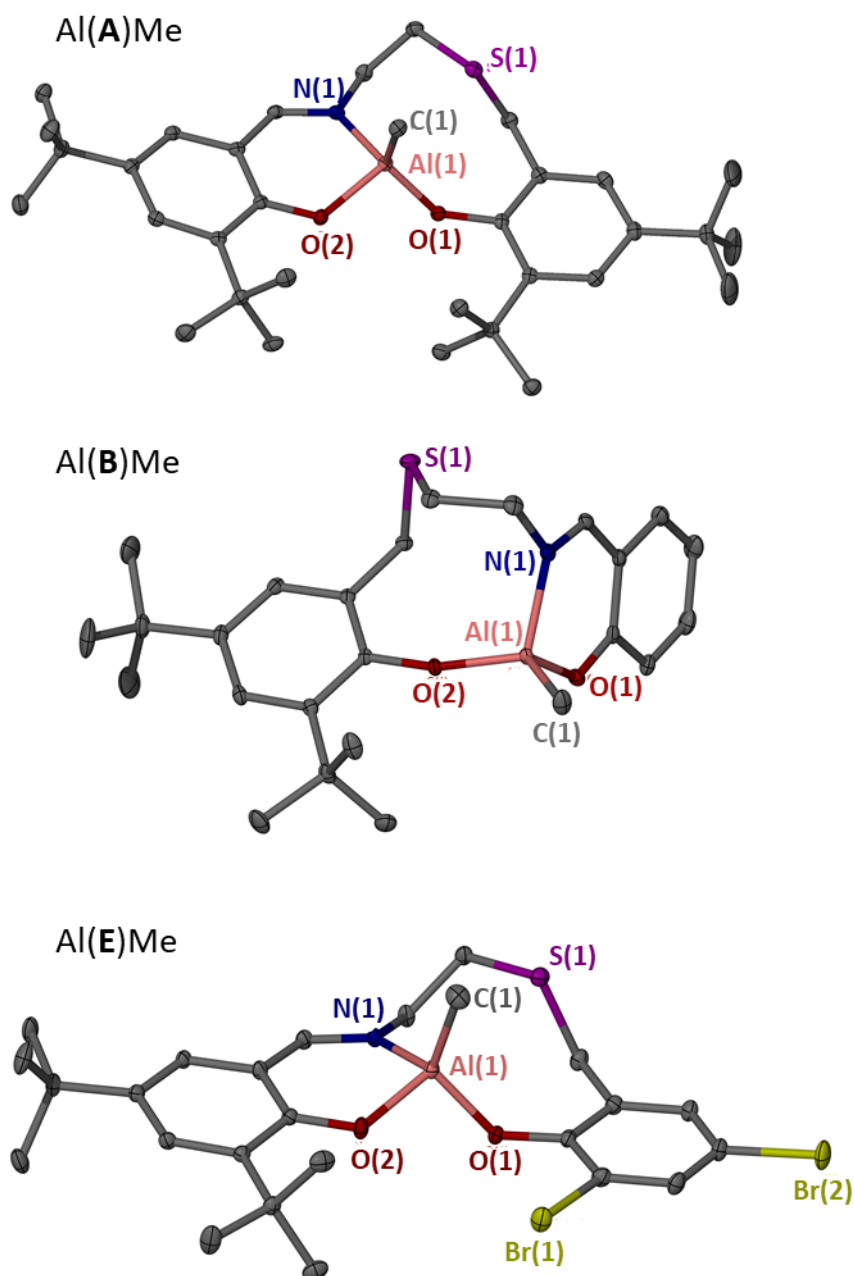


Figure 2.40: Solid state structures of Al(A,B,E)Me. Ellipsoids are shown at the 30% probability level. Hydrogen atoms have been removed for clarity.

Some key bond lengths and angles are shown in **Table 2.11**. As expected from the geometric preferences, the coordination bond angles for the aluminium complexes are all close to the ideal tetrahedral angle of 109.5° {102.85(10)° – 119.57(14)°}. The Al(1) – S(1) distance is 2.879 Å in Al(**E**)Me which is significantly longer than the Fe(1) – S(1) bond in Fe(**A**)Cl. Furthermore, this is longer than the sum of the van der Waals radii, suggesting that there is no bonding interaction and that even a hemilabile interaction is unlikely.

Table 2.11: Selected bond lengths [Å] and angles [°] for Al(**A,B,E**)Me and Al(**A**)Cl. X = Cl(1)/C(1).

	Al(A)Me	Al(B)Me	Al(E)Me	Al(A)Cl
τ_5	-	-	-	0.83
τ_4'	0.91	0.94	0.90	-
M–O(1)	1.7490(17)	1.7048(9)	1.747(2)	1.733(2)
M–O(2)	1.7990(18)	1.7593(10)	1.780(2)	1.788(2)
M–N(1)	1.975(2)	1.9403(12)	1.959(2)	1.951(2)
M–S(1)	-	-	-	2.6863(11)
M–X	1.958(2)	1.9415(15)	1.941(3)	2.1652(11)
O(1)–M–N(1)	111.57(8)	108.34(5)	108.27(11)	121.11(11)
O(2)–M–S(1)	-	-	-	170.80(8)
O(2)–M–X	102.85(10)	114.38(6)	109.46(14)	99.18(8)
N(1)–M–S(1)	-	-	-	85.40(7)
N(1)–M–X	117.03(10)	111.05(7)	119.57(14)	114.86(8)

One aluminium chloride complex, Al(**A**)Cl, was also synthesised to provide a non-paramagnetic analogue to Fe(**A**)Cl. A solid-state structure was obtained (**Figure 2.41**) and, interestingly, there is a bonding interaction between Al(1) and S(1) in this case leading to a five-coordinate complex with a strong tendency towards trigonal bipyramidal geometry ($\tau_5 = 0.83$), when compared with the iron complex. In comparison with the methyl complex, Al(**A**)Me, it is likely that the electronic effect of the chloride ligand reduces the electron density around the iron centre, facilitating sulphur coordination.

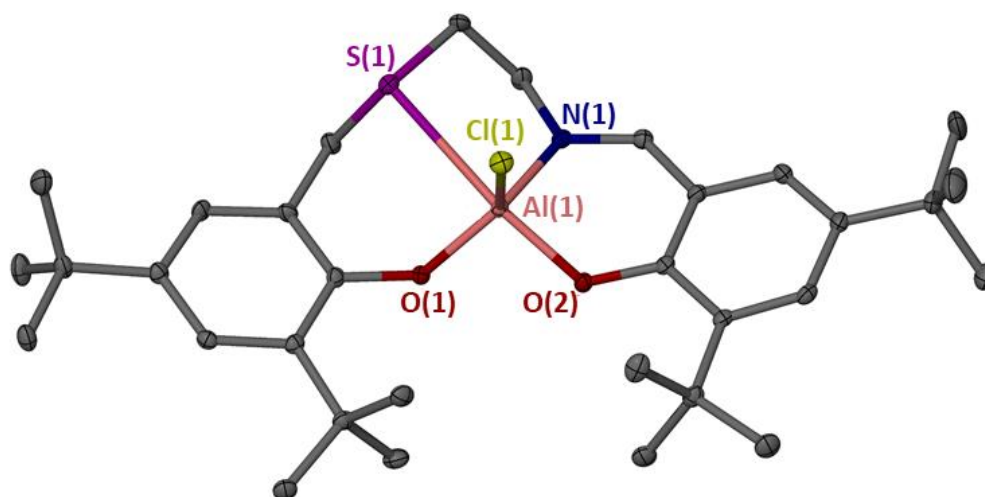


Figure 2.41: Solid state structure of Al(A)Cl. Ellipsoids are shown at the 30% probability level. Hydrogen atoms have been removed for clarity.

2.4.3 *Rac*-lactide polymerisation with Al(A-E)Me

Polymerisations were carried out in toluene with the addition of one equivalent of BnOH for the *in-situ* generation of the classical alkoxide initiating group (**Table 2.12**). Al(A)Me ($R_1 = R_2 = t\text{-Bu}$) achieved only 22% conversion of lactide after 48 h and high conversion was ultimately achieved after 240 h. The resulting polymer was isotactically inclined ($P_m = 0.69$) although significantly less stereoselective than the analogous iron (III) thioen complex. Furthermore, the control was reduced with aluminium and a broader dispersity ($\mathcal{D} = 1.12$) was observed alongside a significant disparity between measured and theoretical molecular weights ($M_n = 9800 \text{ g mol}^{-1}$, $M_{n \text{ theo.}} = 13350 \text{ g mol}^{-1}$).

Table 2.12: ROP of *rac*-lactide with Al(A-E)Me.

Init.	T/°C	Time /hours	Conv. % ^a	P _m ^b	M _n Calc. ^c	M _n ^d	Đ ^d
Al(A)Me	80	48	22	0.64	3300	-	-
Al(A)Me	80	240	92	0.69	13350	9800	1.12
Al(B)Me	80	5	60	0.56	8750	6350	1.06
Al(C)Me	80	5	69	0.58	10050	6650	1.06
Al(D)Me	80	5	72	0.58	10500	7600	1.05
Al(E)Me	80	72	84	0.72	12200	4750	1.09

Conditions: *rac*-LA (0.4 g), [LA]/[Fe]/[BnOH] = 100 : 1 : 1; ^a Determined by ¹H NMR spectroscopy; ^b Probability of isotactic enchainment, determined by ¹H{¹H} NMR spectroscopy; ^c Theoretical molecular weight calculated from conversion (rounded to the nearest 50): {[LA]/[I] × (Conversion × 144.13) / BnOH equiv.} + M_n(BnOH). ^d Determined from GPC (in THF) referenced against polystyrene standards, x 0.58 (rounded to the nearest 50).

Unsubstituted thioen complex Al(B)Me and halogenated analogues Al(C)Me and Al(D)Me all gave reasonable conversion after five hours. The activity follows the same trend as with the iron (III) thioen complexes where the unsubstituted complex is relatively active but gives the lowest stereocontrol ($P_m = 0.56$) and the two halogenated complexes are the most active and give intermediate isotacticity. Al(B-D)Me gave PLA with consistently narrow dispersities ($\text{Đ} = 1.05 - 1.06$) although there was significant disparity between calculated and measured molecular weights. The MALDI-ToF spectrum of the polymer produced by Al(B)Me showed entirely transesterified polymer through a repeating unit of 72 gmol^{-1} . The activity and stereoselectivity of the isomeric pair Al(D/E)Me mirrored that of their iron (III) counterparts with Al(D)Me ($R_1 = \text{Br}$, $R_2 = t\text{-Bu}$) being significantly more active than Al(E)Me ($R_1 = t\text{-Bu}$, $R_2 = \text{Br}$). The selectivity, however, was improved for Al(E)Me and this was the most isoselective aluminium initiator used in this study ($P_m = 0.72$). The polymer initiated by Al(E)Me gave a MALDI-ToF spectrum with three distinct series corresponding to linear polymer, transesterified polymer and polymer ionised by incidental potassium (**Figure 2.42**).

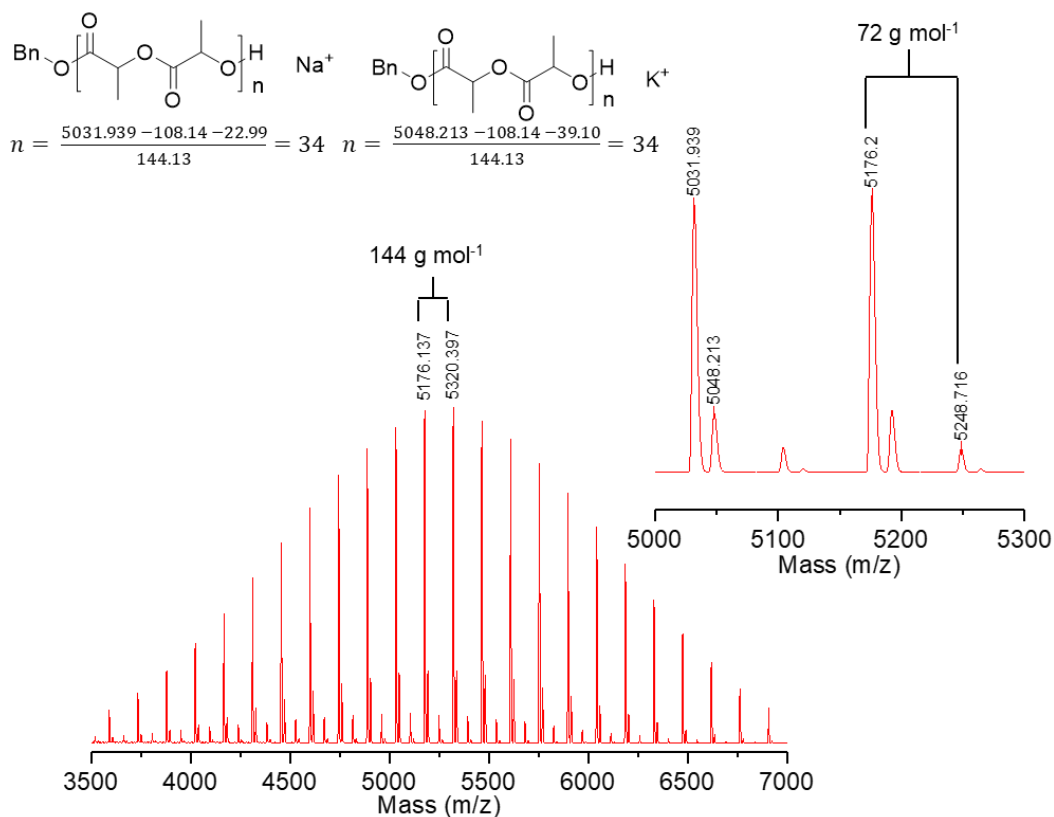


Figure 2.42: MALDI – ToF spectrum of PLA derived from Al(**E**)Me (80 °C, 72 hours) at a ratio of 100 : 1 : 1 ([LA]/[I]/[BnOH]) in toluene. M_n (GPC, corr.) = 4750 gmol⁻¹, M_n (Theo.) = 12200 gmol⁻¹. Main series is linear polymer with BnO + H end groups. Second most intense series shows ionisation by potassium. Transesterified series is also present.

2.4.4 Polymerisation kinetics with Al(**B**)Me

Batch kinetics were carried out for Al(**B**)Me and the semi-logarithmic plot can be seen in **Figure 2.43**. The non-zero intercept (-0.24219) suggests an induction period, after which lactide is consumed with a first-order dependence. The observed rate constant (0.00378 min⁻¹, $R^2 = 0.96$) is much lower than the iron (III) equivalent (Fe(**B**)Cl: 0.0166 min⁻¹, $R^2 = 0.99$) but does compare favourably with the equivalent aluminium salalen.^[110]

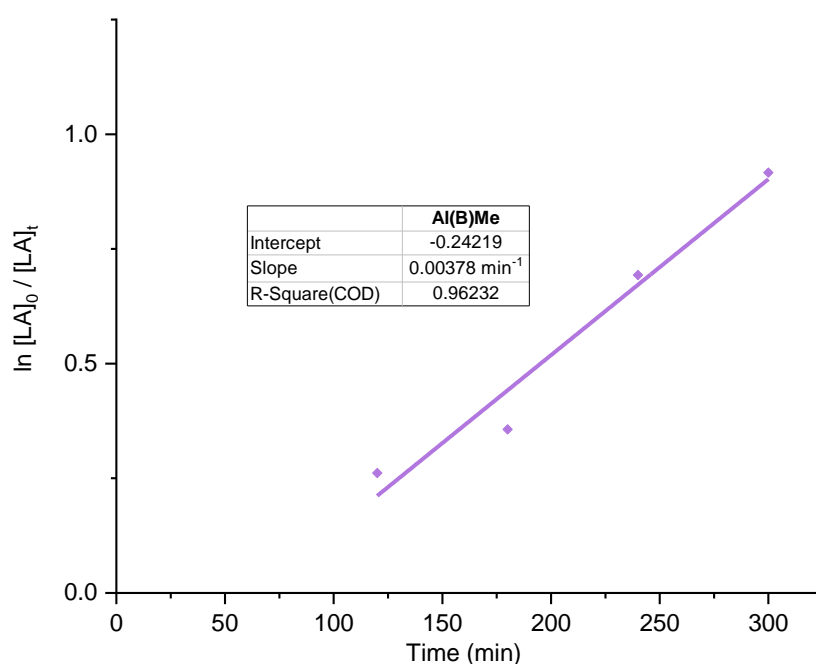


Figure 2.43: Semi-logarithmic plot of ROP of rac-LA with Al(B)Me.

2.4.5 Coordination study with Al(A)Cl

Figure 2.44 shows the ¹H NMR spectra of the sequential addition of BnOH and Et₃N to Al(A)Cl to help understand the role of Et₃N in the ROP of lactide initiated by iron complexes Fe(A–E)Cl (**Scheme 2.06**). Upon addition of BnOH, the CH₂ resonance around $\delta = 5.4$ ppm is split and an -OH resonance around $\delta = 4.3$ ppm is observed. This suggests that the BnOH molecule is coordinated in such a way as rotation is constrained but that deprotonation has not occurred. Upon addition of Et₃N, a broad resonance at $\delta = 5.1$ ppm is observed alongside the disappearance of the -OH peak. This confirms that Et₃N is necessary to fully form the alkoxy species and supports its use throughout the polymerisation studies with iron complexes (**Section 2.2**).

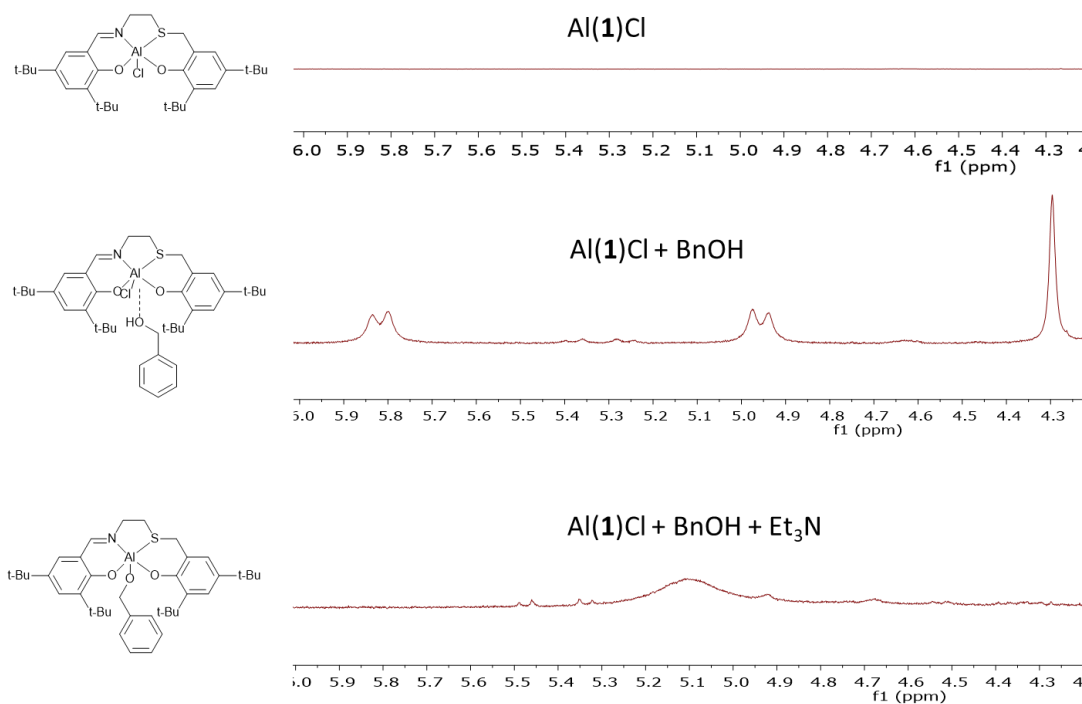


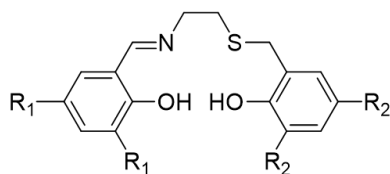
Figure 2.44: ^1H NMR spectra of $\text{Al}(\mathbf{A})\text{Cl}$ with addition of BnOH and Et_3N .

2.5 Summary and conclusions

The key findings from **Chapter 2** are summarised in **Figure 2.45**.

Iron complexes for lactide ROP

- Isoselective ROP with $\text{Fe}(\mathbf{A})\text{Cl}$ ($P_m = 0.89$, $T_m = 181^\circ\text{C}$)
- Thermal and spectrographic characterisation of isotactic PLA
- Reaction rates up to $k_{\text{app}} = 0.025 \text{ min}^{-1}$
- Reaction mechanism investigated



Iron complexes for CO_2 /epoxide coupling

- Complete selectivity to *cis*-CHC
- $\text{Fe}(\mathbf{E})\text{Cl}$ most active complex ($\text{TOF} < 156 \text{ h}^{-1}$)
- Thiolen complexes more active than salen equivalents
- Epoxide substrate scope demonstrated with $\text{Fe}(\mathbf{E})\text{Cl}$

Aluminium complexes for lactide ROP

- Less active and selective than iron analogues
- Al – S bonding influenced by auxiliary ligand
- MALDI-ToF showed high degree of transesterification

Figure 2.45: A summary of the key findings from **Chapter 2**.

Iron complexes Fe(**A–E**)Cl were synthesised and characterised through HR-MS, EA and single-crystal XRD, where possible. Crystals were obtained for Fe(**A**)Cl, [Fe(**A**)₂O] and [Fe(**A**)₂μ₂-CO₃], representing a rare example of atmospheric CO₂ activation through an oxo-bridged intermediate. A methoxy-bridged dimeric structure of the form [Fe(**C**)(μ-OMe)]₂ was also presented.

Fe(**A**)Cl gave highly isotactic PLA ($P_m = 0.89$) with an elevated melting temperature ($T_m = 181$ °C) and excellent control of the reaction was demonstrated in toluene at 80 °C with BnOH and Et₃N. The mechanism was explored and an activated monomer pathway was identified at low temperatures which could be suppressed through pre-activation. Isotactic polymer samples were analysed through ¹H{¹H} NMR, ¹³C{¹H} NMR, pXRD, DSC and TGA.

Fe(**B–E**)Cl polymerised lactide more rapidly than Fe(**A**)Cl, due to varying steric and electronic effects, and this was probed in a kinetic study. Fe(**D**)Cl was the most active giving high conversion after 0.5 hours at 80 °C. Initiators Fe(**B–E**)Cl were significantly less stereoselective than Fe(**A**)Cl and molecular weights tended to be lower than expected.

Fe(**A–E**)Cl and Fe(**A**)OAc were tested as catalysts for the coupling of CHO and CO₂. A high degree of selectivity towards *cis*-CHC was observed and a TOF value of 156 h⁻¹ was observed for Fe(**E**)Cl at 120 °C after six hours. The nature of the auxiliary ligand (Cl or OAc) had little impact on activity. In comparison with analogous salen ligands, thiolen complexes tended to be more active and this was proposed to be a result of a labile Fe-S bond facilitating epoxide binding. With Fe(**E**)Cl, eight equivalents of TBAC were shown to be necessary to achieve full selectivity to *cis*-CHC. A substrate scope showed that terminal epoxides and electron donating groups lead to greater activity than seen with CHO.

Al(**A–E**)Me and Al(**A**)Cl were synthesised and characterised through ¹H NMR, ¹³C NMR and single crystal XRD for Al(**A,B,E**)Me and Al(**A**)Cl. Methyl complexes were shown to have four coordinate geometries with a tetrahedral preference and no Al – S bonding. By contrast, Al(**A**)Cl was five-coordinate, suggesting that metal – sulphur bonding can be influenced by the auxiliary ligand. In comparison with the iron complexes, all

aluminium initiators were slower, less stereoselective and less controlled in terms of molecular weight. MALDI-ToF analysis showed a degree of transesterified polymer in the sample.

2.6 References

- [1] E. D. Cross, L. E. N. Allan, A. Decken, M. P. Shaver, *J. Polym. Sci. Part A Polym. Chem.* **2013**, *51*, 1137–1146.
- [2] Y. Liang, R. L. Duan, C. Y. Hu, L. L. Li, X. Pang, W. X. Zhang, X. S. Chen, *Chinese J. Polym. Sci. (English Ed.)* **2018**, *36*, 185–189.
- [3] Y. Cui, D. Li, B. Gao, Y. Zhou, L. Chen, B. Qiu, Y. Li, Q. Duan, N. Hu, *J. Coord. Chem.* **2016**, *69*, 656–667.
- [4] R. Duan, C. Hu, X. Li, X. Pang, Z. Sun, X. Chen, X. Wang, *Macromolecules* **2017**, *50*, 9188–9195.
- [5] N. Nomura, R. Ishii, Y. Yamamoto, T. Kondo, *Chem. - A Eur. J.* **2007**, *13*, 4433–4451.
- [6] B. Gao, D. Li, Y. Li, Q. Duan, R. Duan, X. Pang, *New J. Chem.* **2015**, *39*, 4670–4675.
- [7] Z. Zhong, P. J. Dijkstra, J. Feijen, *Angew. Chemie - Int. Ed.* **2002**, *41*, 4510–4513.
- [8] M. Cozzolino, V. Leo, C. Tedesco, M. Mazzeo, M. Lamberti, *Dalton Trans.* **2018**, *47*, 13229–13238.
- [9] P. McKeown, M. G. Davidson, J. P. Lowe, M. F. Mahon, L. H. Thomas, T. J. Woodman, M. D. Jones, *Dalton Trans.* **2016**, *45*, 5374–5387.
- [10] H. Du, A. H. Velders, P. J. Dijkstra, J. Sun, Z. Zhong, X. Chen, J. Feijen, *Chem. – A Eur. J.* **2009**, *15*, 9836–9845.
- [11] M. D. Jones, L. Brady, P. McKeown, A. Buchard, P. M. Schäfer, L. H. Thomas, M. F. Mahon, T. J. Woodman, J. P. Lowe, *Chem. Sci.* **2015**, *6*, 5034–5039.
- [12] K. Press, I. Goldberg, M. Kol, *Angew. Chemie - Int. Ed.* **2015**, *54*, 14858–14861.
- [13] P. McKeown, J. Brown-Humes, M. G. Davidson, M. F. Mahon, T. J. Woodman, M. D. Jones, *Dalton Trans.* **2017**, *46*, 5048–5057.
- [14] Y.-L. Duan, Z.-J. Hu, B.-Q. Yang, F.-F. Ding, W. Wang, Y. Huang, Y. Yang, *Dalton Trans.* **2017**, *46*, 11259–11270.
- [15] P. McKeown, M. G. Davidson, G. Kociok-Kohn, M. D. Jones, *Chem. Commun.* **2016**, *3*, 10431–10434.
- [16] A. Pilone, N. De Maio, K. Press, V. Venditto, D. Pappalardo, M. Mazzeo, C. Pellicchia, M. Kol, M. Lamberti, *Dalton Trans.* **2015**, *44*, 2157–2165.
- [17] A. Stopper, T. Rosen, V. Venditto, I. Goldberg, M. Kol, *Chem. - A Eur. J.* **2017**, *23*, 11540–11548.
- [18] S. M. Kirk, G. Kociok-Köhn, M. D. Jones, *Organometallics* **2016**, *35*, 3837–3843.
- [19] R. Lapenta, A. Buonerba, A. De Nisi, M. Monari, A. Grassi, S. Milione, C. Capacchione, *Inorg. Chem.* **2017**, *56*, 3447–3458.
- [20] A. Stopper, J. Okuda, M. Kol, *Macromolecules* **2012**, *45*, 698–704.

- [21] A. Stopper, K. Press, J. Okuda, I. Goldberg, M. Kol, *Inorg. Chem.* **2014**, *53*, 9140–9150.
- [22] B. Han, L. Zhang, S. J. Kyran, B. Liu, Z. Duan, D. J. Darensbourg, *J. Polym. Sci. Part A Polym. Chem.* **2016**, *54*, 1938–1944.
- [23] B. Han, L. Zhang, M. Yang, B. Liu, X. Dong, P. Theato, *Macromolecules* **2016**, *49*, 6232–6239.
- [24] M. Wang, J. Huang, Y. Xu, B. Han, Z. Duan, *Polym. Int.* **2019**, *68*, 1704–1709.
- [25] Q. Zhou, H. Liang, Y. Long, Q. Wu, H. Gao, *J. Organomet. Chem.* **2015**, *798*, 347–353.
- [26] R. P. Pawar, S. U. Tekale, S. U. Shisodia, J. T. Totre, A. J. Domb, *Rec. Pat. Regen. Med.* **2014**, *4*, 40–51.
- [27] B. J. O’Keefe, S. M. Monnier, M. A. Hillmyer, W. B. Tolman, *J. Am. Chem. Soc.* **2001**, *123*, 339–340.
- [28] B. J. O’Keefe, L. E. Breyfogle, M. A. Hillmyer, W. B. Tolman, *J. Am. Chem. Soc.* **2002**, *124*, 4384–4393.
- [29] M. Stolt, A. Södergård, *Macromolecules* **1999**, *32*, 6412–6417.
- [30] X. Wang, K. Liao, D. Quan, Q. Wu, *Macromolecules* **2005**, *38*, 4611–4617.
- [31] P. McKeown, M. D. Jones, O. J. Driscoll, M. F. Mahon, C. K. C. Leung, *Eur. J. Inorg. Chem.* **2018**, *2018*, 5129–5135.
- [32] O. J. Driscoll, C. H. Hafford-Tear, P. McKeown, J. A. Stewart, G. Kociok-Köhn, M. F. Mahon, M. D. Jones, *Dalton Trans.* **2019**, *48*, 15049–15058.
- [33] O. J. Driscoll, C. H. Hafford-Tear, P. McKeown, J. A. Stewart, G. Kociok-Köhn, M. F. Mahon, M. D. Jones, *Dalton Trans.* **2019**, *48*, 15049–15058.
- [34] D. S. McGuinness, E. L. Marshall, V. C. Gibson, J. W. Steed, *J. Polym. Sci. Part A Polym. Chem.* **2003**, *41*, 3798–3803.
- [35] A. B. Biernesser, B. Li, J. A. Byers, *J. Am. Chem. Soc.* **2013**, *135*, 16553–16560.
- [36] A. B. Biernesser, K. R. D. Chiaie, J. B. Curley, J. A. Byers, *Angew. Chemie - Int. Ed.* **2016**, *55*, 5251–5254.
- [37] M. Qi, Q. Dong, D. Wang, J. A. Byers, *J. Am. Chem. Soc.* **2018**, *140*, 5686–5690.
- [38] U. Herber, K. Hegner, D. Wolters, R. Siris, K. Wrobel, A. Hoffmann, C. Lochenie, B. Weber, D. Kuckling, S. Herres-Pawlis, *Eur. J. Inorg. Chem.* **2017**, *2017*, 1341–1354.
- [39] R. D. Rittinghaus, P. M. Schäfer, P. Albrecht, C. Conrads, A. Hoffmann, A. N. Ksiazkiewicz, O. Bienemann, A. Pich, S. Herres-Pawlis, *ChemSusChem* **2019**, *12*, 2161–2165.
- [40] P. Marin, M. J. L. Tschan, F. Isnard, C. Robert, P. Haquette, X. Trivelli, L. M. Chamoreau, V. Guérineau, I. del Rosal, L. Maron, V. Venditto, C. M. Thomas, *Angew. Chemie - Int. Ed.* **2019**, *58*, 1–6.
- [41] A. Stopper, J. Okuda, M. Kol, *Macromolecules* **2012**, *45*, 698–704.

- [42] T. Glaser, T. Lügger, R.-D. Hoffmann, *Eur. J. Inorg. Chem.* **2004**, *2004*, 2356–2362.
- [43] J. A. Castro-Osma, M. North, W. K. Offermans, W. Leitner, T. E. Müller, *ChemSusChem* **2016**, *9*, 791–794.
- [44] Y. Sun, Y. Cui, J. Xiong, Z. Dai, N. Tang, J. Wu, *Dalton Trans.* **2015**, *44*, 16383–16391.
- [45] J. Shao, S. Xiang, X. Bian, J. Sun, G. Li, X. Chen, *Ind. Eng. Chem. Res.* **2015**, *54*, 150206115046006.
- [46] C. Zhang, Q. Lan, T. Zhai, S. Nie, J. Luo, W. Yan, *Polymers (Basel)*. **2018**, *10*, 1181.
- [47] C. Song, *Catal. Today* **2006**, *115*, 2–32.
- [48] J. Artz, T. E. Müller, K. Thenert, J. Kleinekorte, R. Meys, A. Sternberg, A. Bardow, W. Leitner, *Chem. Rev.* **2018**, *118*, 434–504.
- [49] Y. Chen, Z. Wang, Z. Zhong, *Renew. Energy* **2019**, *131*, 208–216.
- [50] M. Mikkelsen, M. Jørgensen, F. C. Krebs, *Energy Environ. Sci.* **2010**, *3*, 43–81.
- [51] M. Cokoja, C. Bruckmeier, B. Rieger, W. A. Herrmann, F. E. Kühn, *Angew. Chemie - Int. Ed.* **2011**, *50*, 8510–8537.
- [52] A. M. Appel, J. E. Bercaw, A. B. Bocarsly, H. Dobbek, D. L. Dubois, M. Dupuis, J. G. Ferry, E. Fujita, R. Hille, P. J. A. Kenis, C. A. Kerfeld, R. H. Morris, C. H. F. Peden, A. R. Portis, S. W. Ragsdale, T. B. Rauchfuss, J. N. H. Reek, L. C. Seefeldt, R. K. Thauer, G. L. Waldrop, *Chem. Rev.* **2013**, *113*, 6621–6658.
- [53] Z. Zhang, Y. Zhu, T. Yang, L. Li, H. Zhu, H. Wang, *J. Clean. Prod.* **2017**, *141*, 463–471.
- [54] C. V Miguel, M. A. Soria, A. Mendes, L. M. Madeira, *J. Nat. Gas Sci. Eng.* **2015**, *22*, 1–8.
- [55] M. Sharifzadeh, L. Wang, N. Shah, *Renew. Sustain. Energy Rev.* **2015**, *47*, 151–161.
- [56] A. S. Lindsey, H. Jeskey, *Chem. Rev.* **1957**, *57*, 583–620.
- [57] D. J. Darensbourg, *Chem. Rev.* **2007**, *107*, 2388–2410.
- [58] G. W. Coates, D. R. Moore, *Angew. Chemie - Int. Ed.* **2004**, *43*, 6618–6639.
- [59] D. J. Darensbourg, M. W. Holtcamp, *Coord. Chem. Rev.* **1996**, *153*, 155–174.
- [60] M. R. Kember, A. Buchard, C. K. Williams, *Chem. Commun.* **2011**, *47*, 141–163.
- [61] A. Decortes, A. M. Castilla, A. W. Kleij, *Angew. Chemie - Int. Ed.* **2010**, *49*, 9822–9837.
- [62] P. P. Pescarmona, M. Taherimehr, *Catal. Sci. Technol.* **2012**, *2*, 2169–2187.
- [63] M. Cokoja, M. E. Wilhelm, M. H. Anthofer, W. A. Herrmann, F. E. Kühn, *ChemSusChem* **2015**, *8*, 2436–2454.
- [64] J. H. Clements, *Ind. Eng. Chem. Res.* **2003**, *42*, 663–674.
- [65] B. Schäffner, F. Schäffner, S. P. Verevkin, A. Börner, *Chem. Rev.* **2010**, *110*, 4554–4581.

- [66] H. L. Parker, J. Sherwood, A. J. Hunt, J. H. Clark, *ACS Sustain. Chem. Eng.* **2014**, *2*, 1739–1742.
- [67] A. Ponrouch, E. Marchante, M. Courty, J.-M. Tarascon, M. R. Palacín, *Energy Environ. Sci.* **2012**, *5*, 8572–8583.
- [68] D. Aurbach, K. Gamolsky, B. Markovsky, Y. Gofer, M. Schmidt, U. Heider, *Electrochim. Acta* **2002**, *47*, 1423–1439.
- [69] L. Wang, C. E. Kefalidis, S. Sinbandhit, V. Dorcet, J.-F. Carpentier, L. Maron, Y. Sarazin, *Chem. - A Eur. J.* **2013**, *19*, 13463–13478.
- [70] D. J. Darensbourg, O. Karroonnirun, S. J. Wilson, *Inorg. Chem.* **2011**, *50*, 6775–6787.
- [71] I. Palard, M. Schappacher, B. Belloncle, A. Soum, S. M. Guillaume, *Chem. - A Eur. J.* **2007**, *13*, 1511–1521.
- [72] M. Cozzolino, T. Rosen, I. Goldberg, M. Mazzeo, M. Lamberti, *ChemSusChem* **2017**, *10*, 1217–1223.
- [73] M. Taherimehr, P. P. Pescarmona, *J. Appl. Polym. Sci.* **2014**, *131*, 41141.
- [74] A. Buchard, M. R. Kember, K. G. Sandeman, C. K. Williams, *Chem. Commun.* **2011**, *47*, 212–214.
- [75] D. J. Darensbourg, P. Bottarelli, J. R. Andreatta, *Macromolecules* **2007**, *40*, 7727–7729.
- [76] F. Della Monica, A. Buonerba, C. Capacchione, *Adv. Synth. Catal.* **2019**, *361*, 265–282.
- [77] K. A. Andrea, F. M. Kerton, *Polym. J.* **2021**, *53*, 29–46.
- [78] D. Alhashmialameer, J. Collins, K. Hattenhauer, F. M. Kerton, *Catal. Sci. Technol.* **2016**, *6*, 5364–5373.
- [79] K. A. Andrea, E. D. Butler, T. R. Brown, T. S. Anderson, D. Jagota, C. Rose, E. M. Lee, S. D. Goulding, J. N. Murphy, F. M. Kerton, C. M. Kozak, *Inorg. Chem.* **2019**, *58*, 11231–11240.
- [80] A. S. Abu-surrah, H. A. N. Abu-shehab, Hamzeh M Abdel-halim, *Transit. Met. Chem.* **2017**, *42*, 117–122.
- [81] K. A. Andrea, T. R. Brown, J. N. Murphy, D. Jagota, D. Mckearney, C. M. Kozak, F. M. Kerton, *Inorg. Chem.* **2018**, *57*, 13494–13504.
- [82] V. Paradiso, V. Capaccio, D. H. Lamparelli, C. Capacchione, *Catalysts* **2020**, *10*, 825.
- [83] A. Buonerba, A. De Nisi, A. Grassi, S. Milione, C. Capacchione, B. Rieger, *Catal. Sci. Technol.* **2015**, *5*, 118–123.
- [84] F. Della Monica, M. Leone, A. Buonerba, A. Grassi, S. Milione, C. Capacchione, *Mol. Catal.* **2018**, *460*, 46–52.
- [85] F. Della Monica, B. Maity, T. Pehl, A. Buonerba, A. De Nisi, M. Monari, A. Grassi, B. Rieger, L. Cavallo, C. Capacchione, *ACS Catal.* **2018**, *8*, 6882–6893.

- [86] F. Della Monica, A. Buonerba, V. Paradiso, S. Milione, A. Grassi, C. Capacchione, *Adv. Synth. Catal.* **2019**, *361*, 283–288.
- [87] O. J. Driscoll, J. A. Stewart, P. McKeown, M. D. Jones, *New J. Chem.* **2020**, *44*, 6063–6067.
- [88] O. J. Driscoll, *The Synthesis and Application of Metal-Based Complexes for Sustainable Catalysis*, University of Bath, **2022**.
- [89] R. Jianming, X. Anguo, W. Hongwei, Y. Hailin, *Des. Monomers Polym.* **2014**, *17*, 345–355.
- [90] X. Pang, R. Duan, X. Li, C. Hu, X. Wang, X. Chen, *Macromolecules* **2018**, *51*, 906–913.
- [91] N. Spassky, M. Wisniewski, C. Pluta, A. L. Borgne, *Macromol. Chem. Phys.* **1996**, *197*, 2627–2637.
- [92] M. Wisniewski, A. Le Borgne, N. Spassky, *Macromol. Chem. Phys.* **1997**, *198*, 1227–1238.
- [93] P. Hormnirun, E. L. Marshall, V. C. Gibson, A. J. P. White, D. J. Williams, *J. Am. Chem. Soc.* **2004**, *126*, 2688–2689.
- [94] J. Beament, M. F. Mahon, A. Buchard, M. D. Jones, *Organometallics* **2018**, *37*, 1719–1724.
- [95] E. L. Whitelaw, G. Loraine, M. F. Mahon, M. D. Jones, *Dalton Trans.* **2011**, *40*, 11469–11473.
- [96] T. M. Ovitt, G. W. Coates, *J. Am. Chem. Soc.* **1999**, *121*, 4072–4073.
- [97] P. Hormnirun, E. L. Marshall, V. C. Gibson, R. I. Pugh, A. J. P. White, *Proc. Natl. Acad. Sci. U. S. A.* **2006**, *103*, 15343–15348.
- [98] H. L. Chen, S. Dutta, P. Y. Huang, C. C. Lin, *Organometallics* **2012**, *31*, 2016–2025.
- [99] N. Maudoux, T. Roisnel, V. Dorcet, J.-F. Carpentier, Y. Sarazin, *Chem. – A Eur. J.* **2014**, *20*, 6131–6147.
- [100] H. Zhang, B. Gao, G. Huang, D. Li, X. Pang, *J. Coord. Chem.* **2021**, *74*, 1641–1650.
- [101] H.-L. Chen, S. Dutta, P.-Y. Huang, C.-C. Lin, *Organometallics* **2012**, *31*, 2016–2025.
- [102] J. Beament, M. F. Mahon, A. Buchard, M. D. Jones, *New J. Chem.* **2017**, *41*, 2198–2203.
- [103] L. Britton, D. Ditz, J. Beament, P. McKeown, H. C. Quilter, K. Riley, M. F. Mahon, M. D. Jones, *Eur. J. Inorg. Chem.* **2019**, *2019*, 2768–2773.
- [104] A. Yeori, S. Gendler, S. Groysman, I. Goldberg, M. Kol, *Inorg. Chem. Commun.* **2004**, *7*, 280–282.
- [105] S. L. Hancock, M. F. Mahon, M. D. Jones, *Dalton Trans.* **2013**, *42*, 9279–9285.
- [106] A. Pilone, K. Press, I. Goldberg, M. Kol, M. Mazzeo, M. Lamberti, *J. Am. Chem. Soc.* **2014**, *136*, 2940–2943.

- [107] S. Gesslbauer, H. Cheek, A. J. P. White, C. Romain, *Dalton Trans.* **2018**, 47, 10410–10414.
- [108] S. Gesslbauer, R. Savela, Y. Chen, A. J. P. White, C. Romain, *ACS Catal.* **2019**, 9, 7912–7920.
- [109] J. Payne, P. McKeown, G. Kociok-Köhn, M. D. Jones, *Chem. Commun.* **2020**, 56, 7163–7166.
- [110] M. A. Bahili, E. C. Stokes, R. C. Amesbury, D. M. C. Ould, B. Christo, R. J. Horne, B. M. Kariuki, J. A. Stewart, R. L. Taylor, P. A. Williams, M. D. Jones, K. D. M. Harris, B. D. Ward, *Chem. Commun.* **2019**, 55, 7679–7682.
- [111] E. L. Whitelaw, G. Loraine, M. F. Mahon, M. D. Jones, *Dalton Trans.* **2011**, 40, 11469–11473.

Chapter 3: Zinc ONS complexes for the production and degradation of polyesters

3.1 Introduction – zinc complexes for lactide polymerisation

Simple zinc salts were first applied to the polymerisation of lactide in 1985 by McNeill and Leiper who examined the effect of polymerisation time as well as the degradation properties of the resultant polylactides (**Figure 3.01**).^[1] The first ligated, single-site zinc initiator was published by Phomphrai using trispyrazolyl- and trisindazolylborate ligands.^[2] Reaction times were long compared to the equivalent magnesium analogues with zinc complexes taking up to six days to reach high conversion. Coates *et al.* introduced zinc initiators based on β -diiminato ligands that were significantly more active than previous zinc initiators for lactide ROP (**88**, 95% conversion, 20 minutes).^[3] A strong heterotactic preference was also observed with **88** ($P_m = 0.94$) particularly at low temperatures ($T = 0\text{ }^\circ\text{C}$). Tolman subsequently reported a diamino monophenol ligand, zinc complexes of which polymerised *rac*-lactide to molecular weights exceeding $100,000\text{ gmol}^{-1}$ in under 20 minutes at room temperature (**89**).^[4]

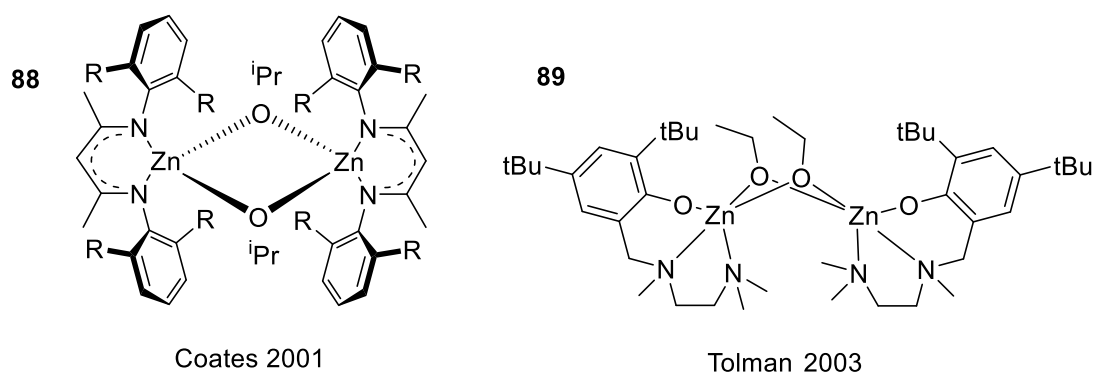


Figure 3.01: Early examples of zinc (II) initiators for lactide ROP.^[3,4]

Schaper and co-workers introduced chiral β -diketiminato ligands to form enantiopure *S,S*-*nacnac* ZnEt complexes (**Figure 3.02**).^[5] Complex **90** produced heterotactic PLA ($P_r = 0.84 - 0.88$) at room temperature through a chain end control mechanism despite the chirality in the ligand framework. This was determined through polarimetric analysis of the remaining *rac*-lactide at 75 % conversion which showed no enantiomeric excess. It was proposed that free rotation around the C-N

bond nullified the effect of chirality and instead induced stereoselectivity through steric bulk. More recent work from the same group increased the steric bulk further by adding N-anthrylmethyl groups.^[6] Complex **91** was predictably slower than the less hindered analogues (95 %, 6 h, 23 °C) but did show increased heteroselectivity ($P_r = 0.93$). This is in keeping with the general trend of increasing the steric bulk having a deleterious effect on activity and a positive effect on stereoselectivity of polymerisation.

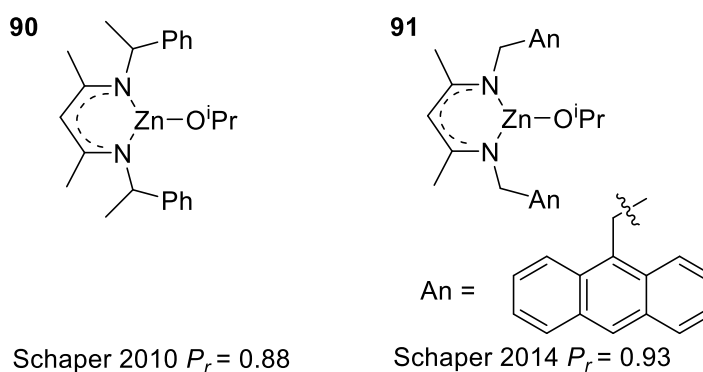


Figure 3.02: β -diketiminato zinc (II) complexes for lactide ROP reported by Schaper *et al.*^[5,6]

Darrensbourg and Karroonnirun published structural variations of the ligand used by Tolman in complex **89**.^[7] Starting from amino-acid precursors allowed the introduction of chiral substituents in the backbone and the resulting complexes were isolated as mononuclear trimethylsilyl amide species (**Figure 3.03**). Reaction times for **92** were significantly extended (≤ 24 h) but the heteroselectivity was increased compared to the Tolman system ($P_r = 0.89$) albeit requiring very low temperatures to achieve this.

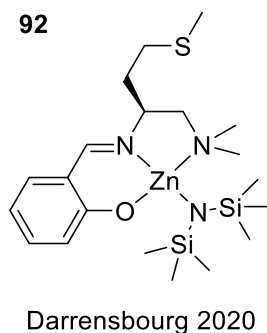


Figure 3.03: Amino acid-based zinc(II) complex for lactide ROP.^[7]

Ma and co-workers have reported various aminophenolate zinc complexes looking at various aspects of chirality and substitution (**Figure 3.04**).^[8–11] A range of ten tetradentate proligands were initially prepared and the trimethylsilyl amine zinc complexes were synthesised.^[8] Most complexes were active at ambient temperatures at high initiator loading ($[LA]/[Zn]/[iOPr] = 200 : 1 : 1$) giving mostly atactic PLA. However, chlorinated analogues such as **93** had a heterotactic bias ($P_m \geq 0.33$). A subsequently published enantiopure analogue, **94**, polymerised lactide with an isotactic bias ($P_m \leq 0.84$), significantly outperforming the other initiators in the study which were present as a mix of diastereomers.^[9] Although, extended reaction times and very low temperatures (56 h, $-38\text{ }^\circ\text{C}$) were required to achieve this selectivity. The diastereoselective synthesis of pyrrolidinyl amino phenolate ligands was further explored.^[11] It was found that substitution at the *ortho*-phenolate, pyrrolidinyl N atom and auxiliary ligand could push the synthesis towards one or other diastereomer and some isotacticity was observed ($P_m \leq 0.81$).

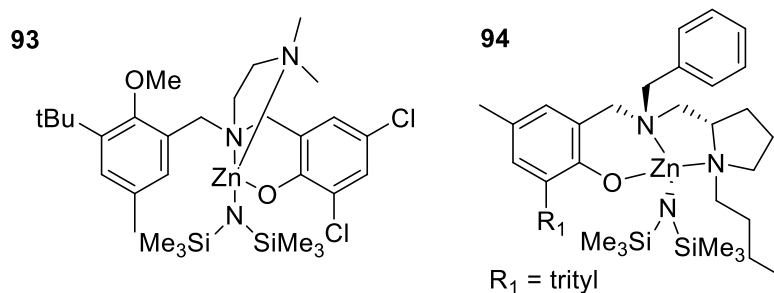


Figure 3.04: Aminophenolate initiators from Ma *et al.*^[8,9]

Further work from Ma attained multiblock isotactic PLA with both chiral oxazolinyl and achiral benzoxazolinyl complexes (**Figure 3.05**).^[12] Chiral complex **95**, gave highly isotactic PLA ($P_m \leq 0.93$) at extremely low temperature (-40 °C), although a strong isotactic bias was maintained at room temperature with relatively low initiator loading ($P_m = 0.87$, $[LA]/[I]/[BnOH] = 1500 : 1 : 1$). Achiral analogue **96** also produced highly isotactic PLA ($P_m = 0.92$) suggesting that chirality is not essential for stereoselective polymerisation, in this case. The range of achiral benzoxazolinyl complexes was expanded to give initiators that furnished atactic to isotactic PLA with relatively high activity at room temperature ($P_m = 0.40 - 0.89$).^[13] Again, the phenolate *ortho*- substituent was found to be paramount when controlling stereospecificity. The introduction of a benzoimidazolyl pendant allowed activity to be increased whilst maintaining high isoselectivity ($P_m \leq 0.93$).^[14] Complex **97** (**Figure 3.06**) was tested at low initiator loading ($[LA]/[I]:[PrOH] = 5000 : 1 : 50$) and reached high conversion after 23 minutes at 110 °C with a TOF value in excess of 11,000 h⁻¹. Some isoselectivity was retained under these conditions ($P_m = 0.78$).

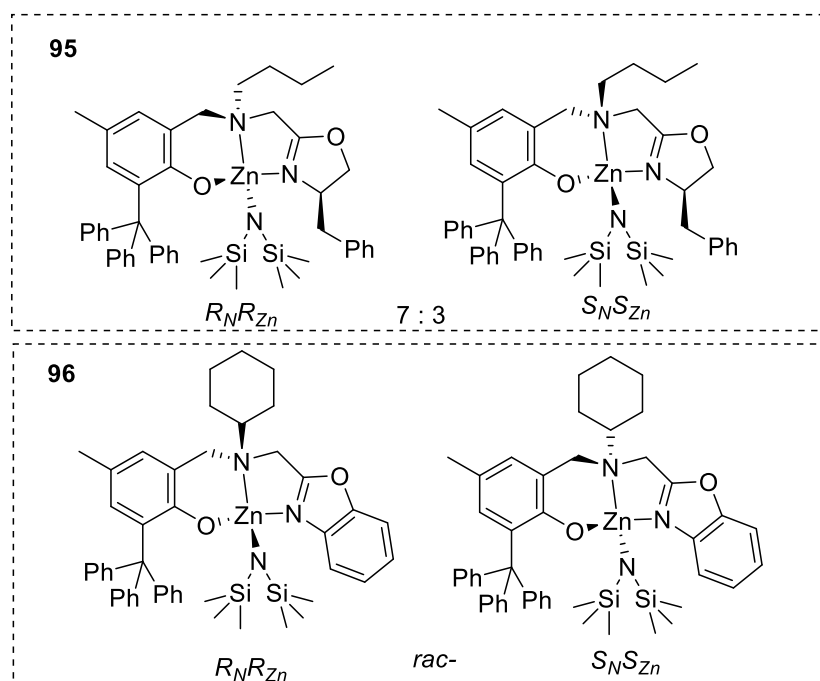


Figure 3.05: Highly isotactic Zn(II) initiators for lactide ROP from Ma *et al.*^[12]

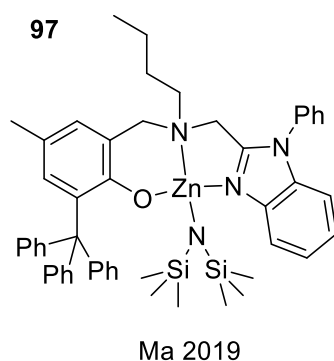


Figure 3.06: Highly active aminophenolate zinc complex.^[14]

Zinc (II) scorpionate complexes were first applied to lactide polymerisation by Otero *et al.* who synthesised nine {NNN} ethyl zinc analogues of which three were active for lactide ROP (**Figure 3.07**).^[15] Initiation was slow, taking up to two days to achieve high conversion with a slight isotactic bias ($P_m \leq 0.68$). Subsequent publications explored {NNO} scorpionate ligands based on bis(pyrazol-1-yl)ethyl with variation and chirality introduced at the ethyl position.^[16–19] The 1:1 reaction between a chiral scorpionate ligand and $ZnEt_2$, **98**, gave moderately heterotactic PLA ($P_r = 0.77$) after three hours at 50 °C, significantly outperforming the mononuclear equivalent.^[16] The 2 : 1 ([Zn]/[L]) reaction with similar ligands gave binuclear complexes including **99** which exhibited an isotactic preference ($P_m = 0.74$) through an enantiomeric site control mechanism.^[17] Interestingly, the mononuclear structure was accessed through the use of zinc with a bulky aminotrimethylsilyl ancillary ligand and furnished PLA with a heterotactic bias ($P_r = 0.78$).^[20] The introduction of a dimethylaminophenyl substituent allowed the synthesis of mononuclear and binuclear complexes of the form $LZnMe$ and LZn_2Me_3 .^[19] The binuclear complex **100** reached high conversion after just two minutes at 60 °C, quicker than the mononuclear counterpart, however, the latter had a slight heterotactic bias ($P_r = 0.68$).

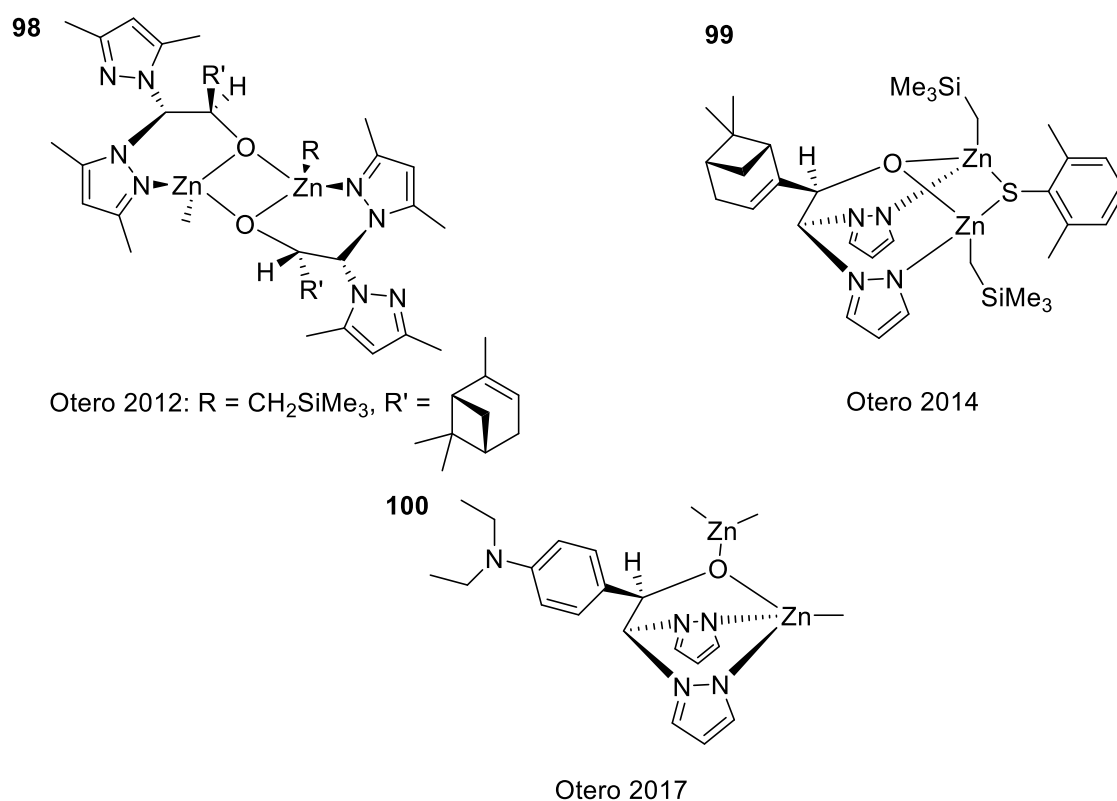


Figure 3.07: Heteroscorpionate zinc (II) complexes reported by Otero *et al.*^[16,17,19]

Cui and co-workers introduced zwitterionic zinc (II) complexes based on heteroscorpionate ligands with appended iminophosphine groups (**Figure 3.08**).^[21] A variety of labile groups were investigated and were shown to have an impact on activity and stereoselectivity. Alkyl or Cl groups gave slow reaction times with a degree of heteroselectivity (**101**: $P_r \leq 0.64$) whereas bulky amido and benzyl alkoxide groups provided higher activity and isoselectivity. In particular, the complex bearing an N(SiHMe₂)₂ group (**102**) gave isotactic PLA with an elevated melting temperature, indicative of a degree of stereocomplex interaction ($P_m = 0.85$, $T_m = 167.4$ °C). Chain end control was postulated based on experiments with enantiopure *L*- and *D*-lactides.

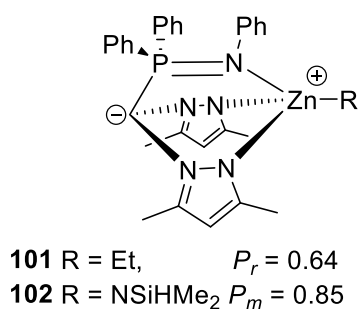
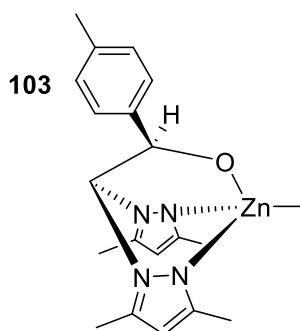


Figure 3.08: Zwitterionic zinc(II) iminophosphine complexes for lactide ROP.^[21]

A simple {NNO} zinc scorpionate methyl complex (**103**) was shown to polymerise lactide without the need for a co-initiator through a ligand-assisted coordination-insertion mechanism (**Figure 3.09**).^[22] The polymerisation of *D*-, *L*- and *rac*- lactides were demonstrated in 45 – 120 minutes at 70 °C with reasonable agreement between theoretical and measured molecular weights and broad dispersities ($\mathcal{D} = 1.36 - 2.19$). Importantly, highly stereocomplexed isotactic PLA was achieved through sequential addition of monomers giving elevated melting temperatures up to 215.33 °C and P_m value up to 0.95.



Hermida-Merino 2022

Figure 3.09: Tolyl substituted heteroscorpionate complex.^[22]

Tetradentate {ONNN} complexes described by Kol *et al.* (**Figure 3.10**) gave well controlled polymerisation of *rac*-lactide at room temperature in 10 – 120 minutes.^[23] It was found that pre-reacting the initiators with benzyl alcohol led to an increase in activity, presumably indicating an initiation period in which the benzoxy complex is

formed. The complex with a chiral bipyrrolidine backbone (**104**) gave isotactic PLA ($P_m \leq 0.81$) whereas alkyl linked complexes (**105**) were more active but less selective ($P_m = 0.69 - 0.71$). This was linked to a degree of enantiomorphic site control. Simple mono-pyrrolidine zinc complexes reported by Jones *et al.* were not stereoselective but were significantly more active.^[24] **106** was active in the melt at very low initiator loading ($[LA]/[Zn]/[BnOH] = 10000 : 1 : 100$), achieving high conversion in as little as three minutes under these conditions.

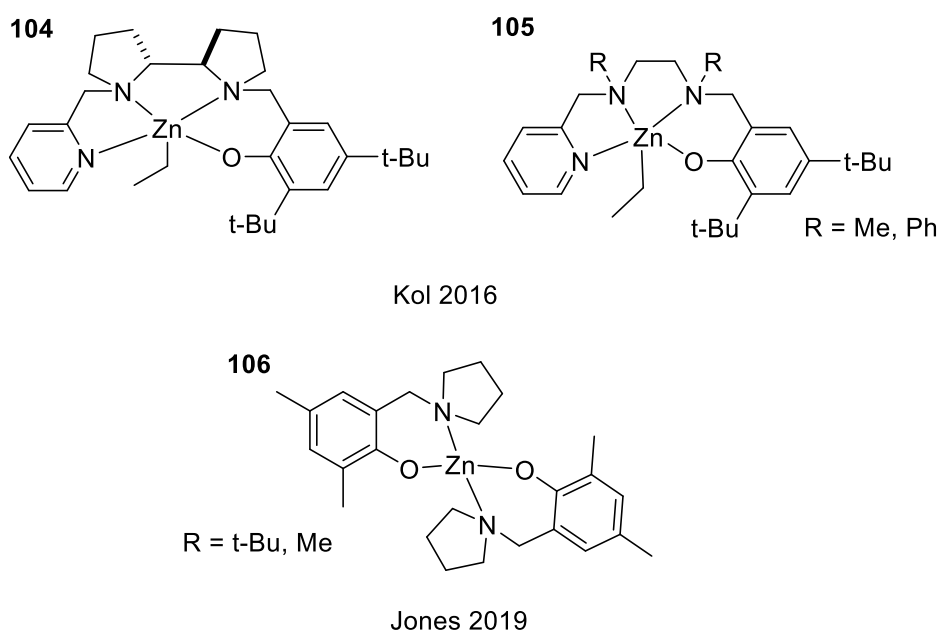


Figure 3.10: Mono and bipyrrolidine zinc (II) complexes for lactide ROP.^[23,24]

Zinc (II) complexes bearing guanidine-based ligands have gained prominence as active initiators for lactide ROP.^[25,26] The first example was introduced by Herres-Pawlis using a bis(guanidine) zinc complex **107**.^[27] The zinc centre was either mono, or bis ligated dependant on the labile group (**Figure 3.11**). All complexes were active in the melt at 150 – 165 °C achieving high molecular weights up to 58,800 gmol⁻¹ but required 1 – 2 days to reach high conversion. Further work from Herres-Pawlis introduced eight chiral bis(guanidine) complexes with cyclic, aliphatic backbones.^[28] All complexes were active for the bulk polymerisation of technical-grade *rac*-lactide with the THF-bridged compounds **108** – **109** being the most active with rate constants of 3.6 x 10⁻⁵ s⁻¹ and 5.7 x 10⁻⁵ s⁻¹ respectively. The use of a cyclohexyl-bridged

bis(guanidine) ligand was further explored through reaction with zinc (II) trifluoromethanesulphonate to give the homoleptic complex **110**.^[29] In a direct comparison with Sn(Oct)₂, **110** was shown to polymerise *L*-lactide with a polymerisation rate constant almost an order of magnitude higher (**110**: $k_p = 1.43 \text{ L mol}^{-1} \text{ s}^{-1}$, Sn(Oct)₂: $k_{app} = 0.167 \text{ L mol}^{-1} \text{ s}^{-1}$) and to give PLLA with a higher crystallinity than seen with Sn(Oct)₂. The rate was measured under industrial conditions using *in-situ* Raman spectroscopy making this the most active robust initiator to date.

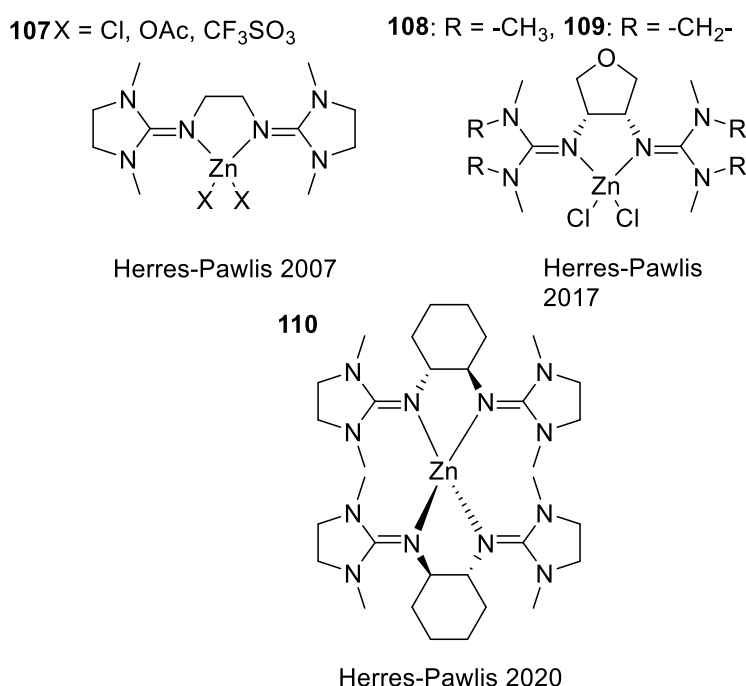


Figure 3.11: Zinc(II) bisguanidine complexes for lactide ROP from Herres-Pawlis *et al.*^[27–29]

Recent work from the Herres-Pawlis group has demonstrated hybrid guanidine ligands bearing carbonyl donors resulting in neutral {NO} coordination to zinc (**Figure 3.12**).^[29–31] A series of four air-stable complexes were initially reported with cyclopentyl or methyl guanidine substituents and chloro or bromo labile groups.^[30] The most active initiator (**111**) gave colourless PLA from technical grade *rac*-lactide. At low initiator loading ($[LA]/[I] = 5000 : 1$), high molecular weights and fast rates of reaction were attained ($k_{app} = 1.26 \times 10^{-4} \text{ s}^{-1}$). Subsequent work introduced substituents with varying electronic profiles to the aromatic backbone.^[31] *Para*

substitution led to an increase in rate with dimethylamine complex **112** giving the biggest increase. Interestingly, the same substitution at the *ortho* position had no effect on activity.

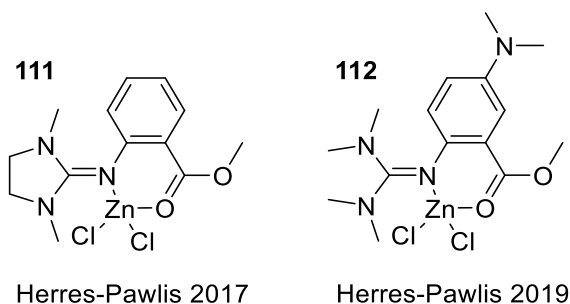


Figure 3.12: {NO} zinc(II) guanidine initiators for lactide ROP.^[30,31]

Jones and co-workers have reported a range of simple, monophenolate zinc complexes that are highly active for the polymerisation of lactide under industrial conditions.^[32–37] A range of seven, simple monophenolate ligands based on ethylenediamine were complexed to zinc to give homoleptic octahedral complexes (**Figure 3.13**).^[32] The most active initiator, **113**, achieved almost complete conversion of *L*-lactide after three minutes at low initiator loading and industrially optimal temperature ($[LA]/[I]/[BnOH] = 10000 : 1 : 100$, 180 °C) giving TOF values in excess of 100,000 h⁻¹. Furthermore, the molecular weight could be controlled through reducing the benzyl alcohol loading to give molecular weights up to 60,600 gmol⁻¹. Reasonable conversion was also attained in the absence of co-initiator, and it was suggested that ligand-assisted coordination-insertion contributed to this. Complexes **114** and **115**, with a tertiary amine donor, were also active under these conditions but required a co-initiator, supporting the idea that the N-H moiety was assisting with polymerisation. **113** was also able to produce isotactic stereoblock PLA through the sequential addition of monomers approach ($P_m = 0.80$, $T_m = 190$ °C). Propylenediamine-based equivalents were subsequently reported and showed higher activity than their ethylene-bridged counterparts.^[33] Complex **116**, a direct analogue of **113**, gave essentially quantitative conversion of *L*-lactide after just one minute at 180 °C and very low initiator loading ($[LA]/[I]/[BnOH] = 10000 : 1 : 100$).

The reaction was also very well controlled with good agreement between theoretical and measured molecular weights and narrow dispersity ($M_{n, \text{theo.}} = 14100 \text{ gmol}^{-1}$, $M_{n, \text{GPC}} = 14400 \text{ gmol}^{-1}$, $\mathcal{D} = 1.27$).

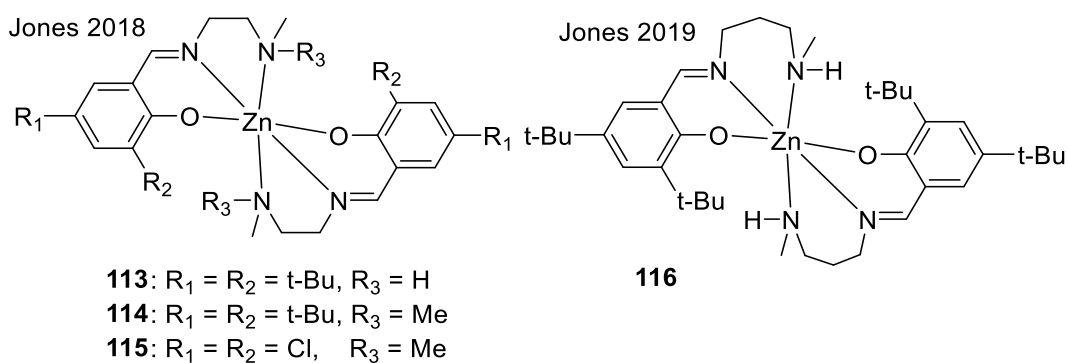


Figure 3.13: Selected highly active zinc(II) monophenolate complexes reported by Jones *et al.*^[32,33]

A series of monophenolate Schiff base ligands with phenyl imine substitution was reported by Payne and co-workers (**Figure 3.14**).^[35] Upon reaction with ZnEt_2 , tetrahedral mononuclear complexes or $\text{Zn}_2\text{L}_2\text{Et}_2$ dimers could be selectively produced. The dimers were, in all cases, superior to the equivalent monomers in terms of activity and control both in the melt and in solution. Dimeric species **117** – **119** reached *ca.* 90 % conversion in less than one minute in the melt at a ratio of $[\text{LA}]/[\text{I}]/[\text{BnOH}] = 3000 : 1 : 1$. Monomeric equivalents required up to 18 minutes to reach lower conversion (47 – 72 %) at identical conditions.

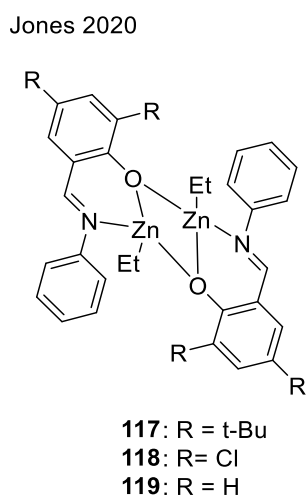


Figure 3.14: Dimeric zinc (II) monophenolate complexes for lactide ROP.^[35]

Three derivatives of the hybrid catalen ligand were complexed to zinc to give dimeric species of the form $(ML)_2$ and applied to *rac*-lactide polymerisation (**Figure 3.15**).^[36] Reasonable activity was displayed at a ratio of 3000 : 1 giving moderate conversions in 50 – 90 minutes with good molecular weight control and a broad range of dispersities ($\mathcal{D} = 1.24 - 2.04$). Higher activities were achieved with homoleptic complex **120** using a monophenolate {ONN} ligand bearing a catam based aminophenolate moiety.^[37] High conversion was attained after eight minutes in the melt at relatively low initiator loading ($[LA]/[I]/[BnOH] = 3000 : 1 : 10$) and room temperature activity was also demonstrated, the latter having a slight heterotactic preference ($P_r = 0.60$).

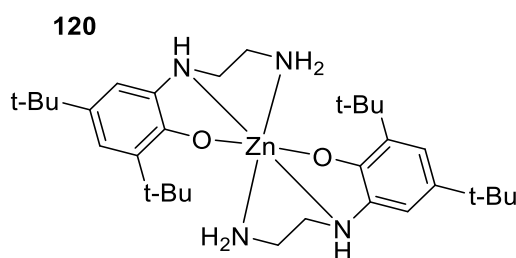


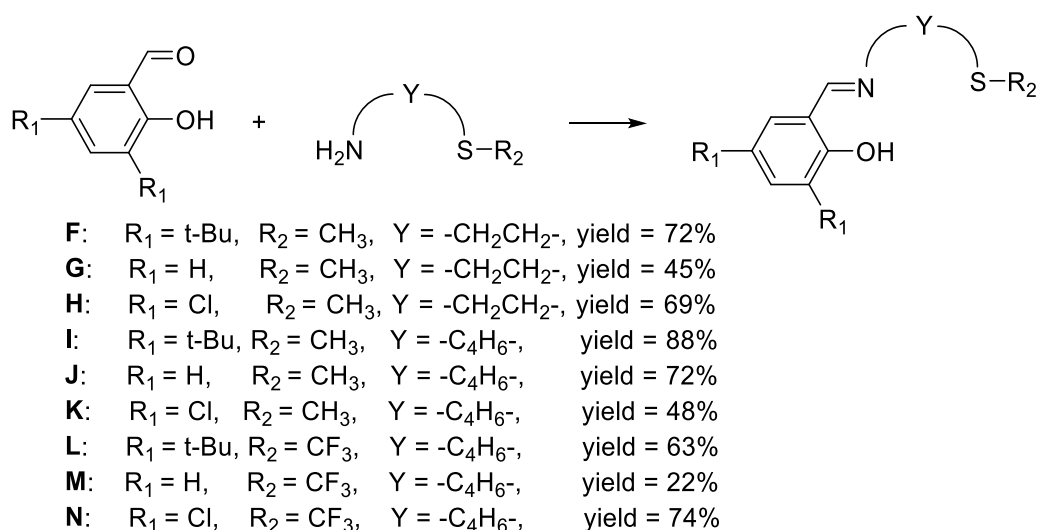
Figure 3.15: Zinc(II) catam-based complex for lactide ROP.^[37]

Based on the success of zinc monophenolate complexes with {ONN} donor ability, a series of ligands were developed with an {ONS} motif. These are applied to lactide polymerisation in the melt and polyester degradation allowing the role of the pendant donor to be compared with the common amine functionality.

3.2 Zinc {ONS} complexes for lactide polymerisation

3.2.1 Synthesis and characterisation of {ONS} monophenolate ligands

Ligands **F** – **NH** were synthesised through a simple condensation reaction between the relevant salicylaldehyde derivative and thio-amine (**Scheme 3.01**). The reaction was performed in methanol and stirred at room temperature for three hours or until a precipitate formed. With the exception of **JH** and **MH**, all ligands were recrystallised from methanol to give yellow to orange powders in moderate to good yields (22 – 88%). **JH** and **MH** were isolated as pale-yellow oils, washed with methanol and solidified upon standing to give the pure product.



Scheme 3.01: Synthesis of {ONS} ligands.

All ligands were characterised through ^1H NMR, ^{13}C { ^1H } NMR and ESI-MS. For ligands bearing a $-\text{CF}_3$ group (**M** – **NH**), ^{19}F NMR was carried out, showing a single species in all cases. The ^1H NMR spectrum of **FH** is shown in **Figure 3.16** where the identity and purity of the ligand can be seen. The nine derivatives bear a range of substituents exploring the sterics and electronics of the phenolate moiety, the flexibility of the linker and the effect of CH_3 or CF_3 thioether substitution.

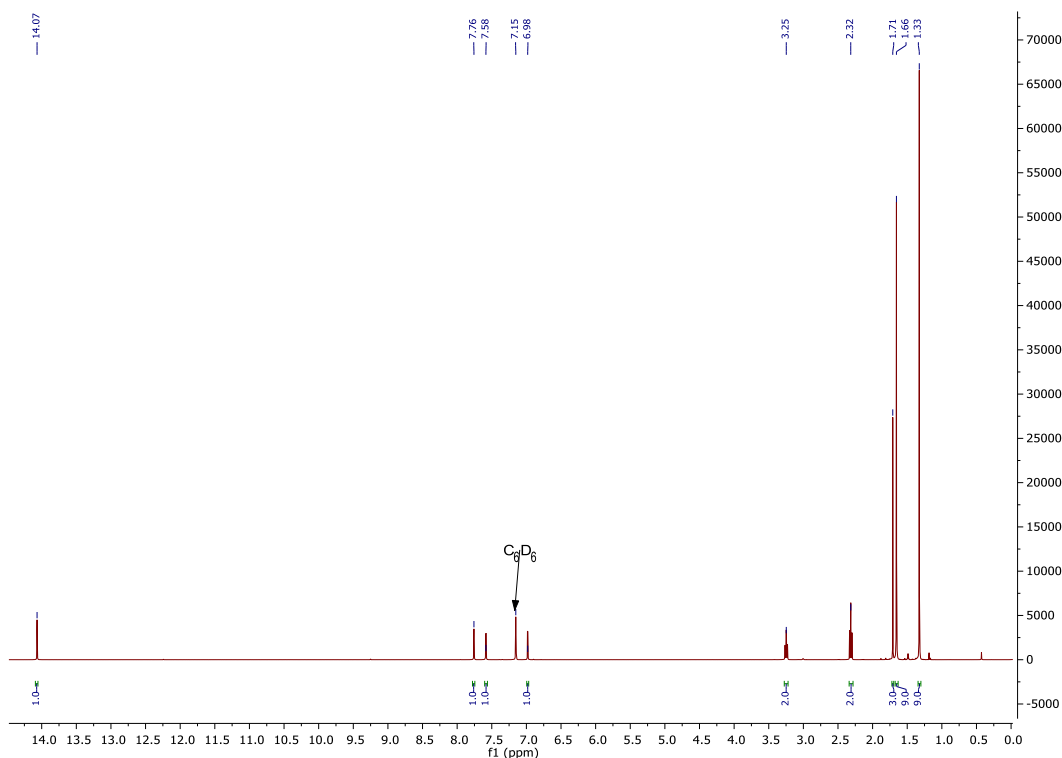
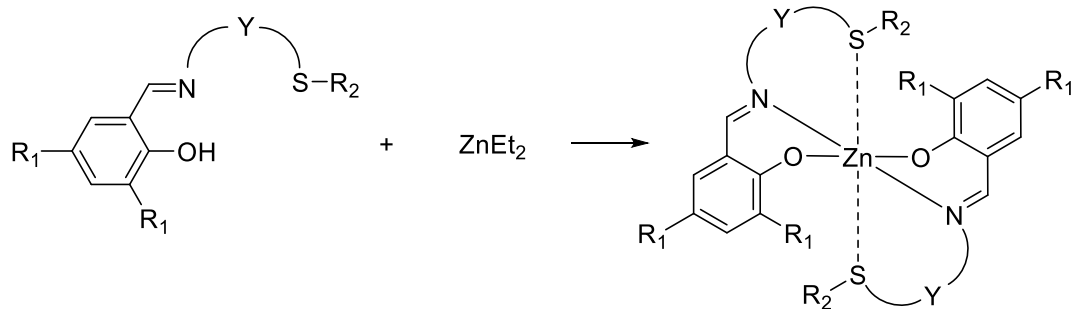


Figure 3.16: ^1H NMR (400 MHz, C_6D_6 , 298K) spectrum of FH.

3.2.2 Synthesis and characterisation of zinc {ONS} complexes

The complexation of ligands **F – NH** to $\text{Zn}(\text{Et})_2$ was carried out in anhydrous toluene under air-sensitive conditions (**Scheme 3.02**). The products crystallised from mixtures of hexane and toluene and were collected as yellow crystalline solids. The ^1H NMR spectra were consistent with the homoleptic complexes $[\text{Zn}(\text{F} - \text{N})_2]$; there was no evidence of ethyl groups for any complexes. The ^1H NMR spectrum of $\text{Zn}(\text{F})_2$ is given in **Figure 3.17**. Compared to the corresponding ligand (**Figure 3.16**), there is a general upfield shift in resonances and no -OH resonance, as would be expected from coordination. For complexes $\text{Zn}(\text{O} - \text{N})_2$, ^{19}F NMR gave a single peak. Elemental analysis (CHN) was also consistent with the homoleptic $\text{Zn}(\text{Lig})_2$ structure in all cases.



- F:** $R_1 = t\text{-Bu}$, $R_2 = \text{CH}_3$, $Y = -\text{CH}_2\text{CH}_2-$, yield = 22%
G: $R_1 = \text{H}$, $R_2 = \text{CH}_3$, $Y = -\text{CH}_2\text{CH}_2-$, yield = 82%
H: $R_1 = \text{Cl}$, $R_2 = \text{CH}_3$, $Y = -\text{CH}_2\text{CH}_2-$, yield = 74%
I: $R_1 = t\text{-Bu}$, $R_2 = \text{CH}_3$, $Y = -\text{C}_4\text{H}_6-$, yield = 40%
J: $R_1 = \text{H}$, $R_2 = \text{CH}_3$, $Y = -\text{C}_4\text{H}_6-$, yield = 50%
K: $R_1 = \text{Cl}$, $R_2 = \text{CH}_3$, $Y = -\text{C}_4\text{H}_6-$, yield = 80%
L: $R_1 = t\text{-Bu}$, $R_2 = \text{CF}_3$, $Y = -\text{C}_4\text{H}_6-$, yield = 24%
M: $R_1 = \text{H}$, $R_2 = \text{CF}_3$, $Y = -\text{C}_4\text{H}_6-$, yield = 50%
N: $R_1 = \text{Cl}$, $R_2 = \text{CF}_3$, $Y = -\text{C}_4\text{H}_6-$, yield = 68%

Scheme 3.02: Synthesis of $\text{Zn}(\text{F-N})_2$.

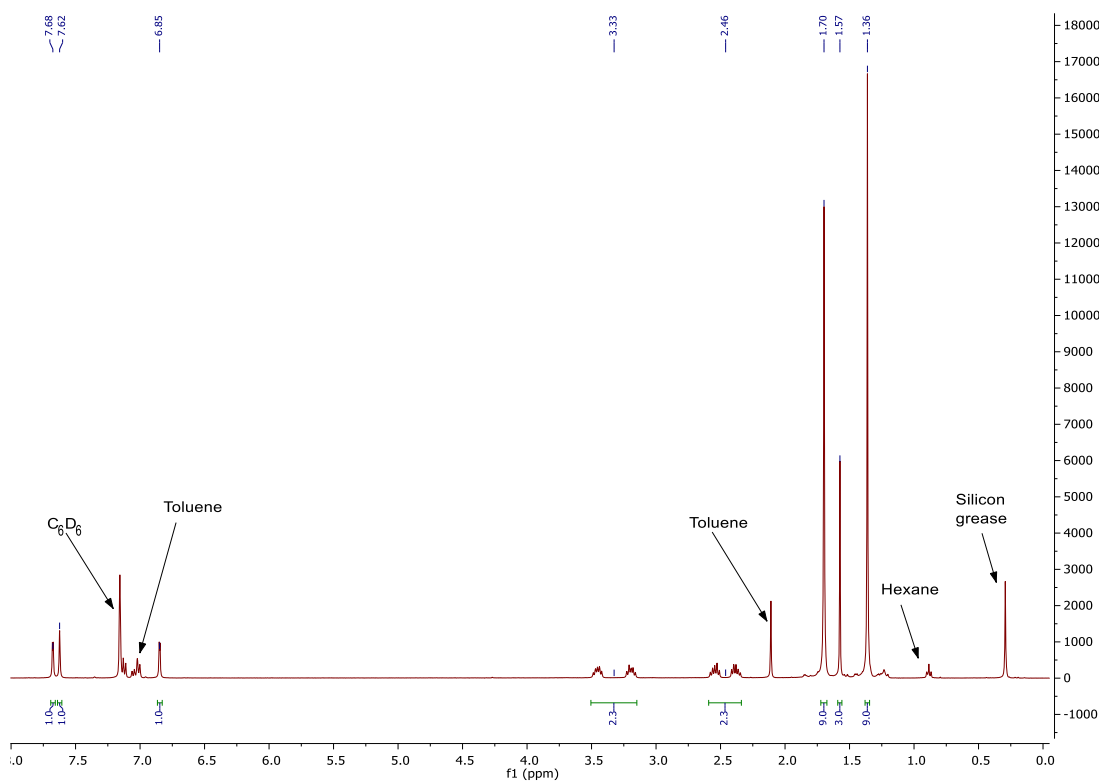


Figure 3.17: ^1H NMR (400 MHz, C_6D_6) of $\text{Zn}(\text{F})_2$.

Analysis by X-ray crystallography yielded seven solid state structures for Zn(**F,G,I,J,K,L,N**)₂. Of these, five were four-coordinate with no evidence of Zn – S bonding (**Figure 3.18**). The geometry index for a four-coordinate complex (τ_4') was calculated (**Table 3.01**) and gave a range of values with Zn(**F,G**)₂ ($R_1 = t\text{-Bu}$, H ; $R_2 = \text{CH}_3$; $Y = -\text{CH}_2\text{CH}_2-$) being closest to tetrahedral geometry (Zn(**F**)₂: $\tau_4' = 0.84$, Zn(**G**)₂: $\tau_4' = 0.70$), presumably facilitated by the flexible ethylene moiety. In the case of Zn(**G**)₂, the N(1) – Zn – N(2) dihedral angle is relatively large {136.49(13)°}, resulting in the reduced tetrahedral preference. The introduction of a rigid phenylene linking group Zn(**I,J,L**)₂ resulted in further deviation from tetrahedral geometry, particularly in the case of Zn(**J**)₂ ($R_1 = H$, $R_2 = \text{CH}_3$, $Y = -\text{C}_6\text{H}_4-$), where two distinct crystallographic structures were present, both of which had a low geometric preference {Zn(**J**)₂ = 0.48, Zn(**J**)₂' = 0.55}. Zn(**I**)₂ and Zn(**L**)₂ differ only in the nature of the thioether substituent and have a geometric preference of 0.64 and 0.68 respectively. This can be explained by a combination of steric and electronic differences between the $-\text{CH}_3$ and $-\text{CF}_3$ groups.

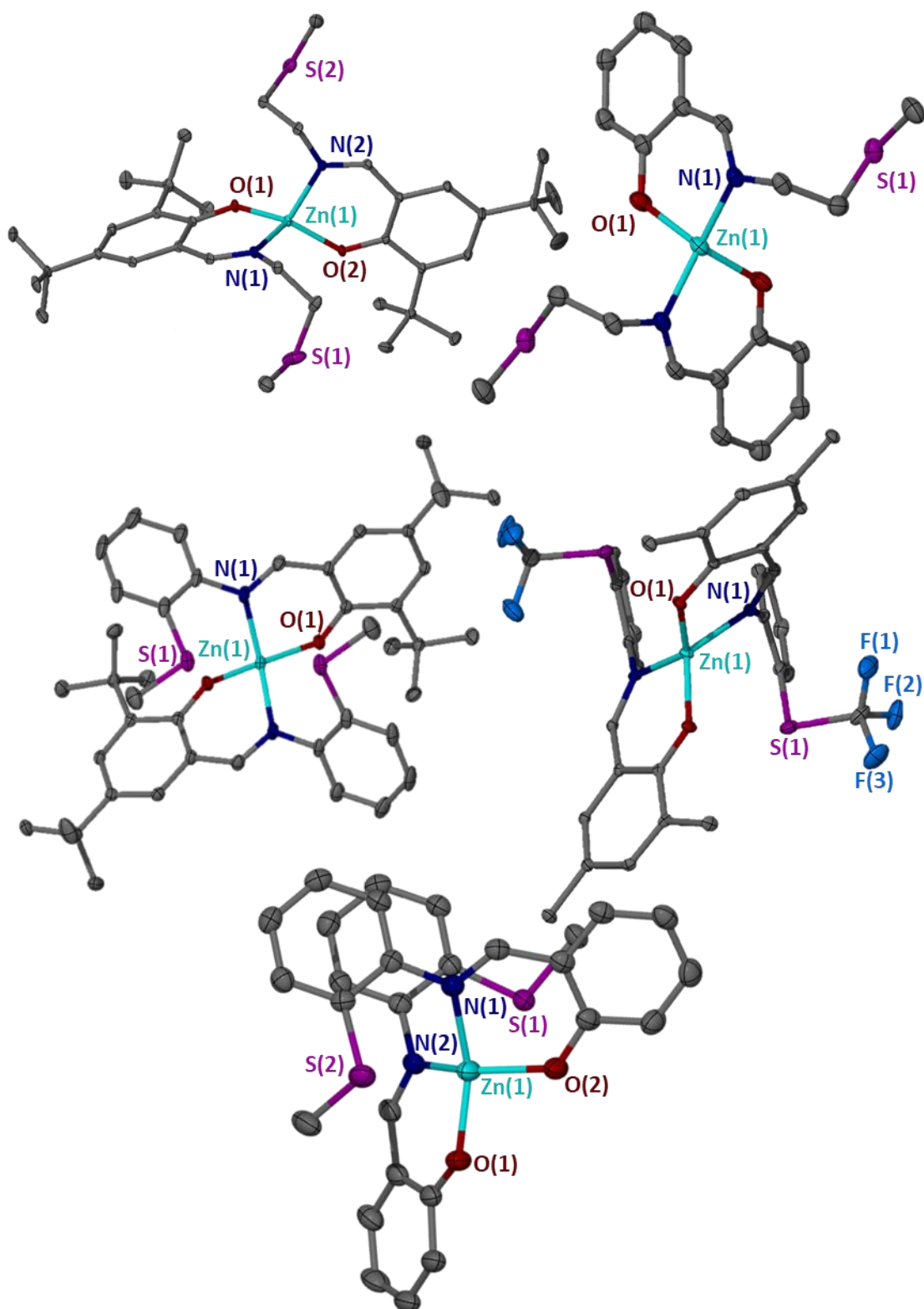


Figure 3.18: Solid state structures of $\text{Zn}(\mathbf{F})_2$ (top left), $\text{Zn}(\mathbf{G})_2$ (top right), $\text{Zn}(\mathbf{I})_2$ (middle left), $\text{Zn}(\mathbf{L})_2$ (middle right) and $\text{Zn}(\mathbf{J})_2$ (bottom). Ellipsoids are shown at the 30% probability level. H and tBu groups have been removed for clarity. Only one structure for $\text{Zn}(\mathbf{J})_2$ is displayed.

Table 3.01: Selected bond lengths (Å) and angles (°) for Zn(**F,G,I,J,L**)₂.

	Zn(F) ₂	Zn(G) ₂	Zn(I) ₂	Zn(J) ₂	Zn(J) ₂ '	Zn(L) ₂
$\tau_4^{[a]}$	0.84	0.70	0.64	0.48	0.55	0.68
Zn – S ^[b]	4.4	4.5	3.1	3.1	3.2	3.4
Zn – O(1)	1.896(2)	1.944(2)	1.9304(11)	1.9555(15)	1.9251(14)	1.9188(17)
Zn – O(2)	1.921(2)	1.944(2)	1.9304(11)	1.9478(15)	1.9251(14)	1.9199(17)
Zn – N(1)	1.989(3)	1.993(2)	2.0539(14)	2.0755(17)	2.0454(16)	2.019(2)
Zn – N(2)	2.003(3)	1.933(2)	2.0539(14)	2.0701(17)	2.0454(16)	2.028(2)
O(1) – Zn – O(2)	121.50 (10)	115.34(13)	118.05(7)	97.62(6)	97.03(9)	105.10(7)
O(1) – Zn – N(1)	97.49 (10)	95.89(9)	93.10(5)	91.34(7)	94.70(6)	94.46(8)
O(1) – Zn – N(2)	115.15(10)	107.08(9)	106.63(5)	149.11(7)	140.88(7)	133.98(8)
O(2) – Zn – N(1)	119.01(10)	107.08(9)	106.63(5)	139.28(7)	140.88(7)	127.79(8)
O(2) – Zn – N(2)	95.98(10)	95.89(9)	93.10(5)	91.84(7)	94.70(6)	94.13(8)
N(1) – Zn – N(2)	108.15(10)	136.49(13)	141.39(8)	100.47(7)	99.30(9)	106.11(9)

[a] Calculated from the two largest coordination angles. [b] Average of Zn – S interatomic distance.

Among the tetrahedral complexes, there was a range of Zn – S average interatomic distances, and this was broadly correlated with tetrahedral preference. The most tetrahedral complexes, Zn(**F** – **G**)₂, had long average Zn – S distances (4.4 – 4.5 Å), larger than the sum of van der Waals radii (Zn: 2.39 Å, S: 1.89)^[96] suggesting a lack of bonding interaction. The phenylene bridge equivalents have much shorter Zn – S bond distances (3.1 – 3.4 Å) due to constrained chelation. Of the phenylene-based complexes, Zn(**L**)₂ has both the greatest tetrahedral preference and the largest average Zn – S distance ($\tau_4' = 0.68$, Zn – S = 3.4 Å). This is a result of the steric or electronic differences between the CH₃ and CF₃ substituents. These distances are within the sum of van der Waals radii implying some degree of interaction. The solid-state structure of Zn(**K**)₂ indicated a five-coordinate complex with one Zn – S bond and a square pyramidal geometry ($\tau_5 = 0.02$) (**Figure 3.19, Table 3.02**). The distance between the zinc centre and the two sulphur atoms are very similar {Zn(1) – S(1) = 2.8032(18) Å, Zn(1) – S(2) = 2.9 Å}. Moreover, Bader's theory of atoms in molecules (QTAIM) predicts a bond critical point between Zn and S(2) ($\rho = 0.185 \text{ e } \text{Å}^{-3}$). These data suggest that the complex can be considered to have octahedral geometry.

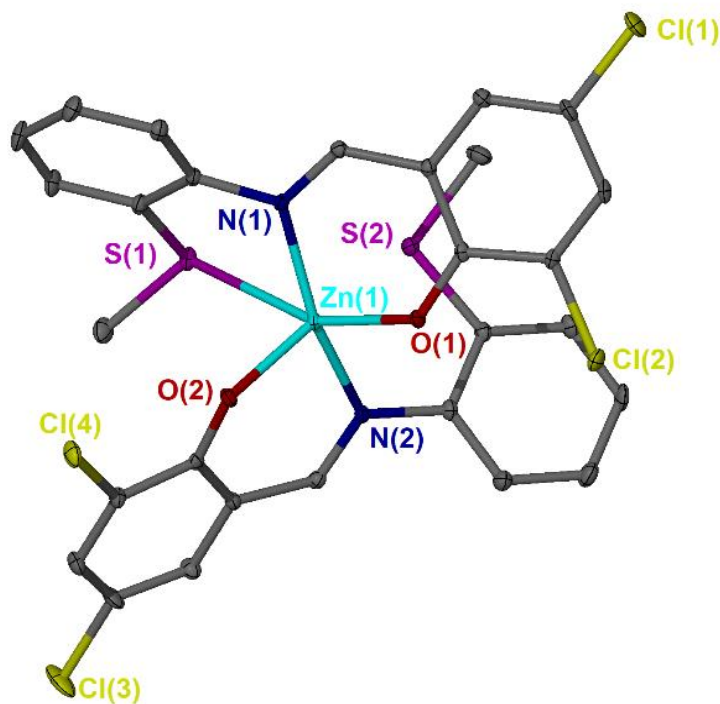


Figure 3.19: Solid-state structure of $\text{Zn}(\mathbf{K})_2$. Ellipsoids are shown at the 30% probability level. H atoms have been removed for clarity.

Table 3.02: Selected bond lengths (Å) and angles (°) for $\text{Zn}(\mathbf{K})_2$.

	$\text{Zn}(\mathbf{K})_2$
$\tau_5^{[a]}$	0.02
Zn – S(1)	2.8032(6)
Zn – O(1)	1.9568(14)
Zn – O(2)	1.9561(15)
Zn – N(1)	2.0528(17)
Zn – N(2)	2.0685(18)
O(1) – Zn – O(2)	110.38(6)
O(1) – Zn – N(1)	90.23(7)
O(1) – Zn – N(2)	93.79(7)
O(2) – Zn – N(1)	105.99(7)
O(1) – Zn – S(1)	157.45(5)
N(1) – Zn – N(2)	158.81(7)

[a] Calculated from the two largest coordination angles. [b] Average of Zn – S interatomic distance.

The complex produced through the complexation of **NH** was shown to be dimeric in the solid state with a $\text{Zn}_2(\mathbf{N})_4$ structure (**Figure 3.20**, **Table 3.03**). The zinc atoms were bridged by the phenoxy groups of two ligands resulting in two five-coordinate centres. A slight preference for trigonal bipyramidal geometry was displayed by Zn(1) ($\tau_5 = 0.54$) whereas Zn(2) was much closer to a square pyramidal geometry ($\tau_5 = 0.33$). The latter appears to be influenced by a relatively small Zn – S distance located *trans* to the apical Zn(2) – N(4) bond (3.4 Å). It could therefore be suggested that Zn(2) has a *pseudo*-octahedral structure, similar to that seen with $\text{Zn}(\mathbf{K})_2$.

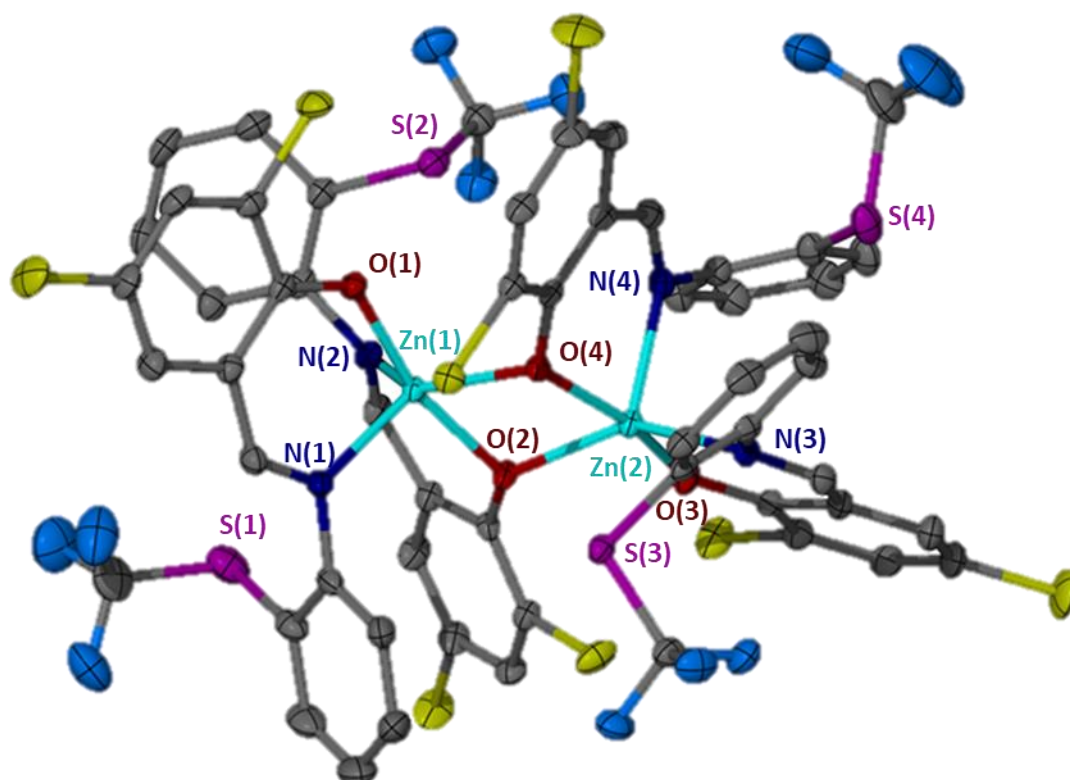


Figure 3.20: Solid-state structure of $\text{Zn}_2(\mathbf{N})_4$. Ellipsoids are shown at the 30% probability level. H atoms have been removed for clarity.

Table 3.03: Selected bond lengths (Å) and angles (°) for Zn₂(N)₄.

	Zn ₂ (N) ₄
$\tau_5^{[a]}$	Zn(1): 0.54, Zn(2): 0.33
Zn(1) – O(1)	1.9559(12)
Zn(1) – O(2)	2.0253(12)
Zn(1) – N(1)	2.0557(15)
Zn(1) – N(2)	2.1288(15)
O(1) – Zn(1) – O(2)	165.19(5)
O(4) – Zn(1) – N(2)	132.75(5)
O(3) – Zn(2) – O(4)	163.05(5)
O(2) – Zn(2) – N(3)	143.43(6)

[a] Calculated from the two largest coordination angles. [b] Average of Zn – S interatomic distance.

A DOSY NMR study was performed to assess whether the dimeric structure of Zn(N)₂ was maintained in a solution of C₆D₆. The DOSY NMR spectrum of Zn(N)₂ showed one species. This was compared to the equivalent spectra of Zn(I)₂ and Zn(L)₂, both of which were monomeric in the solid state and gave single diffusion species. Through comparison between each complex and their respective solvent peak, it was possible to calculate an estimate of the volume and hydrodynamic radii of Zn(I,L,N)₂ in solution (**Table 3.04**). The estimated hydrodynamic radii were sufficiently similar to suggest that they share the same coordination structure {rZn(I)₂ = 7.25 Å, rZn(L)₂ = 6.30 Å, rZn(N)₂ = 7.13 Å}. An approximate measurement of the crystal structure suggests that the complexes are monomeric in solution and that Zn(N)₂ is the best structural description of the analysed compound.

Table 3.04: r_H, c and V for Zn(I)₂, Zn(L)₂ and Zn₂(N)₄

Sample	c _{sa} r _H ^{sa}	r _H / Å	c	V / Å ³
Zn(I) ₂	40.58	7.25	5.58	1,596
Zn(L) ₂	39.69	7.13	5.57	1,518
Zn ₂ (N) ₄	34.26	6.30	5.44	1,047

3.2.3 Lactide polymerisation with Zn(F-N)₂.

Complexes Zn(F-N)₂ were initially tested for the solvent-free polymerisation of *rac*-lactide at a ratio of [LA]/[Zn]/[BnOH] = 300 : 1 : 1 (**Table 3.05**). All complexes were active under these conditions and gave reasonably well-controlled polymerisation in terms of agreement between theoretical and measured molecular weights and dispersities ($\bar{D} = 1.21 - 1.88$). The most notable substituent effect comes from the introduction of a rigid, phenylene linker which tended to give the most active initiators. In contrast, the introduction of the electron-withdrawing CF₃ group, Zn(L-N)₂, had little effect on polymerisation activity. The effect of switching phenolate substitution between H and tBu had a minimal and inconsistent effect on polymerisation outcome. However, the introduction of chloride moieties on the ligand yielded the least active initiators in each series. This is interesting as the introduction of electron-withdrawing groups can often boost activity through increasing the Lewis acidity of the metal centre. In this case, it can be rationalised by considering the tendency towards octahedral geometry shown by Zn(K)₂ and Zn(N)₂ in the solid state with the increased steric hindrance hampering activity. The most active initiators under these conditions were Zn(J)₂ and Zn(L)₂ which both achieved reasonable conversion in a minute or less giving TOF values in excess of 10,000 h⁻¹.

Table 3.05: Solvent-free polymerisation of *rac*-lactide at 130 °C using Zn(1–9)₂, [LA]/[Zn]/[BnOH] = 300:1:1.

Init.	T/°C	Time /minutes	Conv. % ^a	P _m ^b	M _n ^d	M _n Calc. ^c	Đ ^d	TOF / h ⁻¹
Zn(F) ₂	130	3	59	0.55	25600	25600	1.32	3550
Zn(G) ₂	130	7	73	0.55	24450	31650	1.34	1900
Zn(H) ₂	130	25	60	0.60	22400	26050	1.26	450
Zn(I) ₂	130	2	81	0.57	22500	35100	1.59	7300
Zn(J) ₂	130	<1	56	0.57	21050	24300	1.88	10100
Zn(K) ₂	130	3	61	0.57	31350	26500	1.21	3650
Zn(L) ₂	130	1	72	0.59	24950	31250	1.52	12950
Zn(M) ₂	130	2	72	0.51	25500	31250	1.66	6500
Zn(N) ₂	130	10	46	0.58	17950	26600	1.27	850

Conditions: *rac*-LA (1 g), [LA]/[Zn]/[BnOH] = 300:1:1, solvent free. [a] Determined by ¹H NMR spectroscopy. [b] Probability of racemic enchainment, determined by ¹H{¹H} NMR spectroscopy. [c] Theoretical molecular weight calculated from conversion (rounded to the nearest 50): {(conversion × 3 × M_n [LA]) + M_n [BnOH]}. [d] Determined from GPC (in tetrahydrofuran) referenced against polystyrene standards × 0.58. [e] TOF = [LA]_t / ([Zn] × t).

Complexes Zn(F–N)₂ were all active for the polymerisation of *rac*-lactide at decreased initiator loading ([LA]/[Zn]/[BnOH] = 3000 : 1 : 10) (**Table 3.06**). At this ratio, the trends highlighted at lower loading became more pronounced. Ethylene bridged complexes, Zn(F–G)₂, took between 30 and 60 minutes to attain a reasonable conversion with TOF values less than 5000 h⁻¹. Again, the chloro ligated complexes proved to be the slowest in each series with only Zn(N)₂ showing good activity under these conditions (Conversion = 64%, t = 12 min, TOF = 9600 h⁻¹). There was no consistent difference between H- and tBu- phenolate substitution or the modification of the thioether component. Zn(J)₂ and Zn(L)₂ remained the most active initiators giving TOF values of 124,200 h⁻¹ and 65,700 h⁻¹ respectively. The molecular weight control remained predictable and there was a narrowing of dispersities compared to previous data; this effect is often observed with decreased initiator loading (300 : 1 : 1, Đ = 1.21 – 1.88; 3000 : 1 : 10, Đ = 1.08 – 1.48).

Table 3.06: Solvent-free polymerisation of rac-lactide at 130 °C using Zn(1–9)₂, [LA]/[Zn]/[BnOH] = 3000:1:10.

Init.	T/°C	Time /minutes	Conv. % ^a	P _m ^b	M _n ^d	M _n Calc. ^c	Đ ^d	TOF / h ⁻¹
Zn(F) ₂	130	45	52	0.56	20100	22600	1.17	2080
Zn(G) ₂	130	30	73	0.58	11150	31650	1.14	4380
Zn(H) ₂	130	60	40	0.62	4750	5850	1.08	1200
Zn(I) ₂	130	4	71	0.60	23750	30800	1.23	31950
Zn(J) ₂	130	1	69	0.57	25150	29950	1.28	124200
Zn(K) ₂	130	40	53	0.61	22250	23050	1.16	2385
Zn(L) ₂	130	2	73	0.57	16950	31650	1.48	65700
Zn(M) ₂	130	4	70	0.56	27800	30400	1.38	31500
Zn(N) ₂	130	12	64	0.60	20200	27800	1.36	9600

Conditions: rac-LA (1 g), [LA]/[Zn]/[BnOH] = 3000:1:10, solvent free. [a] Determined by ¹H NMR spectroscopy. [b] Probability of racemic enchainment, determined by ¹H(¹H) NMR spectroscopy. [c] Theoretical molecular weight calculated from conversion (rounded to the nearest 50): {(conversion × 3 × M_n [LA]) + M_n [BnOH]}. [d] Determined from GPC (in tetrahydrofuran) referenced against polystyrene standards × 0.58. [e] TOF = [LA]_t / ([Zn] × t).

The most active initiators, Zn(I,J,L,M,N)₂, were tested at a ratio of [LA]/[Zn]/[BnOH] = 10000 : 1 : 30; this is close to the ratios employed with Sn(Oct)₂ in an industrial setting (Table 3.07).^[97] Reasonable dispersities were maintained throughout (Đ = 1.20 – 1.44) with good agreement between theoretical and measured molecular weights, particularly for Zn(I)₂ (M_n GPC = 23600 gmol⁻¹, M_n theo. = 24600 gmol⁻¹). Zn(J)₂ and Zn(L)₂ were clearly the most active initiators converting 68% and 51% in 3 and 9 minutes respectively. With the exception of Zn(J)₂, conversion tended to be limited to around 50%. This could in part reflect a decrease in stirring due to increased viscosity, however analogous systems are able to reach high conversion so there was clearly some initiator decomposition taking place.

Table 3.07: Solvent-free polymerisation of rac-lactide at 130 °C using Zn(I,J,L,M,N)₂. [LA]/[Zn]/[BnOH] = 10000:1:30.

Init.	T/°C	Time /minutes	Conv. % ^a	P _m ^b	M _n ^d	M _n Calc. ^c	Đ ^d	TOF / h ⁻¹
Zn(I) ₂	130	30	51	0.58	23600	24600	1.23	10200
Zn(J) ₂	130	3	68	0.57	29750	32850	1.20	136000
Zn(L) ₂	130	9	51	0.58	21100	24450	1.28	34000
Zn(M) ₂	130	45	54	0.58	14400	26100	1.44	7200
Zn(N) ₂	130	30	55	0.61	17200	26600	1.31	11000

Conditions: rac-LA (3 g), [LA]/[Zn]/[BnOH] = 10000:1:30, solvent free. [a] Determined by ¹H NMR spectroscopy. [b] Probability of racemic enchainment, determined by ¹H(¹H) NMR spectroscopy. [c] Theoretical molecular weight calculated from conversion (rounded to the nearest 50): {(conversion × 3 × M_n [LA]) + M_n [BnOH]}. [d] Determined from GPC (in tetrahydrofuran) referenced against polystyrene standards × 0.58. [e] TOF = [LA]_t / ([Zn] × t).

The most active initiators were further tested for *rac*-lactide polymerisation at low initiator loading at an increased temperature of 180 °C (**Table 3.08**). This is to further mimic industrial conditions where high temperatures are used to reduce the viscosity of the prepared polymer to aid with downstream processing. Zn(**I**,**J**,**L**,**M**,**N**)₂ were all sufficiently robust to show activity under these conditions. All took significantly less time to reduce stirring than at 130 °C and higher conversions were attained. This suggests that any deactivation processes were dependant more on reaction time than monomer conversion. The most active initiator, Zn(**J**)₂, gave 83% conversion after two minutes giving a very high TOF value of 249,000 h⁻¹. Under these conditions, measured molecular weights were generally lower than the theoretical ideal and dispersities were broadened compared to the lower-temperature experiments (\bar{D} = 1.45 – 1.68), possibly due to a degree of initiator decomposition at elevated temperatures.

Table 3.08: Solvent-free polymerisation of *rac*-lactide at 130 °C using Zn(**I**,**J**,**L**,**M**,**N**)₂. [LA]/[Zn]/[BnOH] = 10000:1:30.

Init.	T/°C	Time /minutes	Conv. % ^a	P _m ^b	M _n ^d	M _n Calc. ^c	\bar{D} ^d	TOF / h ⁻¹
Zn(I) ₂	180	3	74	0.57	28100	35750	1.62	148000
Zn(J) ₂	180	2	83	0.57	31350	40050	1.53	249000
Zn(L) ₂	180	6	67	0.58	26850	32350	1.45	67000
Zn(M) ₂	180	3	69	0.58	27150	33300	1.60	138000
Zn(N) ₂	180	12	65	0.62	24400	31400	1.68	32500

Conditions: *rac*-LA (3 g), [LA]/[Zn]/[BnOH] = 10000:1:30, solvent free. [a] Determined by ¹H NMR spectroscopy. [b] Probability of racemic enchainment, determined by ¹H(¹H) NMR spectroscopy. [c] Theoretical molecular weight calculated from conversion (rounded to the nearest 50): {(conversion × 3 × M_n [LA]) + M_n [BnOH]}. [d] Determined from GPC (in tetrahydrofuran) referenced against polystyrene standards × 0.58. [e] TOF = [LA]₀ / ([Zn] × t).

Zn(**J**)₂ and Zn(**L**)₂ were further tested using *L*-lactide, which is the standard industrial monomer for PLA production (**Table 3.09**). For both initiators, activity was reduced compared to the equivalent *rac*-lactide reactions but remained high giving TOF values of 111,000 h⁻¹ for Zn(**J**)₂ and 56,000 h⁻¹ for Zn(**L**)₂. Analogous zinc {ONS} complex **113** (**Figure 3.12**) was more active under identical conditions with *L*-lactide (TOF = 188,000 h⁻¹).^[32] The control of the polymerisation was increased with *L*-lactide in terms of agreement between theoretical and calculated molecular weights (Zn(**J**)₂,

$M_n = 32,050 \text{ gmol}^{-1}$, $M_n(\text{theo.}) = 35,750 \text{ gmol}^{-1}$; $\text{Zn}(\mathbf{L})_2$, $M_n = 28,050 \text{ gmol}^{-1}$, $M_n(\text{theo.}) = 27,050 \text{ gmol}^{-1}$) and relatively narrow dispersities $\text{Zn}(\mathbf{J})_2$, $\mathcal{D} = 1.16$; $\text{Zn}(\mathbf{L})_2$, $\mathcal{D} = 1.15$). $^1\text{H}\{^1\text{H}\}$ NMR analysis showed only one peak in the methine region, suggesting that there are no unwanted epimerisation reactions occurring and this is supported by DSC which gave melting points of 162 °C and 167 °C for $\text{Zn}(\mathbf{J})_2$ and $\text{Zn}(\mathbf{L})_2$ respectively. Throughout the experiments with a high ratio of monomer to initiator, white PLA was produced despite the yellow colouring of the initiators. This is important from an industrial standpoint where white/colourless polymer is desirable.

Table 3.09: Solvent-free polymerisation of L-lactide at 180 °C using $\text{Zn}(\mathbf{J},\mathbf{L})_2$. $[\text{LA}]/[\text{Zn}]/[\text{BnOH}] = 10000:1:30$.

Init.	T/°C	Time /minutes	Conv. % ^a	P_m ^b	M_n ^d	M_n Calc. ^c	\mathcal{D} ^d	TOF / h^{-1e}
$\text{Zn}(\mathbf{J})_2$	180	4	74	0.00 ^[f]	32050	35750	1.16	111000
$\text{Zn}(\mathbf{L})_2$	180	6	56	0.00 ^[f]	28050	27050	1.15	56000

Conditions: rac-LA (3 g), $[\text{LA}]/[\text{Zn}]/[\text{BnOH}] = 10000:1:30$, solvent free. [a] Determined by ^1H NMR spectroscopy. [b] Probability of racemic enchainment, determined by $^1\text{H}\{^1\text{H}\}$ NMR spectroscopy. [c] Theoretical molecular weight calculated from conversion (rounded to the nearest 50): $\{(\text{conversion} \times 3 \times M_n[\text{LA}] + M_n[\text{BnOH}])\}$. [d] Determined from GPC (in tetrahydrofuran) referenced against polystyrene standards $\times 0.58$. [e] $\text{TOF} = [\text{LA}]_t / ([\text{Zn}] \times t)$. [f] One resonance in $^1\text{H}\{^1\text{H}\}$ NMR.

3.2.4 Reactivity trends and mechanistic considerations

The activity shown by complexes $\text{Zn}(\mathbf{F}-\mathbf{N})_2$ show a degree of correlation with the average Zn – S interatomic distance. This data can be plotted against TOF values ($[\text{LA}]/[\text{I}]/[\text{BnOH}] = 3000 : 1 : 10$, **Table 3.04**) to show a volcano-style relationship (**Figure 3.21**) which suggests there is an ideal Zn – S bond distance for this class of complex. $\text{Zn}(\mathbf{F})_2$ and $\text{Zn}(\mathbf{G})_2$ have respective Zn – S distances of 4.38 Å and 4.52 Å respectively; these are the highest values of the compounds analysed and correspond to relatively low activity [$\text{Zn}(\mathbf{F})_2$, $\text{TOF} = 2080 \text{ h}^{-1}$; $\text{Zn}(\mathbf{G})_2$, $\text{TOF} = 4380 \text{ h}^{-1}$]. $\text{Zn}(\mathbf{N})_2$ had a smaller average Zn – S distance, corresponding to a modest increase in activity ($\text{TOF} = 9600 \text{ h}^{-1}$). Relatively low activity was also recorded with $\text{Zn}(\mathbf{K})_2$ ($\text{TOF} = 2385 \text{ h}^{-1}$) which has the shortest average Zn – S bond length that was measured at 2.87 Å. $\text{Zn}(\mathbf{I},\mathbf{J},\mathbf{L})_2$ had Zn – S interatomic distances between 3 – 3.4 Å and were the most active initiators [$\text{Zn}(\mathbf{I})_2$, $\text{TOF} = 31,950 \text{ h}^{-1}$; $\text{Zn}(\mathbf{J})_2$, $\text{TOF} = 124,200 \text{ h}^{-1}$; $\text{Zn}(\mathbf{L})_2$, $\text{TOF} = 65,700 \text{ h}^{-1}$].

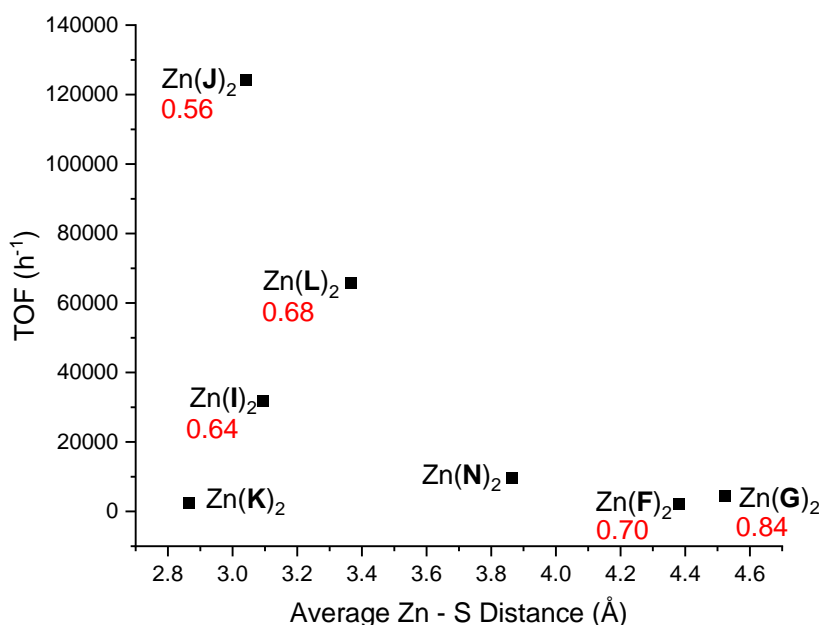


Figure 3.21: Average Zn – S bond distances for selected complexes plotted against TOF at ratio of 3000:1:10 ([LA]/[I]/[BnOH]) showing a volcano-type relationship. Geometric preference for a four-coordinate complex (τ_4') is shown in red for tetrahedral complexes.

Between tetrahedral complexes, Zn(F,G,I,J,L)₂, there was also some correlation between Zn – S bond distance and the preference for tetrahedral geometry; this can help to rationalise the observed trends in reactivity. A shorter Zn – S bond distance tends to distort the geometry of the complexes away from tetrahedral. For the incoming lactide monomer, it is easier to displace a weakly coordinated sulphur donor than to coordinate to a tetrahedral centre. However, when the Zn – S bonds are strong then a coordinatively saturated octahedral complex is formed and activity is low. This explains the correlation observed in **Figure 3.21** and the very high activity of Zn(J)₂ (TOF = 124,200 h⁻¹) which is far higher than the activity of Zn(I)₂ (TOF = 31,950 h⁻¹) despite having very similar Zn – S distances. Comparison of the geometric preference shows that Zn(J)₂ has a much lower tetrahedral preference ($\tau_4' = 0.56$) than Zn(I)₂ ($\tau_4' = 0.64$), probably as a result of the lack of steric hindrance around the phenolate groups.

To gain some insight into the mechanism and the role of the co-initiator, a stoichiometric reaction was performed. On an NMR scale, a 1 : 1 solution of *rac*-lactide and Zn(L)₂ in CDCl₃ was initially heated for 90 minutes at 50 °C (**Figure 3.22**). At this stage, resonances corresponding to ring-opened lactide accounted for 34% of

the sample. This increased to 60% upon addition of benzyl alcohol after ten minutes at room temperature and to 94% after a further 90 minutes at 50 °C. This demonstrates that a co-initiator is required for high conversion to be attained but there is also a degree of reaction taking place in its absence. This could result from some initiation by impurities in the monomer, or through a competing coordination-insertion mechanism facilitated by ligand dissociation. The latter has been previously reported with the analogous zinc ONN complex, **113**.^[32]

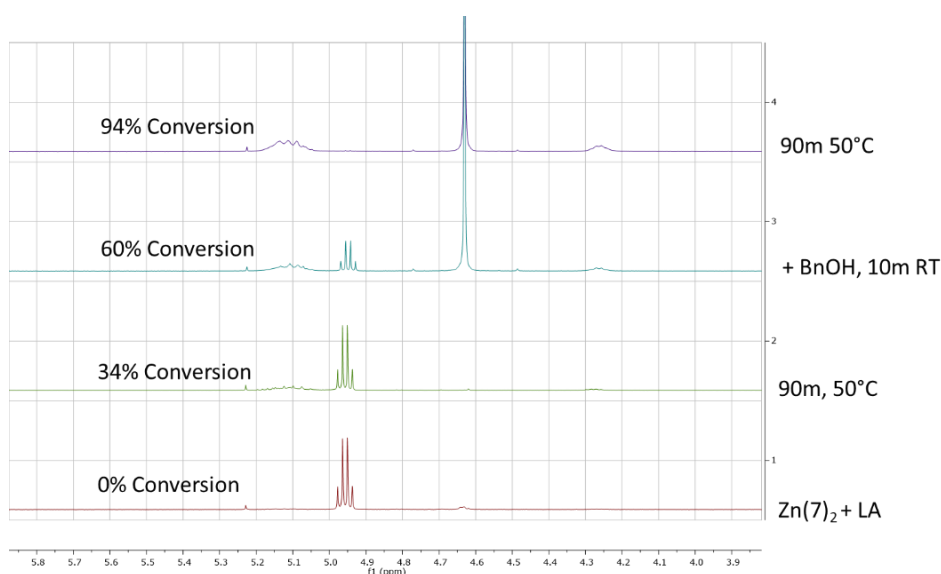


Figure 3.22: ^1H NMR spectra (CDCl_3 , 500MHz) of the methine region for stoichiometric reaction between $\text{Zn}(\mathbf{L})_2$, rac-LA and BnOH.

Further analysis of the ^1H NMR spectra revealed some evidence of ligand dissociation (**Figure 3.23**). Although the aromatic region was relatively unchanged, a new pair of tBu resonances appeared as the reaction progressed. This was corroborated by the presence of a new resonance in the ^{19}F NMR spectrum at the end of the reaction (**Figure 3.24**). This could be evidence of ligand dissociation leading to coordination-insertion or a function of the initiator degradation that was apparent during polymerisations.

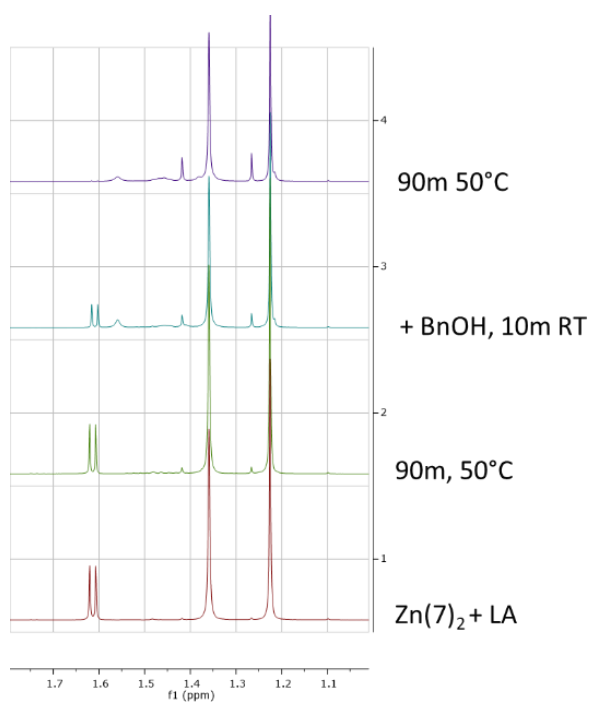


Figure 3.23: ^1H NMR spectra (CDCl_3 , 500MHz) of the methine region for stoichiometric reaction between $\text{Zn}(\text{L})_2$, rac-LA and BnOH.

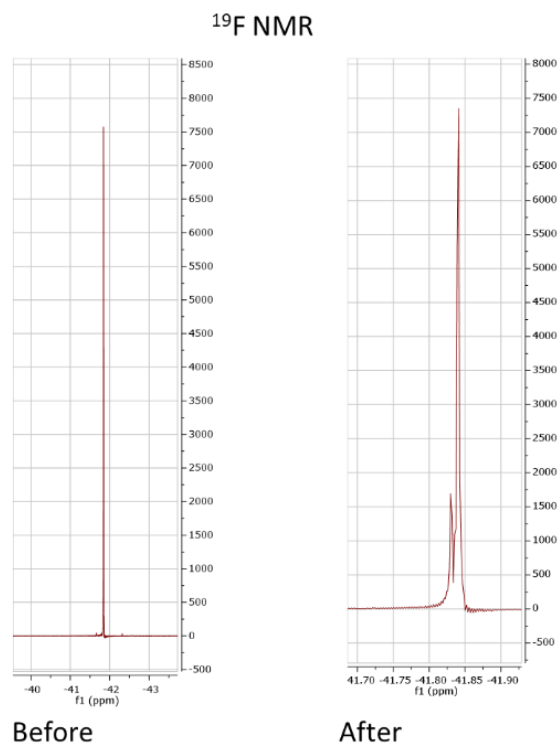


Figure 3.24: ^{19}F NMR spectra (CDCl_3 , 500MHz) of the methine region before and after stoichiometric reaction between $\text{Zn}(\text{L})_2$, rac-LA and BnOH

DOSY NMR of the final reaction mixture was subsequently carried out to ascertain if any coordination-insertion had taken place. If a coordination-insertion mechanism had occurred, then a signal representing ring-opened lactide would be expected at the same diffusion constant as the initiator (**Figure 3.25**). It is clear from the spectrum that the ring-opened lactide has a distinct diffusion and was therefore not bonded to the zinc centre or inserted into the ligand. From this it can be concluded that there is no evidence of coordination-insertion and that an activated monomer mechanism is predominant. The extra signals present in **Figure 3.23** and **Figure 3.24** must therefore be evidence of complex degradation that limits the conversion attainable with this system at low initiator loadings. Furthermore, the degree of conversion observed before addition of benzyl alcohol can be attributed to impurities in the monomer.

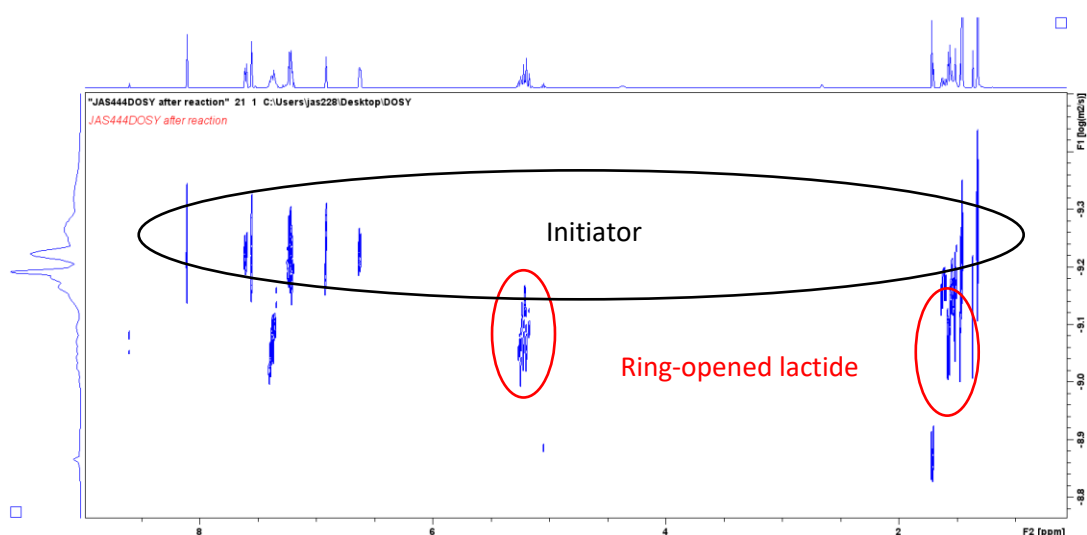


Figure 3.25: DOSY NMR spectrum (CDCl₃, 500 MHz) after stoichiometric reaction between Zn(L)₂, rac-LA and BnOH.

3.2.5 Kinetic study of *rac*-lactide polymerisation with Zn(J)₂ and Zn(L)₂

The work detailed in this section was produced in collaboration with Professor Sonja Herres-Pawlis and Martin Fuchs of Aachen University.

The kinetics of lactide polymerisation with Zn(J)₂ and Zn(L)₂ was probed using *in-situ* Raman spectroscopy. The conditions were chosen to reflect industrial processes and to provide a direct comparison with previously reported systems from Herres-Pawlis and co-workers.^[29,30,40] Technical grade *rac*-lactide was initially used at a ratio of 2500 : 1 with no co-initiator present. Reactions were performed in the melt at 150 °C with mechanical stirring set to 260 rpm. Under these conditions, Zn(L)₂ was the most active initiator giving a rate constant of $1.06 \times 10^{-4} \text{ s}^{-1}$ (**Figure 3.26**). However, the results were disappointing for both initiators with a maximum of 39% conversion achieved over three hours. For the polymer produced from Zn(L)₂, the measured molecular weight was significantly lower than the theoretical molecular weight ($M_{n \text{ calc.}} = 139500 \text{ gmol}^{-1}$, $M_{n \text{ GPC}} = 12500 \text{ gmol}^{-1}$). This suggests that there is significant initiation and chain transfer by monomer impurities.

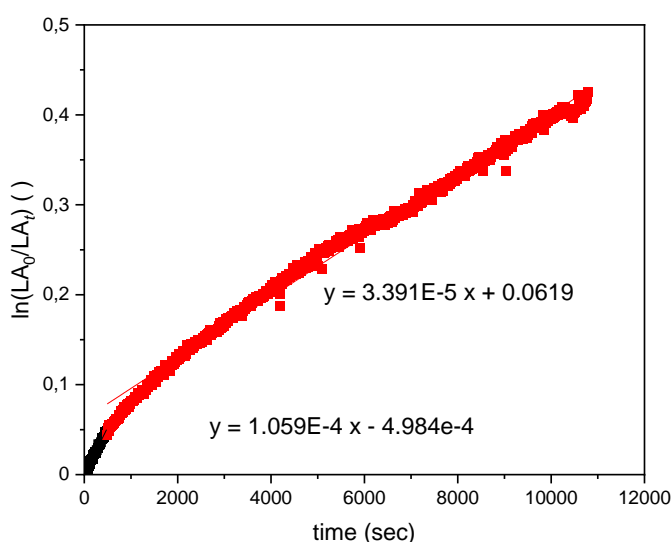


Figure 3.26: Plot of $\ln(LA_0/LA_t)$ vs. time for Zn(L)₂.

The same conditions were subsequently employed using recrystallised *L*-lactide (Figure 3.27 & 3.28). Conversions were lower than seen with technical grade *rac*-lactide for $Zn(J)_2$ and $Zn(L)_2$ giving 7% and 24% respectively in three hours. This can be attributed to a reduction in monomer impurities after recrystallisation, supporting the previous conclusion that ligand-based coordination insertion is not relevant to this system. Furthermore, this explains the low molecular weight observed for *rac*-lactide initiated by $Zn(L)_2$.

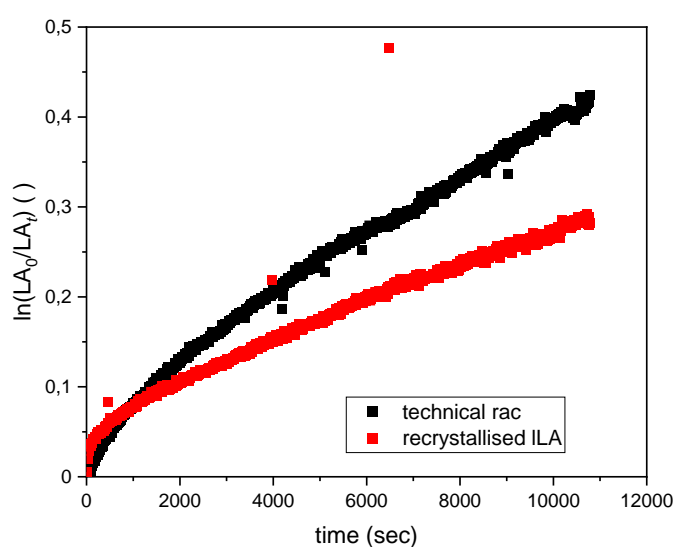


Figure 3.27: Comparison of the semilogarithmic plots for $Zn(J)_2$ and $Zn(L)_2$.

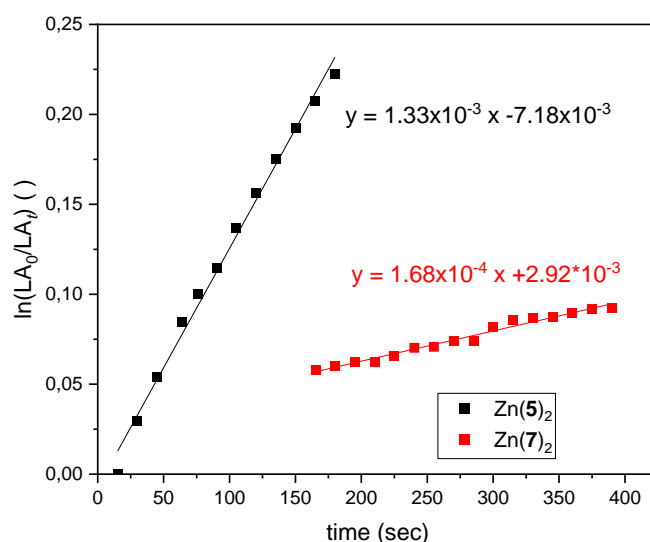


Figure 3.28 Kinetic analysis for $Zn(J,L)_2$. $[LA]/[Zn]/[4-MeBnOH] = 3000 : 1 : 10$. Initial rate.

Due to the continued discrepancy between the very high activity demonstrated in the small-scale polymerisations and the modest activity reported during kinetic runs, the original initiator, BnOH, was used for subsequent experiments. Unfortunately, the nature of the preparation meant that Zn(J)₂ was unsuitable. The activity improved for Zn(L)₂ giving 75% conversion after 45 minutes with $k_{app} = 2.2 \times 10^{-3} \text{ s}^{-1}$ (**Figure 3.29**). The polymerisation was reasonably well controlled ($M_{n, GPC} = 31,200 \text{ gmol}^{-1}$, $M_{n, Calc.} = 32550 \text{ gmol}^{-1}$, $\bar{D} = 1.22$).

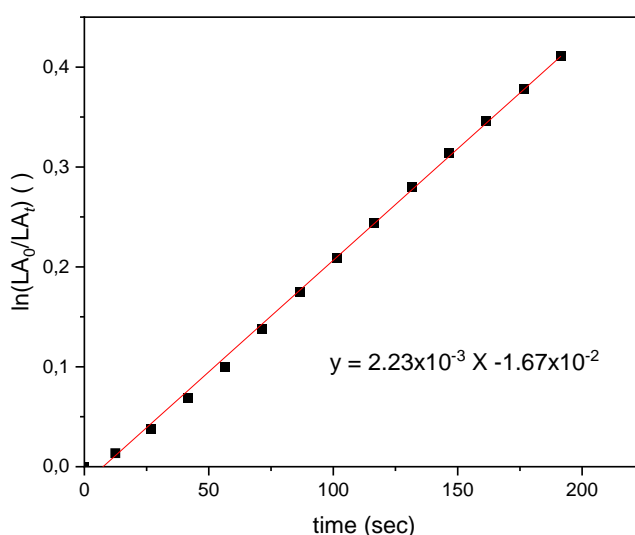


Figure 3.29 Kinetic analysis for Zn(L)₂. [LA]/[Zn]/[BnOH] = 3000 : 1 : 10. Initial rate.

The ratio was increased to [LA]/[I]/[BnOH] = 10000 : 1 : 100 to test the performance of Zn(L)₂ at very low loading. As expected, there was a significantly reduced rate of reaction ($k_{app} = 9.95 \times 10^{-5}$) and only 34% conversion was possible over six hours (**Figure 3.30**). Despite the impressive activity shown by these complexes in sealed flasks with magnetic stirring, the transition to the larger and less air sensitive conditions within the Raman kinetics reactor significantly reduced the efficacy of Zn(J)₂ and Zn(L)₂. The results were ultimately not comparable with the rapid guanidine-based systems reported by Herres-Pawlis.^[29,30] This can be attributed to the deactivation processes discussed in **Section 3.2.4**. Presumably, these are more

apparent with the extended reaction times and larger volumes required for the kinetics experiments.

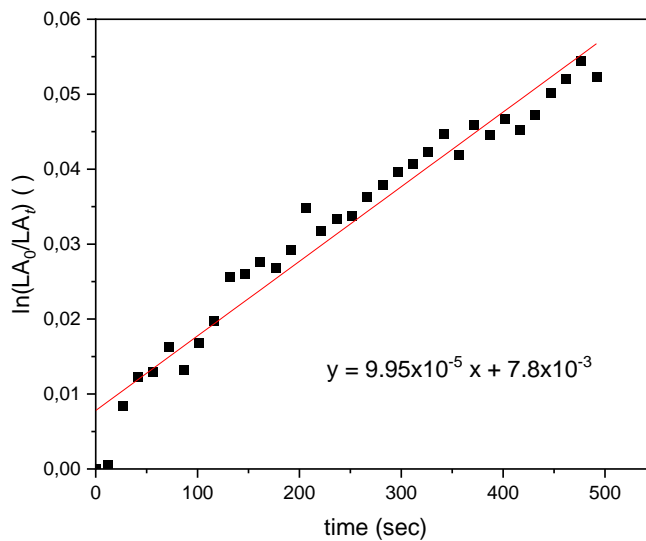


Figure 3.30: Kinetic analysis for Zn(L)₂. [LA]/[Zn]/[BnOH] = 10000 : 1 : 100. Initial rate.

3.3 Introduction – Catalytic PLA degradation

3.3.1 Chemical recycling

The significant issues associated with the production of plastics from crude oil can be offset through the incorporation of abundant and renewable feedstocks. However, equally important is the disposal of plastic waste and its effect on the environment and ecological systems. Traditional hydrocarbon plastics do not biodegrade, instead forming toxic microparticles which are devastating to marine ecosystems.^[3,100,101] This form of pollution is not limited to the oceans and significant microplastic contamination has been found in terrestrial and freshwater environments as well as in animal sources and, recently, in the human bloodstream.^[6,102,103] Mechanical recycling is somewhat effective but inevitably leads to a downgrading of material properties which limits the number of cycles possible; it is therefore a limited strategy for retaining value in the polymer economy.^[10]

Chemical recycling offers an alternative strategy wherein polymers are depolymerised into virgin monomer or degraded to value-added products (**Figure 3.31**).^[38] Depolymerisation offers a potentially unlimited number of monomer to polymer cycles with no material downcycling whereas degradation can be designed to give useful and valuable chemicals or to give a product that can be readily converted to virgin monomer. Both offer an intrinsic economic incentive for industry to consider the end-of-life strategies for their products and are a crucial component of a circular economy for polymers.

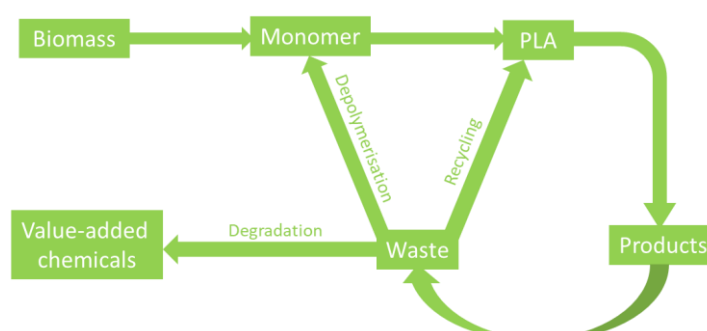


Figure 3.31: Schematic showing a circular economy approach to PLA production and disposal.

Some technologies have been developed which allow for hydrocarbon polymers to be chemically recycled through solvolysis, dissolution and pyrolysis among other strategies.^[49–51] However, the nature of these polymers, particularly for polyolefins, means that there are no convenient chemical target groups for catalytic decomposition and so harsh conditions are often required. Conversely, polyesters such as PLA and PET are ideal for attack by a transesterification catalyst and can form monomer adducts with alcohols (alcoholysis). In the case of PLA, the target products are often alkyl lactates. Alkyl lactates are increasingly useful as high boiling point, “green” solvents with potential for use in many industries such as agriculture, industrial cleaning and pharmaceutical.^[52–55] Low molecular weight alkyl lactates can also be directly converted to virgin lactide monomer.^[56] Furthermore, alkyl lactates can also replace lactic acid in many transformations and so could be considered platform chemicals.^[57] A recent LCA compared PLA alcoholysis to hydrolysis and incineration and found it preferable for every measured environmental impact with the exception of land use and ozone depletion.^[58]

3.3.2 PLA degradation – hydrolysis

DuPont patented an early process for the degradation of PLA to lactate esters in the presence of H₂SO₄ at high temperatures (≤ 190 °C).^[59] Numerous studies have reported PLA degradation to lactate esters through hydrolysis.^[60–64] Moscatelli *et al.* showed that the degradation of small polylactide oligomers was strongly dependent on pH.^[61,62] PLA was shown to degrade readily over 20 days at 30 °C in a strong acid or base environment but was relatively stable where pH was close to neutral.^[64]

3.3.3 PLA degradation – ionic liquids and organocatalysis

Liu and co-workers reported the first example of ionic liquid catalysed PLA degradation to methyl lactate.^[65] Several ionic liquids were tested with 1-butyl-3-methylimidazolium acetate ([Bmim][Ac]) being the most active system. The reaction conditions were optimised, and it was found that PLA solubility was the most important factor. Using optimised conditions (T = 115 °C, [CH₃OH]/[PLA] = 5 : 1,

[IL]/[PLA] = 0.02 : 1), 97.2% PLA conversion was achieved with 92.5% yield of methyl lactate. The reusability of the ionic liquid was also demonstrated with minimal loss of activity over six recycling runs. A subsequent report by the same group demonstrated the beneficial use of acid-modified ionic liquid, [HSO₃-pmim][HSO₄].^[66] Similar results were obtained as with [Bmim][Ac] with PLA conversion and Me-LA yield of 97% and 88.7% respectively and recyclability was demonstrated over six cycles.

The introduction of a Lewis acidic moiety to the ionic liquid, [Bmim]FeCl₄, further improved the activity of the degradation system giving nearly quantitative PLA conversion and 94.6% Me-LA yield. Crucially, this result was achieved with a much lower dosage of catalyst [IL]/[PLA] = 0.0025:1. As with the other ionic liquid catalysts, [Bmim]FeCl₄ could be reused six times without loss of activity. The introduction of zinc acetate to the ionic liquid {2[Bmim][OAc]-Zn(OAc)₂} resulted in the most active ionic liquid PLA degradation catalyst to date.^[67] After one hour, 93.46% of PLA was converted with a Me-LA yield 87.75%, and this could be increased with reaction time or temperature. A kinetic investigation showed that PLA methanolysis was a *pseudo*-first order reaction where $E_a = 20.96 \text{ kJmol}^{-1}$.

Triazabicyclodecane (TBD) was shown to be an active catalyst for PLA degradation by Shand *et al.*^[68] At 1 mol% loading, complete consumption of PLA was observed and several alcoholysis products were demonstrated. Lactate dimers were shown to be a significant by-product, and this could be avoided to give >95% lactate ester yield by increasing the loading to 2.5 mol% or increasing the reaction time to 10 min. 4-dimethylaminopyridine (DMAP) has also been applied to PLA degradation.^[69] Microwave heating was used to heat the reaction to 180 °C allowing for 97% yield of methyl lactate after 10 minutes. The system did not require a solvent and activity was generally maintained when degrading a range of PLA products with varying levels of additives and dyes.

McKeown and co-workers published a simple organocatalyst of the structure [NMe₄]⁺[OCO₂Me]⁻ that was capable of degrading commercial samples of PLA, PCL, PC and PET.^[70] At 50 °C with 4 wt% organocatalyst, full conversion and quantitative Me-LA yield was possible after one hour. Increasing the temperature and alcohol

content allowed the reaction to proceed to completion without extra solvent in 10 minutes. The reaction was also attempted with less harmful solvents. Although THF gave the best results, ethyl acetate and 2-Me-THF produced comparable conversion and yield.

3.3.4 PLA degradation – zinc catalysis

The first example of a zinc complex for PLA degradation was reported by Avilés and co-workers with a dizinc NHC complex (**Figure 3.32**).^[71] Complex **121** was initially shown to be an effective initiator for lactide polymerisation. Upon washing the polymer with methanol, oligomers and methyl lactate were shown to be present from the GPC trace. A more controlled experiment using a commercial source of PLLA demonstrated a linear decline in PLLA and a concurrent linear increase in methyl lactate and small oligomers.

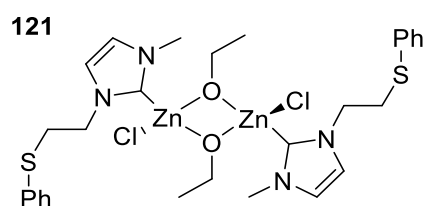


Figure 3.32: Dinuclear Zn (NHC) complex for PLA degradation to methyl lactate reported by Avilés *et al.*^[71]

Jones and co-workers subsequently applied a previously reported homoleptic zinc {ONN} complex **113**, that was highly active for lactide polymerisation, to PLA degradation under mild conditions (**Figure 3.33**).^[34] The effect of many parameters were studied including temperature, concentration, stirring speed and PLA grade and 100% yield of methyl lactate could be achieved in one hour under optimised conditions, although this required a very high catalyst loading of 16 wt% and relatively high temperatures. It was found that catalyst concentration and temperature had the most profound effect on reaction rate and that there was no

evidence of mass-transfer limitations. A detailed kinetic study was used to propose a two-step mechanism that will be discussed further in section 3.3.5.

The introduction of a propyl linker gave complexes **116** and **112** which significantly outperformed their ethylene-linked counterparts.^[33] **116** was particularly quick ($k_{app} = 0.20 \text{ min}^{-1}$) with full PLA consumption observed after 30 minutes at mild conditions and with relatively low catalyst loading (50 °C, 4 wt%). The corresponding rate constant for **122** was $k_{app} = 0.094 \text{ min}^{-1}$ under the same conditions after a one-hour reaction time. Upon increasing the temperature to 130 °C, **116** achieved essentially quantitative conversion to methyl lactate after one hour with 1 wt% catalyst. A conversion of 97% was attained when the reaction was scaled up to 12.25 g PLA with **122**.

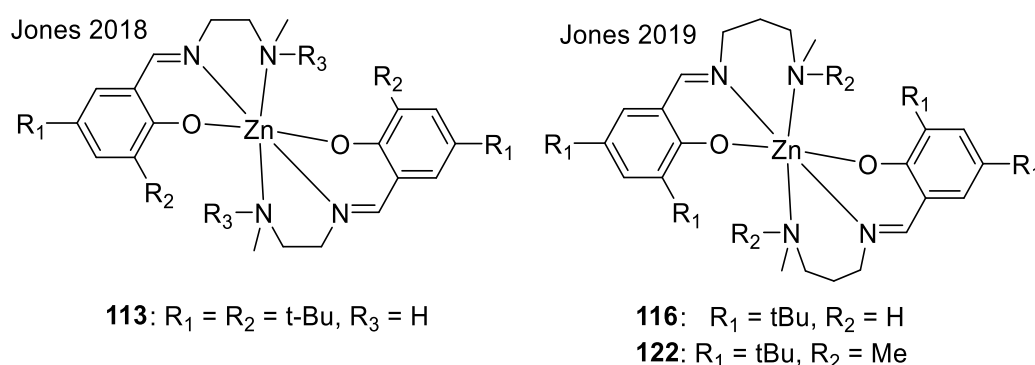


Figure 3.33: Homoleptic zinc {ONS} complexes for PLA degradation reported by Jones and co-workers.^[33,34]

A follow up study presented a detailed kinetic analysis of methyl lactate production from **113** and **116**.^[72] Ethylenediamine-based complex **113** was shown to be robust towards oxygen and moisture and the reaction followed the linear temperature-dependent model given by the Arrhenius equation. The behaviour of **116** was more complex, showing some non-Arrhenius behaviour resulting in more rapid methyl lactate production at lower temperatures. The authors proposed the design of a system whereby PLA is broken down into oligomers at elevated temperatures followed by methyl lactate production at ambient conditions.

Ethylenediamine complex **113** was applied to the degradation of commercial PLA waste sources including a cup, a toy and some 3D printing material.^[73] The waste PLA degraded at similar rates to virgin PLA and a predictive model was developed that could predict conversion and selectivity. The presence of additives was identified as the main source of rate variation with the toy proving to have the most additives and be most difficult to break down. Complex **122** was also applied to post-consumer PLA degradation in a subsequent study.^[74] In addition to the sources tested with **113**, thin-film PLA and a PLA phone case were also degraded. The film was degraded most effectively giving a 71% yield of ethyl lactate after 3 hours at 50 °C. As previously noted, this catalyst was most effective at lower temperatures for the thinner samples, but elevated temperatures were required to solubilise the phone case and toy. The rate of degradation was shown to be reliant on ease of dissolution and the level of additives whereas the dispersity and molecular weight of the polymers had no impact.

Payne and co-workers introduced a Schiff base bidentate ligand and prepared a series of mononuclear (**123 – 125**) and dinuclear (**117 – 119**) zinc complexes that were active for lactide polymerisation and PLA degradation to methyl lactate (**Figure 3.34 & 3.13**).^[35] Monomeric complexes **124** and **125** were the most active degradation catalysts achieving 100% Me-LA yield after 8 h at 80 °C and 8 wt% loading. When the temperature was lowered to 50 °C, with a corresponding increase in reaction time to 18 h, **124** and **125** remained active giving Me-LA yields of 88% and 77% respectively. Kinetic analysis revealed that the loading was important for activity and the rate dropped when it was reduced from 8 wt% ($k_{app} = 0.63 \pm 0.051 \text{ h}^{-1}$) to 4 wt% ($k_{app} = 0.37 \pm 0.021 \text{ h}^{-1}$).

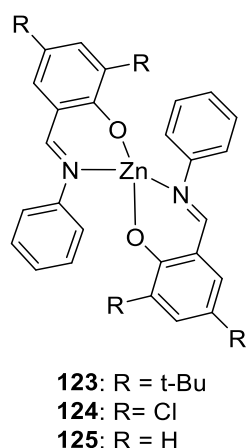


Figure 3.34: Monomeric zinc {ON} complex for PLA degradation reported by Jones *et al.*^[35]

Complex **120** (Figure 3.14), with a catam-like {ONN} coordination motif, was significantly more active for PLA degradation than the catalen equivalent.^[37] At 4 wt% catalyst loading, 100% PLA conversion was possible in 3 h at both 50 °C and 80 °C, both giving Me-LA yields around 90%. The system was proved to be robust to PVC impurities and effective at loadings as low as 2 wt%. The magnesium equivalent showed similar activity and retained more activity at low catalyst loadings. Room temperature degradation was also demonstrated, and 68% conversion was possible over 16 h.

A series of homo- and heteroleptic zinc complexes based on half salan ligands were reported by Payne and co-workers that could catalyse the degradation of several plastics including PLA (Figure 3.35).^[75] Complexes **127** and **128** were the most active catalysts, both converting 100% of PLA after 1.5 h (50 °C, 8 wt%) giving rates of $k_{app} = 0.053 \text{ min}^{-1}$ and $k_{app} = 0.044 \text{ min}^{-1}$ respectively.

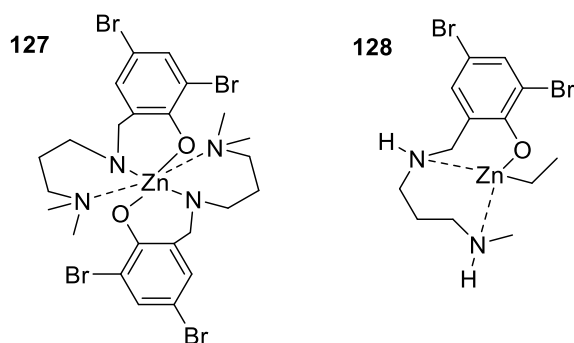
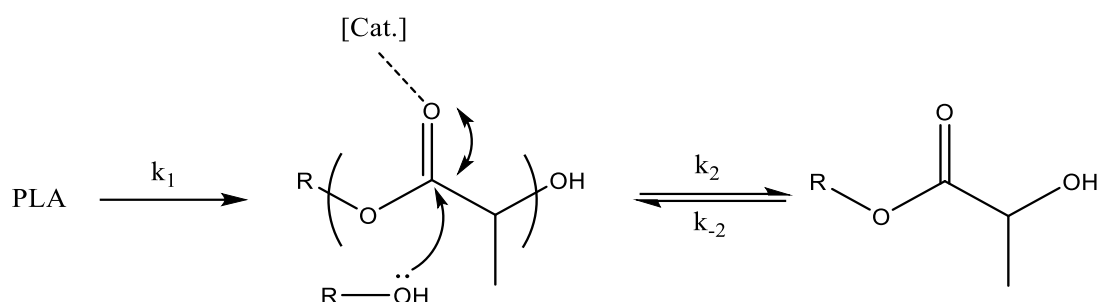


Figure 3.35: Half-salan zinc complexes for PLA degradation.^[75]

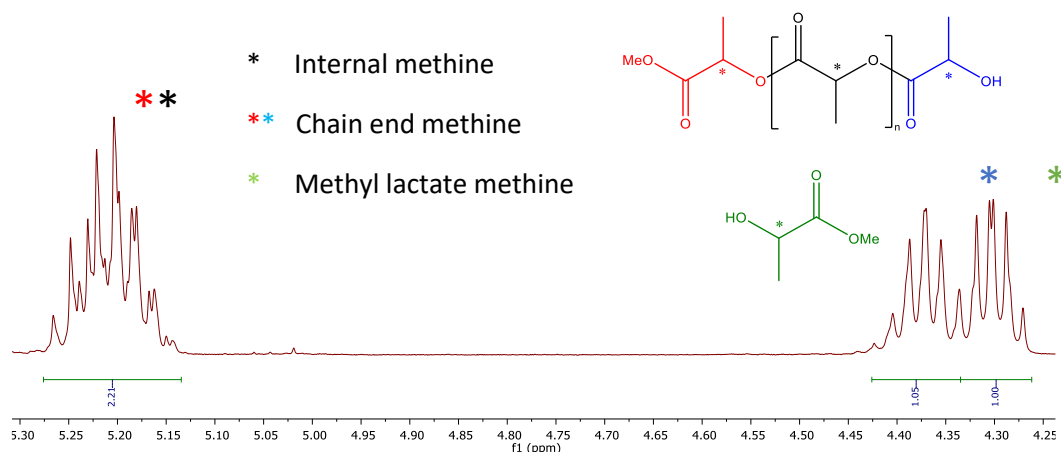
3.3.5 PLA degradation – mechanism and characterisation

The zinc-catalysed degradation of PLA has been shown to occur through a two-step mechanism (**Scheme 3.03**).^[34] The carbonyl group is activated by the catalyst allowing for nucleophilic attack by the alcohol. The polymer initially breaks down irreversibly into oligomers before a reversible step where the alkyl lactate is formed.



Scheme 3.03: Mechanism for the degradation of PLA to alkyl lactate.

The reaction can be followed through ¹H NMR spectroscopy where three distinct signals can be observed in the methine region (*ca.* δ = 4.2 – 5.2 ppm). The most downfield signal corresponds to an overlapping combination of internal and chain end methine protons (**figure 3.36**). The former represents the PLA starting material whereas the latter is a measure of the oligomeric intermediate species. The middle peak is also related to the oligomers and the upfield signal corresponds to the alkyl lactate product. From the relative integration of the three signals, the percentage composition of each component can be calculated.



$$[\text{Me-LA}] = 1/(1+2.21+1.05) = 23.5\%$$

$$[\text{Int}] = (2.21-1.05)/(1+2.21+1.05) = 27.2\%$$

$$[\text{CE}] = 1.05/(1+2.21+1.05) = 24.6\%$$

$$[\text{CE}] = 1.05/(1+2.21+1.05) = 24.6\%$$

Figure 3.36: ^1H NMR (CDCl_3 , 400 MHz) spectrum of PLA Vegware cup degradation into methyl lactate (Me-LA) using $\text{Zn}(\text{I})_2$ (8 wt% - mol% relative to ester linkages) at 80°C for 8 h in THF.

From the relative quantities of each component, it was possible to calculate three key parameters from the following equations:

$$X_{int} = 1 - \frac{[int]}{[int]_0}$$

$$S_{\text{Me-LA}} = \frac{[\text{Me-LA}]}{[int]_0 - [int]}$$

$$Y_{\text{Me-LA}} = X_{int} S_{\text{Me-LA}}$$

The conversion of internal methine (X_{int}) gives the overall conversion of PLA to oligomers and alkyl lactate. $S_{\text{Me-LA}}$ refers to the selectivity of the catalyst towards methyl lactate and $Y_{\text{Me-LA}}$ gives the overall yield of methyl lactate. These parameters can be used to assess the activity and selectivity of the catalysts towards PLA degradation.

3.4 Polyester degradation with {ONS} zinc complexes

3.4.1 PLA degradation with Zn(F–N)₂

Complexes Zn(F–N)₂ were applied to the catalytic degradation of PLA to methyl lactate and moderate activity was observed with all catalysts (**Table 3.10**). A PLLA cup (0.25 g, $M_n = 45510 \text{ gmol}^{-1}$) was used for degradation as a proxy for consumer waste. Polymer and catalyst (8 wt%, 20 mg) were added in a glovebox and dissolved in bench THF. Upon solubilisation of PLA at 80 °C, MeOH was added to the mixture to initiate the reaction. Initial conditions were chosen to provide direct comparisons with published zinc catalysts (80 °C, 8 wt% catalyst loading, 8 h). Reactivity trends were generally not consistent with polymerisation efficacy. Ethylene-bridged complexes, Zn(F–H)₂, were more competitive than seen during lactide polymerisation with Zn(G)₂ giving the highest yield and selectivity to Me-LA of all the tested catalysts ($S_{\text{Me-LA}} = 72\%$, $Y_{\text{Me-LA}} = 63\%$). The poor polymerisation activity of Zn(G)₂ could be advantageous as Me-LA would be less likely to be re-polymerised to oligomers i.e., $k_2 > k_{-2}$.

Internal methine conversion was greatest for Zn(I)₂ and Zn(J)₂ giving internal methine conversion of 94% and 96% respectively, although less Me-LA was produced than with Zn(G)₂ [Zn(I)₂, $S_{\text{Me-LA}} = 50\%$, $Y_{\text{Me-LA}} = 47\%$; Zn(J)₂, $S_{\text{Me-LA}} = 62\%$, $Y_{\text{Me-LA}} = 59\%$]. The slowest of the phenylene-bridged, S-Me complexes was Zn(K)₂ ($R_1 = \text{Cl}$, $R_2 = \text{Me}$, $Y = -\text{C}_4\text{H}_6-$), presumably as a result of the crowded steric profile. However, reasonable conversion of internal methine was still achieved ($X_{\text{int}} = 78\%$). The activity was significantly reduced by the introduction of trifluoromethyl groups at the thioether position with H and tBu groups at the R₁ position. Catalysts Zn(L)₂ and Zn(M)₂ both converted 39% of internal methine with correspondingly low yields of Me-LA. This could be related to the sensitivity of Zn(L)₂ to moisture or contaminants combined with the use of bench solvents for degradation reactions. Conversely, Zn(N)₂ performed relatively well ($X_{\text{int}} = 81\%$, $S_{\text{Me-LA}} = 50\%$, $Y_{\text{Me-LA}} = 41\%$).

Table 3.10: Degradation of PLLA cup to Me-LA using Zn(F-N)₂ at 80 °C^a

Init.	T/°C	Time /hours	Cat. Loading/wt%	Y _{Me-LA} /%	S _{Me-LA} /%	X _{int} /%
Zn(F) ₂	80	8	8	24	33	72
Zn(G) ₂	80	8	8	63	72	87
Zn(H) ₂	80	8	8	13	20	65
Zn(I) ₂	80	8	8	47	50	94
Zn(J) ₂	80	8	8	59	62	96
Zn(K) ₂	80	8	8	32	41	78
Zn(L) ₂	80	8	8	6	16	39
Zn(M) ₂	80	8	8	7	17	39
Zn(N) ₂	80	8	8	41	50	81

^a Reaction conditions: 0.25 g of PLLA cup ($M_n = 45\,510\text{ g mol}^{-1}$), $V_{\text{THF}} : V_{\text{MeOH}} = 4 : 1$, $n_{\text{MeOH}} : n_{\text{ester}} = 7 : 1$, 8 wt% cat. loading (1.3–2.1 mol% relative to ester linkages). $Y_{\text{Me-LA}}$, $S_{\text{Me-LA}}$ and X_{int} determined by ¹H NMR upon solvent removal.

The most active degradation catalysts, Zn(G,I,J,N)₂ were tested at 50 °C with an extended reaction time of 18 hours (Table 3.11). Although all complexes were active at this temperature, conversion was reduced for all complexes; this is consistent with literature examples.^[35,76] Zn(G)₂ gave the highest conversion of internal methine and the highest yield and selectivity to Me-LA ($X_{\text{int}} = 77\%$, $S_{\text{Me-LA}} = 41\%$, $Y_{\text{Me-LA}} = 31\%$). The most notable reduction in activity came from Zn(I)₂ and Zn(J)₂, which were the most active catalysts at 80 °C, and gave internal methine conversions of 57% and 56% respectively. Zn(N)₂ was slightly more active giving 62% PLA conversion and 16% yield of Me-LA.

Table 3.11: Degradation of PLLA cup to Me-LA using Zn(G,I,J,N)₂ at 80 °C^a

Init.	T/°C	Time /hours	Cat. Loading/wt%	Y _{Me-LA} /%	S _{Me-LA} /%	X _{int} /%
Zn(G) ₂	80	8	8	63	72	87
Zn(I) ₂	80	8	8	47	50	94
Zn(J) ₂	80	8	8	59	62	96
Zn(N) ₂	80	8	8	41	50	81

^a Reaction conditions: 0.25 g of PLLA cup ($M_n = 45\,510\text{ g mol}^{-1}$), $V_{\text{THF}} : V_{\text{MeOH}} = 4 : 1$, $n_{\text{MeOH}} : n_{\text{ester}} = 7 : 1$, 8 wt% cat. loading (1.3–2.1 mol% relative to ester linkages). $Y_{\text{Me-LA}}$, $S_{\text{Me-LA}}$ and X_{int} determined by ¹H NMR upon solvent removal.

3.4.2 Kinetics of PLA degradation with Zn(G)₂ and Zn(N)₂

Kinetic analysis was attempted for Zn(G,I,J,N)₂ of which only Zn(G)₂ and Zn(N)₂ were amenable to sampling (**Figure 3.37**). Complexes Zn(I)₂ and Zn(J)₂ quenched after the first sample was taken for ¹H NMR analysis, suggesting that rapid deactivation of the catalysts occurred upon brief exposure to air. Zn(G)₂ and Zn(N)₂ were more robust and gave rate constants of $0.00528 \pm 1.63 \times 10^{-4} \text{ min}^{-1}$ ($R^2 = 0.995$) and $0.00567 \pm 4.17 \times 10^{-4} \text{ min}^{-1}$ ($R^2 = 0.979$) respectively. Statistically, there is no significant difference between the two rate constants. It should be noted that, for Zn(G)₂, the final conversion, selectivity and yield during the kinetic runs ($X_{\text{int}} = 94\%$, $S_{\text{Me-LA}} = 59\%$, $Y_{\text{Me-LA}} = 55\%$) were all lower than the initial testing where no samples were taken ($X_{\text{int}} = 99\%$, $S_{\text{Me-LA}} = 72\%$, $Y_{\text{Me-LA}} = 71\%$). This is presumably a result of slight deactivation during sampling and implies that the apparent rate constant is understated.

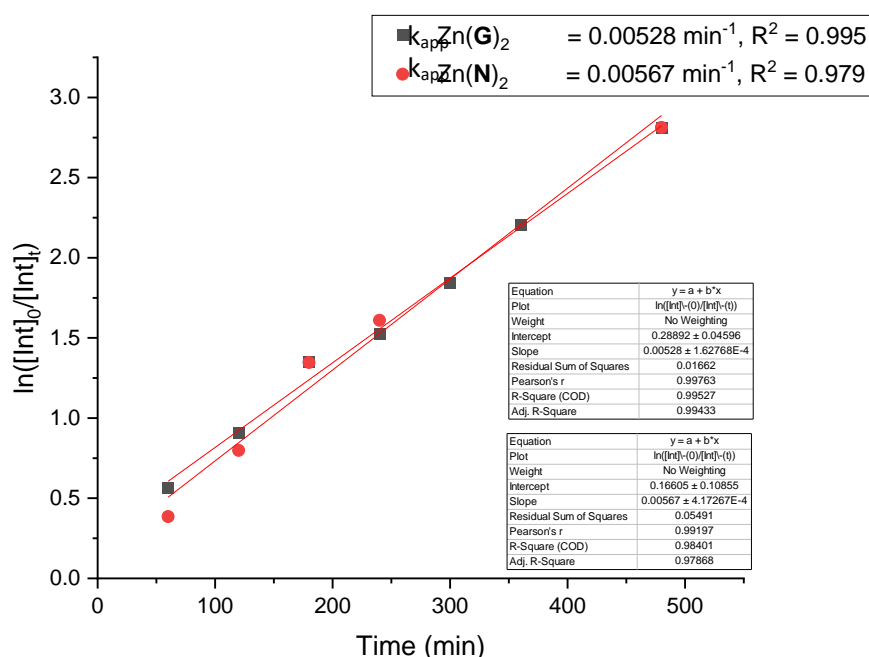


Figure 3.37: Semi-logarithmic plot for PLA degradation with Zn(G)₂ and Zn(N)₂.

From the data acquired during the kinetic runs, it was also possible to look at the reaction profiles through the varying percentages of internal, chain end and Me-LA methine signals (**Figure 3.38** & **Figure 3.39**). Consumption of PLA was initially most

rapid with Zn(**G**)₂ with 43% internal methine converted after one hour compared to 32% for Zn(**N**)₂. However, after three hours, both reaction mixtures contained 26% internal methine units and remained approximately equal down to 6% remaining after 8 hours. This could reflect the aforementioned deactivation of Zn(**G**)₂ during sampling and the reduction in conversion compared to initial testing. The proportion of chain end methine grew more rapidly during the first hour for Zn(**G**)₂ and had a greater peak concentration, which was seen at 3 hours for both catalysts (Zn(**G**)₂, [CE]_{max} = 48%, Zn(**N**)₂, [CE]_{max} = 41%). For Zn(**G**)₂, Me-LA production was consistent and linear ($R^2 = 0.99$) over the reaction time. For Zn(**N**)₂, the Me-LA percentage was low for the first two time points and then rapidly increased and was greater for Zn(**N**)₂ (33%) than Zn(**G**)₂ (27%) after three hours. The acceleration of Me-LA production for Zn(**N**)₂ could be rationalised by considering the concurrent peak in oligomer concentration driving the reaction towards Me-LA. The lack of this effect with Zn(**G**)₂, coupled with the high percentage of chain end methine suggests that the second reversible step (k_2) was slower for Zn(**G**)₂ resulting in a reduced selectivity and yield of Me-LA. It is therefore likely that the deactivation process that was previously discussed primarily affected the conversion of oligomers to product rather than the consumption of PLA.

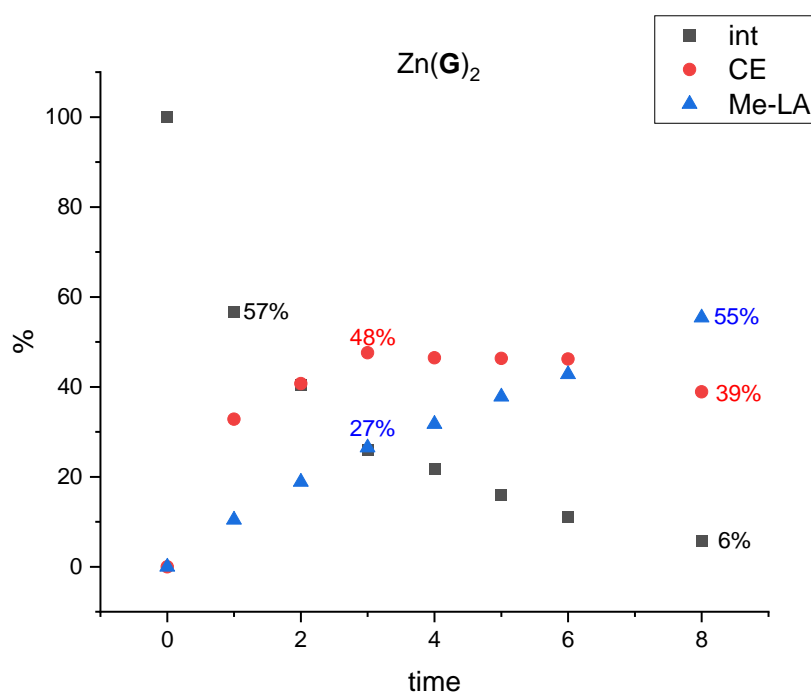


Figure 3.38: Reaction profile for PLA degradation with Zn(**G**)₂.

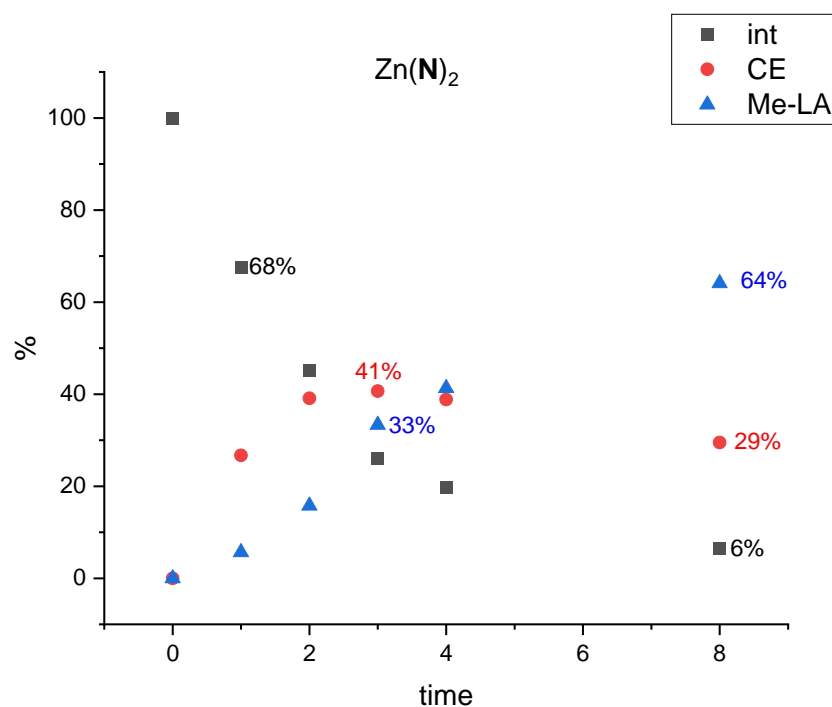
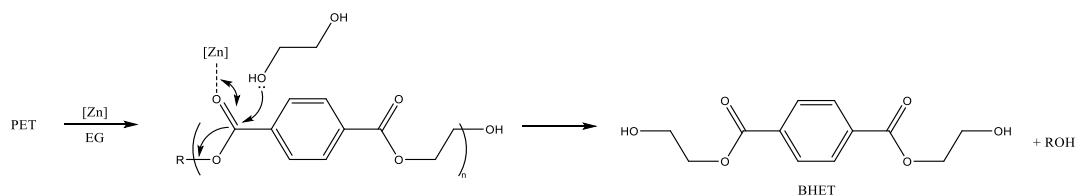


Figure 3.39: Reaction profile for PLA degradation with Zn(N)₂.

3.4.3 PET degradation with Zn(F-N)₂

Despite the increasing prevalence of PLA in the polymer economy, crude-oil based polymers still dominate the market and therefore the chemical recycling of these materials is of utmost importance. PET is one of the most important commodity plastics and accounted for 9% of all polymer production in 2015.^[77] Despite a relatively effective and widespread mechanical recycling program, the sheer volume of disposable PET products mean that it is a significant contributor to plastic waste and does not readily degrade in the environment.^[78] The targeted product for this work was bis(2-hydroxyethyl) terephthalate (BHET) through glycolysis with two equivalents of ethylene glycol (**Scheme 3.04**). BHET is a useful chemical that can be used to make unsaturated polymer resins or can be repolymerised to give virgin PET.^[79,80] The production of BHET from waste PET is one of the oldest and most well-established commercial chemical recycling processes.^[81] During the catalysed reaction, the ester carbonyl is activated through interaction with the zinc complex allowing for nucleophilic attack by the alcohol to give the hydroxyl terminated product.



Scheme 3.04: Mechanism for the production of BHET from PET with a zinc catalyst.

There are many reported catalysts for PET glycolysis including metal salts, simple base catalysts and ionic liquids, however there are limited examples of discrete metal complexes for this reaction.^[51,81–84] Zinc acetate is generally considered to be the benchmark metal salt catalyst and so there have been recent examples of ligated zinc complexes for PET degradation.^[79] Zinc catalen complex **126** degraded PET from a carbonated drink bottle in four hours to give 49% yield of isolated BHET, slightly outperforming the commercial zinc acetate reference.^[36] A high ratio of EG/PET (27.5 eq.) was employed to prevent repolymerisation and to drive the reaction towards the products. No external solvent was required although high temperature was required for the reaction to proceed. The reaction was assumed to be complete when the PET had fully solubilised.

Complex **120** achieved full PET consumption after one hour under the same conditions.^[37] This could be reduced to 20 minutes when using thin-film PET as a proxy for manufacturing waste. Complex **127** gave similar results with reduced catalyst loading.^[75]

The conditions used for this work were based on the work with discrete zinc complexes that have been discussed.^[35–37,75] The PET (0.25 g) and catalyst (8 wt%, 0.02 g) were dissolved in 27.5 equivalents (2 mL) of ethylene glycol. The reaction was heated to 180 °C and stopped when full PET dissolution was observed. The product was collected through recrystallisation from water and pure, white BHET was isolated in all cases (**Figures 3.40**).

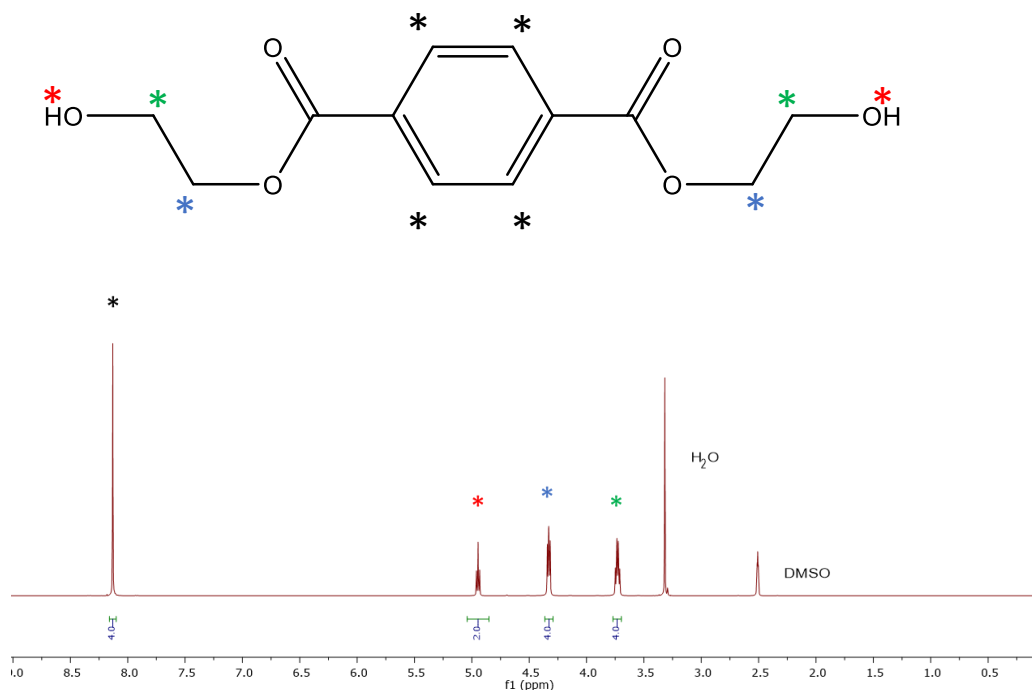


Figure 3.40: ^1H NMR ($\text{D}_6\text{-DMSO}$, 400 MHz) spectrum of recrystallised BHET from PET carbonated drink bottle degradation using $\text{Zn}(\text{G})_2$.

Complexes $\text{Zn}(\text{G,I,J,N})_2$ were applied to the glycolysis of a PET carbonated drink bottle ($M_n \sim 40000 \text{ gmol}^{-1}$) (**Table 3.12**). Full dissolution was observed between 1.5 and 4 hours giving approximately 50% conversion in all cases; this is probably a result of product lost during recrystallisation, consistent with analogous systems.^[35,36] Interestingly, the most active catalysts, $\text{Zn}(\text{G})_2$ and $\text{Zn}(\text{N})_2$, were the only ones amenable to sampling during PLA kinetic experiments. This could suggest that resistance to bench reagents is important for activity. $\text{Zn}(\text{G})_2$ was the most active catalyst taking 1.5 hours to consume PET. It was therefore applied to the degradation of thin film PET, a proxy for manufacturing waste, where PET consumption was observed after 0.75 hours. This is probably related to ease of dissolution of the thinner material.

Table 3.12: Degradation of PET to BHET using Zn(G,I,J,N)₂.

Init.	T/°C	Time /hours	Cat. Loading/wt%	Y _{BHET} (g/%)
Zn(G) ₂	180	1.5	8	0.16 (48%)
Zn(G) ₂ ^a	180	0.75	8	0.17 (51%)
Zn(I) ₂	180	4	8	0.18 (55%)
Zn(J) ₂	180	4	8	0.14 (42%)
Zn(N) ₂	180	3.5	8	0.17 (51%)

Reaction conditions: 0.25 g of carbonated drinks bottle ($M_n \sim 40\,000 \text{ g mol}^{-1}$), 27.5 equivalents of EG (relative to ester linkages), 8 wt% cat. loading (0.02 g, 1.9–3.4 mol% relative to ester linkages). b 0.25 g PET thin film.

3.5 Aluminium {ONS} complexes for lactide polymerisation

3.5.1 Synthesis and characterisation of aluminium {ONS} complexes

The complexation of ligands **I** – NH with aluminium was attempted to target the bis-ligated methyl complexes, $\text{Al}(\text{Lig})_2\text{Me}$. The ligands were prepared according to the procedure detailed in **Scheme 3.01** then reacted in a 2 : 1 ratio with AlMe_3 in anhydrous toluene. The resulting complexes crystallised from mixtures of hexane and toluene. Four complexes were successfully synthesised and characterised. The solid-state structures of aluminium complexes made from **KH**, **LH** and **MH** showed the expected monomeric structures with no sulphur – aluminium bonding and *pseudo*-trigonal bipyramidal geometry ($\tau_5 = 0.75 - 0.83$) (**Figure 3.41**, **Table 3.13**). The largest coordination angle for each of the three complexes is situated between the two nitrogen donors [$\text{N}(1) - \text{Al} - \text{N}(2) = 166.65 - 178.67^\circ$].

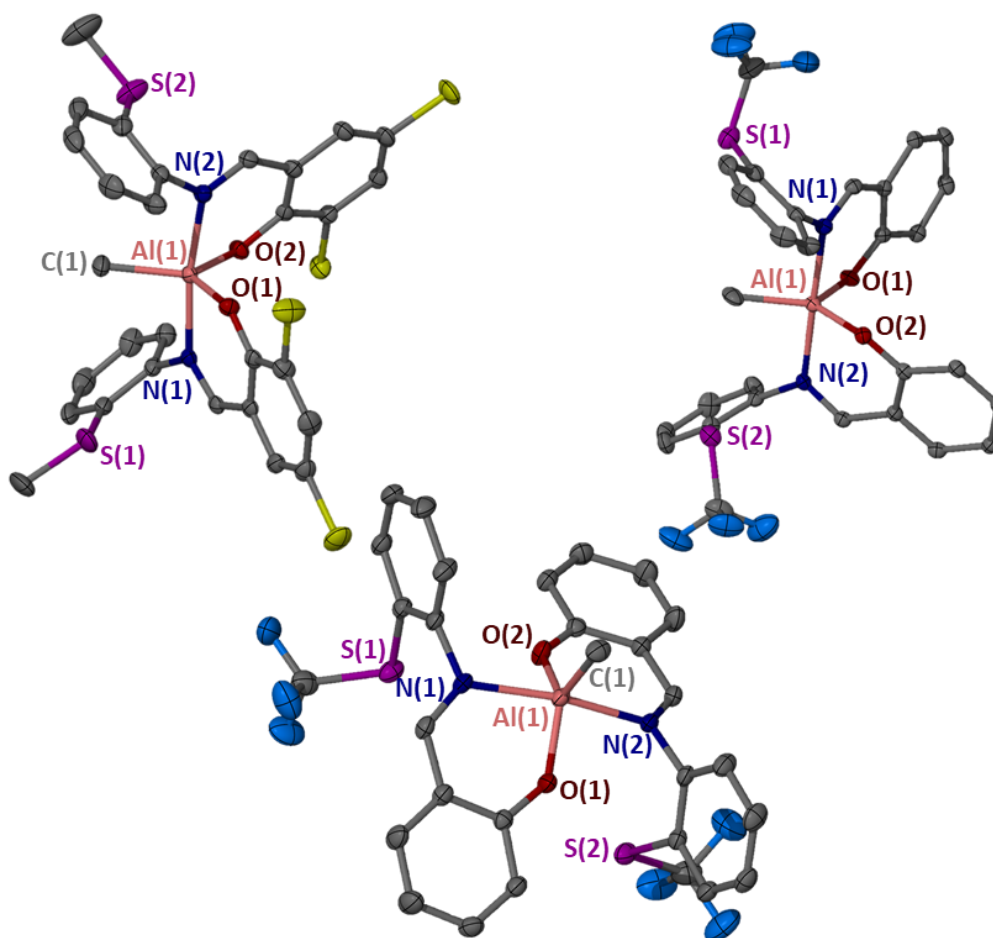


Figure 3.41: Solid state structures of $\text{Al}(\text{K})_2\text{Me}$ (top-left, ellipsoids are shown at the 50% probability level and all hydrogen atoms have been removed for clarity. Two molecules of toluene have been removed, one of which is disordered over two sites. There are two crystallographically unique molecules of the complex in the unit cell, only one is shown), $\text{Al}(\text{L})_2\text{Me}$ (top-right ellipsoids are shown at the 50% probability level. All hydrogen atoms and the carbon atoms of the tBu groups have been removed for clarity) and $\text{Al}(\text{M})_2\text{Me}$ (bottom, ellipsoids are shown at the 50% probability level and all H-atoms have been removed for clarity).

The solid-state structure of the complex formed from IH showed a 1:1 ligand to metal precursor complex, $\text{Al}(\text{I})\text{Me}_2$ (**Figure 3.42**). A fairly strong tetrahedral preference was observed ($\tau_4' = 0.89$). The steric profile of the ligand presumably prevented the formation of the bis-ligated species, but the resulting complex was sterically unencumbered, allowing for the tetrahedral structure. The interatomic distance between aluminium and sulphur atoms is around 4.3 Å, suggesting that there is no bonding interaction.

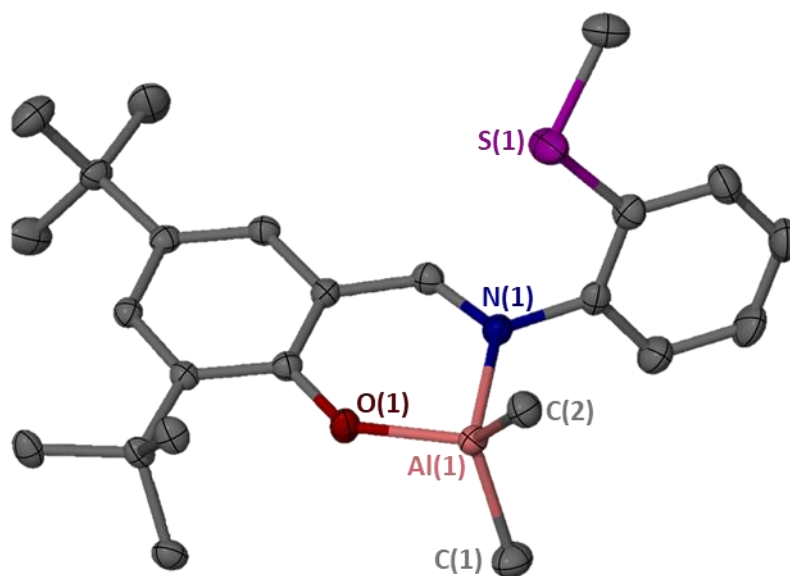


Figure 3.42: Solid state structure of Al(I)Me₂, ellipsoids are drawn at the 50% probability level and all H-atoms have been removed for clarity.

Table 3.13: Selected bond lengths (Å) and angles (°) for Al(K,L,M)₂Me and Al(I)Me₂.

	Al(K) ₂ Me	Al(L) ₂ Me	Al(M) ₂ Me	Al(I)Me ₂
τ_4 ^[a]	-	-	-	0.89
τ_5 ^[a]	0.78	0.83	0.75	-
Al – O(1)	1.7927(13)	1.7814(17)	1.7803(9)	1.7777(16)
Al – O(2)	1.7949(12)	1.7950(18)	1.7803(9)	-
Al – N(1)	2.0827(15)	2.101(2)	2.0848(10)	1.956(2)
Al – N(2)	2.0777(15)	2.102(2)	2.0848(10)	-
Al – C(1)	1.9724(18)	1.946(3)	1.962(2)	1.966(3)
Al – C(2)	-	-	-	1.961(3)
O(1) – Al – O(2)	112.21(6)	107.23(8)	121.80(7)	-
O(2) – Al – C(1)	122.75(8)	128.85(11)	119.10(4)	-
O(1) – Al – C(1)	125.04(8)	123.91(11)	119.10(4)	111.05(10)
N(1) – Al – N(2)	171.55(6)	178.67(9)	166.65(7)	-
C(1) – Al – C(2)	-	-	-	120.51(12)

[a] Calculated from the two largest coordination angles.

Analysis of the ^1H NMR spectra supported the bis-ligated methyl structures of $\text{Al}(\mathbf{K},\mathbf{L},\mathbf{M})_2\text{Me}$. The example ^1H NMR spectrum of $\text{Al}(\mathbf{L})_2\text{Me}$ is shown in **Figure 3.43** where the methyl ligand signal can be seen clearly at $\delta = -1.06$ ppm. The ^1H NMR spectrum of $\text{Al}(\mathbf{I})\text{Me}_2$ showed six protons in the aluminium methyl region supporting the structure taken from the solid-state analysis (**Figure 3.44**).

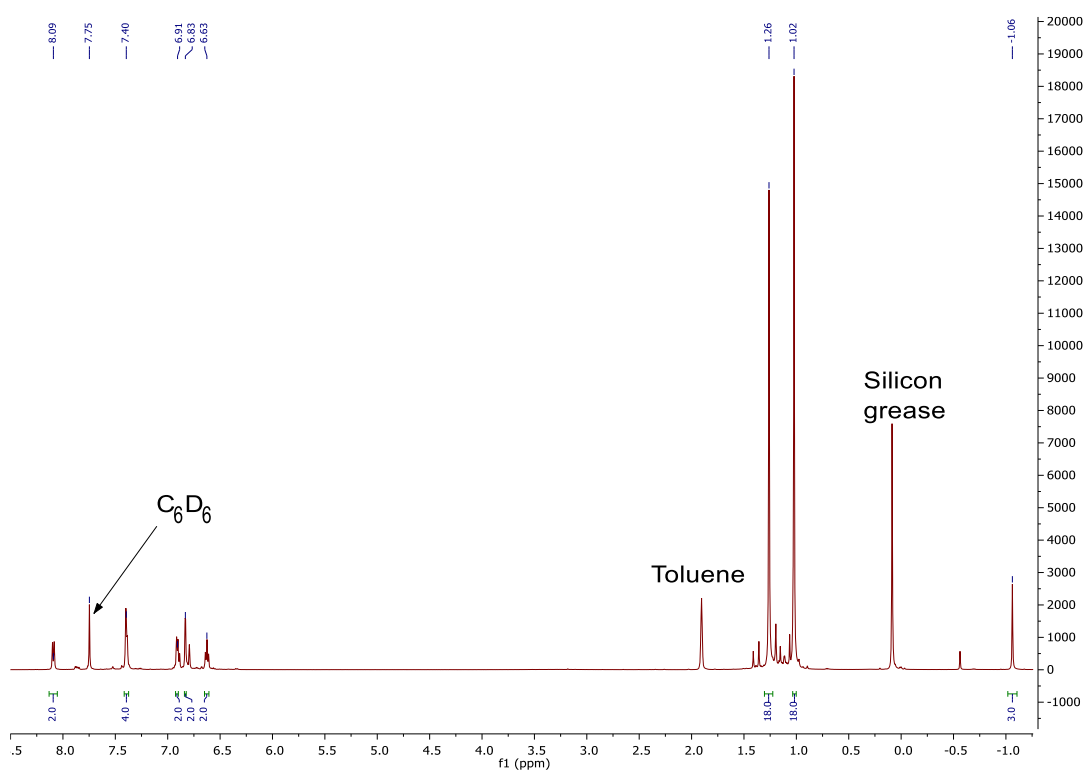


Figure 3.43: ^1H NMR spectrum (500 MHz, tol-d_9) spectrum of $\text{Al}(\mathbf{L})_2\text{Me}$.

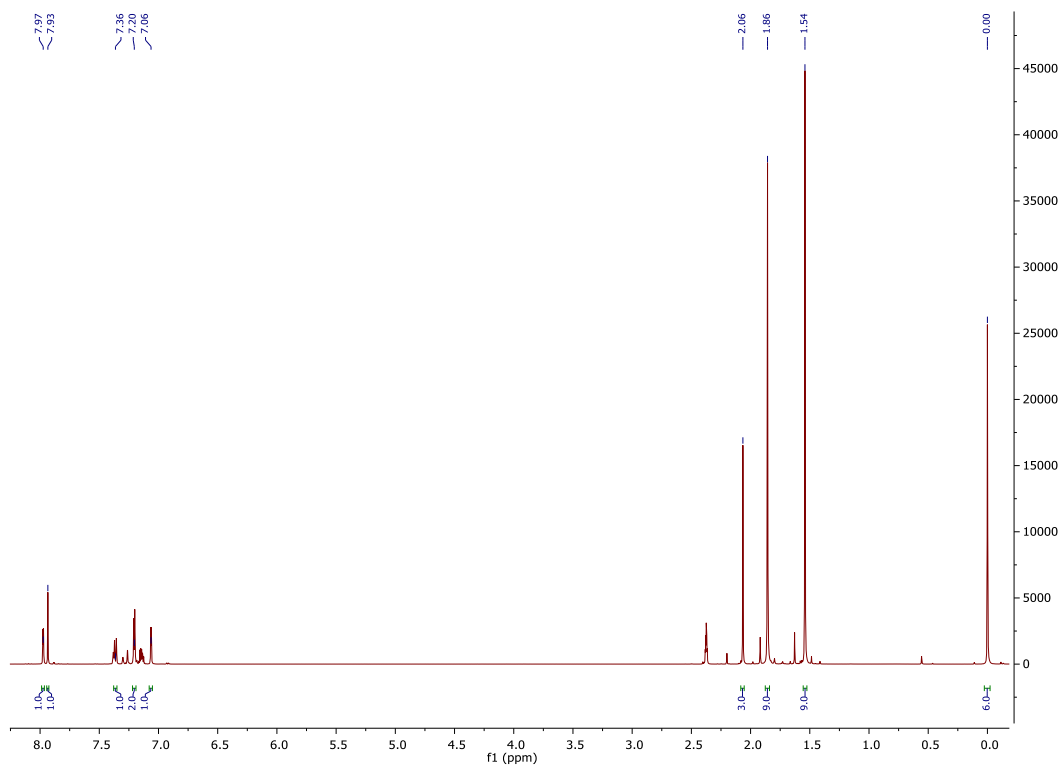


Figure 3.44: ^1H NMR spectrum (500 MHz, tol-d9) spectrum of $\text{Al}(\text{I})\text{Me}_2$.

3.5.2 *Rac*-lactide polymerisation with $\text{Al}(\text{K,L,M})_2\text{Me}$ and $\text{Al}(\text{I})\text{Me}_2$

The four aluminium complexes that were successfully synthesised were applied to the polymerisation of *rac*-lactide, initially at 80 °C in toluene at a ratio of $[\text{LA}]/[\text{I}]/[\text{BnOH}] = 100 : 1 : 1$ (**Table 3.14**). The four complexes were active over a 6 – 8-hour reaction time with $\text{Al}(\text{M})_2\text{Me}$ being the most active, giving 90% conversion in six hours. Conversely, $\text{Al}(\text{K})_2\text{Me}$ gave the slowest reaction and there was insufficient product for GPC or $^1\text{H}\{^1\text{H}\}$ NMR analysis. $\text{Al}(\text{I})\text{Me}_2$ and $\text{Al}(\text{K})_2\text{Me}$ gave well controlled polymerisation with reasonable dispersities ($\text{Đ} = 1.19 - 1.20$) and predictable molecular weights. For $\text{Al}(\text{M})_2\text{Me}$, the molecular weight was roughly half of the calculated molecular weight ($M_{\text{n GPC}} = 6800 \text{ gmol}^{-1}$, $M_{\text{n calc.}} = 13100 \text{ gmol}^{-1}$). This could either result from two chains growing per metal centre, or through a polymer degradation process at high conversion. Despite the tendency of aluminium complexes to show stereoselectivity for lactide ROP, all complexes gave atactic PLA.

Init.	[LA]/[I]/[BnOH]	Time /min	Conv. % ^a	P _r ^b	M _n ^d	M _n Calc. ^c	Đ ^d	TOF / h ⁻¹
Al(I)Me ₂	300 : 1 : 1	50	34	0.51	9590	14800	2.13	122
Al(K) ₂ Me	300 : 1 : 1	60	7	0.50	8500	3150	1.78	21
Al(L) ₂ Me	300 : 1 : 1	25	63	0.43	16050	27350	1.36	454
Al(M) ₂ Me	300 : 1 : 1	4	64	0.54	14300	27800	1.21	2835
Al(M) ₂ Me	3000 : 1 : 10	12	56	0.55	15850	24300	1.14	8400
Al(M) ₂ Me	10000 : 1 : 30	90	56	0.51	32150	27000	1.16	3733

Table 3.14: Rac-lactide polymerisation with Al(I)Me₂ and Al(L,K,M)₂Me.

Conditions: *rac*-LA (0.4 g), [LA]/[Al]/[BnOH] = 100 : 1 : 1; ^a Determined by ¹H NMR spectroscopy; ^b Probability of isotactic enchainment, determined by ¹H(¹H) NMR spectroscopy; ^c Theoretical molecular weight calculated from conversion (rounded to the nearest 50): {[LA]/[I] × (Conversion × 144.13) / BnOH equiv.} + M_n(BnOH). ^d Determined from GPC (in THF) referenced against polystyrene standards, × 0.58 (rounded to the nearest 50).

Initiators Al(I)Me₂ and Al(K–M)₂Me were further tested for the polymerisation of *rac*-lactide under solvent-free conditions at a ratio of [LA]/[I]/[BnOH] = 300 : 1 : 1 (**Table 3.15**). Al(I)Me₂ and Al(K)₂Me performed poorly under these conditions giving 34% and 7% conversion after 50 and 60 minutes respectively. By contrast, Al(L)₂Me was relatively quick giving 63% conversion in 25 minutes with a turnover frequency of 454 h⁻¹. Al(M)Me₂ was clearly the most active initiator of the series, in keeping with the solvated polymerisation data. A conversion of 63% was attained after four minutes with a relatively narrow dispersity (Đ = 1.21). The ratio was increased to [LA]/[I]/[BnOH] = 3000 : 1 : 10 and the polymerisation reached moderate conversion after 12 minutes giving a TOF value of 8,400 h⁻¹. A narrowing of dispersity was also observed, which is common when the initiator loading is lowered (Đ = 1.14). To further test the capabilities of Al(M)₂Me, ratio was further increased to [LA]/[I]/[BnOH] = 10000 : 1 : 30. The reaction time increased significantly but some activity was retained giving 56% conversion after 90 minutes. The control of polymerisation also improved, with a relatively narrow dispersity maintained (Đ = 1.16) and good agreement between calculated and measured molecular weights (M_{n,calc} = 27000 gmol⁻¹, M_{n,GPC} = 32150 gmol⁻¹).

Init.	T/°C	Time /hours	Conv. % ^a	P _r ^b	M _n ^d	M _n Calc. ^c	Đ ^d
Al(I)Me ₂	80	8	56	0.44	7000	8200	1.20
Al(K) ₂ Me	80	6	60	0.48	8500	8750	1.19
Al(L) ₂ Me	80	8	29	-	-	-	-
Al(M) ₂ Me	80	6	90	0.51	6800	13100	1.29

Table 3.15: Solvent-free *rac*-lactide polymerisation with Al(I)Me₂ and Al(L,K,M)₂Me, 130 °C.

^a Determined by ¹H NMR spectroscopy; ^b Probability of isotactic enchainment, determined by ¹H{¹H} NMR spectroscopy; ^c Theoretical molecular weight calculated from conversion (rounded to the nearest 50): {[LA]/[I] × (Conversion × 144.13) / BnOH equiv.} + M_n (BnOH). ^d Determined from GPC (in THF) referenced against polystyrene standards, × 0.58 (rounded to the nearest 50).

3.5.3 Polymerisation kinetics with Al(M)₂Me

The semi-logarithmic plot for *rac*-lactide polymerisation with Al(M)₂Me at 80 °C in toluene is shown in **Figure 3.45**. As seen with thioen complex, Al(B)Me, the negative intercept ($c = -0.173$) implies an initiation period probably related to forming the active benzoxy complex. After initiation, lactide was consumed with a first-order dependence with the rate constant $k_{app} = 0.0062 \text{ min}^{-1}$, nearly double that of the most active thioen complex detailed in **Section 2.4.3** ($k_{app} = 0.00378 \text{ min}^{-1}$).

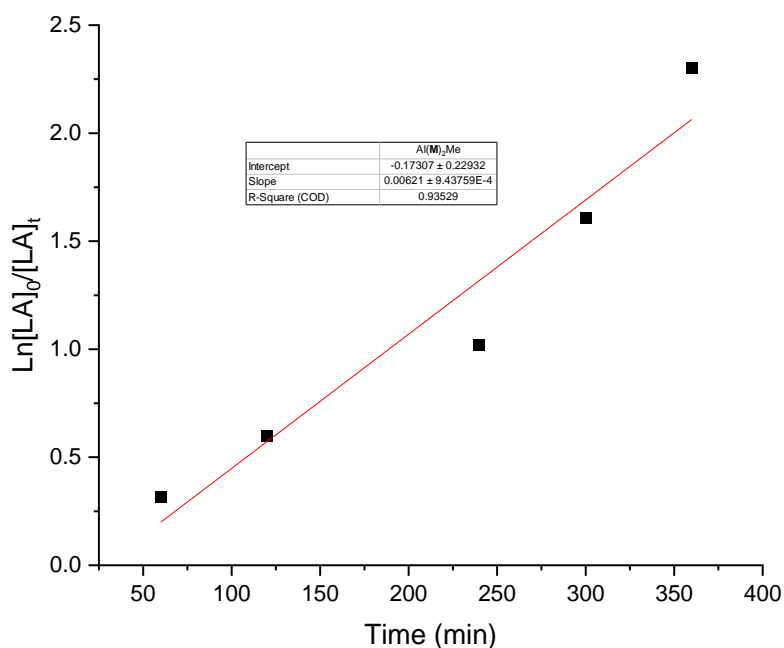


Figure 3.45: Semi-logarithmic plot of *rac*-lactide polymerisation with Al(M)₂Me.

3.6 Summary and conclusions

A summary of the key findings in **Chapter 3** are shown in **Figure 3.46**.

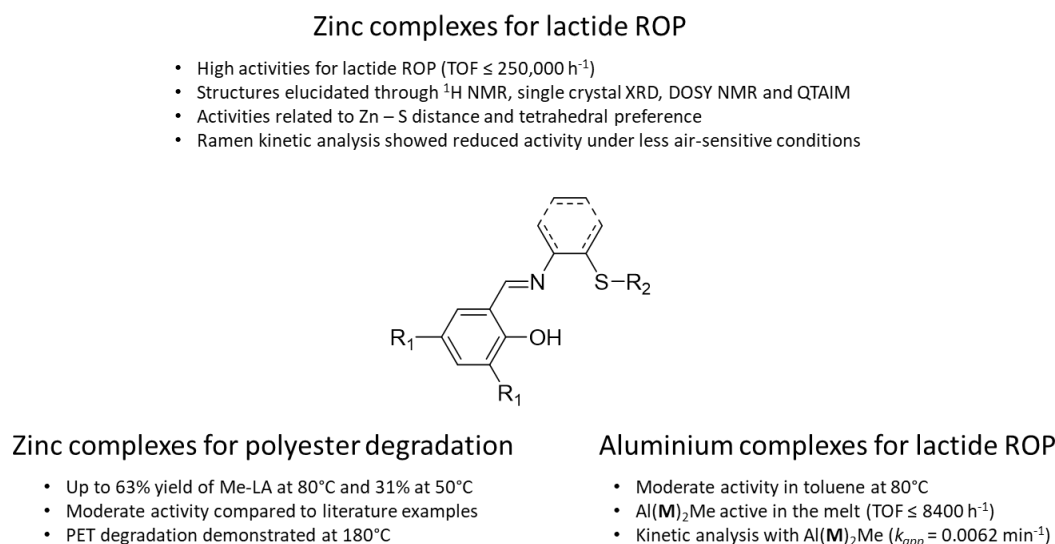


Figure 3.46: A summary of key findings from **Chapter 3**.

A series of monophenolate {ONS} ligands were prepared and complexed with zinc to give $\text{Zn}(\mathbf{F-N})_2$. Complexes were characterised through NMR, EA and X-ray crystallography where possible. Seven solid-state structures were obtained and shown to be monomeric in solution. High activities for *rac*-lactide were observed with low initiator loading ($[\text{LA}]/[\text{Zn}]/[\text{BnOH}] = 10,000 : 1 : 33$ at 180 °C) with TOF values up to $250,000 \text{ h}^{-1}$ for $\text{Zn}(\mathbf{J})_2$. Kinetic analysis using *in situ* Raman spectroscopy was carried out and the polymerisation activity was significantly reduced under these conditions with technical grade *rac*-lactide. Polymerisation activities were shown to correlate with Zn – S interatomic distance and tetrahedral preference and a mechanistic investigation gave no evidence of ligand-assisted coordination insertion.

$\text{Zn}(\mathbf{F-N})_2$ was shown to degrade commercial PLA samples to methyl lactate, a promising green solvent. Conversion of internal methine reached 96% with $\text{Zn}(\mathbf{J})_2$ and a corresponding yield and selectivity to methyl lactate of 62% and 59% respectively. The most active catalysts were also active at 50 °C over 18 h reaching a conversion

of 77% with Zn(**G**)₂. PET degradation to BHET was also demonstrated with full consumption of thin-film PET reached after 45 minutes with Zn(**G**)₂.

Four aluminium complexes of phenylene-bridged {ONS} ligands were prepared and characterised. All complexes were active for *rac*-lactide polymerisation in toluene and Al(**M**)₂Me showed promising activity in the melt reaching a TOF value of 8,400 h⁻¹ at [LA]/[Al]/[BnOH] = 3000 : 1 : 10.

3.7 References

- [1] I. C. McNeill, H. A. Leiper, *Polym. Degrad. Stab.* **1985**, *11*, 267–285.
- [2] M. H. Chisholm, N. W. Eilerts, J. C. Huffman, S. S. Iyer, M. Pacold, K. Phomphrai, *J. Am. Chem. Soc.* **2000**, *122*, 11845–11854.
- [3] B. M. Chamberlain, M. Cheng, D. R. Moore, T. M. Ovitt, E. B. Lobkovsky, G. W. Coates, *J. Am. Chem. Soc.* **2001**, *123*, 3229–3238.
- [4] C. K. Williams, L. E. Breyfogle, S. K. Choi, W. Nam, Young Victor G., M. A. Hillmyer, W. B. Tolman, *J. Am. Chem. Soc.* **2003**, *125*, 11350–11359.
- [5] F. Drouin, P. Oguadinma, T. Whitehorne, R. Prud'homme, F. Schaper, *Organometallics* **2010**, *29*, 2139–2147.
- [6] T. J. J. Whitehorne, B. Vabre, F. Schaper, *Dalton Trans.* **2014**, *43*, 6339–6352.
- [7] D. J. Darensbourg, O. Karroonnirun, *Inorg. Chem.* **2010**, *49*, 2360–2371.
- [8] L. Wang, H. Ma, *Dalton Trans.* **2010**, *39*, 7897–7910.
- [9] H. Wang, H. Ma, *Chem. Commun.* **2013**, *49*, 8686–8688.
- [10] Y. Yang, H. Wang, H. Ma, *Inorg. Chem.* **2015**, *54*, 5839–5854.
- [11] H. Wang, Y. Yang, H. Ma, *Inorg. Chem.* **2016**, *55*, 7356–7372.
- [12] C. Kan, J. Hu, Y. Huang, H. Wang, H. Ma, *Macromolecules* **2017**, *50*, 7911–7919.
- [13] J. Hu, C. Kan, H. Ma, *Inorg. Chem.* **2018**, *57*, 11240–11251.
- [14] Y. Gong, H. Ma, *Chem. Commun.* **2019**, *55*, 10112–10115.
- [15] C. Alonso-Moreno, A. Garcés, L. F. Sánchez-Barba, M. Fajardo, J. Fernández-Baeza, A. Otero, A. Lara-Sánchez, A. Antiñolo, L. Broomfield, M. I. López-Solera, A. M. Rodríguez, *Organometallics* **2008**, *27*, 1310–1321.
- [16] A. Otero, J. Fernández-Baeza, L. F. Sánchez-Barba, J. Tejada, M. Honrado, A. Garcés, A. Lara-Sánchez, A. M. Rodríguez, *Organometallics* **2012**, *31*, 4191–4202.
- [17] M. Honrado, A. Otero, J. Fernández-Baeza, L. F. Sánchez-Barba, A. Garcés, A. Lara-Sánchez, A. M. Rodríguez, *Organometallics* **2014**, *33*, 1859–1866.
- [18] M. Honrado, A. Otero, J. Fernández-Baeza, L. F. Sánchez-Barba, A. Garcés, A. Lara-Sánchez, A. M. Rodríguez, *Eur. J. Inorg. Chem.* **2016**, *2016*, 2562–2572.
- [19] A. Otero, J. Fernández-Baeza, L. F. Sánchez-Barba, S. Sobrino, A. Garcés, A. Lara-Sánchez, A. M. Rodríguez, *Dalton Trans.* **2017**, *46*, 15107–15117.
- [20] M. Honrado, A. Otero, J. Fernández-Baeza, L. F. Sánchez-Barba, A. Garcés, A. Lara-Sánchez, A. M. Rodríguez, *Dalton Trans.* **2014**, *43*, 17090–17100.
- [21] Z. Mou, B. Liu, M. Wang, H. Xie, P. Li, L. Li, S. Li, D. Cui, *Chem. Commun.* **2014**, *50*, 11411–11414.

- [22] C. Moya-Lopez, I. Bravo, J. A. Castro-Osma, D. Chapron, P. Bourson, C. Vagner, M. Cochez, N. Leoné, A. Lara-Sánchez, C. Alonso-Moreno, D. Hermida-Merino, *Polymers (Basel)*. **2022**, *14*, 232.
- [23] T. Rosen, Y. Popowski, I. Goldberg, M. Kol, *Chem. – A Eur. J.* **2016**, *22*, 11533–11536.
- [24] H. Shere, P. McKeown, M. F. Mahon, M. D. Jones, *Eur. Polym. J.* **2019**, *114*, 319–325.
- [25] I. dos Santos Vieira, S. Herres-Pawlis, *Eur. J. Inorg. Chem.* **2012**, *2012*, 765–774.
- [26] P. M. Schäfer, S. Herres-Pawlis, *Chempluschem* **2020**, *85*, 1044–1052.
- [27] J. Börner, S. Herres-Pawlis, U. Flörke, K. Huber, *Eur. J. Inorg. Chem.* **2007**, *2007*, 5645–5651.
- [28] A. Metz, P. McKeown, B. Esser, C. Gohlke, K. Kröckert, L. Laurini, M. Scheckenbach, S. N. McCormick, M. Oswald, A. Hoffmann, M. D. Jones, S. Herres-Pawlis, *Eur. J. Inorg. Chem.* **2017**, *2017*, 5557–5570.
- [29] A. Hermann, S. Hill, A. Metz, J. Heck, A. Hoffmann, L. Hartmann, S. Herres-Pawlis, *Angew. Chemie Int. Ed.* **2020**, *59*, 21778–21784.
- [30] P. M. Schäfer, M. Fuchs, A. Ohligschläger, R. Rittinghaus, P. McKeown, E. Akin, M. Schmidt, A. Hoffmann, M. A. Liauw, M. D. Jones, S. Herres-Pawlis, *ChemSusChem* **2017**, *10*, 3547–3556.
- [31] P. M. Schäfer, P. McKeown, M. Fuchs, R. D. Rittinghaus, A. Hermann, J. Henkel, S. Seidel, C. Roitzheim, A. N. Ksiazkiewicz, A. Hoffmann, A. Pich, M. D. Jones, S. Herres-Pawlis, *Dalton Trans.* **2019**, *48*, 6071–6082.
- [32] P. McKeown, S. N. McCormick, M. F. Mahon, M. D. Jones, *Polym. Chem.* **2018**, *9*, 5339–5347.
- [33] P. McKeown, L. A. Román-Ramírez, S. Bates, J. Wood, M. D. Jones, *ChemSusChem* **2019**, *12*, 5233–5238.
- [34] L. A. Román-Ramírez, P. McKeown, M. D. Jones, J. Wood, *ACS Catal.* **2019**, *9*, 409–416.
- [35] J. Payne, P. McKeown, M. F. Mahon, E. A. C. Emanuelsson, M. D. Jones, *Polym. Chem.* **2020**, *11*, 2381–2389.
- [36] J. Payne, P. McKeown, O. Driscoll, G. Kociok-Köhn, E. A. C. Emanuelsson, M. D. Jones, *Polym. Chem.* **2021**, *12*, 1086–1096.
- [37] J. M. Payne, G. Kociok-Köhn, E. A. C. Emanuelsson, M. D. Jones, *Macromolecules* **2021**, *54*, 8453–8469.
- [38] S. Alvarez, *Dalton Trans.* **2013**, *42*, 8617–8636.
- [39] K. Masutani, Y. Kimura, in *Poly(Lactic Acid) Sci. Technol. Process. Prop. Addit. Appl., The Royal Society Of Chemistry*, **2015**, pp. 1–36.
- [40] R. D. Rittinghaus, P. M. Schäfer, P. Albrecht, C. Conrads, A. Hoffmann, A. N. Ksiazkiewicz, O. Bienemann, A. Pich, S. Herres-Pawlis, *ChemSusChem* **2019**, *12*, 2161–2165.

- [41] J. R. Jambeck, R. Geyer, C. Wilcox, T. R. Siegler, M. Perryman, A. Andrady, R. Narayan, K. L. Law, *Science* **2015**, *347*, 768–771.
- [42] A. L. Andrady, *Mar. Pollut. Bull.* **2011**, *62*, 1596–1605.
- [43] J. R. Jambeck, R. Geyer, C. Wilcox, T. R. Siegler, A. Andrady, R. Narayan, K. L. Law, R. Geyer, **2021**, *347*, 768–771.
- [44] A. A. Horton, A. Walton, D. J. Spurgeon, E. Lahive, C. Svendsen, *Sci. Total Environ.* **2017**, *586*, 127–141.
- [45] H. A. Leslie, M. J. M. van Velzen, S. H. Brandsma, A. D. Vethaak, J. J. Garcia-Vallejo, M. H. Lamoree, *Environ. Int.* **2022**, *163*, 107199.
- [46] O. Setälä, V. Fleming-Lehtinen, M. Lehtiniemi, *Environ. Pollut.* **2014**, *185*, 77–83.
- [47] K. Ragaert, L. Delva, K. Van Geem, *Waste Manag.* **2017**, *69*, 24–58.
- [48] J. Payne, P. McKeown, M. D. Jones, *Polym. Degrad. Stab.* **2019**, *165*, 170–181.
- [49] Y.-B. Zhao, X.-D. Lv, H.-G. Ni, *Chemosphere* **2018**, *209*, 707–720.
- [50] G. Lopez, M. Artetxe, M. Amutio, J. Bilbao, M. Olazar, *Renew. Sustain. Energy Rev.* **2017**, *73*, 346–368.
- [51] V. Sinha, M. R. Patel, J. V Patel, *J. Polym. Environ.* **2010**, *18*, 8–25.
- [52] V. Piemonte, S. Sabatini, F. Gironi, *J. Polym. Environ.* **2013**, *21*, 640–647.
- [53] C. T. Bowmer, R. N. Hooftman, A. O. Hanstveit, P. W. M. Venderbosch, N. Van Der Hoeven, *Chemosphere* **1998**, *37*, 1317–1333.
- [54] F. G. Calvo-Flores, M. J. Monteagudo-Arrebola, J. A. Dobado, J. Isac-García, *Top. Curr. Chem.* **2018**, *376*, DOI 10.1007/s41061-018-0191-6.
- [55] C. S. M. Pereira, V. M. T. M. Silva, A. E. Rodrigues, *Green Chem.* **2011**, *13*, 2658–2671.
- [56] P. P. Upare, Y. K. Hwang, J.-S. Chang, D. W. Hwang, *Ind. Eng. Chem. Res.* **2012**, *51*, 4837–4842.
- [57] Y. Fan, C. Zhou, X. Zhu, *Catal. Rev.* **2009**, *51*, 293–324.
- [58] V. Aryan, D. Maga, P. Majgaonkar, R. Hanich, *Resour. Conserv. Recycl.* **2021**, *172*, 105670.
- [59] L. D. Brake, *Prep. Alkyl Esters by Depolymerization.* **1993**.
- [60] P. Coszach, J. C. Bogaert, J. Willocq, *Chem. Recycl. PLA by alcoholysis n.d.*
- [61] F. Codari, S. Lazzari, M. Soos, G. Storti, M. Morbidelli, D. Moscatelli, *Polym. Degrad. Stab.* **2012**, *97*, 2460–2466.
- [62] S. Lazzari, F. Codari, G. Storti, M. Morbidelli, D. Moscatelli, *Polym. Degrad. Stab.* **2014**, *110*, 80–90.
- [63] C. F. Van Nostrum, T. F. J. Veldhuis, G. W. Bos, W. E. Hennink, *Polymer (Guildf).* **2004**, *45*, 6779–6787.

- [64] J. H. Jung, M. Ree, H. Kim, *Catal. Today* **2006**, *115*, 283–287.
- [65] X. Song, X. Zhang, H. Wang, F. Liu, S. Yu, S. Liu, *Polym. Degrad. Stab.* **2013**, *98*, 2760–2764.
- [66] X. Song, H. Wang, X. Zheng, F. Liu, S. Yu, *J. Appl. Polym. Sci.* **2014**, *131*, 40817–40823.
- [67] X. Song, Z. Bian, Y. Hui, H. Wang, F. Liu, S. Yu, *Polym. Degrad. Stab.* **2019**, *168*, 108937.
- [68] F. A. Leibfarth, N. Moreno, A. P. Hawker, J. D. Shand, *J. Polym. Sci. Part A Polym. Chem.* **2012**, *50*, 4814–4822.
- [69] C. Alberti, N. Damps, R. R. R. Meißner, S. Enthaler, *ChemistrySelect* **2019**, *4*, 6845–6848.
- [70] P. McKeown, P. McKeown, M. Kamran, M. Kamran, M. G. Davidson, M. G. Davidson, M. D. Jones, M. D. Jones, L. A. Román-Ramírez, J. Wood, *Green Chem.* **2020**, *22*, 3721–3726.
- [71] C. Fliedel, D. Vila-Viçosa, M. J. Calhorda, S. Dagorne, T. Avilés, *ChemCatChem* **2014**, *6*, 1357–1367.
- [72] L. A. Román-Ramírez, P. McKeown, M. D. Jones, J. Wood, *ACS Omega* **2020**, *5*, 5556–5564.
- [73] L. A. Román-Ramírez, P. McKeown, C. Shah, J. Abraham, M. D. Jones, J. Wood, *Ind. Eng. Chem. Res.* **2020**, *59*, 11149–11156.
- [74] L. A. Román-Ramírez, M. Powders, P. McKeown, M. D. Jones, J. Wood, *J. Polym. Environ.* **2020**, *28*, 2956–2964.
- [75] J. M. Payne, M. Kamran, M. G. Davidson, M. D. Jones, *ChemSusChem* **2022**, *15*, e202200255.
- [76] R. Petrus, D. Bykowski, P. Sobota, *ACS Catal.* **2016**, *6*, 5222–5235.
- [77] I. Taniguchi, S. Yoshida, K. Hiraga, K. Miyamoto, Y. Kimura, K. Oda, *ACS Catal.* **2019**, *9*, 4089–4105.
- [78] H. Zhang, Z.-G. Wen, *Waste Manag.* **2014**, *34*, 987–998.
- [79] F. M. Lamberti, L. A. Román-Ramírez, J. Wood, *J. Polym. Environ.* **2020**, *28*, 2551–2571.
- [80] S. M. Al-Salem, P. Lettieri, J. Baeyens, *Waste Manag.* **2009**, *29*, 2625–2643.
- [81] N. George, T. Kurian, *Ind. Eng. Chem. Res.* **2014**, *53*, 14185–14198.
- [82] K. Troev, G. Grancharov, R. Tsevi, I. Gitsov, *J. Appl. Polym. Sci.* **2003**, *90*, 1148–1152.
- [83] S. Wang, C. Wang, H. Wang, X. Chen, S. Wang, *Polym. Degrad. Stab.* **2015**, *114*, 105–114.
- [84] R. Esquer, J. J. García, *J. Organomet. Chem.* **2019**, *902*, 120972.

Chapter 4: Redox switchable initiators for co-polymerisation

4.1 Copolymers and redox-switchable initiators

Co-polymerisation, where two or more monomers are combined in a polymeric chain, has resulted in some of the most important plastics that are in use today.^[1] There are numerous examples of commercially available, bio-based co-polymers where one or more components can be sourced from renewable feedstocks.^[2] These include: bio-PET, made from bio-derived ethylene glycol and terephthalic acid;^[3] polyurethanes, made with polyols derived from plant oil^[4] and polyamides such as nylon 56.^[5]

Despite the numerous benefits of PLLA and the improved thermal properties that can be attained through stereocomplexation, the application of polylactides is still limited by poor thermal properties and a lack of elasticity.^[6] Alongside other strategies, such as forming composites and the use of additives, co-polymerisation is an excellent synthetic tool for accessing improved properties whilst continuing to benefit from the sustainability and abundance of lactide.^[7] A common method is to form end-functionalised PLA and react with another telechelic polymer, such as polyethylene glycol (PEG), to form di- or multi-block co-polymers that have found use in biomedical applications such as drug delivery and tissue engineering.^[8] A recent example of this is the targeted release of chemotherapy agents using a PLA-PEG nanoparticle drug-delivery system.^[9]

An important challenge for lactide co-polymerisation is the synthesis of controlled co-polymers from a melt or solution mixture of monomers, to limit the number of synthetic steps. An important example of this is poly(lactic-co-glycolic acid) (PLGA) which also finds extensive use in the biomedical industry as one of the most important bioresorbable polymers.^[10] It can be formed through ring-opening co-polymerisation (ROCOP) of lactide and glycolide with an initiator such as tin octanoate and a suitable alcohol, although the properties are typically affected by the monomer ratios rather than precise control of the microstructure.^[11] There has been significant research into the controlled formation of PLGA nanostructures. For example, Chvalun recently published work detailing the controlled formation of PLGA nano-spheres initiated by bismuth subsalicylate through nanoprecipitation.^[12]

Copolymerisation of lactide can also be useful for improving the degradability of the polymer. Buchard *et al.* prepared a novel cyclic xanthate comonomer that introduced sulphur-based linkages that were cleavable by UV light.^[13] This allowed for biodegradable PLA oligomers to be quickly accessed and a mass loss of 40% was achieved over six hours of degradation, with as little as 3% xanthate incorporation. There was also little effect on the thermal properties of the final polymer.

One emerging strategy is the modification of monomer selectivity through redox control of the initiator; this is usually achieved through the use of redox reagents to alter the oxidation state of a metal.^[14] There are many examples utilising salen ligands containing ferrocenyl groups where the oxidation state of the iron can be modulated to alter the structure and activity of the initiators. White and co-workers published the first example of this for lactide ROP with a titanium salen complex **129** substituted at the *para*-phenolate positions with two ferrocene units (**Figure 4.01**).^[15] There was a significant difference in reactivity between the neutral complex and the diferrocenium 2+ cation, allowing the polymerisation to be switched on or off with the addition of redox reagents. Similar complexes of cerium, yttrium and indium have also been reported.^[16,17]

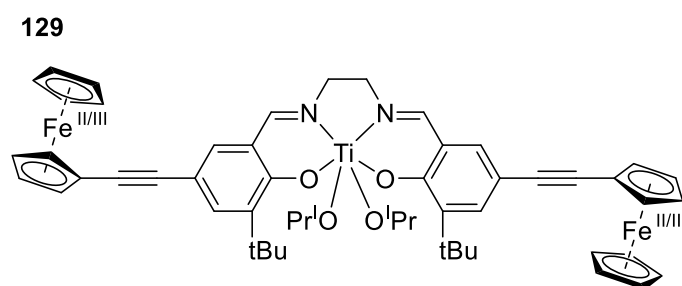


Figure 4.01: Ferrocene-substituted titanium salen complex for on/off lactide polymerisation.^[15]

More recently, the salfen ligand, a salen containing a ferrocene backbone, has been applied for switchable lactide polymerisation (**Figure 4.02**).^[18] The proximity of the ferrocene moiety to the metal centre allows it to exert more influence over the complex both electronically and geometrically.^[19] Long and co-workers published a

titanium salfen complex (**130**).^[19] Interestingly, the initiator was inactive in both reduced and oxidised forms until it was reduced in the presence of lactide, at which point reasonably active polymerisation could occur. This allowed for on/off polymerisation of lactide controlled by the addition of redox reagents. The first example of a successful copolymerisation of this type was reported by Diaconescu and co-workers using a zirconium salfan complex (**131**).^[20] A switch in selectivity between monomers was observed depending on oxidation state and, through sequential addition of redox reagents, block co-polymers of *L*-lactide and ϵ -caprolactone could be formed.

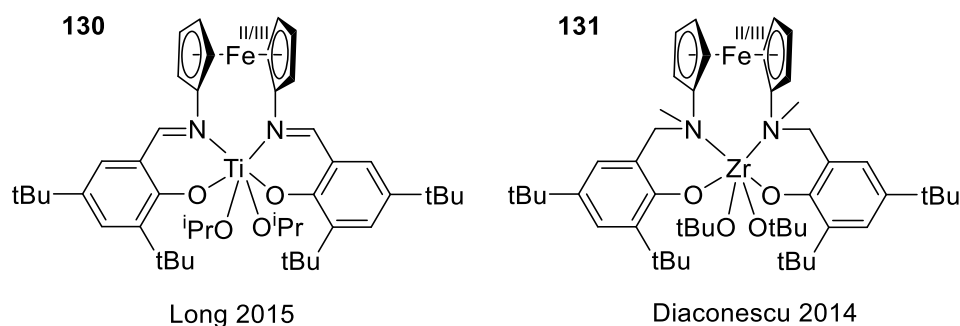


Figure 4.02: Salfen and salfan complexes for on/off lactide polymerisation and lactide ϵ -CL copolymerisation.^[19,20]

Diaconescu presented an analogous aluminium complex, **132**, with redox-switching capabilities (**Figure 4.03**).^[18] With the goal of creating controlled block copolymers, a range of common monomers were tested with the initiator in both reduced and oxidised forms. Significant differences in activity were found for several cyclic lactones, trimethylene carbonate (TMC) and CHO leading to a range of di- and tri-block copolymers controlled by the addition of redox reagents.

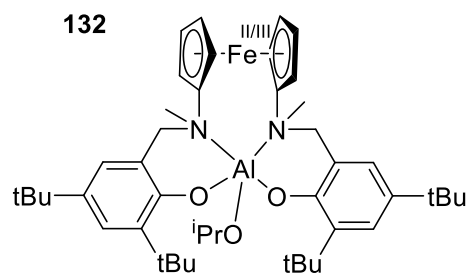


Figure 4.03: Aluminium salfan complex for redox-switchable co-polymerisation of lactones, ethers and TMC.^[18]

Further work from the same group looked at a dinuclear yttrium complex supported by salfen ligands (**Figure 4.04**).^[21] The CV of complex **133** showed two reversible redox peaks suggesting that the complex had 3 readily available states. This was confirmed using redox reagents although the exact nature of the two oxidised species could not be confirmed. During polymerisation studies, lactones were found to polymerise favourably with increasingly reduced complex whereas the opposite was true of the cyclic ethers. Di- and tri- block copolymers were made by exploiting this switch.

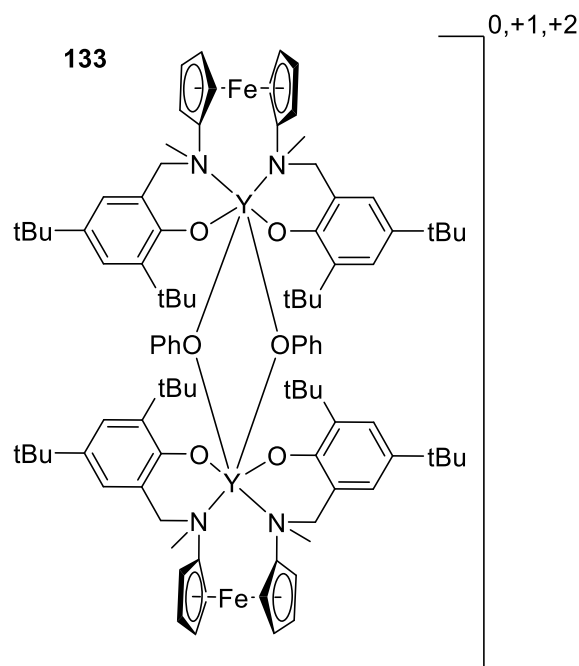


Figure 4.04: Dinuclear yttrium complex with three possible states for switchable copolymerisation.^[21]

Another strategy towards switchable polymerisation is the direct manipulation of the oxidation state of the metal centre (**Figure 4.05**). This was first reported for on-off homopolymerisation of lactide with cerium (III/IV) complexes containing a ferrocene-bridged phosphasalen ligand (**134**).^[22] The switch was made using standard redox reagents (FcBAR^{F} and CoCp_2) and it was confirmed through XANES and Mössbauer spectroscopy that the cerium centre was oxidised or reduced while the ferrocene moiety remained unaffected. The *in-situ* oxidation of the complex led to a loss of activity, that could be regained through reduction. A theoretical study concluded that the Ce(III) complex is more active due to the steric effect of the larger ionic radius favouring the coordination of the lactide, coupled with increased nucleophilicity. Okuda and co-workers demonstrated similar results with cerium (III/IV) complexes with a bisphenolate (OSSO) ligand (**135**).^[17] Using redox reagents, the reaction could be stopped and restarted without loss of activity over three additions.

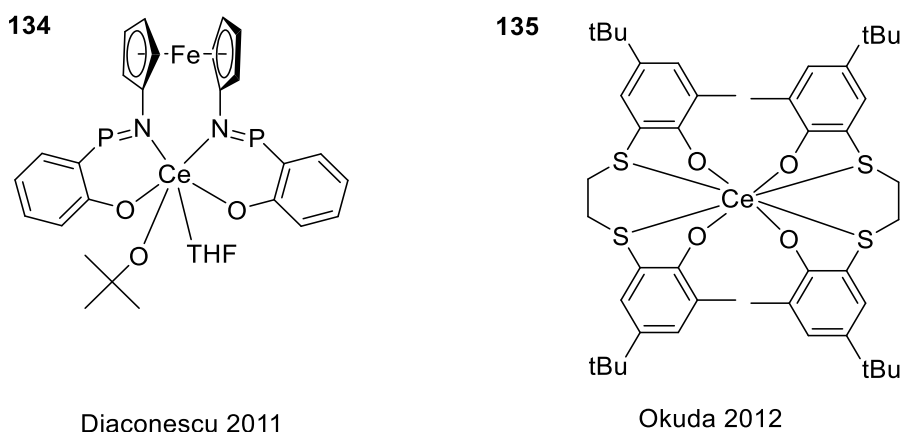


Figure 4.05: Redox switchable cerium (III/IV) complexes for on/off lactide polymerisation.^[17,22]

An iron bis(imino)pyridine complex (**136**) reported by Byers and co-workers also attained on/off polymerisation of lactide through the direct manipulation of the oxidation state at the metal centre (**Figure 4.06**).^[23] Continued work by the Byers group using the same complex demonstrated a switch in monomer selectivity between lactide and epoxides when redox stimuli was applied. Initially this was in the form of reagents, with CoCp_2 or FcPF_6 added to reduce or oxidise the complex

respectively.^[24] This led to a clear switch in selectivity between lactide and CHO polymerisation which was successfully exploited to give di- and tri-block copolymers with controllable chain lengths.

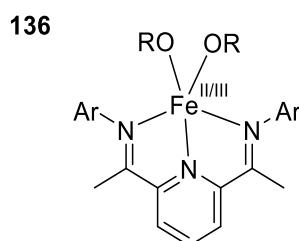


Figure 4.06: Bis(imino pyridine) iron (II/III) complex for switchable lactide copolymerisation.^[23–26]

Subsequent work with complex **136** was the first example of using electrochemistry to change the oxidation state of a polymerisation initiator.^[25] There are some distinct advantages to using electrochemistry to affect the redox switch; crucially, it avoids the use of sequential additions of reagents and also allows the switch to be made remotely. The established selectivity differences between the reduced and oxidised form of **136**, coupled with a reversible redox potential, allowed for the switching of monomer selectivity through the application of a suitable potential to the system. Multiblock copolymers of lactide and CHO were attained through this process. A heterogenized analogue of **136** has also been reported that accessed semi-conductive surfaces patterned with polymer brushes.^[26] The modification of the electrode surface with different materials and conductive areas resulted in a range of surface films with domains of PLA or PCHO depending on the potential applied to these regions.

A recent publication from Chen and co-workers applied a bimetallic salen complex with cobalt and manganese to the electrochemically switchable co-polymerisation of lactide, CO₂ and epoxides (**Figure 4.07**).^[27] CV analysis demonstrated a reversible switch between Co(III)-Mn(III) and Co(II)-Mn(II) oxidation states, and this was confirmed in the solid state through XPS. Initial studies demonstrated that the Co(II)-

Mn(II) oxidation states favoured lactide ROP whereas the oxidised form, Co(III)-Mn(III), favoured the ROCOP of CO₂ and epoxides. Initiator **137** was able to prepare multiblock copolymers based on oxidation state manipulation with PLA being formed until oxidation, at which point polycarbonate blocks were formed. The complex was subsequently reduced resulting in full consumption of remaining lactide. The GPC trace showed steadily increasing molecular weight, supporting the conversion data from ¹H NMR spectroscopy.

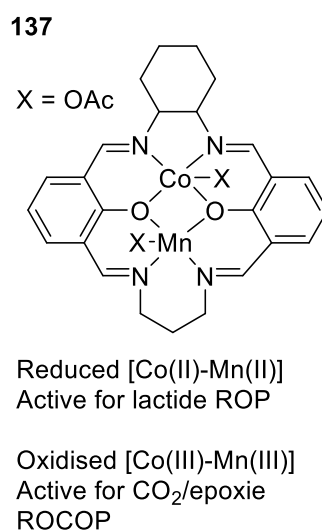


Figure 4.07: Electrochemically switchable co-polymerisation initiator from Chen *et al.*^[27]

4.2 Redox behaviour of iron (III) bisphenolate complexes

4.2.1 Identification of redox active iron (III) complexes

Cyclic voltammetry (CV) experiments were carried out with iron(III) complexes (**Figure 4.08**) in order to identify reversible, or quasi-reversible, $\text{Fe}^{3+}/\text{Fe}^{2+}$ redox peaks. The reversibility of the electron transfer event is crucial if the oxidation state of the complex is to be changed reliably throughout a copolymerisation experiment. CV was performed using a glassy carbon working electrode, a platinum coil counter electrode and a platinum wire as a *pseudo*-reference electrode. Ferrocene was introduced as an internal reference and so potentials are quoted vs. Fc/Fc^+ . All experiments were performed in anhydrous acetonitrile with 0.1 M tetrabutylammonium hexafluorophosphate (TBAPF_6) electrolyte and 5 – 10 mg of complex.

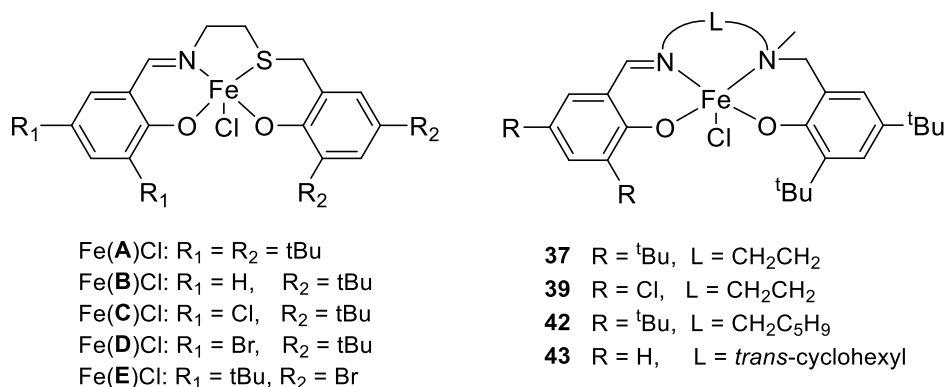


Figure 4.08: Iron (III) chloride complexes tested for reversible redox activity.

Due to the excellent polymerisation activity demonstrated by iron (III) thienopyridine complexes, these were the first to be tested with CV. Unfortunately, there was no evidence of a reversible redox peak at reducing potentials, suggesting that they are redox inactive under conditions relevant to this study. An example CV with Fe(**A**)Cl is shown in **Figure 4.09** where only a small reduction peak can be observed with no corresponding oxidation. Similar results were obtained with Fe(**B-E**)Cl suggesting that this family of complexes is not suitable for electrochemical switching.

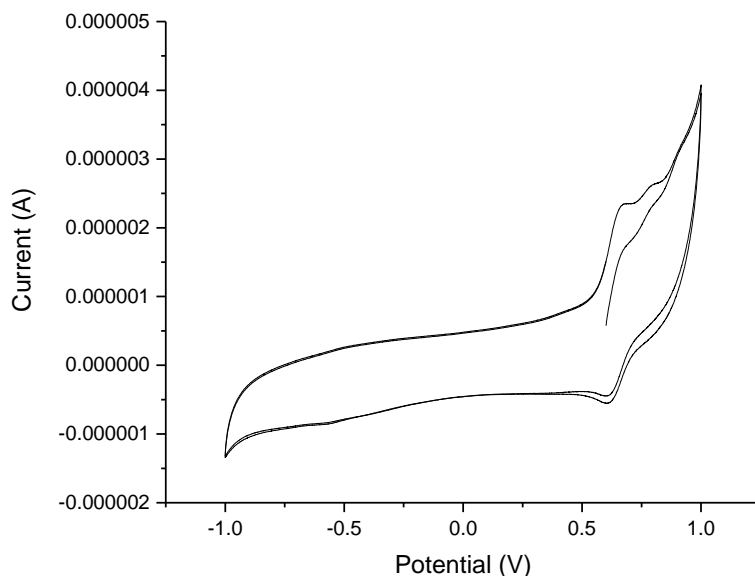


Figure 4.09: CV of Fe(A)Cl in acetonitrile with 0.1 M TBAPF₆ electrolyte.

The electrochemical behaviour of a series of recently reported iron (III) salen complexes (**37**, **39**, **42**, **43**) were subsequently assessed.^{28,29} All four complexes exhibited *quasi*-reversible redox peaks between -0.764 and -0.934 V vs. Fc/Fc⁺ that could be attributed to the Fe³⁺/Fe²⁺ redox couple. There is clearly a strong ligand influence as salen and thioen ligands are very similar yet show very different electrochemical behaviour. The CV of Fe(**37**)Cl referenced to Fc/Fc⁺ (a/a') is shown in **Figure 4.10** where a clear reduction peak can be observed (b) whereas the corresponding oxidation (b') is much weaker, suggesting a partially reversible system.

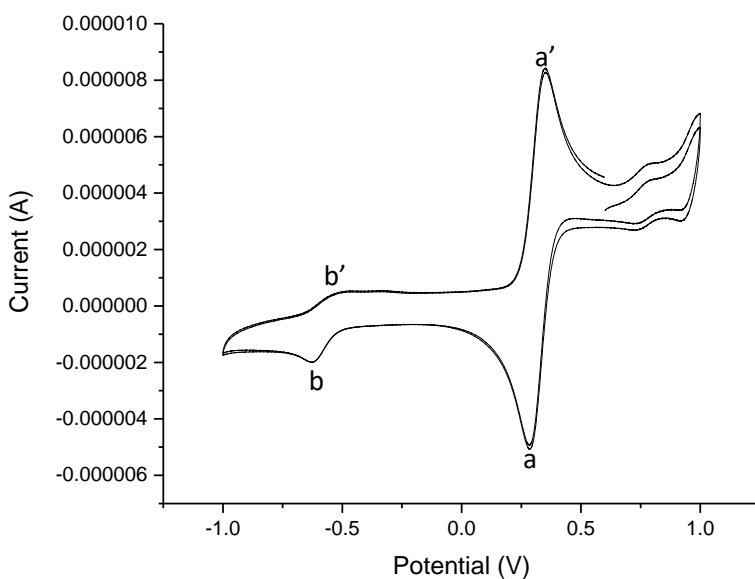


Figure 4.10: CV of **37** in acetonitrile with 0.1 M TBAPF₆ electrolyte and ferrocene as internal reference.

With **39**, containing chloro substituents, there is a far clearer oxidation peak (*b'*), and the Fe³⁺/Fe²⁺ couple (*b/b'*) appears almost fully reversible (**Figure 4.11**). There is an extra redox couple at more reducing potential, *c/c'*, which could represent the same Fe³⁺/Fe²⁺ transition following the loss of the chloride auxiliary ligand. Compared to **37**, the reduction potential vs. Fc/Fc⁺ (*a/a'*) is lower, and this could be linked to electronic structure and, possibly, polymerisation activity.

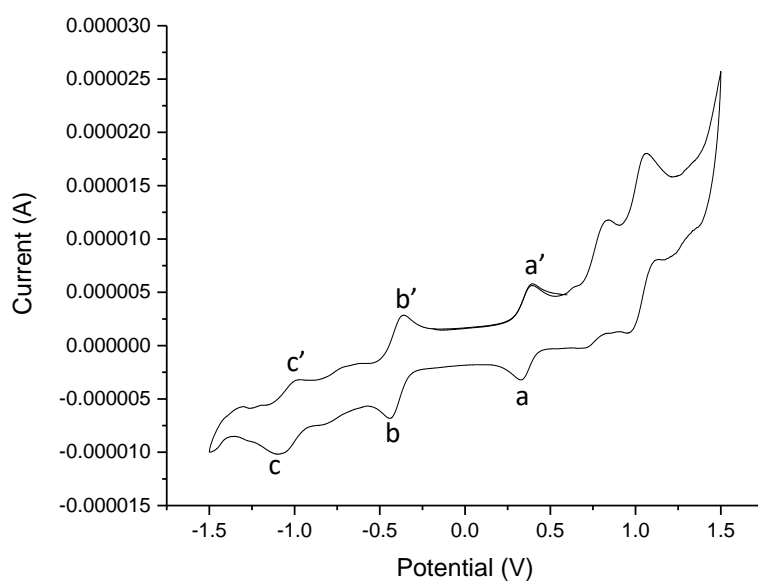


Figure 4.11: CV of **39** in acetonitrile with 0.1 M TBAPF₆ electrolyte and ferrocene as internal reference.

4.2.2 Electrochemical characterisation of Fe (III) salalen complexes.

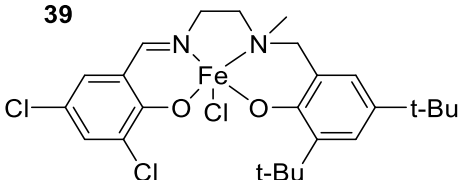
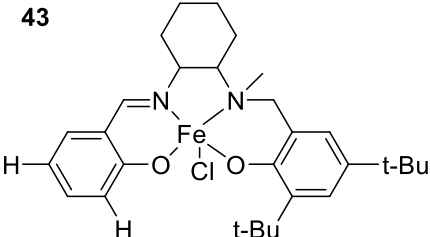
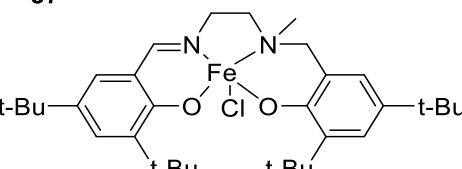
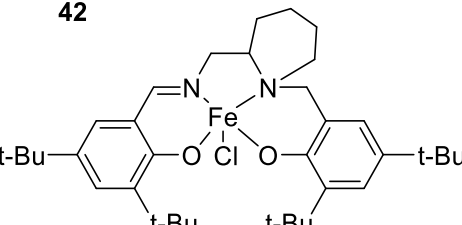
The voltage required to reduce an iron (III) complex to iron (II) can be seen as a direct measure of the electronics around the metal centre; the reducibility of the iron centre is related to the electron density imparted by the ligand system. For more electron-rich systems, it would necessarily be more difficult to complete the one-electron reduction to iron (II) whereas a more electron deficient system should more readily accept an electron. This suggests that the reduction potential of the complexes would correlate with Lewis acidity and therefore polymerisation activity; electron poor initiators tend to give the fastest rates.

The reduction potential for four salalen complexes is given in **Table 4.01** alongside the reaction time and conversion from the ROP of *rac*-lactide as reported by Driscoll and co-workers.^[28] Chlorinated analogue **39** has the lowest reduction potential of the four complexes tested ($E_{1/2} = -0.764$ V vs. Fc/Fc⁺) and this can be related to the electron-withdrawing chloro groups drawing electron density away from the metal centre. It is also the most active initiator giving 93% conversion of lactide in four

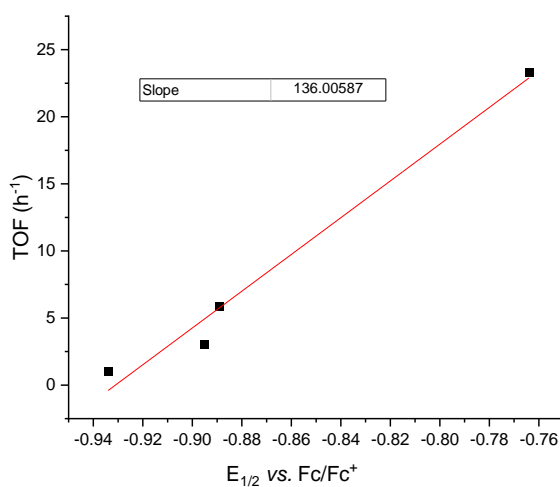
hours. The reduction potential of the other three complexes that were analysed, **37**, **42** and **43**, are higher than that of **39** and there is only a small variation between them ($E_{1/2} = -0.889 - -0.934$ V vs. Fc/Fc⁺), correlating with very similar lactide conversions. This can be rationalised by considering the electronics of the ligands as they all bear *t*-butyl groups as the sole phenolate substituents and differ only in the aliphatic linker. They are also significantly less active than **39**, in keeping with the large gap in reduction potential. Despite being tightly grouped, the reduction potential of **37**, **42** and **43** do correlate with polymerisation activity. This effect is presumably not influenced by sterics and so there must be a subtle electronic influence imparted by the linker either directly or through alteration of the geometry. This could prove an interesting technique for comparing the relative effect of sterics and electronics within redox active complexes.

From the conversion and reaction time data in **Table 4.01**, it is possible to work out turnover frequency (TOF) values for the lactide polymerisation activity of the four salalens. These values were plotted against the reduction potentials in **Table 4.01**, where a linear relationship ($R^2 = 0.981$) between reduction potential and TOF can be observed (**Figure 4.12**). As many of the polymerisations reached similarly high conversion, the TOF values are not necessarily representative of the overall reaction, and it would be ideal to use rate constants instead. Furthermore, there are only four data points and so the data cannot be overly analysed. However, this does indicate a probable link between reduction potential and polymerisation activity that could be usefully employed for screening and characterisation purposes.

Table 4.01: Reduction potential and polymerisation data for four iron salen complexes.²⁸

Initiator	$E_{1/2}$ vs. (Fc/Fc ⁺) ^a	Reaction time /h	Conversion /%	TOF /h ⁻¹
39 	-0.76	4	93	23.3
43 	-0.89	16	95	5.9
37 	-0.90	24	72	3.0
42 	-0.93	96	92	1.0

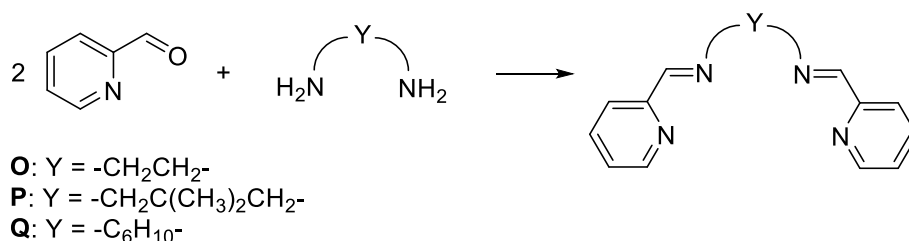
Polymerisation conditions: [LA]/[Fe] = 100:1 in PO (2 mL), 80°C, ^a Taken from cyclic voltammetry in anhydrous acetonitrile with 0.1 M TBAPF₆. Glassy carbon working electrode, platinum counter electrode, platinum reference electrode. Ferrocene used as internal reference.

**Figure 4.12:** Plot of $E_{1/2}$ vs. TOF for **37**, **39**, **42**, **43**. $R^2 = 0.981$.

4.3 Redox switching with iron (II) {N4} complexes

4.3.1 Synthesis and characterisation of iron (II) {N4} complexes

As the ligands described in **Section 4.2** were ultimately unsuitable for electrochemical switching, a series of iron (II) complexes with neutral {N4} ligands were prepared based on the success achieved by Byers' electrochemically switchable iron (II) complex.^[25] Ligands **O** – **Q** were prepared through a simple condensation reaction with diamine linkers and two equivalents of picolinaldehyde (**Scheme 4.01**). The identity of the ligands was confirmed through ¹H NMR and HR-MS.



Scheme 4.01: Synthesis of neutral {N4} ligands **O-Q**.

Ligands **O-Q** were complexed to FeCl₂ in anhydrous acetonitrile to give the dichloride complexes Fe(**O-Q**)Cl₂ in relatively low yields (27 – 37%). Identity was confirmed primarily through elemental analysis (CHN) where values were consistently within 1% of the expected range. A solid-state structure was obtained for Fe(**P**)Cl₂ (**Figure 4.13**) showing the expected coordination motif. Unfortunately, the data were of poor quality and so further interpretation of the structure was not feasible, but the coordination motif was unequivocal.

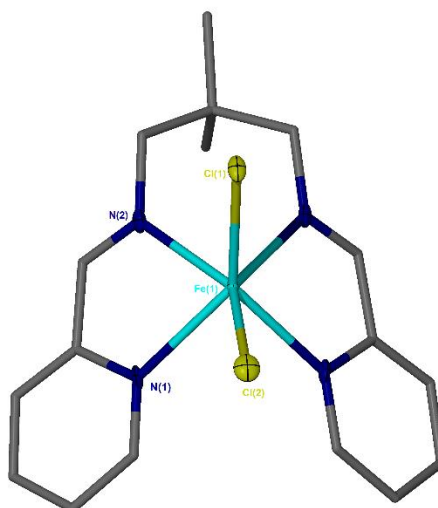


Figure 4.13: Solid state structure of $\text{Fe}(\mathbf{P})\text{Cl}_2$. Ellipsoids are shown at the 30% probability level. Only central atoms of $\text{Fe}(\mathbf{P})\text{Cl}_2$ are shown as ellipsoids due to incomplete data set due to weakly diffracting nature of crystals. Bond lengths and angles are not provided due to poor quality dataset.

4.3.2 Electrochemical characterisation of $\text{Fe}(\mathbf{O}-\mathbf{Q})\text{Cl}_2$

CV analysis for complexes $\text{Fe}(\mathbf{O}-\mathbf{Q})\text{Cl}_2$ was carried out to identify reversible redox behaviour suitable for the switching of oxidation states. The CV of $\text{Fe}(\mathbf{O})\text{Cl}_2$ is shown in **Figure 4.14** where a reversible redox peak centred around 0.2 V can be observed. This is presumably indicative of an $\text{Fe}^{2+}/\text{Fe}^{3+}$ transition. **Figure 4.15** shows the CV of $\text{Fe}(\mathbf{O})\text{Cl}_2$ against an internal ferrocene reference (a/a'). From this, the potential at which oxidation state change occurs (b/b') could be identified as $E_{1/2} = -0.33$ V vs. Fc/Fc^+ . The reversibility of the redox couple, combined with the polymerisation activity of $\text{Fe}(\mathbf{O})\text{Cl}_2$ make this a good candidate for electrochemical switching.

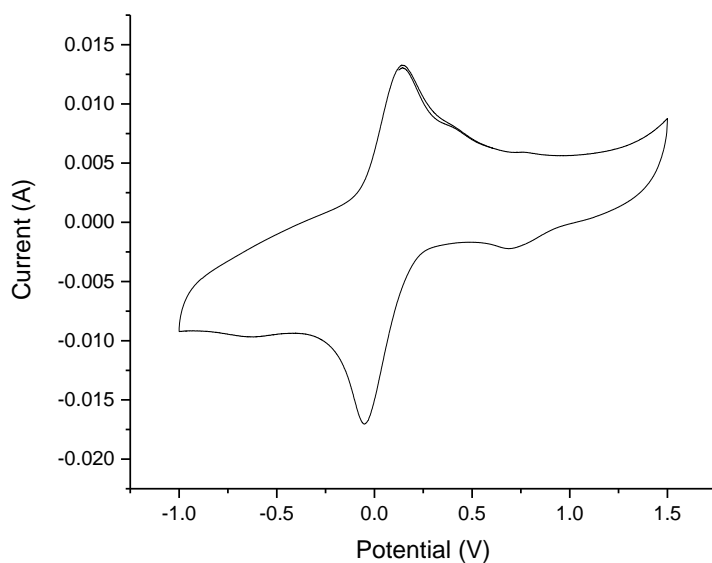


Figure 4.14: Cyclic voltammogram of Fe(O)Cl₂ in acetonitrile with 0.1 M TBPAF₆.

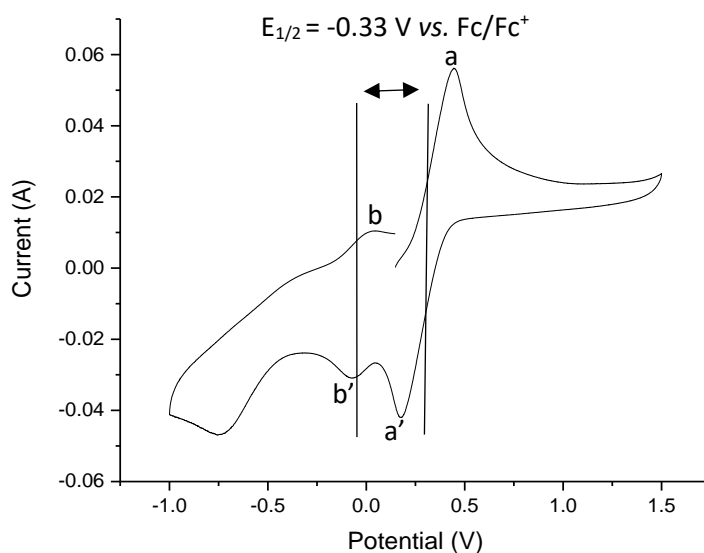


Figure 4.15: Cyclic voltammogram of Fe(O)Cl₂ in acetonitrile with 0.1 M TBPAF₆ and ferrocene as internal reference.

The CV of Fe(P)Cl₂ referenced against ferrocene (a/a') can be seen in **Figure 4.16**. The $E_{1/2}$ value is more positive than Fe(O)Cl₂, suggesting the complex is less susceptible to oxidation. A quasi-reversible redox peak (b/b'/b'') is present, and it appears that there is one oxidation peak followed by two, smaller reduction peaks. This could perhaps suggest a two-electron process oxidation and two one-electron reductions,

although the nature of these transitions is unclear. The CV of $\text{Fe}(\mathbf{Q})\text{Cl}_2$ (Figure 4.17) displayed a similar profile and, when ferrocene was added, the signals completely overlapped, suggesting a redox potential of approximately 0 V vs. Fc/Fc^+ . This suggests that $\text{Fe}(\mathbf{Q})\text{Cl}_2$ is the most difficult complex to oxidise.

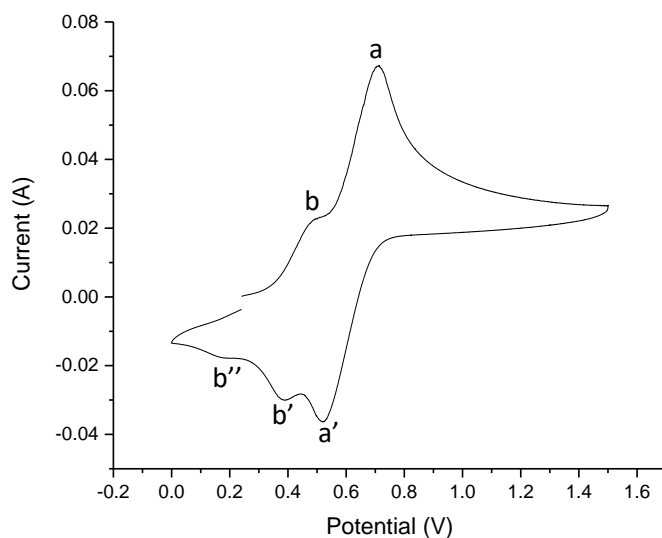


Figure 4.16: Cyclic voltammogram of $\text{Fe}(\mathbf{P})\text{Cl}_2$ in acetonitrile, 0.1 M TBAPF_6 with ferrocene as internal standard

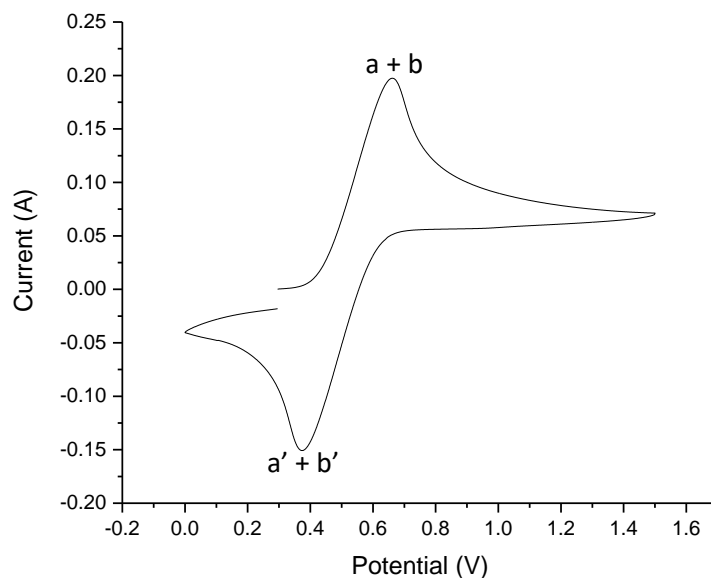


Figure 4.17: Cyclic voltammogram of $\text{Fe}(\mathbf{P})\text{Cl}_2$ in acetonitrile, 0.1 M TBAPF_6 with ferrocene as internal reference.

4.3.3 Lactide polymerisation with Fe(O-Q)Cl₂

Complexes Fe(O-Q)Cl₂ were initially tested for lactide polymerisation activity under solvent-free conditions at a ratio of [LA]/[I]/[BnOH]/[Et₃N] = 300 : 1 : 1 : 1 (**Table 4.02**). Fe(O)Cl₂ showed good activity, taking three minutes to reach 70% conversion. Both Fe(P)Cl₂ and Fe(Q)Cl₂ gave only 12% conversion after 60 minutes and insufficient samples was acquired for further analysis. Fe(O)Cl₂ was further tested at increased lactide to initiator ratio. With 600 equivalents of lactide, 41% conversion was attained after six minutes and the reaction time increased to nine minutes with 900 equivalents of lactide, showing that the system is robust enough to handle relatively low initiator loading. The molecular weights were consistently higher than the theoretical values and did not increase linearly with increased lactide concentration. This suggests inconsistent initiation, perhaps suggesting that not all complex is activated for initiation by the co-initiator and Et₃N. Dispersities were relatively broad (\bar{D} = 1.50 – 1.86), which is typical for a melt polymerisation. Due to the paramagnetic nature of the complexes, only one ¹H{¹H} NMR spectrum was procured which showed that atactic polymer was produced.

Table 4.02: Solvent-free polymerisation of *rac*-lactide with Fe(O-Q)Cl₂ at 130 °C.

Init.	[LA]/[I]/[BnOH]/[Et ₃ N]	Time /minutes	Conv. % ^a	P _r ^b	M _n ^d	M _n Calc. ^c	\bar{D} ^d
Fe(O)Cl ₂	300 : 1 : 1 : 1	3	70	0.60	46850	30400	1.64
Fe(P)Cl ₂	300 : 1 : 1 : 1	60	12	- ^e	- ^e	- ^e	- ^e
Fe(Q)Cl ₂	300 : 1 : 1 : 1	60	12	- ^e	- ^e	- ^e	- ^e
Fe(O)Cl ₂	600 : 1 : 1 : 1	6	41	- ^e	87150	35550	1.50
Fe(O)Cl ₂	900 : 1 : 1 : 1	9	44	- ^e	67350	57200	1.86

[a] Determined by ¹H NMR spectroscopy. [b] Probability of racemic enchainment, determined by ¹H{¹H} NMR spectroscopy. [c] Theoretical molecular weight calculated from conversion (rounded to the nearest 50): {(conversion × 3 × M_n [LA]) + M_n [BnOH]}. [d] Determined from GPC (in tetrahydrofuran) referenced against polystyrene standards × 0.58. [e] Not determined

To establish the feasibility of electrochemical switching with Fe(O)Cl₂, a series of screening tests were carried out (**Table 4.03**). Initially, polymerisation activity was tested in solution in the absence and presence of a chemical oxidant (FcPF₆). When the reaction was carried out in toluene for three hours at 80 °C, 77% conversion was observed. In an identical experiment with the addition of one equivalent of FcPF₆, 7% conversion was observed. This suggests that the oxidised form of the complex was

far less active for lactide polymerisation, which is ideal for the purpose of switchable catalysis.

Table 4.03: Screening tests for switchable polymerisation with Fe(O)Cl₂.

Init.	T / °C	[LA]/[I]/[BnOH] / [Et ₃ N]/FcPF ₆]	Solvent	[TBAPF ₆]	Reactor	Time /h	Conv. % ^a
Fe(O)Cl ₂	80	100 : 1 : 1 : 1 : 0	Toluene	-	Young's tap flask	3	77
Fe(O)Cl ₂	80	100 : 1 : 1 : 1 : 1	Toluene	-	Young's tap flask	3	7
Fe(O)Cl ₂	60	100 : 1 : 1 : 1 : 0	Acetonitrile	-	Young's tap flask	3	0
Fe(O)Cl ₂	60	100 : 1 : 1 : 1 : 0	THF	-	Young's tap flask	3	0
Fe(O)Cl ₂	40	100 : 1 : 1 : 1 : 0	DCM	-	Young's tap flask	3	0
Fe(O)Cl ₂	60	100 : 1 : 1 : 1 : 0	Toluene / DCM = 3 : 1	-	Young's tap flask	3	80
Fe(O)Cl ₂	60	100 : 1 : 1 : 1 : 0	Toluene / DCM = 3 : 1	0.1 M	Young's tap flask	4	76
Fe(O)Cl ₂	60	100 : 1 : 1 : 1 : 0	Toluene / DCM = 3 : 1	0.1 M	E-chem cell	3	31

[a] Determined by ¹H NMR spectroscopy

Toluene is an ideal solvent for conducting lactide polymerisation as it has a high boiling point and readily dissolves PLA. However, its non-polar nature means that it cannot dissolve the electrolyte required for the application of a stable potential across a solution. Furthermore, the heating of an electrochemical cell is not straightforward and so the temperature should be as low as possible. This is another reason to avoid toluene as it does not dissolve lactide at low temperatures. A series of alternative solvents were therefore tested for this reaction. No activity was observed when coordinating solvents, acetonitrile and THF, were used, presumably due to competition around the coordination sphere. DCM was able to dissolve all the reaction components but has a low boiling point and the temperature used (40 °C) was insufficient to polymerise lactide in this case.

A 3 : 1 mixture of toluene and DCM proved effective at 60 °C and 80% conversion was observed after three hours in a sealed flask. This conversion was only slightly reduced with the addition of electrolyte and a reaction time of four hours. Finally, an identical reaction was carried out in a two-chamber electrochemical cell with a flow of argon. A conversion of 31% was attained over three hours. This suggests that the complex is suitable in many ways for on-off polymerisation controlled by electrochemical means, however there are many technical challenges to realising this potential.

An electrochemical cell was developed according to the schematic diagram in **Figure 4.18**. A two-chamber cell was modified to include ground glass joints at the chamber openings and a Young's tap connection suitable for attaching to an argon line. The cell was dried in an oven for at least two hours. The electrodes were secured in Suba Seals which were used to seal the chamber openings. The system was flushed with argon before being submerged in an oil bath at the appropriate temperature. The reaction mixture and electrolyte were introduced into the working chamber and the platinum counter electrode was in contact with an electrolyte solution. For CV analysis, a glassy carbon electrode was employed; this was switched for a vitreous carbon electrode with a high surface area for bulk electrolysis.

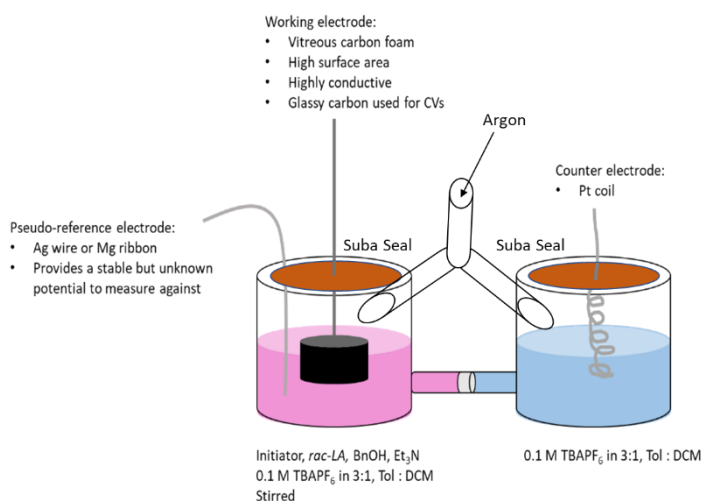


Figure 4.18: Schematic diagram of electrochemical reaction protocol.

There were numerous problems that were encountered when running the reaction under the conditions described in **Figure 4.18** and no conversion of lactide was achieved in subsequent reactions. The first problem related to the reaction mixtures being made up in a glovebox and added to the cell with a syringe. This had the potential to introduce a small amount of air into the system and may have hampered the activity of $\text{Fe}(\text{O})\text{Cl}_2$. Although every effort was made to secure gaps, the use of Suba Seals with electrodes is not an ideal airtight system and this is another way in which air could have contaminated the system. A constant flow of argon through the cell was used to try and counteract this potential issue. Related is the problem of solvent evaporation. As previously mentioned, a 3 : 1 mixture of toluene and DCM was required to solubilise the reagents whilst maintaining reasonable activity for lactide polymerisation. In practice, a combination of an imperfect seal, strong flow of argon and heating to 60 °C saw the DCM quickly removed. This invariably caused the electrolyte and some lactide to crash out of solution, rendering the applied potential to be lost.

4.4 Summary and conclusion

The redox behaviour of several iron (III) bisphenolate complexes were studied and quasi-reversible redox peaks were observed for five salalen complexes. These were not ultimately suitable for electrochemical switching. However, the redox potential of the $\text{Fe}^{2+}/\text{Fe}^{3+}$ couple could be related to the Lewis acidity of the complex and was shown to correlate with activity.

A series of three neutral {NNNN} ligands were synthesised and complexed to FeCl_2 . Of the complexes produced, $\text{Fe}(\text{O})\text{Cl}_2$ showed good activity towards lactide polymerisation. Furthermore, CV analysis demonstrated a reversible redox peak assigned to the $\text{Fe}^{2+}/\text{Fe}^{3+}$ transition, making it an ideal candidate for switchable polymerisation. A solvent system capable of dissolving both reagents and electrolyte was devised (toluene/DCM = 3 : 1) and good conversion was achieved in a reaction flask. Unfortunately, when the reaction was attempted with the electrochemical equipment, a combination of solvent evaporation and contamination with air led to a complete loss of activity. To achieve switchable polymerisation with this, or a

similar system, would require either a more active initiator capable of room temperature polymerisation in DCM, or a more air-tight cell where the solvent would not evaporate during the reaction.

4.5 References

- [1] A. Parthiban, *Synth. Appl. Copolym.* **2014**, 1–28.
- [2] H. Nakajima, P. Dijkstra, K. Loos, *Polymers (Basel)*. **2017**, *9*, 523.
- [3] L. Chen, R. E. O. Pelton, T. M. Smith, *J. Clean. Prod.* **2016**, *137*, 667–676.
- [4] J. Datta, E. Głowińska, *Ind. Crops Prod.* **2014**, *61*, 84–91.
- [5] Y. F. Guo, X. M. Hao, Y. L. Li, Y. Yang, X. Chen, J. M. Wang, *Adv. Mater. Res.* **2014**, *1048*, 31–35.
- [6] S. Jacobsen, H. G. Fritz, *Polym. Eng. Sci.* **1999**, *39*, 1303–1310.
- [7] K. Masutani, Y. Kimura, *Polym. Int.* **2017**, *66*, 260–276.
- [8] K. Avgoustakis, *Curr. Drug Deliv.* **2004**, *1*, 321–333.
- [9] S. Shahrad, M. Rajabi, H. Javadi, A. A. Karimi Zarchi, M. H. Darvishi, *Sci. Rep.* **2022**, *12*, 4718.
- [10] J. Panyam, V. Labhasetwar, *Adv. Drug Deliv. Rev.* **2003**, *55*, 329–347.
- [11] C. E. Astete, C. M. Sabliov, *J. Biomater. Sci. Polym. Ed.* **2006**, *17*, 247–289.
- [12] E. Razuvaeva, N. Sedush, E. Shirokova, S. Moskvichev, D. Streltsov, S. Chvalun, *Colloids Surfaces A Physicochem. Eng. Asp.* **2022**, *648*, 129198.
- [13] C. Hardy, G. Kociok-Köhn, A. Buchard, *Chem. Commun.* **2022**, *58*, 5463–5466.
- [14] C. Chen, *ACS Catal.* **2018**, *8*, 5506–5514.
- [15] C. K. A. Gregson, V. C. Gibson, N. J. Long, E. L. Marshall, P. J. Oxford, A. J. P. White, *J. Am. Chem. Soc.* **2006**, *128*, 7410–7411.
- [16] E. M. Broderick, N. Guo, C. S. Vogel, C. Xu, J. Sutter, J. T. Miller, K. Meyer, P. Mehrkhodavandi, P. L. Diaconescu, *J. Am. Chem. Soc.* **2011**, *133*, 9278–9281.
- [17] A. Sauer, J.-C. Buffet, T. P. Spaniol, H. Nagae, K. Mashima, J. Okuda, *ChemCatChem* **2013**, *5*, 1088–1091.
- [18] J. Wei, P. L. Diaconescu, *Acc. Chem. Res.* **2019**, *52*, 415–424.
- [19] L. A. Brown, J. L. Rhinehart, B. K. Long, *ACS Catal.* **2015**, *5*, 6057–6060.
- [20] X. Wang, A. Thevenon, J. L. Brosmer, I. Yu, S. I. Khan, P. Mehrkhodavandi, P. L. Diaconescu, *J. Am. Chem. Soc.* **2014**, *136*, 11264–11267.

- [21] S. Deng, P. L. Diaconescu, *Inorg. Chem. Front.* **2021**, *8*, 2088–2096.
- [22] E. M. Broderick, N. Guo, T. Wu, C. S. Vogel, C. Xu, J. Sutter, J. T. Miller, K. Meyer, T. Cantat, P. L. Diaconescu, *Chem. Commun.* **2011**, *47*, 9897.
- [23] A. B. Biernesser, B. Li, J. A. Byers, *J. Am. Chem. Soc.* **2013**, *135*, 16553–16560.
- [24] A. B. Biernesser, K. R. D. Chiaie, J. B. Curley, J. A. Byers, *Angew. Chemie - Int. Ed.* **2016**, *55*, 5251–5254.
- [25] M. Qi, Q. Dong, D. Wang, J. A. Byers, *J. Am. Chem. Soc.* **2018**, *140*, 5686–5690.
- [26] M. Qi, H. Zhang, Q. Dong, J. Li, R. A. Musgrave, Y. Zhao, N. Dulock, D. Wang, J. A. Byers, *Chem. Sci.* **2021**, *12*, 9042–9052.
- [27] Y. Huang, C. Hu, X. Pang, Y. Zhou, R. Duan, Z. Sun, X. Chen, *Angew. Chemie Int. Ed.* **2022**, *61*, e202202660.
- [28] P. McKeown, M. D. Jones, O. J. Driscoll, M. F. Mahon, C. K. C. Leung, *Eur. J. Inorg. Chem.* **2018**, *2018*, 5129–5135.
- [29] M. Cozzolino, V. Leo, C. Tedesco, M. Mazzeo, M. Lamberti, *Dalton Trans.* **2018**, *47*, 13229–13238.

Chapter 5: Experimental

5.1 General experimental methods

All chemicals were commercially obtained from Sigma-Aldrich and used as received. This is with the exception of the *rac*-lactide, which was singly recrystallised from dry toluene and stored under argon. 3,5-di-*tert*-butyl-2-hydroxybenzyl bromide was prepared according to literature methods.^[1] For the synthesis of metal complexes under anhydrous conditions, dry solvents, a MBraun LABmaster dp glovebox, standard Schlenk line techniques and oven-dried glassware were used. Dried and degassed reaction solvents, used in the preparation of these complexes, were collected under inert gas conditions from a Solvent Purification System (SPS).

¹H NMR spectra of ligands, complexes and polymerisations were recorded on a Bruker 400 II MHz or 500 MHz instrument and referenced to residual solvent peaks. Polymerisation conversion was recorded from the integration of the methine region of the polymer (5.12 - 5.20 ppm) against that of the monomer (4.94 – 5.01). The tacticity of polymers was determined from its ¹H{¹H} NMR spectrum, decoupling from the polymer doublet at 1.62 ppm. ¹H{¹H} NMR was recorded on a Bruker AV 400 MHz spectrometer. The following abbreviations are used in the report of spectra: s, singlet; d, doublet; dd, doublet of doublets; t, triplet; q, quartet; m, multiplet.

Electrospray ionisation (ESI) mass spectra of ligands and Fe(III) complexes were collected using a MicroToF electrospray quadrupole time-of-flight mass spectrometer, with the sample dissolved in acetonitrile at approximately 1 µg mL⁻¹ concentration. Spectra were recorded in positive loop injection mode set for a range of 50 - 1500 m/z.

Typical polymerisation procedure (solution, iron complexes)

Rac-lactide (0.4 g, 2.8 × 10⁻³ mol) was added to an ampoule with a Young's cap in 4 mL of toluene, with initiator (2.8 × 10⁻⁵ mol), benzyl alcohol (2.88 µL, 2.8 × 10⁻⁵ mol), and triethylamine (3.87 µL, 2.8 × 10⁻⁵ mol). An oil bath was heated to the appropriate temperature and the polymerisation ran for the chosen time. Once complete the solvent was immediately removed in vacuo and the crude product analysed via ¹H NMR. The pure polymer was obtained by washing with > 30 mL methanol.

Typical polymerisation procedure (solution, pre-activated iron complexes)

Initiator (2.8×10^{-5} mol), benzyl alcohol (2.88 μ L, 2.8×10^{-5} mol), and triethylamine (3.87 μ L, 2.8×10^{-5} mol) were added to an ampoule with a Young's cap in 4 mL of toluene. The solution was stirred for the chosen time at 80 °C. The solution was cooled to room temperature and taken into a glovebox where *rac*-lactide (0.4 g, 2.8×10^{-3} mol) was added. The solution was then heated to 40 °C for the chosen polymerisation time. Once complete the solvent was immediately removed in vacuo and the crude product analysed via ^1H NMR. The pure polymer was obtained by washing with > 30 mL methanol.

Typical polymerisation procedure (solution, aluminium complexes)

Rac-lactide (0.4 g, 2.8×10^{-3} mol) was added to an ampoule with a Young's cap in 4 mL of toluene, with initiator (2.8×10^{-5} mol) and benzyl alcohol (2.88 μ L, 2.8×10^{-5} mol). An oil bath was heated to the appropriate temperature and the polymerization ran for the chosen time. Once complete the solvent was immediately removed in vacuo and the crude product analysed via ^1H NMR. The pure polymer was obtained by washing with > 30 mL methanol.

Typical polymerisation procedure (melt, zinc and aluminium complexes)

Lactide (1.0 g, 6.9×10^{-3} mol) was added to an ampoule with a Young's cap with initiator (2.3×10^{-5} mol) and benzyl alcohol (2.40 μ L, 2.3×10^{-5} mol). An oil bath was heated to the appropriate temperature and the polymerisation ran for the chosen time. Once complete, the crude product analysed via ^1H NMR. The pure polymer was obtained by washing with > 30 mL methanol.

Typical degradation procedure

Degradation reactions were performed in a Young's ampoule under argon. The flask containing PLA (0.25 g, Vegware™, PLLA cup, $M_n = 45,510 \text{ g mol}^{-1}$), was taken into a glovebox and loaded with metal complex (8 wt%, 0.02 g). The polymer was then dissolved in THF (4 mL) with heating and stirring assisting dissolution. The flask was then submerged in a preheated oil bath (80 °C) to which MeOH (1 mL) was added. Aliquots were taken for ^1H NMR (CDCl_3) analysis of the methine region. After the

reaction, the solvent was removed *in vacuo* and the residual methyl lactate (Me-La) was analysed further. PET reactions were carried out in a Young's ampoule containing 0.25 g of carbonated drinks bottle or thin films. Catalyst (8 wt%, 0.02 g) was added in a glove box. EG (27.5 eq, 1.5 mL) was added and the flask was submerged in a pre-heated oil bath at 180 °C. When full dissolution of the PET was observed, water was added and the mixture was filtered. BHET crystallised from the mixture and was collected, dried at 100°C *in vacuo* for 4 hours and weighed to obtain isolated yields.

General CO₂ / epoxide coupling reaction method and procedure

All CO₂ / epoxide coupling reactions were carried out in a ratio of 1 : 8 : 1200 [catalyst (0.08 mol%)]/[co-catalyst (0.64 mol%)]/[epoxide] where tetrabutylammonium chloride (TBAC) was the co-catalyst and cyclohexene (CHO) was generally the epoxide.

The catalyst (4.21×10^{-5} mol) and TBAC (0.094 g, 3.37×10^{-4} mol) were added as solids to a glass reactor vial in a glovebox. CHO (5 mL) was added to the vial *via* syringe to form a dark purple mixture. The vial was transferred out of the glovebox and placed in the autoclave under a flow of argon. The autoclave was cycled five times with CO₂ and finally left pressurised at 10 bar. The temperature was ramped to 80 °C and left for 24 hours with mechanical stirring. After this time, the autoclave was cooled in an ice bath before bleeding to the air. An aliquot was taken of the crude dark red product mixture and analysed *via* ¹H NMR spectroscopy to determine conversion and selectivity. ESI-MS was used to confirm the cyclic carbonate product was present in the mixture and GPC analysis to confirm no polymer was present. GPC was carried out at 1 mL min⁻¹ at 35 °C with a THF eluent using a PLgel 5 µm.

GPC was carried out on an Agilent 1260 Infinity series instrument at 1 mL min⁻¹ at 35 °C with a THF eluent using a PL gel 5 µm MIXED-D 300 x 7.5 mm column. Detection was carried out using a differential refractive index detector (referenced to 11 polystyrene standards of narrow molecular weight, ranging from M_w 615-568000 Da).

MALDI-ToF analysis was carried out on a Bruker Autoflex speed instrument in reflector positive mode, using DCTB as the matrix at a concentration of 10 mg mL⁻¹.

50 μL of this solution was co-applied with 2 μL of 0.1 M NaTFA solution and 10 μL of the analyte at a concentration of 10 mg mL^{-1} . 1 μL of this homogenised solution was applied to a steel target plate for analysis. Materials characterization (GPC, MALDI-ToF) facilities were provided through MC² at the University of Bath.

The DSC analyses were recorded on a TA Instruments DSC Q20. The sample was held at 40 °C for 1 minute, heated to 200 °C at 10 °C/min held at this temperature for 1 minute, cooled to 40 °C at 5 °C/min held at this temperature for 1 minute and finally heated to 200 °C at 10 °C/min - the T_m values are quoted for the second heating cycle. TGA analysis was recorded on a Setaram KEP Technologies Setsys Evolution TGA-DTA/DSC instrument. The sample chamber was purged with Ar (20 mL min^{-1}) for 20 minutes before being heated to 500 °C at 10 °C/min.

All crystallographic data was collected on a SuperNova or Excalibur, EOS detector diffractometer using radiation $\text{CuK}\alpha$ ($\lambda = 1.54184 \text{ \AA}$) or $\text{Mo-K}\alpha$ ($\lambda = 0.71073 \text{ \AA}$) radiation all recorded at 150(2) K. All structures were solved by direct methods and refined on all F^2 data using the SHELXL-2014 suite of programs. All hydrogen atoms were included in idealised positions and refined using the riding model, all refinement details are given in the .cif file. All models were straightforward with the following exceptions: $[\text{Fe}(\mathbf{A})]_2(\mu_2\text{-CO}_3)$: The asymmetric unit comprises half of a carbonate bridged dimer (in which C33 and O4 are coincident with a crystallographic 2-fold rotation axis) and a portion of solvent. The latter was extremely disordered, and ultimately treated with the solvent mask algorithm in Olex-2. An allowance for the presence of one molecule of CH_2Cl_2 , per asymmetric unit, has been made in the formula as presented. $\text{Al}(\mathbf{E})\text{Me}$: one solvent molecule of toluene is disordered over a centre of inversion and has been refined with 50% occupation, geometric constraints and ADP restraints.

Experimental procedure for Raman kinetics

All polymerisation samples were prepared in a N_2 filled glovebox. The initiator, co-initiator (4-MeBnOH or BnOH) and the lactide were stored in the same glovebox. Technical grade L- and D-lactide were stored at -30 °C. Technical grade lactide was used without further purification. L-lactide was recrystallised one time from toluene

and dried under vacuum before use. All polymerisations were carried out under Ar atmosphere in a stainless-steel reactor. The reactor was heated to 150 °C under vacuum and flushed with Ar three times prior to the reaction. In all cases a stirrer speed of 260 rpm was used. All polymerisations were monitored by *in situ*-Raman spectroscopy using a Kaiser Optical Systems RXN1 spectrometer equipped with a probe head with a sapphire lens ($d = 0.1$ mm) at a wavelength of 785 nm and 450 mW. *Peaxact 4* was used to calculate the kinetic data by integration of the Raman spectrum. The boundaries for lactide were 627 – 713 cm^{-1} . To determine the average molar masses and the mass distributions of these polylactide samples GPC was used. A GPCmax VE 2001 from Viscotek was used with THF as the mobile phase and a flow rate of 1 mL min^{-1} , combining an HPLC pump with two Malvern Viscotek T columns (porous styrene divinylbenzene copolymer) with a maximum pore size of 500 and 5000 Å, a refractive index detector (VE 3580) and a viscometer (Viscotek 270 Dual Detector).

Sample preparation:

a) Polymerisation of technical grade *rac*-lactide:

Technical grade *rac*-lactide (4.0 g, 27.75 mmol, 1250 eq) and the respective initiator (0.022 mmol, 1.0 eq) were weighed out and thoroughly combined using an agate mortar. The mixture was placed in a screw cap vial and transferred to the reactor under Ar flow. As soon as the reactor was closed the Raman measurements were started. Spectra collection was conducted every 15 seconds. After 3 hours of reaction time the heating and stirring were stopped and the reaction mixture was exposed to air to end the polymerisation. An aliquot of the mixture was used to determine the conversion *via* $^1\text{H-NMR}$ spectroscopy in CDCl_3 . A further portion of the reaction mixture was dissolved in CH_2Cl_2 (2.0 ml) and PLA was precipitated from cold EtOH (0 °C). The polymer was dried under vacuum and analysed *via* GPC.

b) Polymerisation of recrystallised L-lactide:

Recrystallised L-lactide (8.0 g, 55.5 mmol, 2500 eq,) and the respective initiator (0.022 mmol, 1.0 eq) were weighed out and thoroughly combined using an agate mortar. The mixture was placed in a screw cap vial and transferred to the reactor under Ar flow. As soon as the reactor was closed the Raman measurements were started. Spectra collection was conducted every 15 seconds. After 3 hours of reaction time the heating and stirring were stopped and the reaction mixture was exposed to air to end the polymerisation. An aliquot of the mixture was used to determine the conversion *via* $^1\text{H-NMR}$ spectroscopy in CDCl_3 . A further portion of the reaction mixture was dissolved in CH_2Cl_2 (2.0 ml) and PLA was precipitated from cold EtOH (0 °C). The polymer was dried under vacuum and analysed *via* GPC.

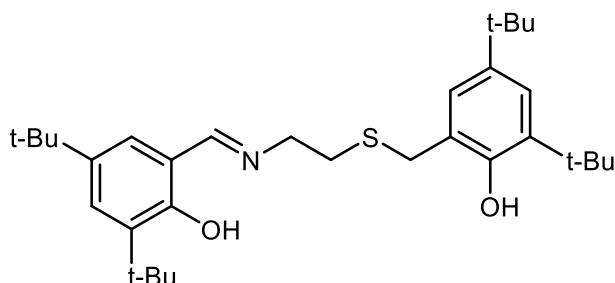
c) Polymerisation of recrystallised L-lactide with added co-initiator (4-MeBnOH):

Recrystallised L-lactide (8.0 g, 55.5 mmol, 3000 eq,) 4-MeBnOH (22.6 mg, 0.19 mmol, 10 eq) and the respective initiator (0.019 mmol, 1.0 eq) were weighed out and thoroughly combined using an agate mortar. The mixture was placed in a screw cap vial and transferred to the reactor under Ar flow. As soon as the reactor was closed the Raman measurements were started. Spectra collection was conducted every 15 seconds. After 3 hours of reaction time the heating and stirring were stopped and the reaction mixture was exposed to air to end the polymerisation. An aliquot of the mixture was used to determine the conversion *via* $^1\text{H-NMR}$ spectroscopy in CDCl_3 . A further portion of the reaction mixture was dissolved in CH_2Cl_2 (2.0 ml) and PLA was precipitated from cold EtOH (0 °C). The polymer was dried under vacuum and analysed *via* GPC.

d) Polymerisation of recrystallised L-lactide with added co-initiator (BnOH) Recrystallised l-lactide (8.0 g, 55.5 mmol, 3000 or 10000 eq) and Zn(7)₂ (1.0 eq) were weighed out and placed in a screw cap vial. The mixture was transferred to the reactor und Ar flow. The reactor was closed and the mixture was allowed to melt. After 1 min BnOH (10.0 or 100.0 eq) was added thereto and the Raman measurement was started. Spectra collection was conducted every 15 seconds. After the desired reaction time the heating and stirring was stopped and the reaction mixture was exposed to air to end the polymerisation. An aliquot of the mixture was used to determine the conversion *via* ¹H-NMR spectroscopy in CDCl₃. A further portion of the reaction mixture was dissolved in CH₂Cl₂ (2.0 ml) and PLA was precipitated from cold EtOH (0 °C). The polymer was dried under vacuum and analysed *via* GPC.

5.2 Thiolen complexes of iron and aluminium for *rac*-lactide polymerisation

5.2.1 Ligand synthesis and characterisation



AH₂: A solution of 3,5-di-*tert*-butyl-2-hydroxybenzaldehyde (3.02 g, 12.9 mmol) and 2-amino-ethanethiol (1.0 g, 12.9 mmol) in methanol (20 mL) was stirred until a precipitate formed. The pale yellow solid was collected and dried (2.86 g, 76%). The solid (2.6 g, 8.9 mmol) and triethylamine (0.90 g, 1.24 mL, 8.9 mmol) were dissolved in THF (20 mL). A solution of 3,5-di-*tert*-butyl-2-hydroxybenzyl bromide (2.54 g, 8.9 mmol) in THF (20 mL) was added dropwise and the mixture was stirred for three hours. The white precipitate was filtered off and the solvent removed *in vacuo* to give a yellow oil. Recrystallisation from methanol gave the product as a yellow powder (4.22 g, 8.2 mmol 64%).

¹H NMR (400 MHz, CDCl₃) δ 8.24 (s, 1H, CH), 7.34 (d, *J* = 2.4 Hz, 1H, Ar-H), 7.23 (d, *J* = 2.5 Hz, 1H, Ar-H), 7.03 (d, *J* = 2.4 Hz, 1H, Ar-H), 6.91 (d, *J* = 2.4 Hz, 1H, Ar-H), 3.81 (s, 2H, CH₂), 3.63 (t, *J* = 6.7, 2H, CH₂), 2.68 (t, *J* = 6.7 Hz, 2H, CH₂), 1.39 (s, 9H, C(CH₃)₃), 1.38 (s, 9H, C(CH₃)₃), 1.26 (s, 9H, C(CH₃)₃), 1.23 (s, 9H, C(CH₃)₃). Note: OH peak not observed in spectrum.

¹³C{¹H} NMR (101 MHz, CDCl₃) δ 167.1 (C=N), 157.9 (Ar), 152.0 (Ar), 142.2 (Ar), 140.1 (Ar), 137.2 (Ar), 136.7 (Ar), 127.1 (Ar), 125.9 (Ar), 125.3 (Ar), 123.7 (Ar), 121.5 (Ar), 117.6 (Ar), 59.1 (CH₂), 35.0 (CH₂), 34.9 (C), 34.5 (C), 34.2 (C), 34.1 (C), 31.5 (CH₃), 31.4 (CH₃ + CH₂), 29.7 (CH₃), 29.4 (CH₃).

m/z calc. [C₃₂H₅₀NO₂S]⁺ (methanol) = 512.3562, found 512.3557.

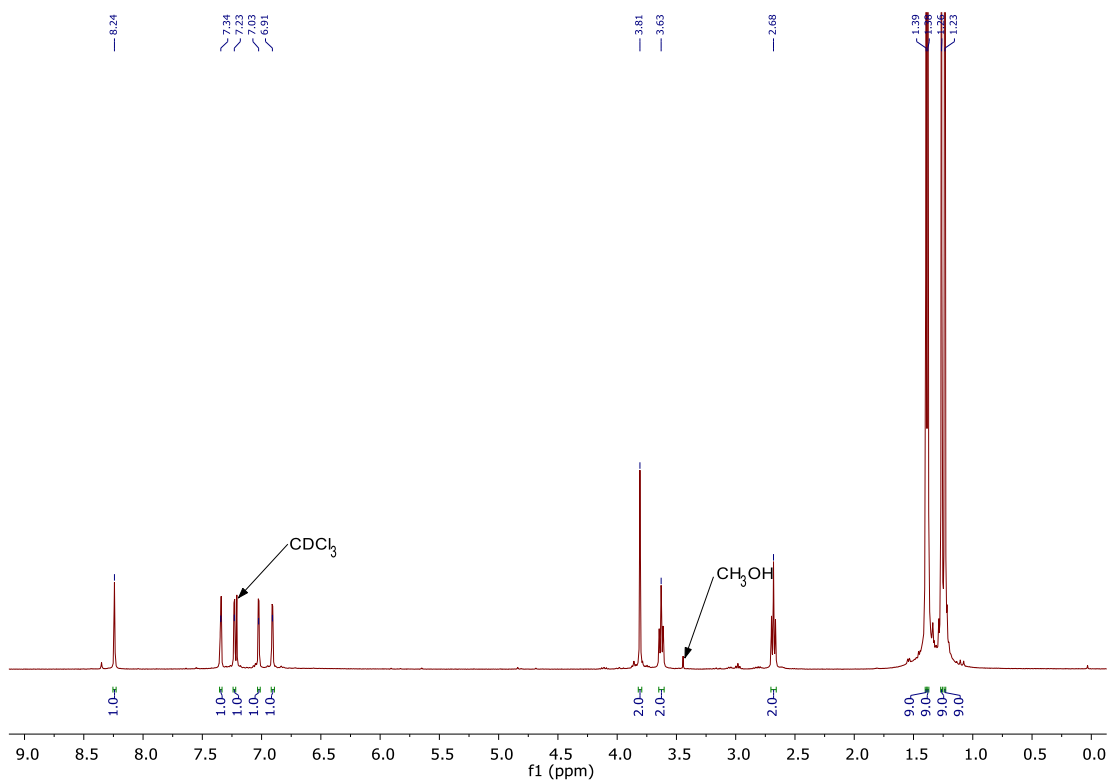


Figure 5.01: ^1H NMR (400 MHz, CDCl_3 , 298K) spectrum of AH_2 .

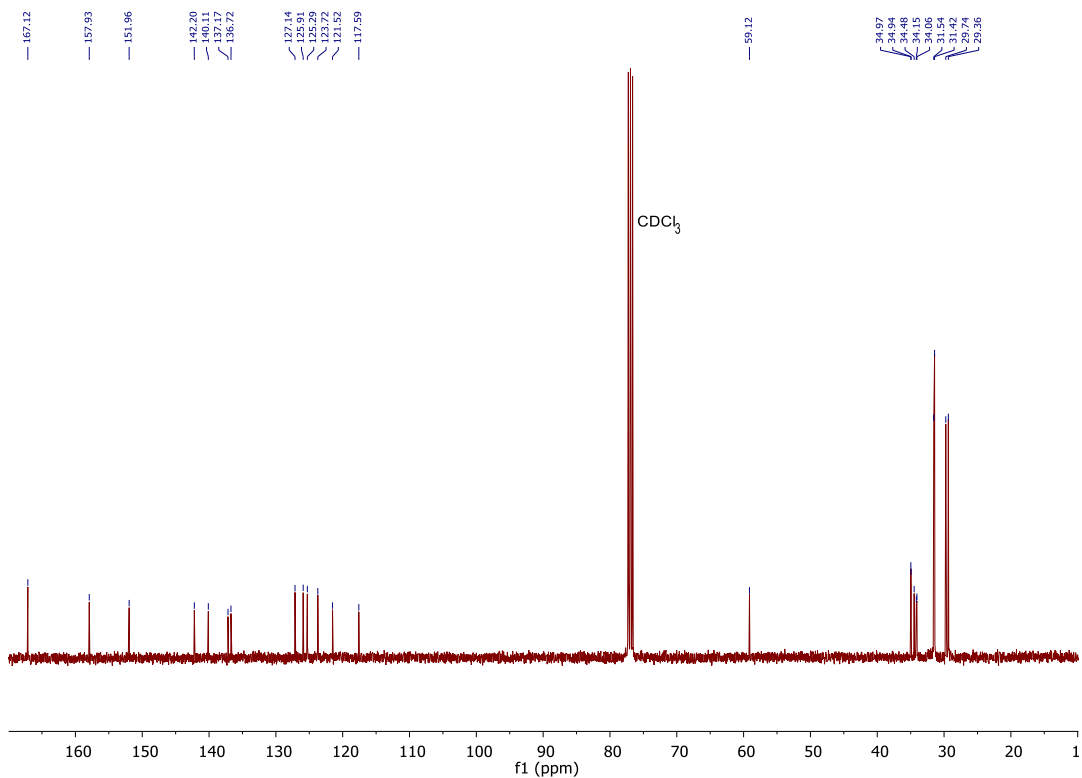
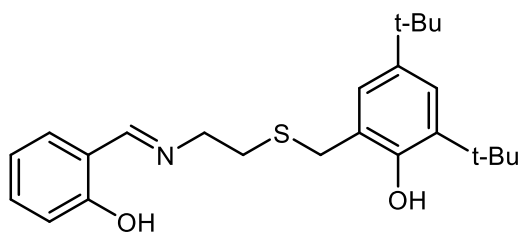


Figure 5.02: $^{13}\text{C}\{^1\text{H}\}$ NMR (101 MHz, CDCl_3 , 298K) spectrum of AH_2 .



BH₂: A solution of salicylaldehyde (1.22 g, 1.04 mL, 10 mmol) and 2-aminoethanethiol (0.77 g, 10 mmol) in THF (20 mL) was refluxed for three hours. Triethylamine (1.01 g, 1.39 mL, 10 mmol) was added and the solution was stirred for 15 minutes. A solution of 3,5-di-*tert*-butyl-2-hydroxybenzyl bromide in THF (20 mL) was added dropwise and the mixture was refluxed for three hours. The white precipitate was filtered off and the solvent removed *in vacuo* to give a yellow oil. Recrystallisation from methanol gave the product as a yellow powder (2.93 g, 7.3 mmol, 73%).

¹H NMR (400 MHz, CDCl₃) δ 8.24 (s, 1H, CH), 7.27 (ddd, *J* = 8.3, 7.3, 1.7 Hz, 1H, Ar-H), 7.22 (d, *J* = 2.5 Hz, 1H, Ar-H), 7.19 (dd, *J* = 7.7, 1.7 Hz, 1H, Ar-H), 6.93 – 6.89 (m, 1H, Ar-H), 6.88 (d, *J* = 2.5 Hz, 1H, Ar-H), 6.84 (td, *J* = 7.5, 1.1 Hz, 1H, Ar-H), 3.79 (s, 2H, CH₂), 3.63 (td, *J* = 6.7, 1.2 Hz, 2H, CH₂), 2.68 (t, *J* = 6.8 Hz, 2H, CH₂), 1.37 (s, 9H, C(CH₃)₃), 1.23 (s, 9H, C(CH₃)₃). Note: OH peak not observed in spectrum.

¹³C{¹H} NMR (101 MHz, CDCl₃) δ 166.0 (C=N), 161.0 (Ar), 151.9 (Ar), 142.2 (Ar), 137.2 (Ar), 132.4 (Ar), 131.4 (Ar), 125.2 (Ar), 123.7 (Ar), 121.5 (Ar), 118.6 (Ar), 118.5 (Ar), 117.0 (Ar), 59.0 (CH₂), 34.9 (CH₂), 34.4 (C), 34.2 (C), 31.5 (CH₂), 31.5 (CH₃), 29.7 (CH₃).

m/z calc. [C₂₄H₃₄NO₂S]⁺ (methanol) = 400.2310, found 400.2352.

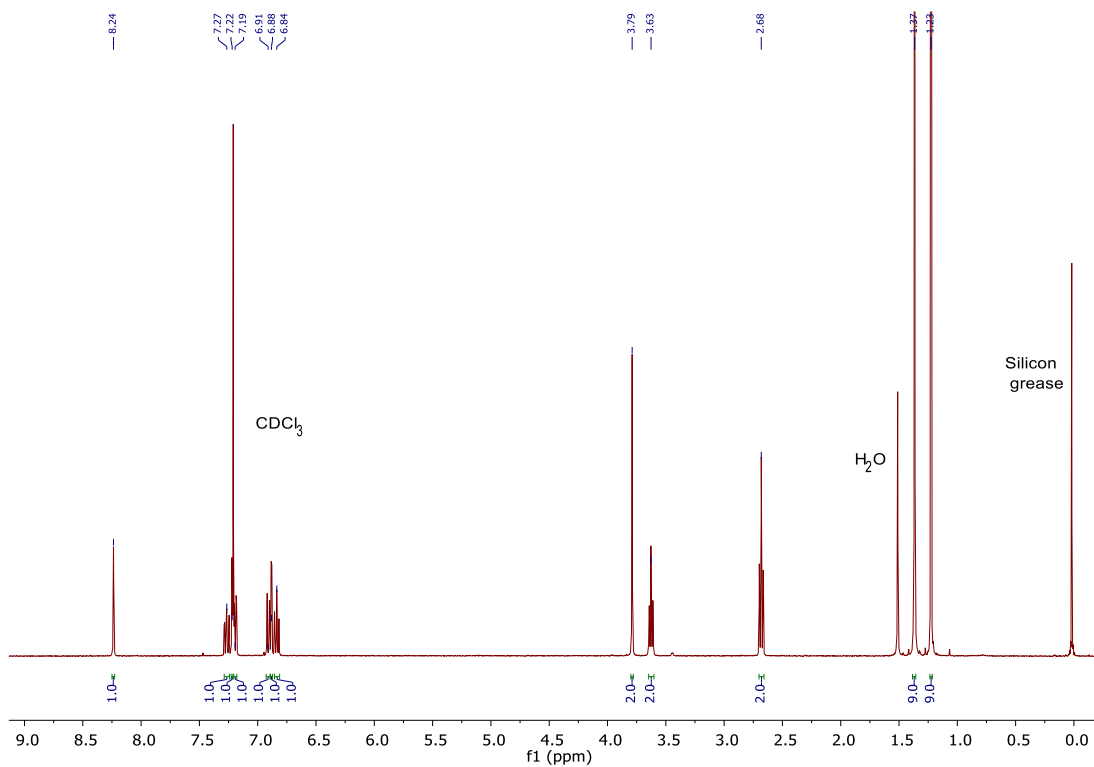


Figure 5.03: ^1H NMR (400 MHz, CDCl_3 , 298K) spectrum of BH_2 .

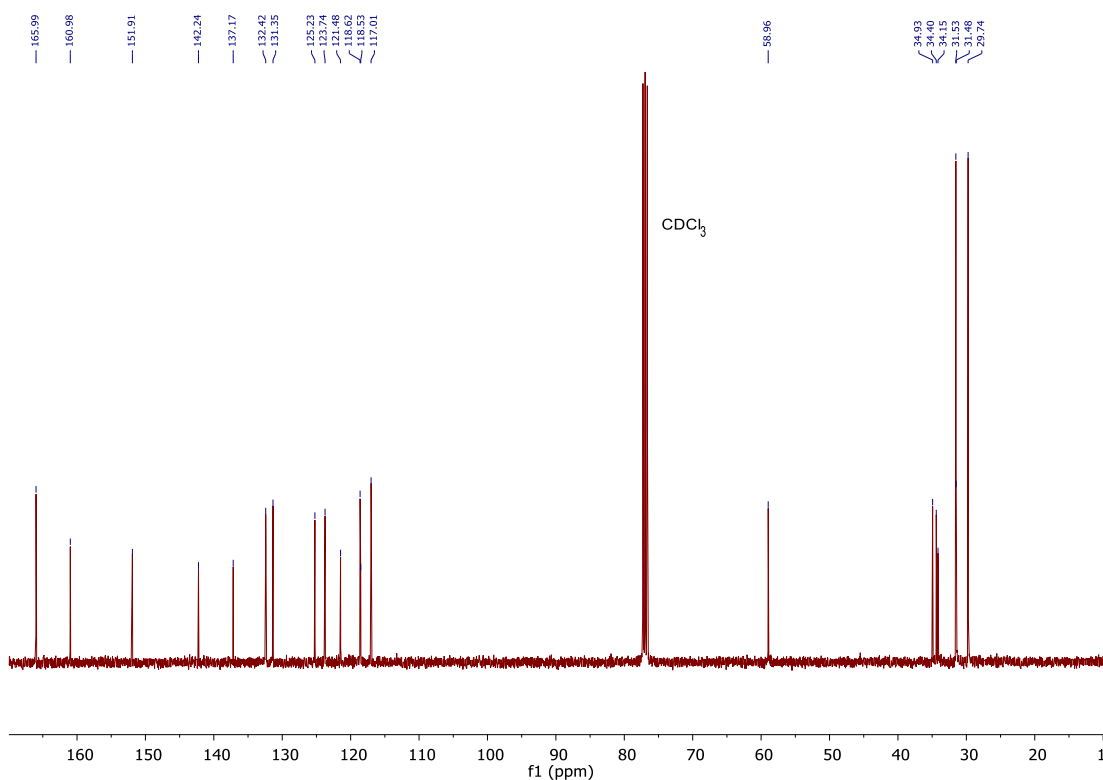
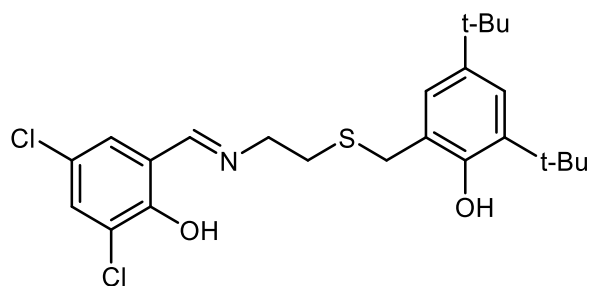


Figure 5.04: $^{13}\text{C}\{^1\text{H}\}$ NMR (101 MHz, CDCl_3 , 298K) spectrum of BH_2 .



CH₂: A solution of 3,5-dichlorosalicylaldehyde (1.91 g, 10 mmol) and 2-aminoethanethiol (0.77 g, 10 mmol) in THF (20 mL) was stirred for two hours at room temperature. Triethylamine (1.01 g, 1.39 mL, 10 mmol) was added and the solution was stirred for a further 15 minutes. A solution of 3,5-di-*tert*-butyl-2-hydroxybenzyl bromide in THF (20 mL) was added dropwise and the mixture was stirred for three hours. The white precipitate was filtered off and the solvent removed *in vacuo* to give an orange oil. Recrystallisation from methanol gave the product as a yellow powder (1.76 g, 37%).

¹H NMR (400 MHz, CDCl₃) δ 8.13 (s, 1H, CH), 7.36 (d, *J* = 2.4 Hz, 1H, Ar-H), 7.23 (d, *J* = 2.4 Hz, 1H, Ar-H), 7.09 (d, *J* = 2.6 Hz, 1H, Ar-H), 6.88 (d, *J* = 2.4 Hz, 1H, Ar-H), 3.78 (s, 2H, CH₂), 3.64 (t, *J* = 6.5, 2H, CH₂), 2.70 (t, *J* = 6.6 Hz, 2H, CH₂), 1.37 (s, 9H, C(CH₃)₃), 1.23 (s, 9H, C(CH₃)₃). Note: OH peak not observed in spectrum.

¹³C{¹H} NMR (101 MHz, CDCl₃) δ 164.4 (C=N), 156.5 (Ar), 151.8 (Ar), 142.4 (Ar), 137.2 (Ar), 132.3 (Ar), 129.0 (Ar), 125.2 (Ar), 123.9 (Ar), 122.9 (Ar), 122.7 (Ar), 121.3 (Ar), 119.3 (Ar), 58.1 (CH₂), 34.9 (CH₂), 34.5 (C), 34.2 (C), 31.5 (CH₃), 31.3 (CH₂), 29.7 (CH₃).

m/z calc. [C₂₄H₃₂Cl₂NO₂S]⁺ (acetonitrile) = 468.1522, found = 468.1514.

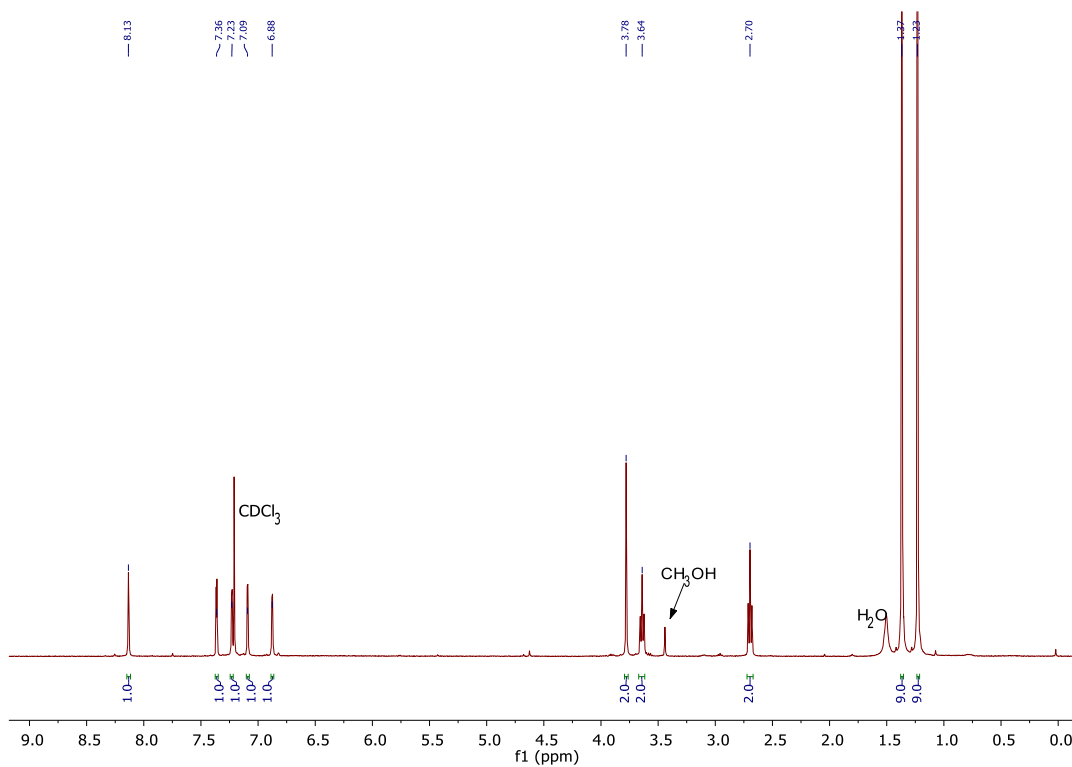


Figure 5.05: ¹H NMR (400MHz, CDCl₃, 298K) spectrum of CH₂.

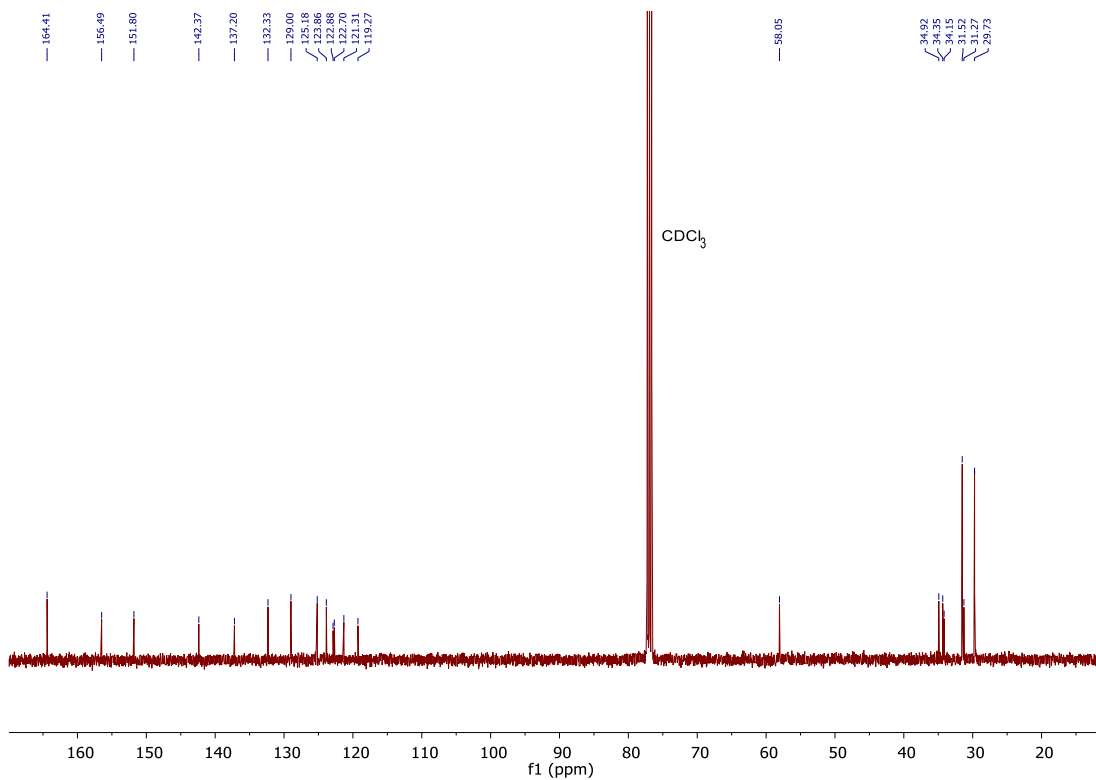
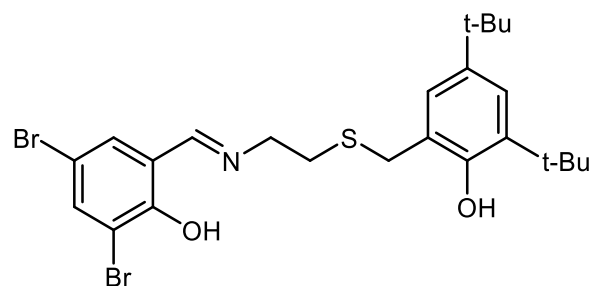


Figure 5.06: ¹³C{¹H} NMR (101 MHz, CDCl₃, 298K) spectrum of CH₂.



DH₂: A solution of 3,5-di-bromo-2-hydroxybenzaldehyde (2.80 g, 10 mmol) and 2-amino-ethanethiol (0.77 g, 10 mmol) in THF (20 mL) was refluxed for four hours. Triethylamine (1.01 g, 1.39 mL, 10 mmol) was added and the solution was stirred for a further 15 minutes. A solution of 3,5-di-*tert*-butyl-2-hydroxybenzyl bromide in THF (20 mL) was added dropwise and the mixture was refluxed for twelve hours. The white precipitate was filtered off and the solvent removed *in vacuo* to give a yellow oil. Recrystallisation from methanol gave the product as a yellow solid (2.32 g, 42%).

¹H NMR (400 MHz, CDCl₃) δ 8.10 (s, 1H, CH), 7.65 (d, *J* = 2.3 Hz, 1H, Ar-H), 7.26 (d, *J* = 2.3 Hz, 1H, Ar-H), 7.24 (s, 1H, Ar-H), 6.88 (d, *J* = 2.4 Hz, 1H, Ar-H), 3.78 (s, 2H), 3.64 (t, *J* = 6.5, 2H, CH₂), 2.69 (t, *J* = 6.5 Hz, 2H, CH₂), 1.37 (s, 9H, C(CH₃)₃), 1.24, (s, 9H, C(CH₃)₃).

Note: OH peak not observed in spectrum.

¹³C{¹H} NMR (101 MHz, CDCl₃) δ 164.2 (C=N), 158.0 (Ar), 151.8 (Ar), 142.4 (Ar), 137.8 (Ar), 137.2 (Ar), 132.7 (Ar), 125.2 (Ar), 123.9 (Ar), 121.3 (Ar), 119.7 (Ar), 112.4 (Ar), 109.5 (Ar), 57.9 (CH₂), 34.9 (CH₂), 34.3 (C), 34.2 (C), 31.5 (CH₃), 31.3 (CH₂), 29.7 (CH₃).

m/z calc. [C₂₄H₃₂Br₂NO₂S]⁺ (acetonitrile) = 556.0515, found = 556.0489.

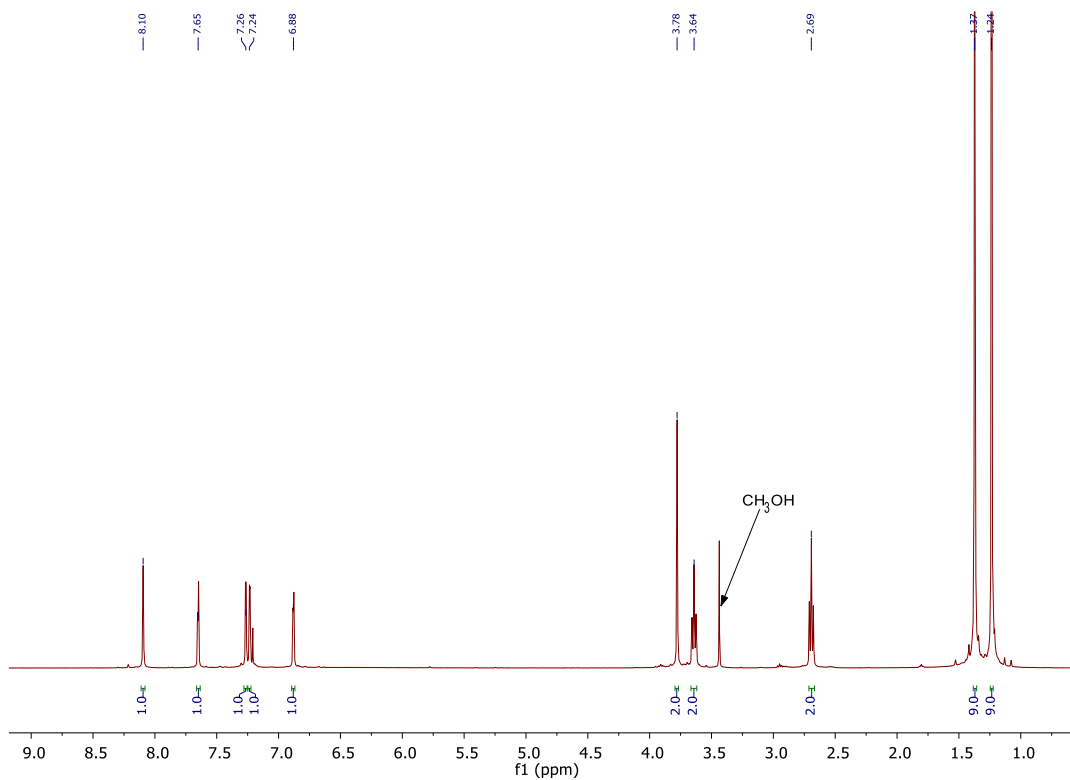


Figure 5.07: ^1H NMR (400MHz, CDCl_3 , 298K) spectrum of DH_2 .

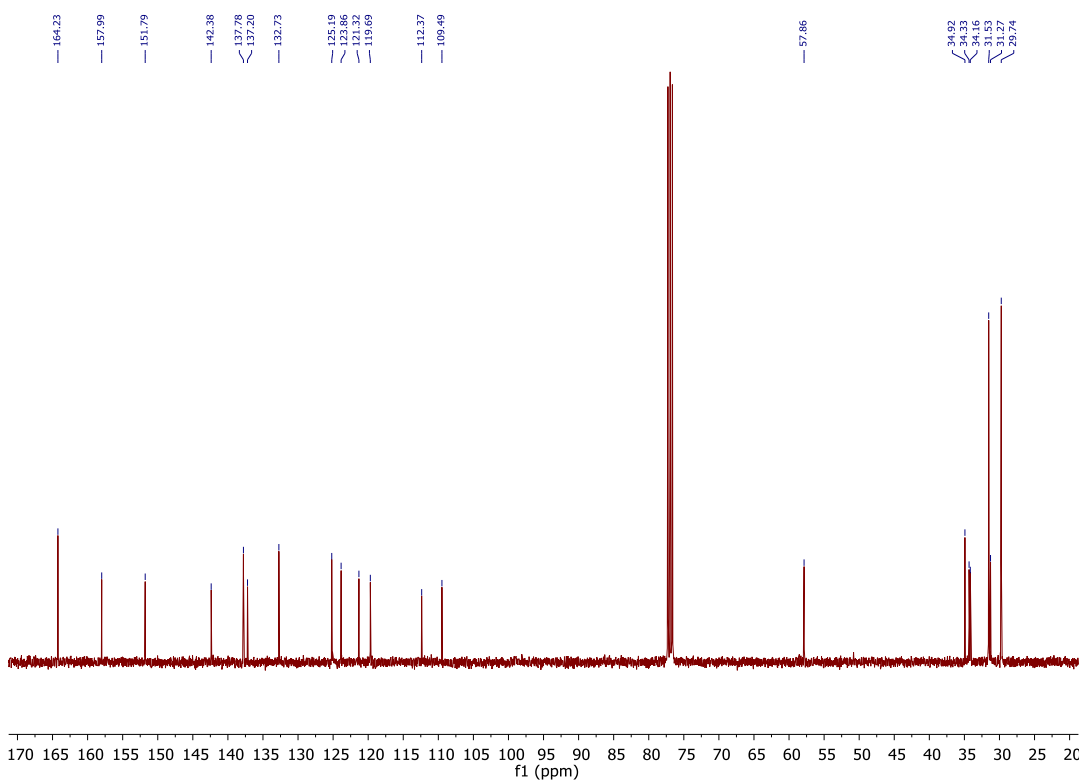
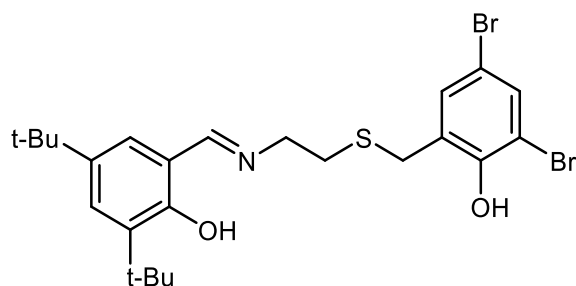


Figure 5.08: $^{13}\text{C}\{^1\text{H}\}$ NMR (101 MHz, CDCl_3 , 298K) spectrum of DH_2 .



EH₂: A solution of 3,5-di-*tert*-butyl-2-hydroxybenzaldehyde (2.34 g, 10 mmol) and 2-amino-ethanethiol (0.77 g, 10 mmol) in THF (20 mL) was stirred for two hours. Triethylamine (1.01 g, 1.39 mL, 10 mmol) was added and the solution was stirred for a further 15 minutes. A solution of 3,5-di-bromo-2-hydroxybenzyl bromide in THF (20 mL) was added dropwise and the mixture was stirred for three hours. The white precipitate was filtered off and the solvent removed *in vacuo* to give an orange oil. Recrystallisation from methanol gave the product as an orange oily solid (2.83 g, 51%).

¹H NMR (400 MHz, CDCl₃) δ 8.29 (s, 1H, CH), 7.48 (dd, *J* = 2.3, 0.9 Hz, 1H, Ar-H), 7.34 (d, *J* = 2.4 Hz, 1H, Ar-H), 7.28 (d, *J* = 2.4 Hz, 1H, Ar-H), 7.05 (d, *J* = 2.5 Hz, 1H, Ar-H), 3.73 (s, 2H, CH₂), 3.71 (td, *J* = 6.8, 1.2 Hz, 2H, CH₂), 2.77 (t, *J* = 6.7 Hz, 2H, CH₂), 1.40 (s, 9H, C(CH₃)₃), 1.26 (s, 9H, C(CH₃)₃). Note: OH peak not observed in spectrum.

¹³C{¹H} NMR (101 MHz, CDCl₃) δ 167.2 (C=N), 157.9 (Ar), 150.0 (Ar), 140.1 (Ar), 136.7 (Ar), 133.2 (Ar), 132.6 (Ar), 127.4 (Ar), 127.2 (Ar), 126.0 (Ar), 117.7 (Ar), 112.4 (Ar), 111.4 (Ar), 59.1 (CH₂), 35.0 (CH₂), 34.1 (C), 32.5 (C), 31.5 (CH₂), 31.5 (CH₃), 29.4 (CH₃).

m/z calc. [C₂₄H₃₂Br₂NO₂S]⁺ (acetonitrile) = 556.0515, found = 556.0547.

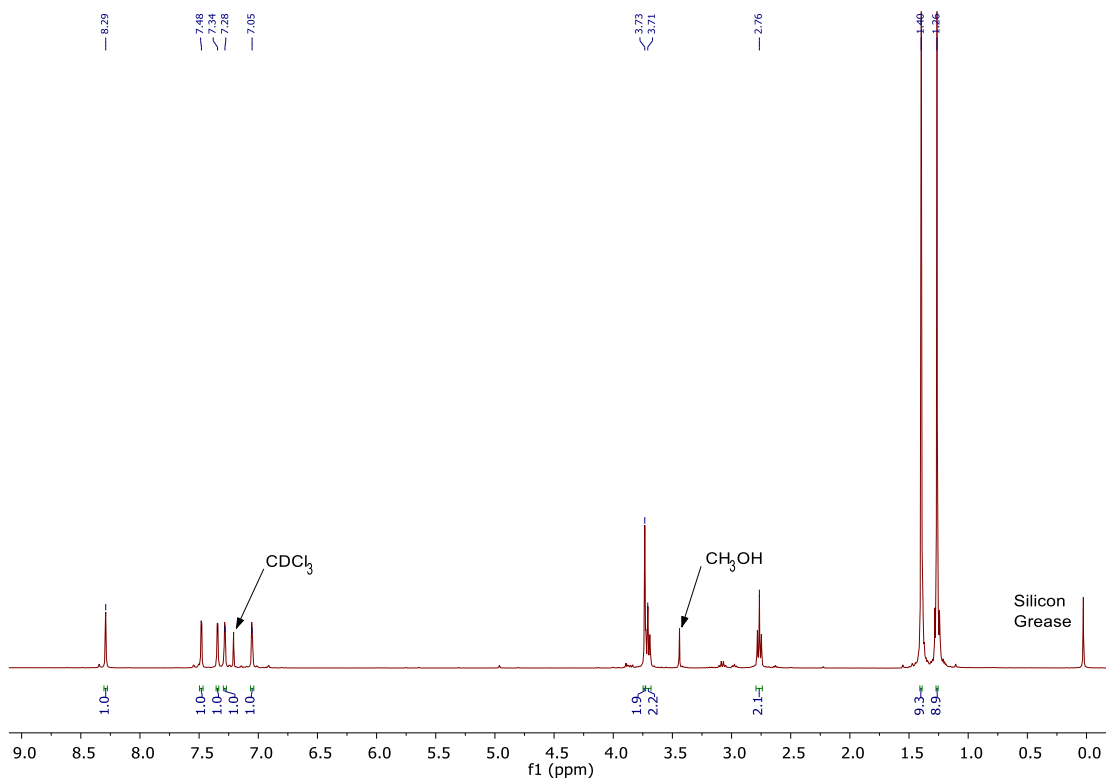


Figure 5.09: ^1H NMR (400 MHz, CDCl_3 , 298K) spectrum of EH_2 .

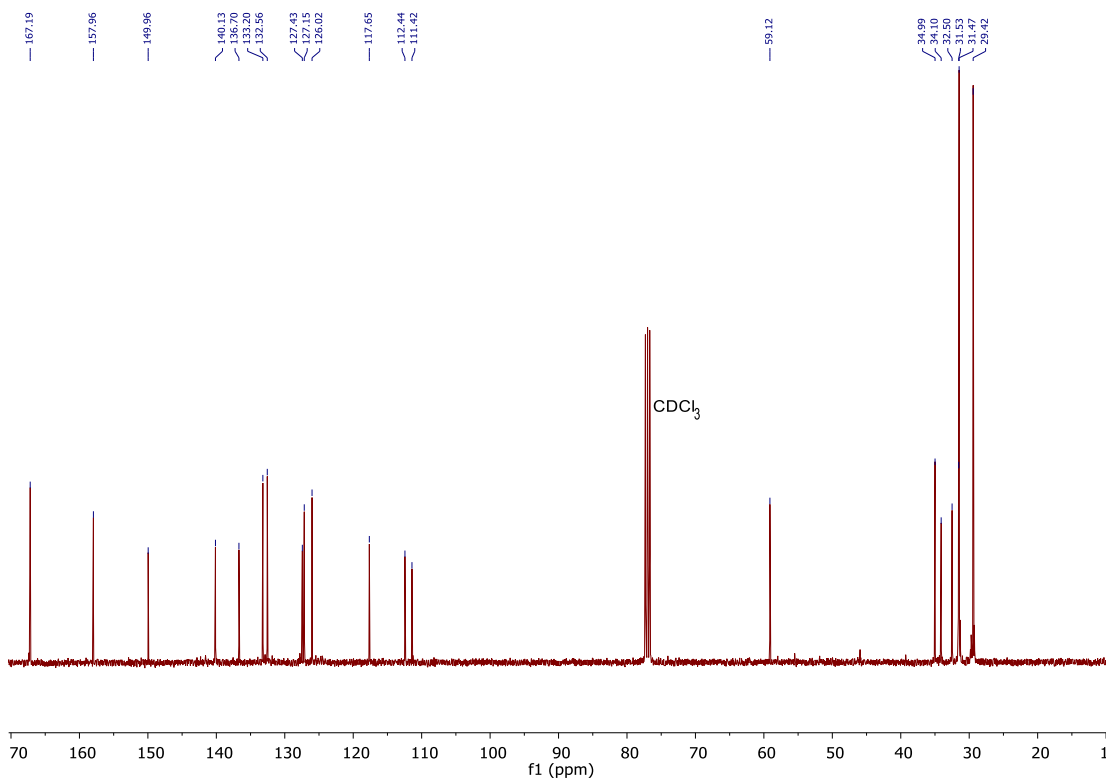


Figure 5.10: $^{13}\text{C}\{^1\text{H}\}$ NMR (101 MHz, CDCl_3 , 298K) spectrum of EH_2 .

5.2.2 Synthesis and characterisation of iron thiolen complexes

Fe(A)Cl

Ligand **AH**₂ (1.75 mmol, 0.90 g) was added to a Schlenk flask and dried under vacuum for one hour. Dry toluene (10 mL) was added inside a glovebox along with FeCl₃ (1.75 mmol, 0.28 g) and Et₃N (3.50 mmol, 0.36 g, 0.49 mL). The solution was stirred at room temperature for 72 hours then at 50 °C for 24 hours. The solvent was filtered under argon and the filtrate was reduced to give a black solid. The product was extracted into hexane (7 mL) which was removed to give the product as a black solid (0.673 g, 1.12 mmol, 64%).

Elemental analysis (C₃₂H₄₇NO₂SFeCl) Calcd in %: C, 63.94; H, 7.88; N, 2.33. Found: C, 63.40; H, 7.88; N, 2.26.

m/z calc. [Fe(**A**)⁺] = [C₃₂H₄₇NO₂SFe]⁺ (acetonitrile) = 565.2677, found 565.2672.

Fe(B)Cl

Ligand **BH**₂ (0.66 mmol, 0.26 g) was added to a Schlenk flask and dried under vacuum for one hour. Dry toluene (6 mL) was added inside a glovebox along with FeCl₃ (0.66 mmol, 0.11 g) and Et₃N (1.32 mmol, 0.13 g, 0.18 mL). The solution was stirred at room temperature for 72 hours then at 50 °C for 24 hours. The solvent was filtered under argon and the filtrate was reduced to give a black solid. The solvent was filtered under argon and the filtrate was reduced to give a black solid. The product was extracted into hexane (7 mL) which was removed to give the product as a black solid (0.22 g, 0.44 mmol, 66%).

Elemental analysis (C₂₄H₃₁NO₂SFeCl) Calcd in %: C, 58.97; H, 6.39; N, 2.78. Found: C, 58.97; H, 7.46; N, 2.46.

m/z calc. [Fe(**B**)⁺] = [C₂₄H₃₁NO₂SFe]⁺ (acetonitrile) = 453.1425, found 453.1430.

Fe(C)Cl

Ligand **CH**₂ (1 mmol, 0.47 g) was added to a Schlenk flask and dried under vacuum for one hour. Dry toluene (10 mL) was added inside a glovebox along with FeCl₃ (1 mmol,

0.16 g) and Et₃N (2 mmol, 0.10 g, 0.14 mL). The solution was stirred at room temperature for 72 hours then at 50 °C for 24 hours. The solvent was filtered under argon and the filtrate was reduced to give a black solid. The solid was washed with hexane (5 mL) to give the product (0.57 g, 0.97 mmol, 97%).

Elemental analysis (C₂₄H₂₉Cl₂NO₂SFeCl) Calcd in %: C, 51.68; H, 5.24; N, 2.51. Found: C, 50.62; H, 6.43; N, 2.24.

m/z calc. [Fe(**C**)⁺] = [C₂₄H₂₉Cl₂NO₂SFe]⁺ (acetonitrile) = 521.0646, found 521.0659.

Fe(**D**)Cl

Ligand **DH**₂ (1 mmol, 0.58 g) was added to a Schlenk flask and dried under vacuum for one hour. Dry toluene (10 mL) was added inside a glovebox along with FeCl₃ (1 mmol, 0.16 g) and Et₃N (2 mmol, 0.10 g, 0.14 mL). The solution was stirred at room temperature for 72 hours then at 50 °C for 24 hours. The solvent was filtered under argon and the filtrate was reduced to give a black solid. The solvent was filtered under argon and the filtrate was reduced to give a black solid. The product was extracted into hexane (7 mL) which was removed to give the product as a black solid (0.19 g, 0.30 mmol, 30 %).

Elemental analysis (C₂₄H₂₉Br₂NO₂SFeCl) Calcd in %: C, 44.58; H, 4.52; N, 2.17. Found: C, 44.96; H, 5.82; N, 1.86.

m/z calc. [Fe(**D**)⁺] = [C₂₄H₂₉Br₂NO₂SFe]⁺ (acetonitrile) = 608.9630, found 608.9642.

Fe(**E**)Cl

Ligand **EH**₂ (1 mmol, 0.58 g) was added to a Schlenk flask and dried under vacuum for one hour. Dry toluene (10 mL) was added inside a glovebox along with FeCl₃ (1 mmol, 0.16 g) and Et₃N (2 mmol, 0.10 g, 0.14 mL). The solution was stirred at room temperature for 72 hours then at 50 °C for 24 hours. The solvent was filtered under argon and the filtrate was reduced to give a black solid. The solid was washed with hexane (5 mL) to give the product (0.49 g, 0.75 mmol, 75%).

Elemental analysis (C₂₄H₂₉ClBr₂FeNO₂S) Calcd in %: C, 44.58; H, 4.52; N, 2.17.

Elemental analysis with half molecule of toluene: (C_{27.5}H₃₃ClBr₂FeNO₂S) Calcd in %: C, 47.68; H, 4.80; N, 2.02. Found: C, 47.72; H, 5.20; N, 2.17.

m/z calc. [Fe(E)⁺] = [C₂₄H₂₉FeBr₂NO₂S]⁺ (acetonitrile) = 608.9630, found 608.9628.

5.2.3 MALDI-ToF spectra examples

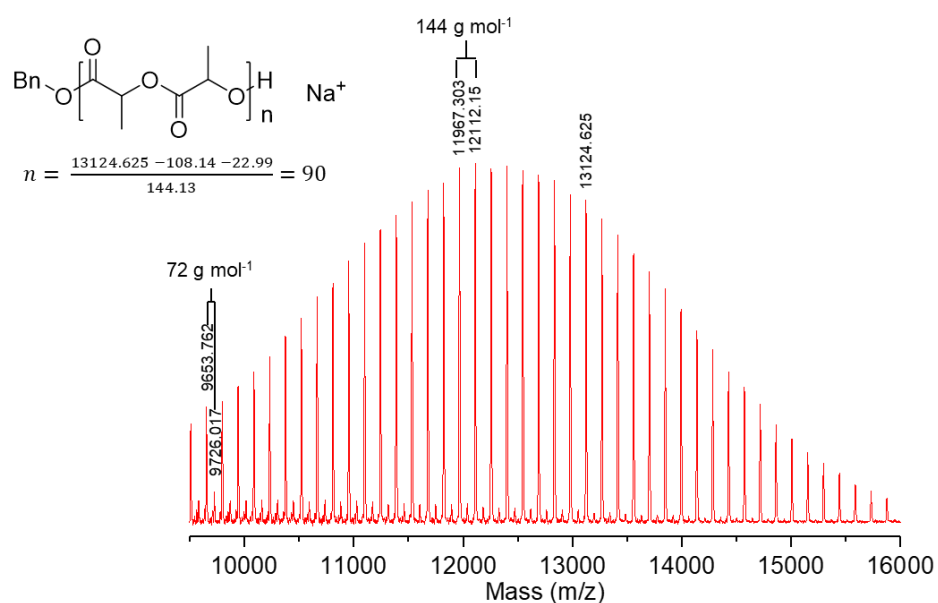


Figure 5.11: MALDI – ToF spectrum of PLA derived from Fe(A)Cl (50 °C, 48 hours) at a ratio of 100:1:1:1 ([LA]:[I]:[BnOH]:[Et₃N]) in toluene. M_n (GPC, corr.) = 13500 gmol⁻¹, M_n(Theo.) = 13800 gmol⁻¹. Main series is linear polymer with BnO + H end groups, with some transesterification.

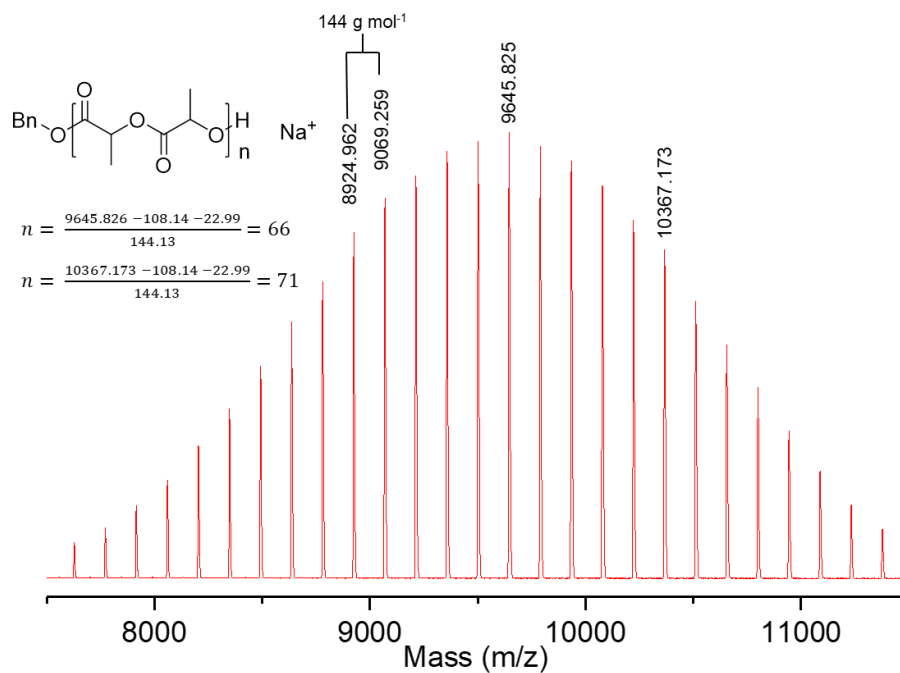


Figure 5.12: MALDI – ToF spectrum of PLA derived from Fe(C)Cl (80 °C, 3 hours) at a ratio of 100:1:1:1 ([LA]:[I]:[BnOH]:[Et₃N]) in toluene. M_n (GPC, corr.) = 9100 gmol⁻¹, M_n (Theo.) = 11050 gmol⁻¹. Linear polymer with BnO + H end groups.

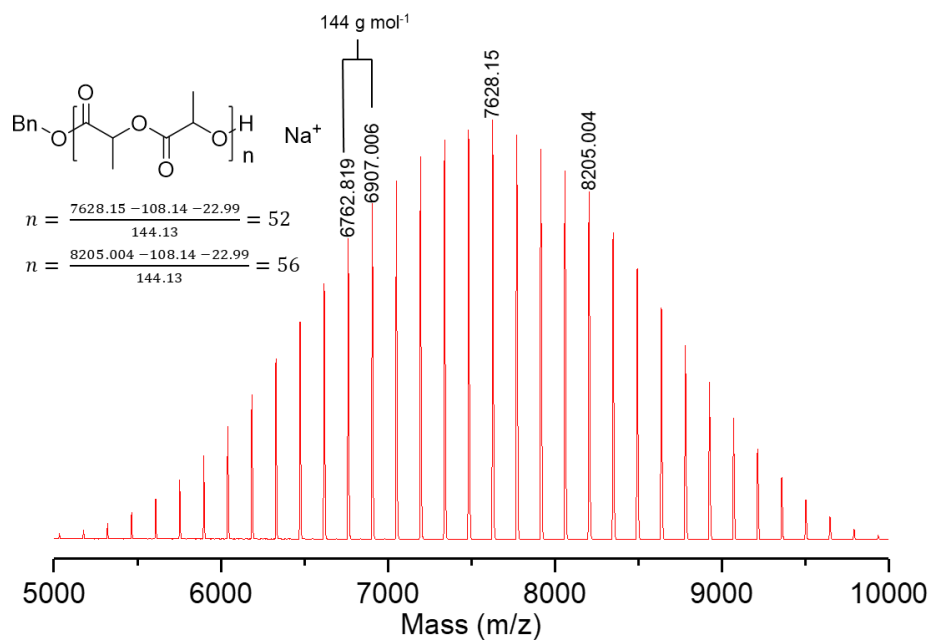


Figure 5.13: MALDI – ToF spectrum of PLA derived from Fe(4)Cl (80 °C, 3 hours) at a ratio of 100:1:1:1 ([LA]:[I]:[BnOH]:[Et₃N]) in toluene. M_n (GPC, corr.) = 7950 gmol⁻¹, M_n (Theo.) = 12050 gmol⁻¹. Linear polymer with BnO + H end groups.

5.2.4 Example GPC spectra

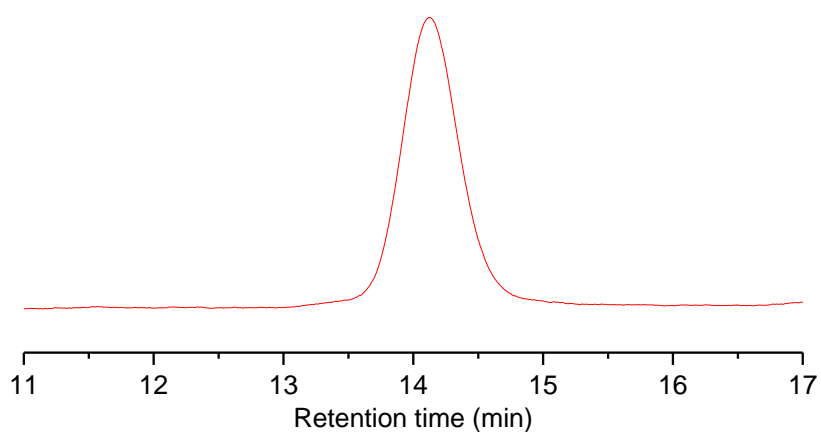


Figure 5.14: GPC trace of PLA initiated by Fe(A)Cl (80 °C, 4 hours) at a ratio of 100 : 1 : 1 : 1 ([LA]/[I]/[BnOH]/[Et₃N]) toluene. M_n (GPC, corr.) = 9850 gmol⁻¹, \mathcal{D} = 1.06, M_n (theo.) = 11750 gmol⁻¹.

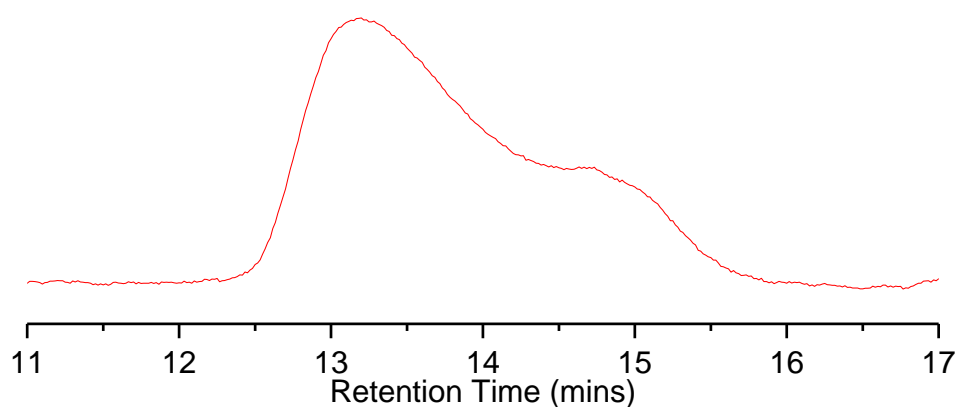


Figure 5.15: GPC trace of PLA initiated by Fe(A)Cl (40 °C, 96 hours) at a ratio of 100:1:1:1 ([LA]:[I]:[BnOH]:[Et₃N]) in toluene. M_n (GPC, corr.) = 11350 gmol⁻¹, \mathcal{D} = 1.51, M_n (theo.) = 13950 gmol⁻¹. Shows bimodality.

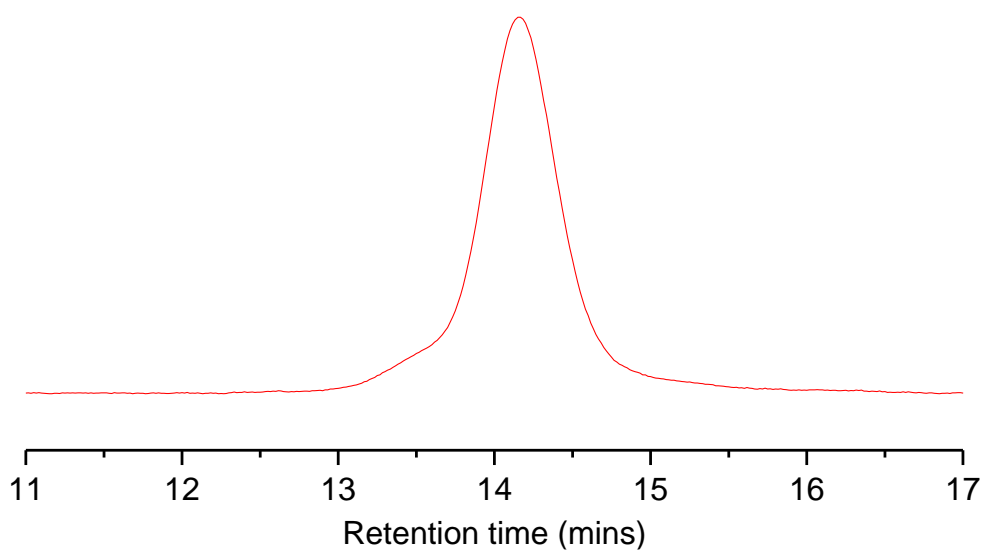


Figure 5.16: GPC trace of PLA initiated by Fe(B)Cl (80 °C, 2 hours) at a ratio of 100:1:1:1 ([LA]:[I]:[BnOH]:[Et₃N]) in toluene. M_n (GPC, corr.) = 9500 gmol⁻¹, \bar{D} = 1.11, M_n (theo.) = 12800 gmol⁻¹.

5.2.5 Example ¹H{¹H} NMR spectra

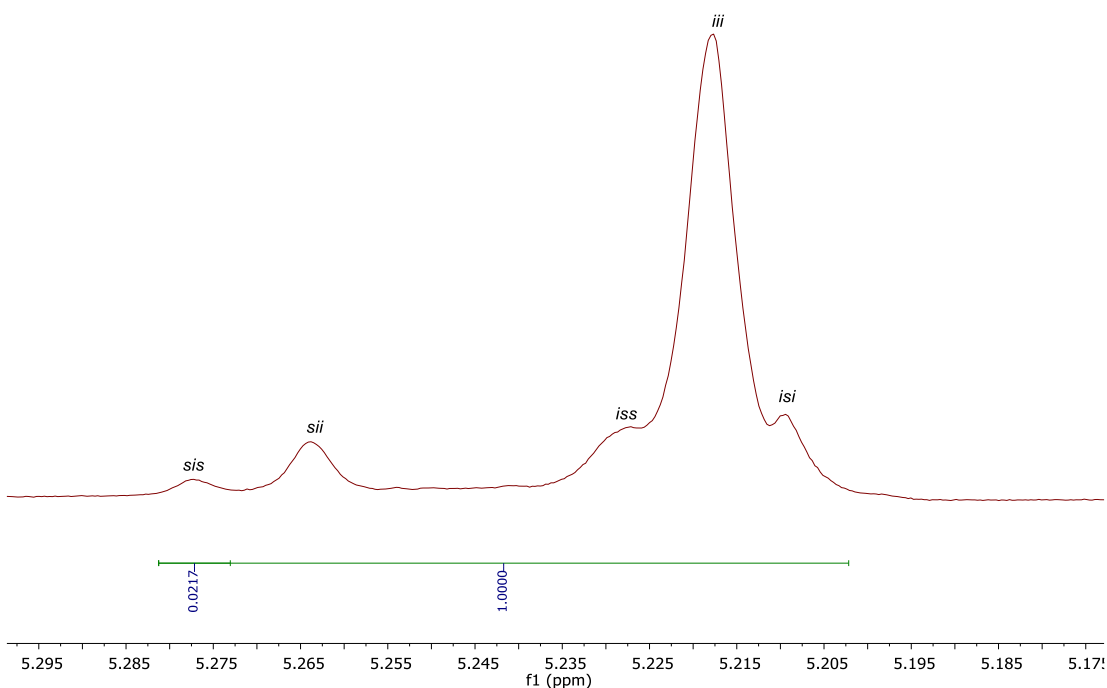


Figure 5.17: ¹H{¹H} NMR spectrum of isotactically enriched PLA from Fe(A)Cl. P_m = 0.79.

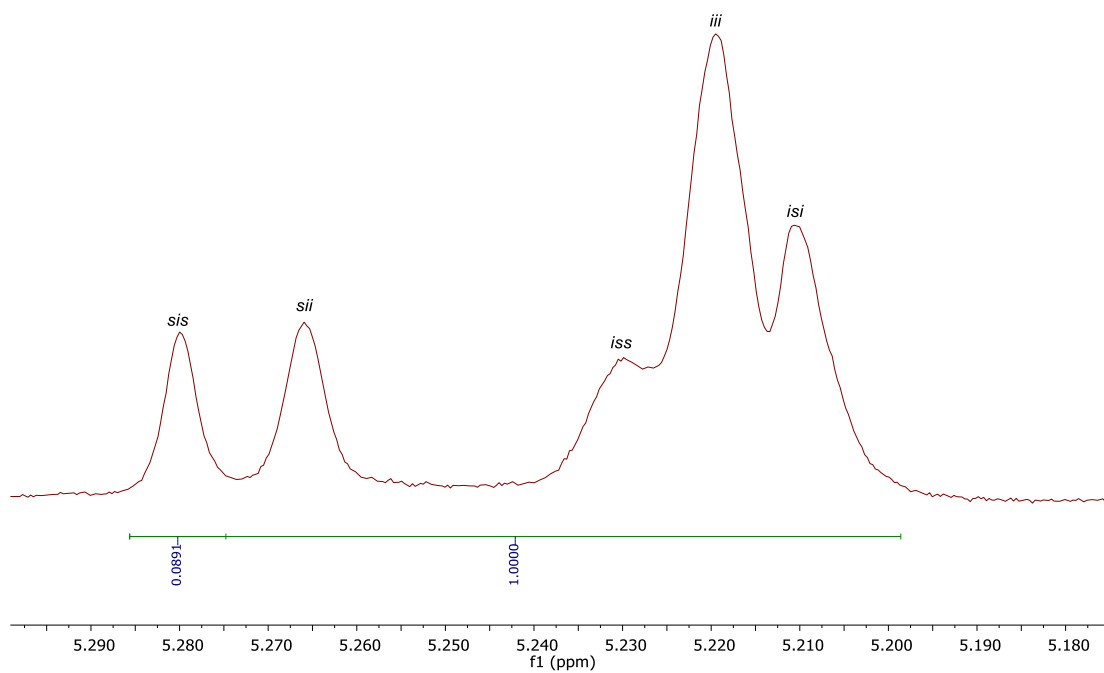


Figure 5.18: $^1\text{H}\{^1\text{H}\}$ NMR spectrum of PLA from $\text{Fe}(\text{B})\text{Cl}$. $P_m = 0.58$.

5.2.6 Synthesis and characterisation of aluminium thioen complexes

Al(A)Me

Ligand **AH**₂ (1 mmol, 0.53 g) was dissolved in toluene (10 mL). AlMe₃ (1 mmol, 0.5 mL 2.0 M) was added dropwise and the solution stirred for four hours. The product crystallised from a mixture of hexane and toluene as a yellow solid (0.24 g, 0.44 mmol, 44%).

¹H NMR (400 MHz, C₆D₆) δ 7.70 (d, *J* = 2.6 Hz, 1H, Ar-H), 7.61 (s, 1H, CH), 7.50 (d, *J* = 2.6 Hz, 1H, Ar-H), 7.10 (d, *J* = 2.6 Hz, 1H, Ar-H), 6.92 (d, *J* = 2.5 Hz, 1H, Ar-H), 3.75 (d, *J* = 13.4 Hz, 1H, CH₂), 3.53 (d, *J* = 12.3 Hz, 1H, CH₂), 2.84 – 2.75 (m, 2H, CH₂), 2.59 (m, 1H, CH₂), 1.97 – 1.92 (m, 1H, CH₂), 1.76 (s, 9H, C(CH₃)₃), 1.52 (s, 9H, C(CH₃)₃), 1.28 (s, 9H, C(CH₃)₃), 1.26 (s, 9H, C(CH₃)₃), -0.14 (s, 3H, Al-CH₃).

¹³C{¹H} NMR (101 MHz, C₆D₆) δ 173.0 (C=N), 161.6 (Ar), 153.8 (Ar), 141.0 (Ar), 140.6 (Ar), 139.8 (Ar), 138.4 (Ar), 132.4 (Ar), 129.0 (Ar), 126.2 (Ar), 126.0 (Ar), 123.5 (Ar), 118.5 (Ar), 60.7 (CH₂), 35.5 (C), 35.3 (C), 34.2 (C), 34.1 (C), 33.0 (CH₂), 31.7 (CH₃), 31.3 (CH₃), 30.2 (CH₃), 29.5 (CH₃), 28.7 (CH₂), -11.89 (Al-CH₃).

Elemental analysis (C₃₃H₅₀NO₂SAI) Calcd in %: C, 71.83; H, 9.13; N, 2.54. Found: C, 70.96; H, 9.12; N, 2.98.

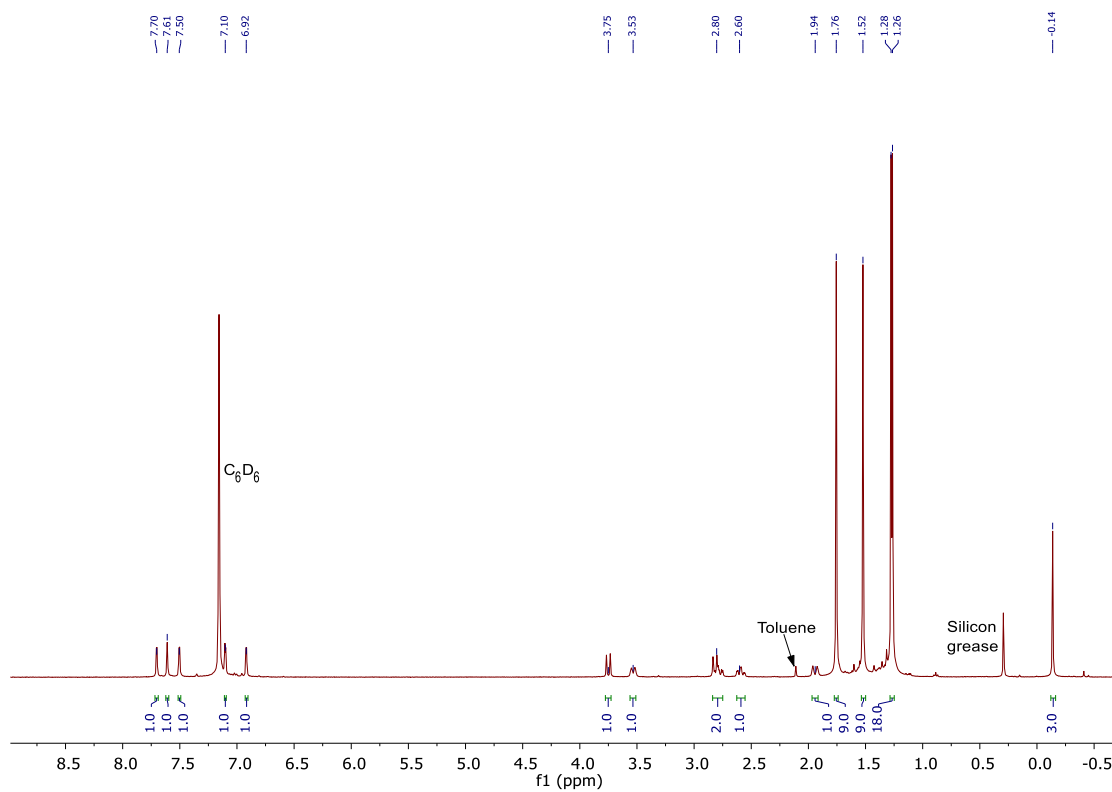


Figure 5.19: ¹H NMR (400 MHz, C₆D₆, 298K) spectrum of Al(A)Me.

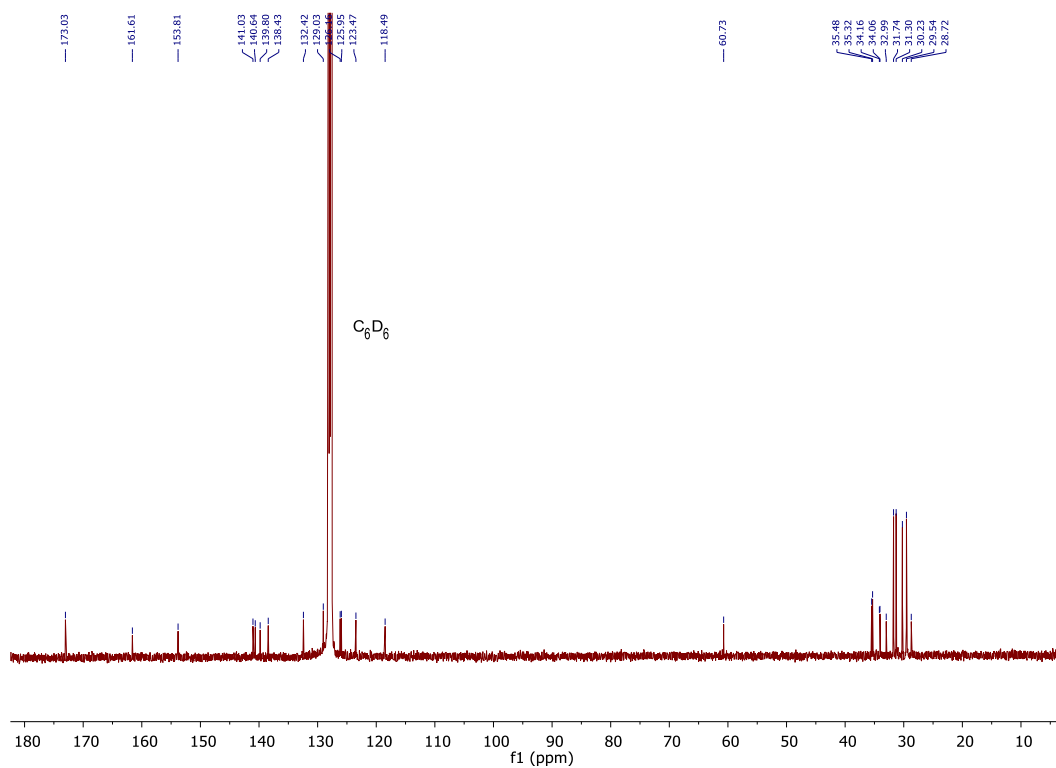


Figure 5.20: ¹³C{¹H} NMR (101 MHz, C₆D₆, 298K) spectrum of Al(A)Me.

Al(**B**)Me

Ligand **B**H₂ (1 mmol, 0.40 g) was dissolved in toluene (10 mL). AlMe₃ (1 mmol, 0.5 mL 2.0 M) was added dropwise and the solution stirred for four hours. The product crystallised from a mixture of hexane and toluene as a yellow solid (0.18 g, 0.42 mmol, 42%).

¹H NMR (400 MHz, C₆D₆) δ 7.50 (d, *J* = 2.6 Hz, 1H), 7.47 (s, 1H), 7.12 – 6.94 (m, 4H), 6.79 (dd, *J* = 7.8, 1.8 Hz, 1H), 6.53 (ddd, *J* = 7.9, 6.9, 1.4 Hz, 1H), 3.50 (dd, *J* = 17.5, 12.6 Hz, 2H), 3.04 – 2.62 (m, 2H), 2.38 (m, 1H), 1.85 (m, 1H), 1.70 (s, 9H), 1.31 (s, 9H), -0.17 (s, 3H).

¹³C{¹H} NMR (101 MHz, C₆D₆) δ 170.8 (C=N), 163.2 (Ar), 152.6 (Ar), 139.5 (Ar), 136.2 (Ar), 133.5 (Ar), 124.6 (Ar), 124.5 (Ar), 124.3 (Ar), 122.2 (Ar), 120.9 (Ar), 117.4 (Ar), 116.7 (Ar), 59.3 (CH₂), 34.0 (C), 32.9 (C), 32.7 (CH₂), 30.5 (CH₃), 28.9 (CH₃), 27.9 (CH₂), -12.4 (Al-CH₃).

Elemental analysis (C₂₅H₃₄NO₂SAI) Calcd in %: C, 68.31; H, 7.80; N, 3.19. Elemental analysis with half O atom (oxy-bridged dimer) Calcd in %: C, 66.64; H, 7.22; N, 3.24 Found: C, 66.97; H, 7.65; N, 3.50.

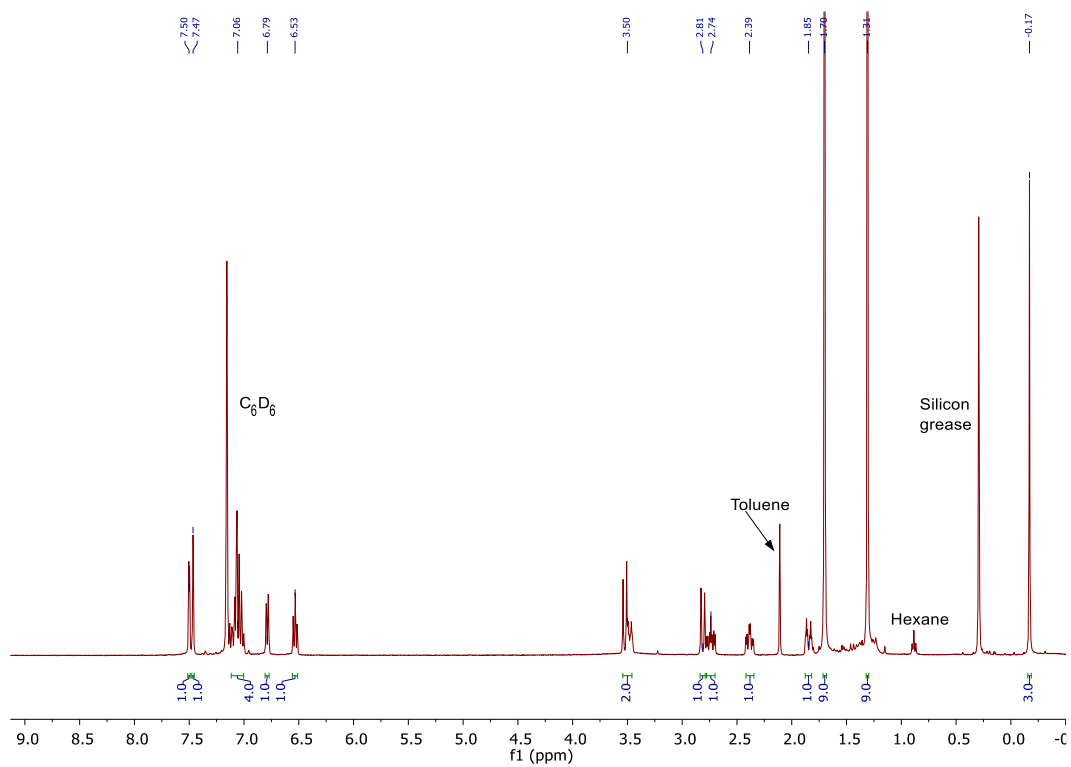


Figure 5.21: ^1H NMR (400 MHz, C_6D_6) spectrum of $\text{Al}(\text{B})\text{Me}$.

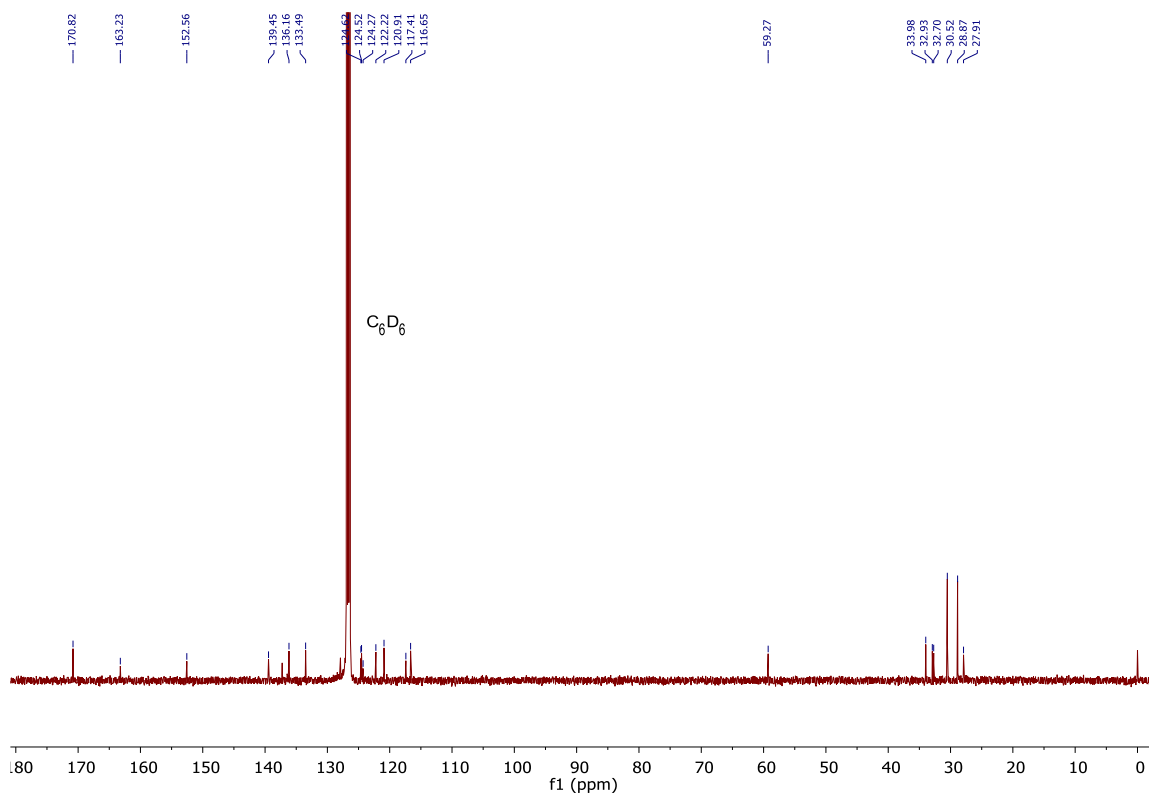


Figure 5.22: $^{13}\text{C}\{^1\text{H}\}$ NMR (101 MHz, C_6D_6 , 298K) spectrum of $\text{Al}(\text{B})\text{Me}$.

Al(C)Me

Ligand CH_2 (1 mmol, 0.47 g) was dissolved in toluene (10 mL). AlMe_3 (1 mmol, 0.5 mL, 2.0 M) was added dropwise and the solution stirred for four hours. The product crystallised from a mixture of hexane and toluene as a yellow solid (0.21 g, 0.41 mmol, 41%).

^1H NMR (400 MHz, C_6D_6) δ 7.52 (d, $J = 2.5$ Hz, 1H, Ar-H), 7.26 (d, $J = 2.6$ Hz, 1H, Ar-H), 7.10 (d, $J = 2.6$ Hz, 1H, Ar-H), 7.02 (s, 1H, CH), 6.50 (d, $J = 2.6$ Hz, 1H, Ar-H), 3.29 (m, 2H, CH_2), 3.02 (d, $J = 12.2$ Hz, 1H, CH_2), 2.51 (m, 1H, CH_2), 2.33 (m, 1H, CH_2), 1.78 (m, 1H, CH_2), 1.70 (s, 9H), 1.32 (s, $J = 1.1$ Hz, 9H), -0.21 (s, 3H).

$^{13}\text{C}\{^1\text{H}\}$ NMR (101 MHz, C_6D_6) δ 170.7 (C=N), 158.5 (Ar), 153.9 (Ar), 140.8 (Ar), 138.8 (Ar), 136.4 (Ar), 131.6 (Ar), 129.2 (Ar), 125.2 (Ar), 125.0 (Ar), 123.9 (Ar), 121.6 (Ar), 119.4 (Ar), 60.2 (CH_2), 35.2 (C), 35.1 (CH_2), 34.2 (C), 31.8 (CH_3), 30.2 (CH_3), 29.9 (CH_2), -12.4 (Al- CH_3).

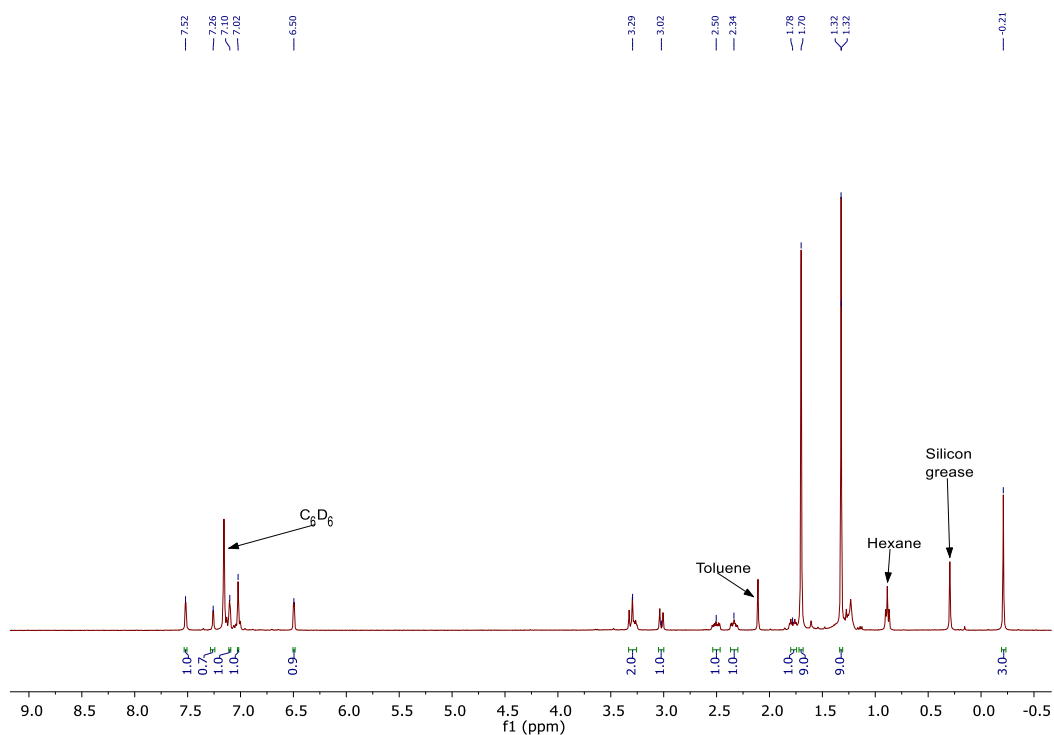


Figure 5.23: ^1H NMR (400 MHz, C_6D_6) spectrum of Al(C)Me .

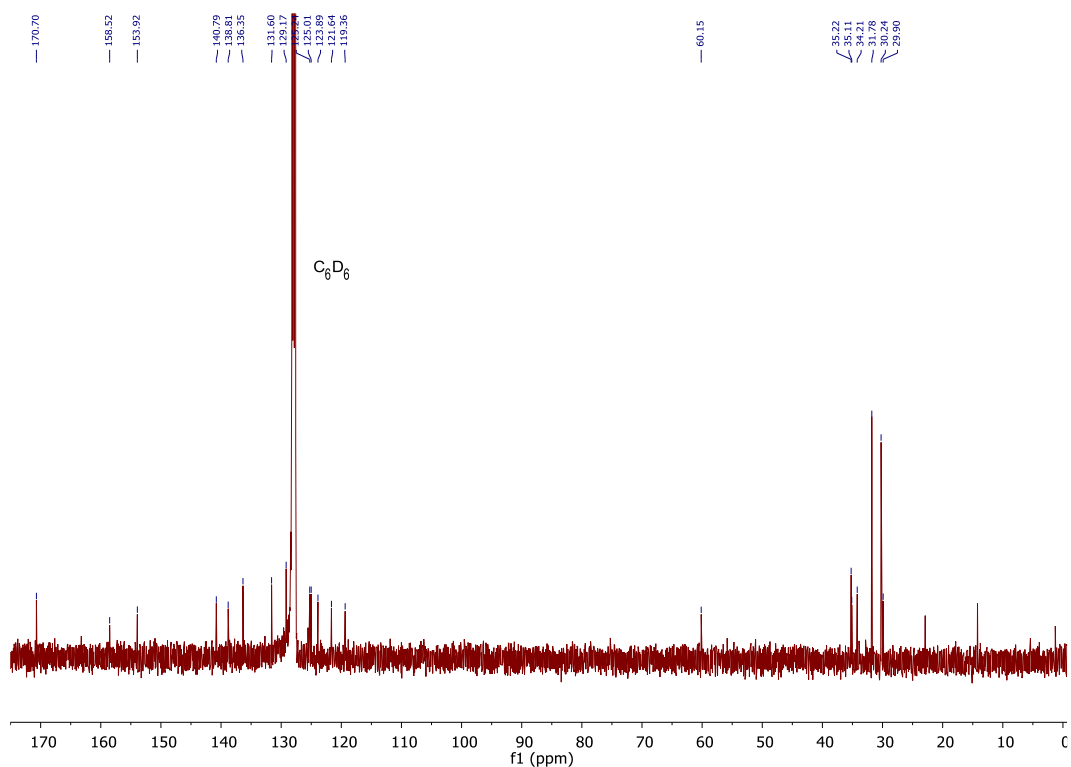


Figure 5.24: $^{13}\text{C}\{^1\text{H}\}$ NMR (101 MHz, C_6D_6 , 298K) spectrum of $\text{Al}(\text{C})\text{Me}$.

$\text{Al}(\text{D})\text{Me}$

Ligand DH_2 (1 mmol, 0.60 g) was dissolved in toluene (10 mL). AlMe_3 (1 mmol, 0.5 mL, 2.0 M) was added dropwise and the solution stirred for four hours. The product crystallised from a mixture of hexane and toluene as a yellow solid (0.09 g, 0.15 mmol, 15%)

^1H NMR (400 MHz, C_6D_6) δ 7.62 (d, $J = 2.5$ Hz, 1H, Ar-H), 7.53 (d, $J = 2.6$ Hz, 1H, Ar-H), 7.10 (d, $J = 2.6$ Hz, 1H, Ar-H), 6.97 (s, 1H, CH), 6.67 (d, $J = 2.5$ Hz, 1H, Ar-H), 3.28 (m, 2H, CH_2), 3.04 (d, $J = 12.0$ Hz, 1H, CH_2), 2.54 – 2.42 (m, 1H, CH_2), 2.40 – 2.30 (m, 1H, CH_2), 1.83 – 1.74 (m, 1H, CH_2), 1.72 (s, 9H), 1.32 (s, 9H), -0.22 (s, 3H).

$^{13}\text{C}\{^1\text{H}\}$ NMR (126 MHz, C_6D_6) δ 170.5 (C=N), 159.5 (Ar), 153.7 (Ar), 141.6 (Ar), 140.5 (Ar), 138.6 (Ar), 135.2 (Ar), 125.0 (Ar), 124.7 (Ar), 123.7 (Ar), 119.6 (Ar), 117.5 (Ar), 108.3 (Ar), 59.8 (CH_2), 35.0 (C), 34.9 (CH_2), 34.0 (CH_2), 31.6 (CH_3), 30.1 (CH_3), 29.8 (C), -11.1 (Al- CH_3).

Elemental analysis ($\text{C}_{25}\text{H}_{32}\text{NO}_2\text{SBr}_2\text{Al}$) Calcd in %: C, 50.26; H, 5.40; N, 2.34. Found: C, 50.73; H, 6.03; N, 2.22.

Al(E)Me

Ligand EH₂ (1 mmol, 0.58 g) was dissolved in toluene (10 mL). AlMe₃ (1 mmol, 0.5 mL 2.0 M) was added dropwise and the solution stirred for four hours. The product crystallised from a mixture of hexane and toluene as a yellow solid (0.32 g, 0.54 mmol, 54%).

¹H NMR (400 MHz, C₆D₆) δ 7.72 (d, *J* = 2.5 Hz, 1H, Ar-H), 7.58 (d, *J* = 2.5 Hz, 1H, Ar-H), 7.46 (s, 1H, CH), 7.05 (d, *J* = 2.2 Hz, 1H, Ar-H), 6.84 (d, *J* = 2.5 Hz, 1H, Ar-H), 3.46 (d, *J* = 12.9 Hz, 1H, CH₂), 3.37 (d, *J* = 13.1 Hz, 1H, CH₂), 2.54 (dd, *J* = 18.5, 11.9 Hz, 2H, CH₂), 2.17 (ddd, *J* = 14.5, 10.8, 2.9 Hz, 1H, CH₂), 1.79 (dd, *J* = 16.2, 4.0 Hz, 1H, CH₂), 1.61 (s, 9H, C(CH₃)₃), 1.27 (s, 9H, C(CH₃)₃), -0.16 (s, 3H, Al-CH₃).

¹³C{¹H} NMR (126 MHz, C₆D₆) δ 172.6 (C=N), 161.5 (Ar), 153.6 (Ar), 140.9 (Ar), 139.9 (Ar), 134.0 (Ar), 132.3 (Ar), 132.0 (Ar), 129.7 (Ar), 128.6 (Ar), 118.5 (Ar), 116.0 (Ar), 110.4 (Ar), 60.8 (CH₂), 35.4 (C), 33.9 (CH₂), 31.1 (C), 31.1 (CH₃) 29.4 (CH₃), 28.7 (CH₂), -13.2 (Al-CH₃).

Elemental analysis (C₂₅H₃₂NO₂SBr₂Al) Calcd in %: C, 50.26; H, 5.40; N, 2.34. Found: C, 53.00; H, 5.54; N, 2.34.

Al(A)Cl

Ligand **AH₂** (0.67 mmol, 0.36 g) was dissolved in toluene (7 mL). AlMe₂Cl (0.67 mmol, 0.67 mL 1.0 M) was added dropwise and the solution stirred for four hours. The product crystallised from a mixture of hexane and toluene as a yellow solid (0.19 g, 0.36 mmol, 53%).

¹H NMR (400 MHz, C₆D₆) δ 7.76 (d, *J* = 2.6 Hz, 1H, Ar-H), 7.59 (d, *J* = 2.6 Hz, 1H, Ar-H), 7.38 (s, 1H, CH), 7.12 (d, *J* = 2.6 Hz, 1H, Ar-H), 6.80 (d, *J* = 2.5 Hz, 1H, Ar-H), 3.63 (d, *J* = 12.0 Hz, 1H, CH₂), 3.14 (d, *J* = 13.2 Hz, 1H, CH₂), 2.99 (d, *J* = 12.0 Hz, 1H, CH₂), 2.89 – 2.81 (m, 1H, CH₂), 2.49 – 2.41 (m, 1H, CH₂), 1.95 – 1.90 (m, 1H, CH₂), 1.86 (s, 9H, C(CH₃)₃), 1.64 (s, 9H, C(CH₃)₃), 1.34 (s, 9H, C(CH₃)₃), 1.28 (s, 9H, C(CH₃)₃).

¹³C{¹H} NMR (101 MHz, C₆D₆) δ 174.3 (C=N), 162.7 (Ar), 153.8 (Ar), 141.5 (Ar), 141.2 (Ar), 140.1 (Ar), 139.6 (Ar), 133.2 (Ar), 129.0 (Ar), 125.2 (Ar), 124.4 (Ar), 123.7 (Ar), 118.3 (Ar), 58.2 (CH₂), 35.7 (CH₂), 35.6 (CH₂), 34.3 (C), 34.1 (C), 32.6 (C), 31.8 (CH₃), 31.3 (CH₃), 30.6(CH₃), 29.7 (CH₃), 28.8 (C).

Elemental analysis (C₃₂H₄₇NO₂SAICl) Calcd in %: C, 67.17; H, 8.28; N, 2.45. Found: C, 64.37; H, 8.11; N, 2.40.

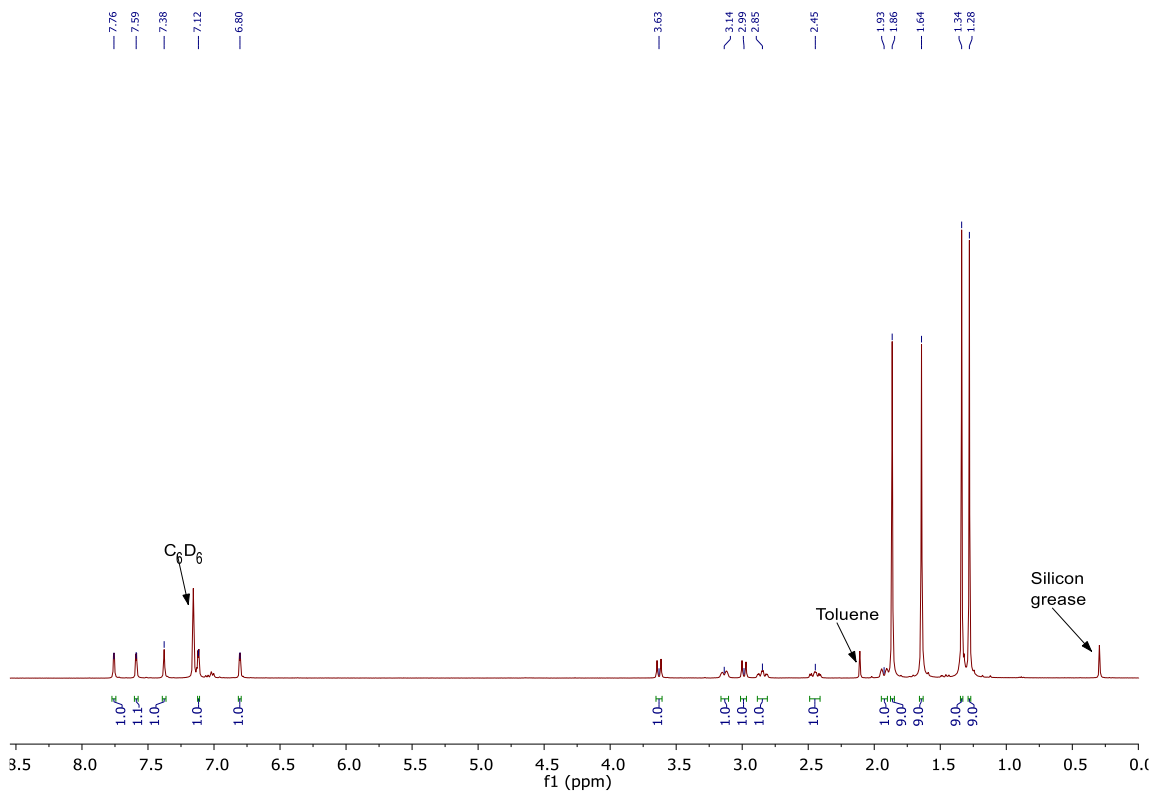


Figure 5.29: ¹H NMR (400 MHz, C₆D₆, 298K) spectrum of Al(A)Cl.

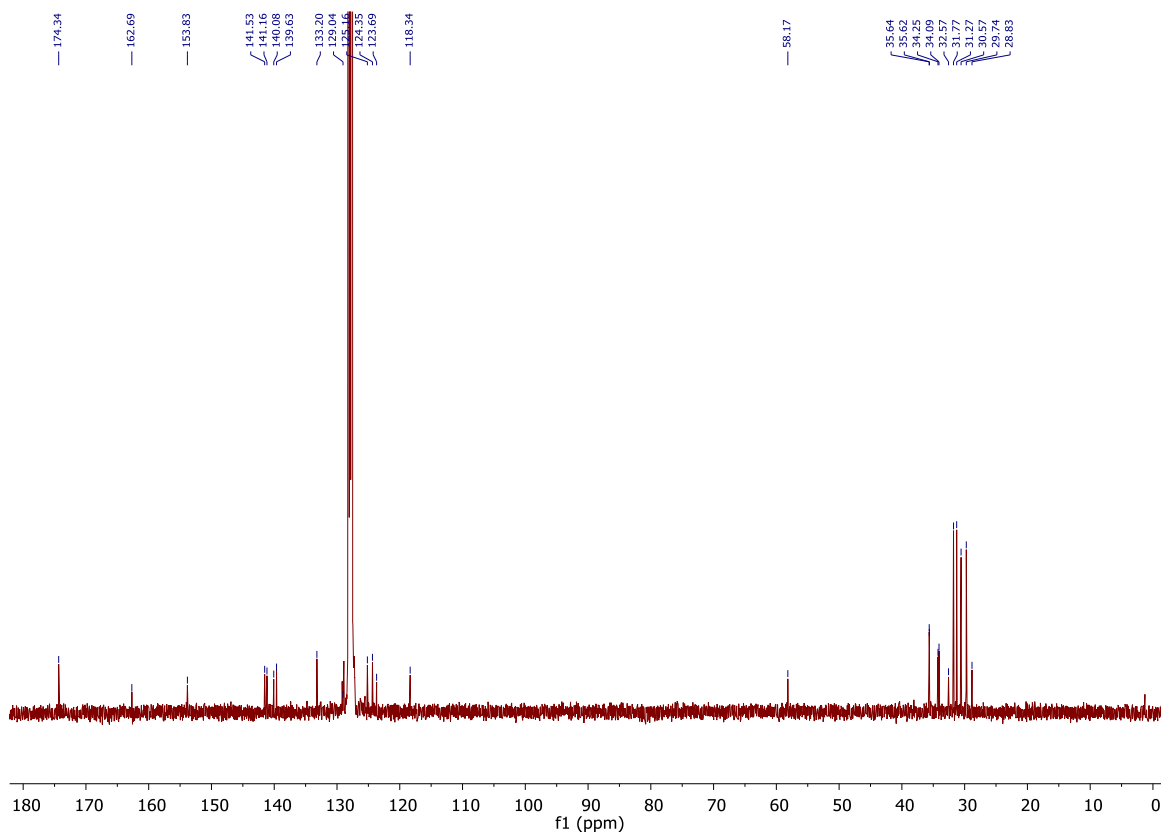


Figure 5.30: ¹³C{¹H} NMR (101 MHz, C₆D₆, 298K) spectrum of Al(A)Cl.

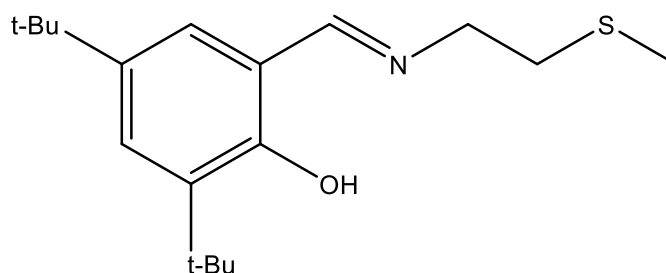
5.2.7 Crystallographic data

Figure 5.031: X-ray crystallographic parameters

Compound reference	Fe(1)Cl	[Fe(1)] ₂ (μ ₂ -CO ₃)	Al(1)Me	Al(2)Me	Al(5)Me	Al(1)Cl
CCDC Number	1919287	1919288	1919289	1919290	1919291	1919292
Chemical formula	C ₃₂ H ₄₇ ClFeNO ₂ S	C ₆₇ H ₉₈ Cl ₄ Fe ₂ N ₂ O ₇ S ₂	C ₃₆ H ₅₇ AlNO ₂ S	C ₂₅ H ₃₄ AlNO ₂ S	C ₅₇ H ₇₂ Al ₂ Br ₄ N ₂ O ₄ S ₂	C ₁₂₈ H ₁₈₈ Al ₄ Cl ₄ N ₄ O ₈ S ₄
Formula Mass	601.06	1361.09	594.86	439.57	1286.88	2288.77
Crystal system	Monoclinic	Monoclinic	Triclinic	Monoclinic	Triclinic	Monoclinic
<i>a</i> /Å	13.4079(3)	23.3269(4)	9.9001(4)	17.2120(2)	11.1417(3)	13.4161(6)
<i>b</i> /Å	9.2706(3)	18.0743(4)	12.7503(4)	6.41290(10)	11.6135(4)	9.3492(4)
<i>c</i> /Å	25.6987(13)	16.4495(3)	15.4058(5)	23.0053(4)	12.7689(5)	25.2864(13)
α /°	90	90	69.764(3)	90	65.306(3)	90
β /°	95.826(3)	90.2440(17)	75.233(3)	98.219(2)	79.826(3)	96.027(4)
γ /°	90	90	78.789(3)	90	79.276(3)	90
Unit cell volume/Å ³	3177.8(2)	6935.3(2)	1752.22(11)	2513.22(7)	1465.83(9)	3154.1(3)
Temperature/K	150(2)	150.00(10)	150(2)	150(2)	150(2)	150(2)
Space group	<i>P</i> 2 ₁ / <i>c</i>	<i>C</i> 2/ <i>c</i>	<i>P</i> 1	<i>P</i> 2 ₁ / <i>n</i>	<i>P</i> 1	<i>P</i> 2 ₁ / <i>c</i>
No. of formula units per unit cell, <i>Z</i>	4	4	2	4	1	1
Radiation type	Cu K α	Cu K α	Mo K α	Cu K α	Cu K α	Cu K α
Absorption coefficient, μ /mm ⁻¹	5.400	5.737	0.148	1.630	4.660	2.171
No. of reflections measured	12033	24104	26474	9801	9574	21891
No. of independent reflections	5583	6545	6638	4761	5662	5780
<i>R</i> _{int}	0.0482	0.0385	0.0374	0.0203	0.0327	0.0745
Final <i>R</i> ₁ values (<i>I</i> > 2 σ (<i>I</i>))	0.0466	0.0521	0.0536	0.0334	0.0380	0.0486
Final <i>wR</i> (<i>F</i> ²) values (<i>I</i> > 2 σ (<i>I</i>))	0.0984	0.1424	0.1428	0.0902	0.0879	0.0949
Final <i>R</i> ₁ values (all data)	0.0693	0.0606	0.0816	0.0365	0.0508	0.0803
Final <i>wR</i> (<i>F</i> ²) values (all data)	0.1092	0.1494	0.1581	0.0930	0.0941	0.1075

5.3 Zinc and aluminium {ONS} complexes for polyester production and degradation

5.3.1 Synthesis and characterisation of {ONS} monophenolate ligands



FH A solution of 3,5-di-*tert*-butyl-2-hydroxybenzaldehyde (2.34 g, 10 mmol) and 2-(methylthio) ethylamine (0.91 g, 10 mmol) in methanol (30 mL) was stirred at room temperature for two hours. The solvent was removed *in vacuo* to give a yellow oil. The crude product was recrystallised from methanol to give a yellow powder (2.21 g, 72%).

^1H NMR (400 MHz, C_6D_6) δ 14.07 (s, 1H, OH), 7.76 (s, 1H, CH), 7.58 (d, $J = 2.5$ Hz, 1H, Ar-H), 6.98 (d, $J = 2.5$ Hz, 1H, Ar-H), 3.25 (t, $J = 6.9$ Hz, 2H, CH_2), 2.32 (t, $J = 6.9$ Hz, 2H), 1.71 (s, 3H, CH_3), 1.66 (s, 9H, $\text{C}(\text{CH}_3)_3$), 1.33 (s, 9H, $\text{C}(\text{CH}_3)_3$).

$^{13}\text{C}\{^1\text{H}\}$ NMR (101 MHz, CDCl_3) δ 166.9 (C=N), 158.1, 140.1, 136.7, 127.1, 126.0, 117.8 (Ar), 59.1, 35.2 (CH_2), 35.0, 34.1 (CH), 31.5, 29.5 (CH_3), 16.0 (S- CH_3).

m/z calc. $[\text{C}_{18}\text{H}_{30}\text{NOS}]^+$ (acetonitrile) = 308.2043, found = 308.2051.

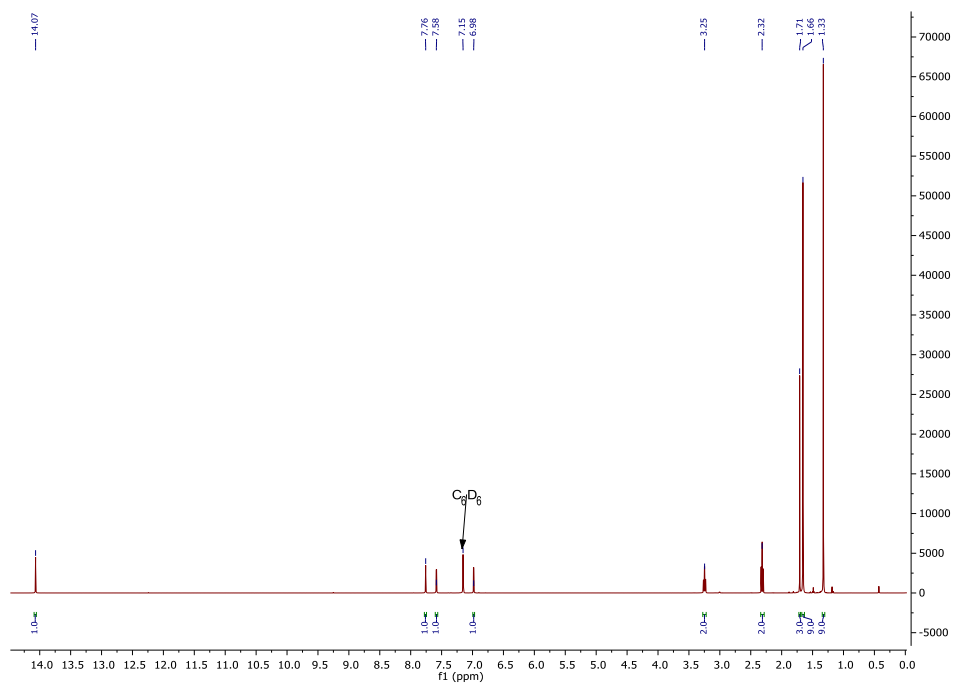


Figure 5.32: 1H NMR (400 MHz, C_6D_6 , 298K) spectrum of FH.

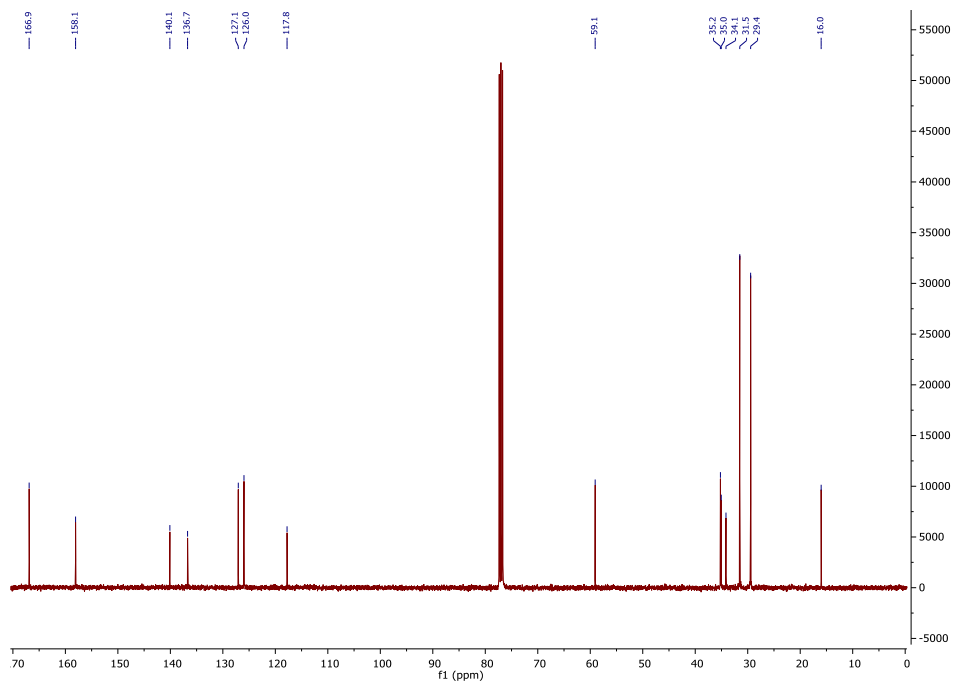
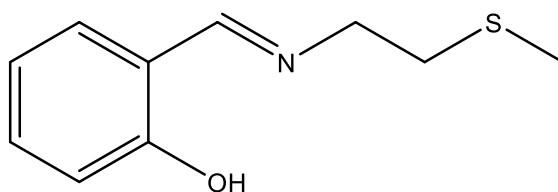


Figure 5.33: $^{13}C\{^1H\}$ NMR (101 MHz, $CDCl_3$) of FH.



GH A solution of salicylaldehyde (1.22 g, 1.04 mL, 10.0 mmol) and 2-(methylthio) ethylamine (0.91 g, 10.0 mmol) in methanol (30 mL) was stirred at room temperature for two hours. The solvent was removed *in vacuo* to give a yellow oil (0.87 g, 45%).

^1H NMR (400 MHz, CDCl_3) δ 8.39 (s, 1H, CH), 7.33 (m, 1H, Ar-H), 7.30 – 7.27 (m, 1H, Ar-H), 6.98 (dd, $J = 8.2, 1.0$ Hz, 1H, Ar-H), 6.90 (td, $J = 7.5, 1.1$ Hz, 1H, Ar-H), 3.82 (t, $J = 6.7$ Hz, 2H, CH_2), 2.85 (t, $J = 6.8$ Hz, 2H, CH_2), 2.16 (s, 3H, CH_3).

$^{13}\text{C}\{^1\text{H}\}$ NMR (101 MHz, CDCl_3) δ 165.8 (C=N), 161.1, 132.4, 131.4, 118.7, 118.6, 117.0 (Ar), 59.0, 35.1 (CH_2), 16.0 (S- CH_3).

m/z calc. $[\text{C}_{10}\text{H}_{14}\text{NOS}]^+$ (acetonitrile) = 196.0791, found = 196.0803.

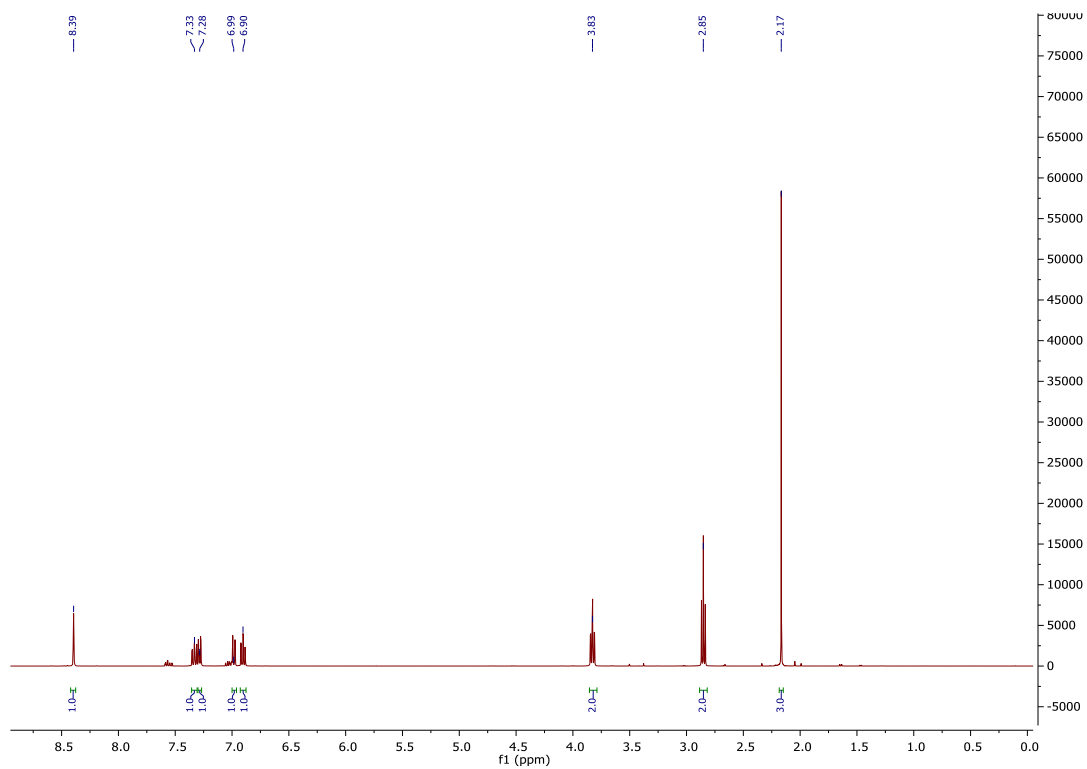


Figure 5.34: ^1H NMR (400 MHz, CDCl_3 , 298K) spectrum of GH.

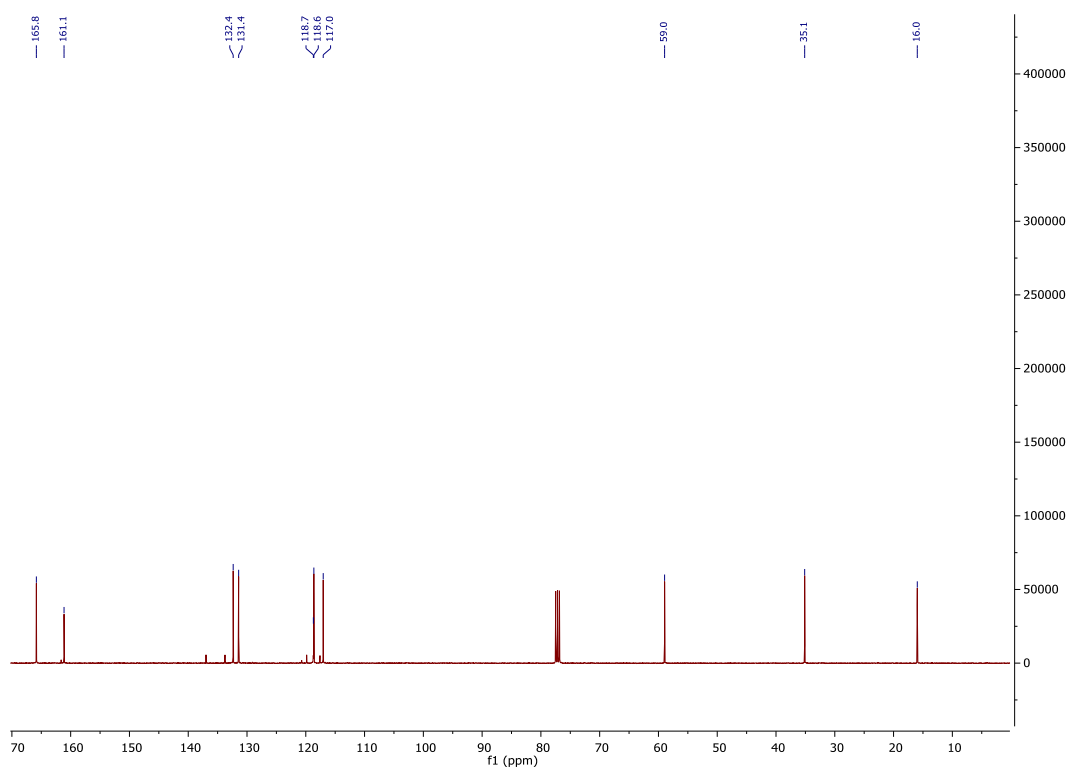
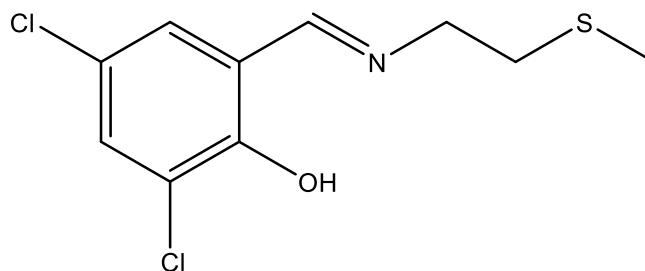


Figure 5.35: $^{13}\text{C}\{^1\text{H}\}$ NMR (101 MHz, CDCl_3) of GH.



HH A solution of 3,5-dichloro-2-hydroxybenzaldehyde (1.91 g, 10.0 mmol) and 2-(methylthio) ethylamine (0.91 g, 10.0 mmol) in methanol (30 mL) was stirred at room temperature for two hours. The solvent was removed *in vacuo* to give a yellow oil. The crude product was recrystallised from methanol to give a yellow powder (1.81 g, 69%).

^1H NMR (400 MHz, CDCl_3) δ 8.30 (t, $J = 1.2$ Hz, 1H, CH), 7.43 (d, $J = 2.5$ Hz, 1H, Ar-H), 7.19 (d, $J = 2.5$ Hz, 1H, Ar-H), 3.89 – 3.84 (m, 2H, CH_2), 2.86 (t, $J = 6.6$ Hz, 2H, CH_2), 2.15 (s, 3H, CH_3).

$^{13}\text{C}\{^1\text{H}\}$ NMR (101 MHz, CDCl_3) δ 164.3 (C=N), 156.9, 132.3, 129.1, 123.0, 122.6, 119.3 (Ar), 57.9, 34.9 (CH_2), 15.9 (S- CH_3).

m/z calc. $[\text{C}_{10}\text{H}_{11}\text{Cl}_2\text{NOS}]^+$ (acetonitrile) = 264.0011, found = 264.0020.

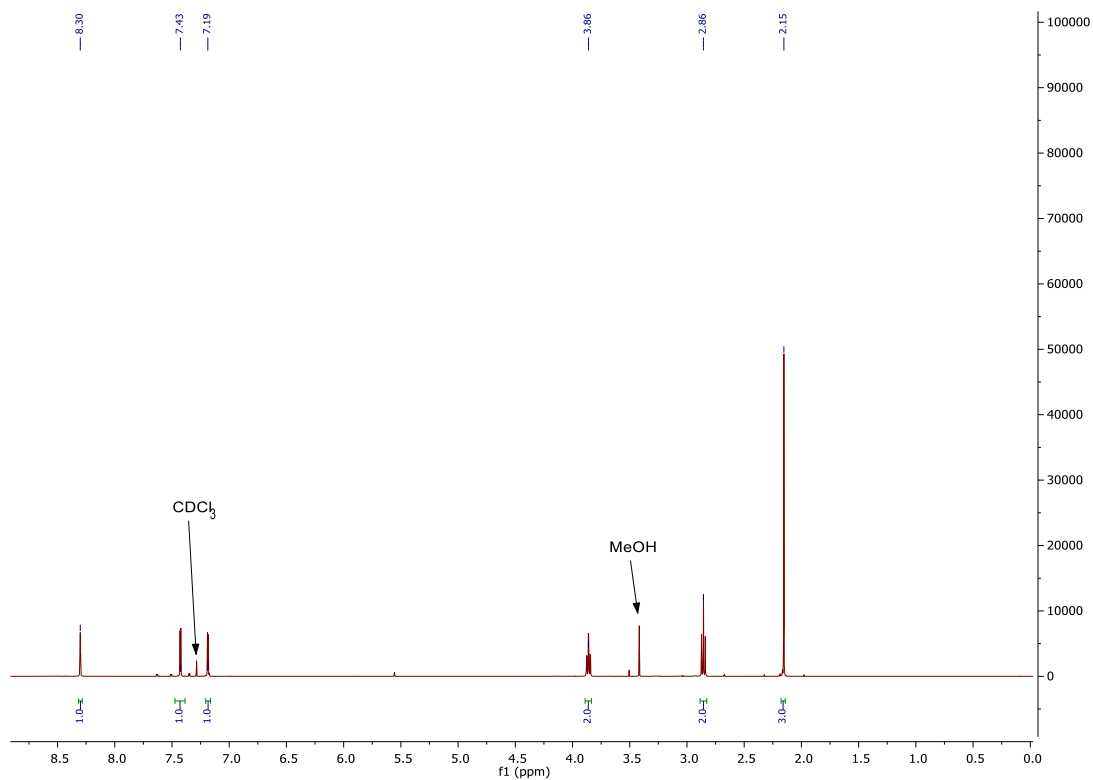


Figure 5.36: ^1H NMR (400 MHz, CDCl_3) of HH.

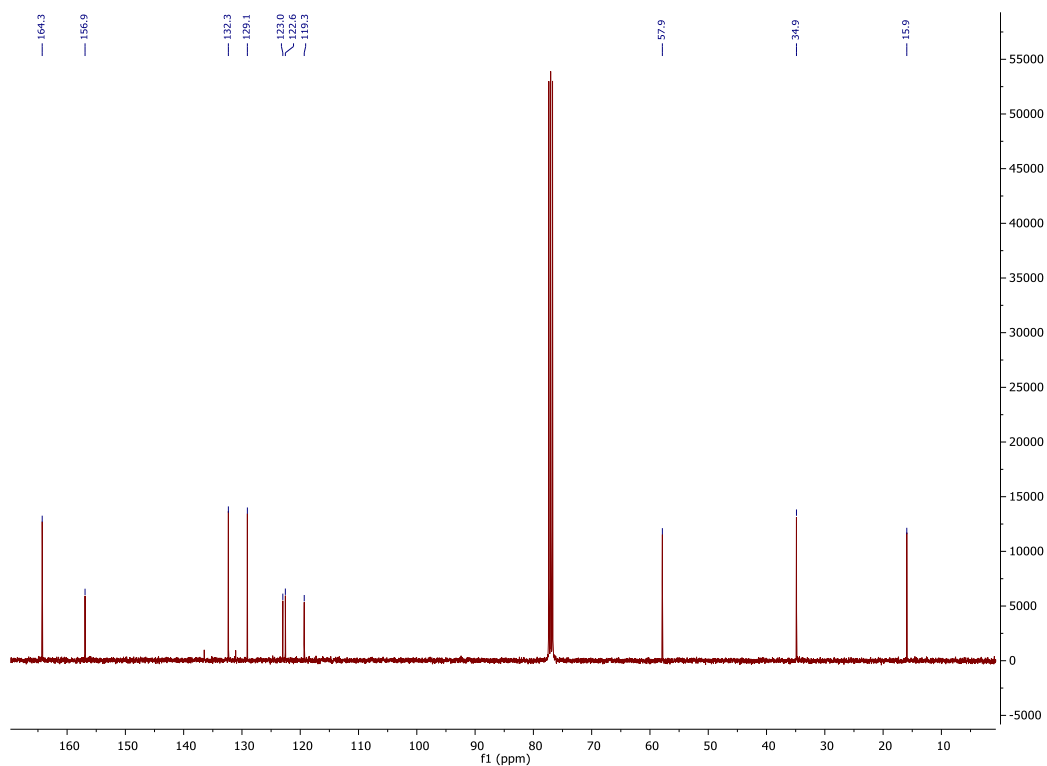
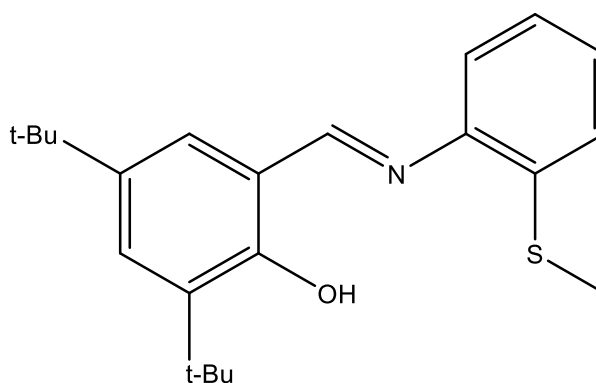


Figure 5.37: $^{13}\text{C}\{^1\text{H}\}$ NMR (101 MHz, CDCl_3) of HH.



4H A solution of 3,5-di-*tert*-butyl-2-hydroxybenzaldehyde (2.34 g, 10.0 mmol) and 2-(methylthio) aniline (1.39 g, 1.25 mL, 10.0 mmol) in methanol (30 mL) was stirred at room temperature for two hours until a precipitate formed. The crude product was collected and recrystallised from methanol to give a yellow powder (3.12 g, 88%).

^1H NMR (500 MHz, CDCl_3) δ 8.55 (s, 1H, CH), 7.39 (d, $J = 2.5$ Hz, 1H, Ar-H), 7.17 (d, $J = 4.7$ Hz, 1H, Ar-H), 7.17 (d, $J = 1.3$ Hz, 1H, Ar-H), 7.15 (d, $J = 2.4$ Hz, 1H, Ar-H), 7.13 – 7.10 (m, 1H, Ar-H), 7.06 (dd, $J = 7.5, 1.2$ Hz, 1H, Ar-H), 2.40 (s, 3H, CH_3), 1.42 (s, 9H, $\text{C}(\text{CH}_3)_3$), 1.26 (s, 9H, $\text{C}(\text{CH}_3)_3$).

$^{13}\text{C}\{^1\text{H}\}$ NMR (126 MHz, CDCl_3) δ 163.3 (C=N), 158.4, 146.0, 140.5, 137.1, 134.6, 128.3, 127.0, 126.9, 125.2, 124.8, 118.4, 117.5 (Ar), 35.2 (CH_2), 34.2 (CH_2), 31.5 (CH_3), 31.3 (CH), 29.5 (CH_3), 29.3 (CH), 14.8 (S- CH_3).

m/z calc. $[\text{C}_{22}\text{H}_{30}\text{NOS}]^+$ (acetonitrile) = 356.2043, found = 356.2061.

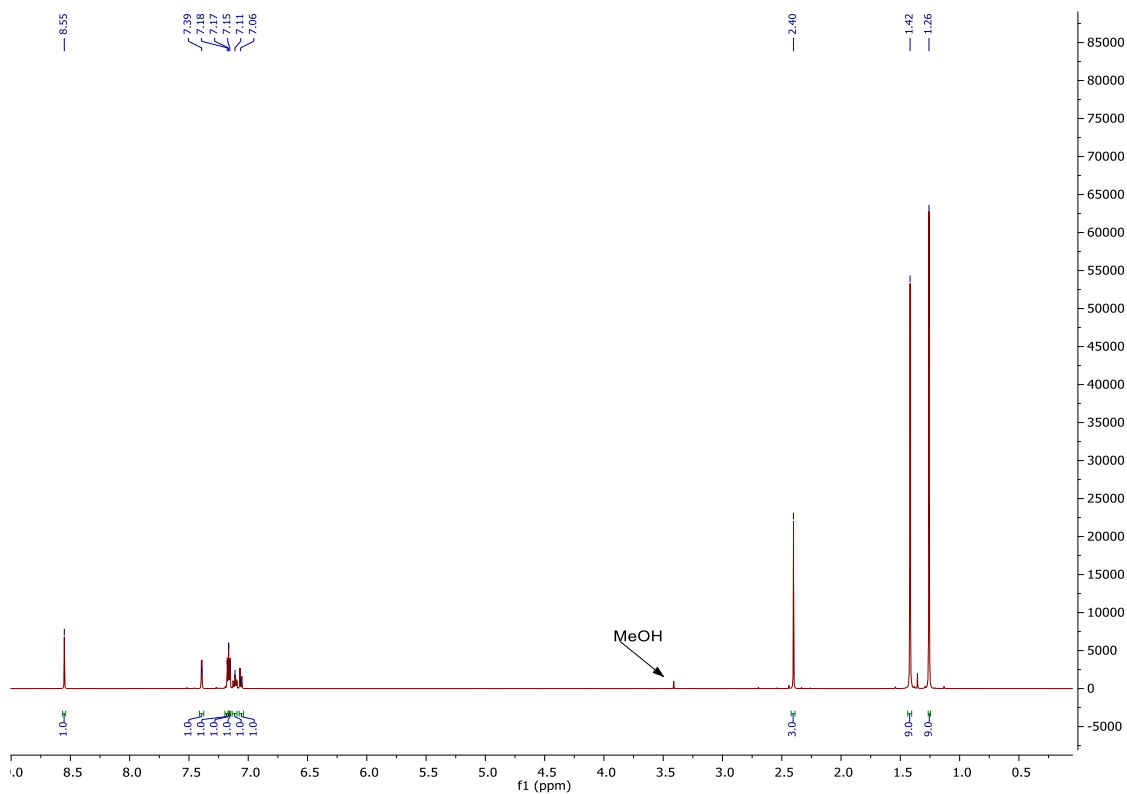


Figure 5.38: ^1H NMR (500 MHz, CDCl_3) of 1H.

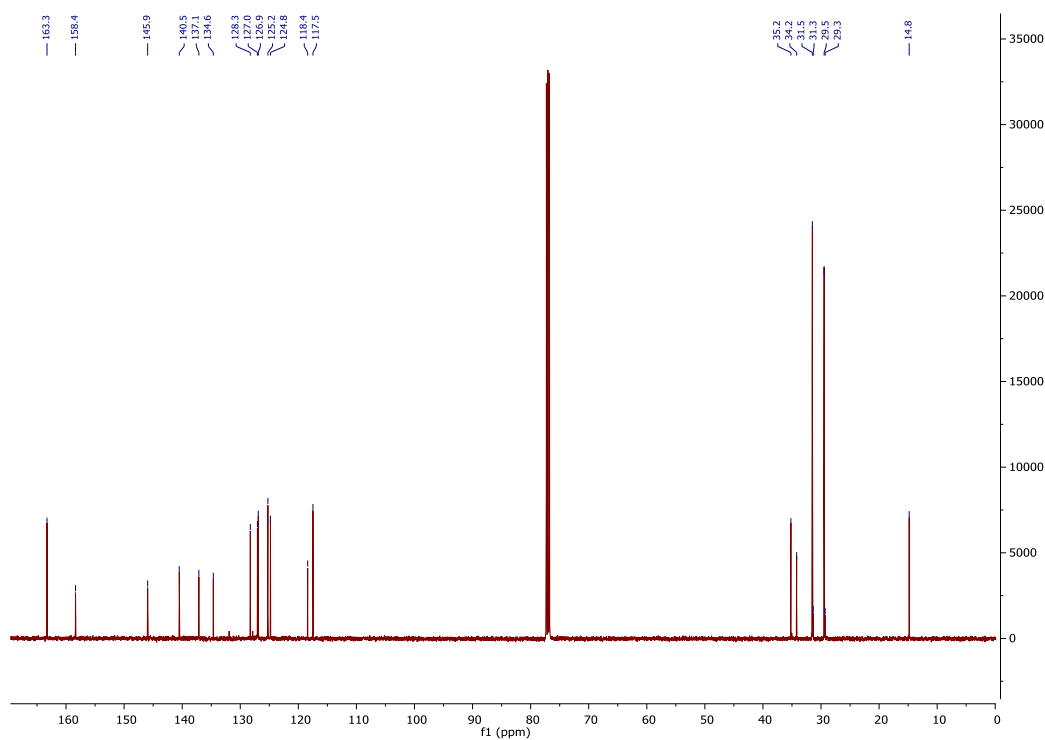
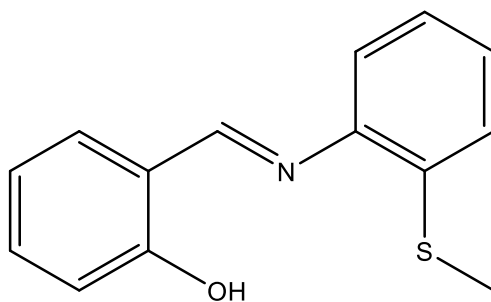


Figure 5.39: $^{13}\text{C}\{^1\text{H}\}$ NMR (126 MHz, CDCl_3) of 1H.



JH A solution salicylaldehyde (1.22 g, 1.04 mL, 10.0 mmol) and 2-(methylthio) aniline (1.39 g, 1.25 mL, 10.0 mmol) in methanol (30 mL) was stirred at room temperature for two hours. A yellow oil precipitated out of solution and was collected through separation. The crude product was washed with methanol to give a yellow oil which solidified overnight (1.74 g, 72%).

^1H NMR (500 MHz, CDCl_3) δ 8.56 (s, 1H, CH), 7.33 (m, 1H, Ar-H), 7.32 – 7.29 (m, 1H, Ar-H), 7.22 – 7.15 (m, 2H, Ar-H), 7.15 – 7.08 (m, 2H, Ar-H), 6.99 (dd, $J = 8.3, 1.0$ Hz, 1H, Ar-H), 6.86 (td, $J = 7.5, 1.1$ Hz, 1H, Ar-H), 2.40 (s, 3H, CH_3).

$^{13}\text{C}\{^1\text{H}\}$ NMR (126 MHz, CDCl_3) δ 161.8 (C=N), 161.2, 145.3, 134.9, 133.4, 132.4, 127.5, 125.4, 125.1, 119.2, 119.1, 117.5, 117.2 (Ar), 14.9 (S- CH_3).

m/z calc. $[\text{C}_{14}\text{H}_{14}\text{NOS}]^+$ (acetonitrile) = 244.0791, found = 244.0788.

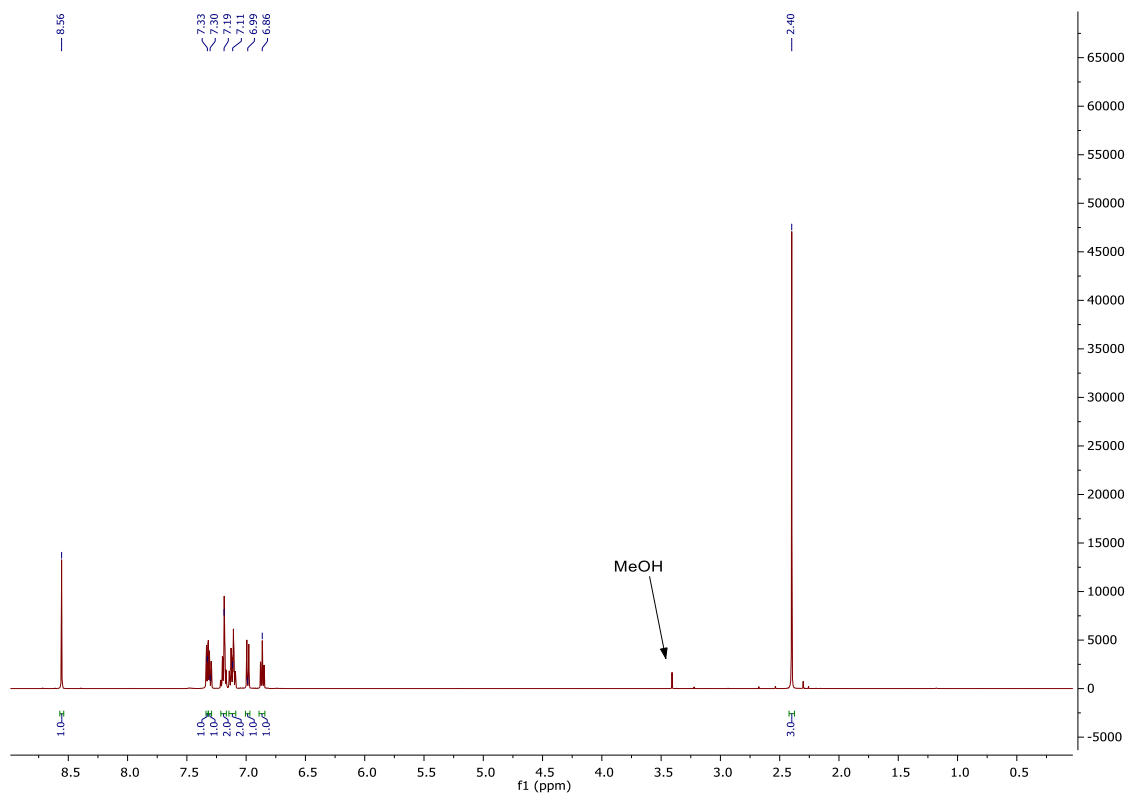


Figure 5.40: ^1H NMR (500 MHz, CDCl_3) of JH.

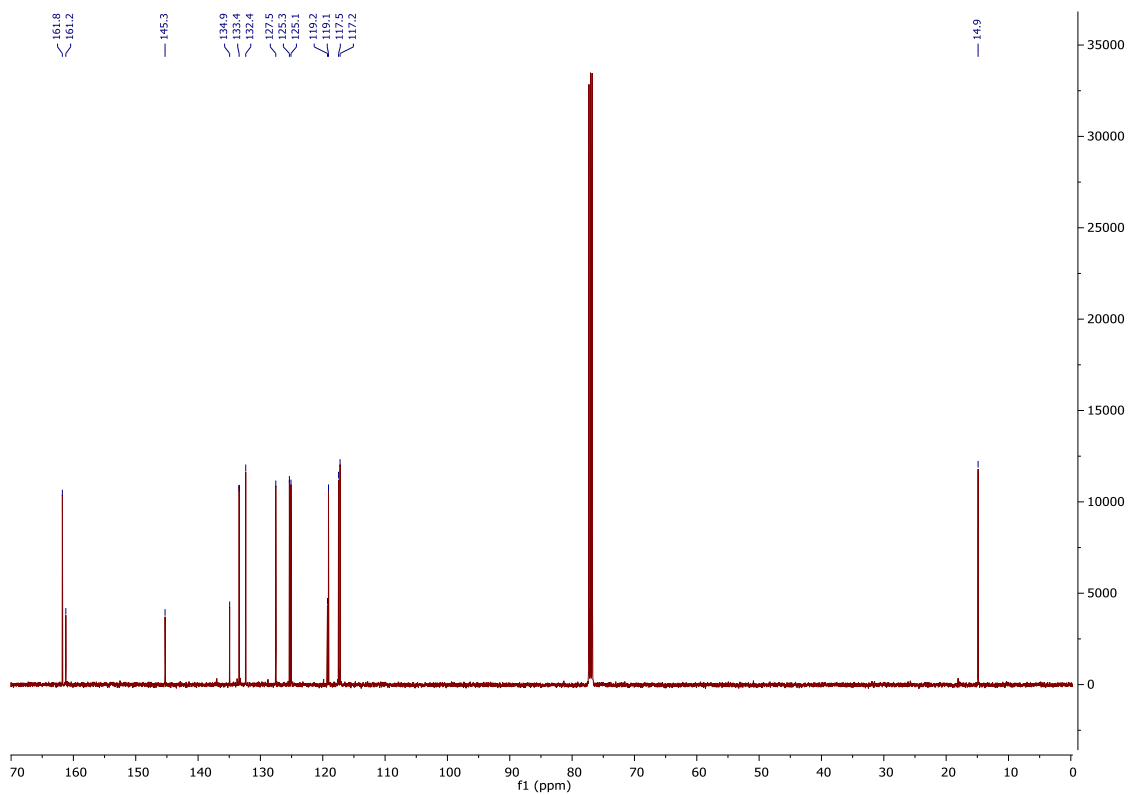
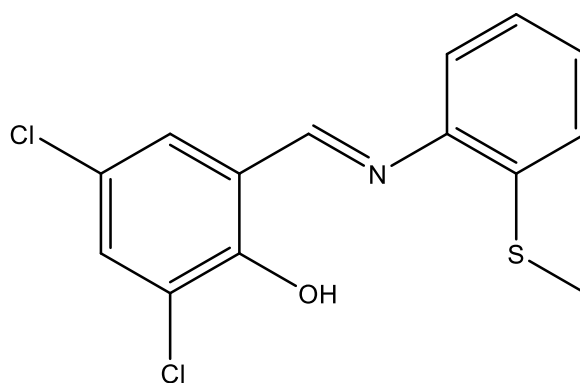


Figure 5.41: $^{13}\text{C}\{^1\text{H}\}$ NMR (126 MHz, CDCl_3) of JH.



KH A solution of 3,5-dichloro-2-hydroxybenzaldehyde (1.91 g, 10.0 mmol) and 2-(methylthio) aniline (1.39 g, 1.25 mL, 10.0 mmol) in methanol (30 mL) was stirred at room temperature for one minute before an orange precipitate was formed. The crude product was collected and recrystallised from methanol to give a bright orange product (1.5 g, 48%).

^1H NMR (400 MHz, CDCl_3) δ 8.66 (s, 1H), 7.48 – 7.36 (m, 2H), 7.26 – 7.15 (m, 2H), 7.09 (dd, $J = 8.2, 1.1$ Hz, 1H), 6.97 (td, $J = 7.5, 1.1$ Hz, 1H), 2.50 (s, 3H).

$^{13}\text{C}\{^1\text{H}\}$ NMR (126 MHz, CDCl_3) δ 161.8 (C=N), 161.2, 145.3, 134.9, 133.4, 132.4, 127.53, 125.4, 125.1, 119.2, 119.1, 117.5, 117.2 (Ar), 14.9 (S- CH_3).

m/z calc. $[\text{C}_{14}\text{H}_{11}\text{Cl}_2\text{NOS}]^+$ (acetonitrile) = 312.0011, found = 312.0006.

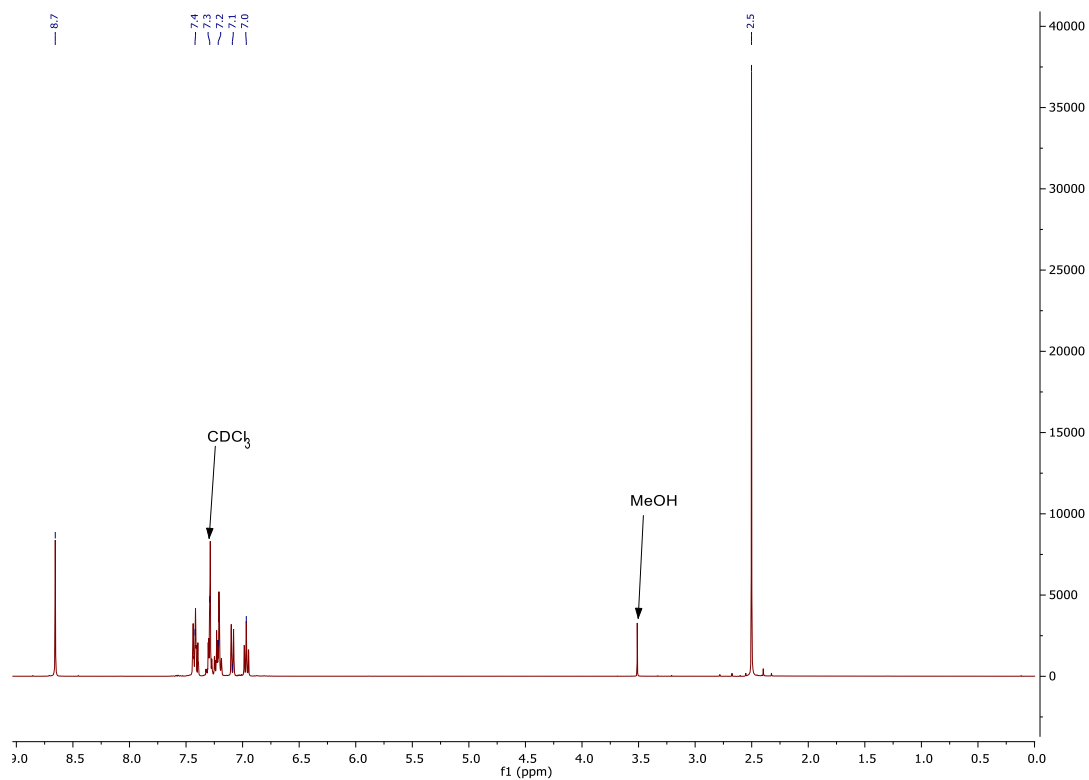


Figure 5.42: ¹H NMR (400 MHz, CDCl₃) of KH.

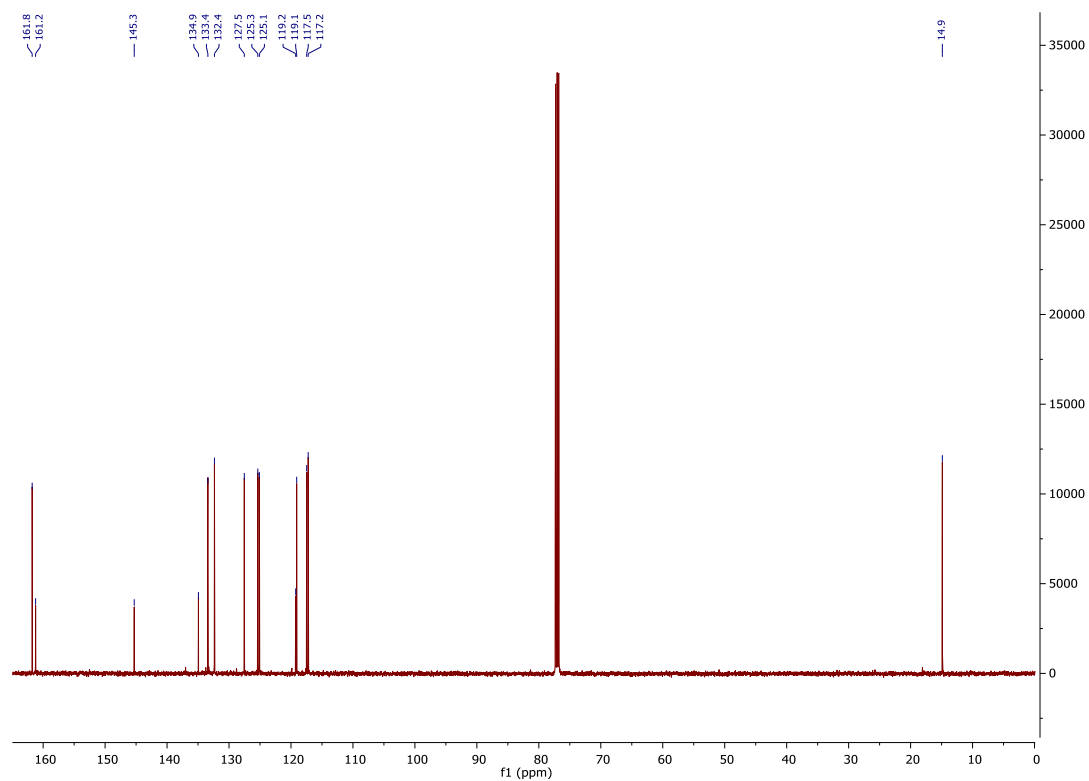
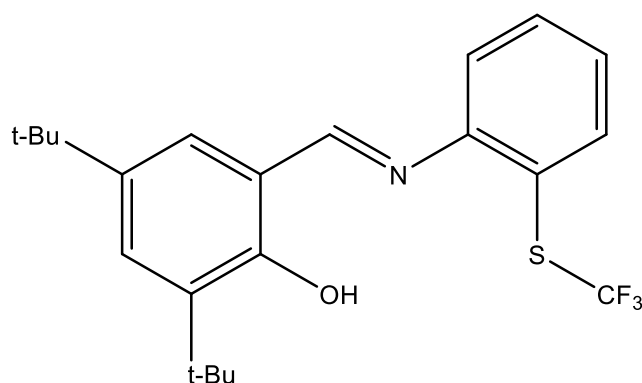


Figure 5.43: ¹³C{¹H} NMR (126 MHz, CDCl₃) of KH.



LH A solution of 3,5-di-*tert*-butyl-2-hydroxybenzaldehyde (2.34 g, 10.0 mmol) and 2-(trifluoromethylthio) aniline (1.93 g, 10.0 mmol) in methanol (30 mL) was stirred at room temperature for two hours. The solvent was removed *in vacuo* to give a yellow oil. The crude product was recrystallised from methanol to give a yellow powder (2.57 g, 63%).

^1H NMR (500 MHz, CDCl_3) δ 13.14 (s, 1H, OH), 8.50 (s, 1H, CH), 7.70 – 7.68 (m, 1H, Ar-H), 7.46 (td, $J = 7.7, 1.5$ Hz, 1H, Ar-H), 7.43 (d, $J = 2.5$ Hz, 1H, Ar-H), 7.23 (td, $J = 7.7, 1.4$ Hz, 1H, Ar-H), 7.18 – 7.17 (m, 1H, Ar-H), 1.42 (s, 9H, $\text{C}(\text{CH}_3)_3$), 1.26 (s, 9H, $\text{C}(\text{CH}_3)_3$).

$^{13}\text{C}\{^1\text{H}\}$ NMR (126 MHz, CDCl_3) δ 165.2 (CH), 158.6, 152.2, 140.7, 137.6, 137.3, 132.4, 128.9, 127.1, 127.0, 119.6, 119.6, 119.5, 118.1 (Ar), 35.2, 34.2 (CH), 31.5, 29.4 (CH_3).

^{19}F NMR (471 MHz, CDCl_3) δ -41.80.

m/z calc. $[\text{C}_{22}\text{H}_{27}\text{F}_3\text{NOS}]^+$ (acetonitrile) = 410.1760, found = 410.1778.

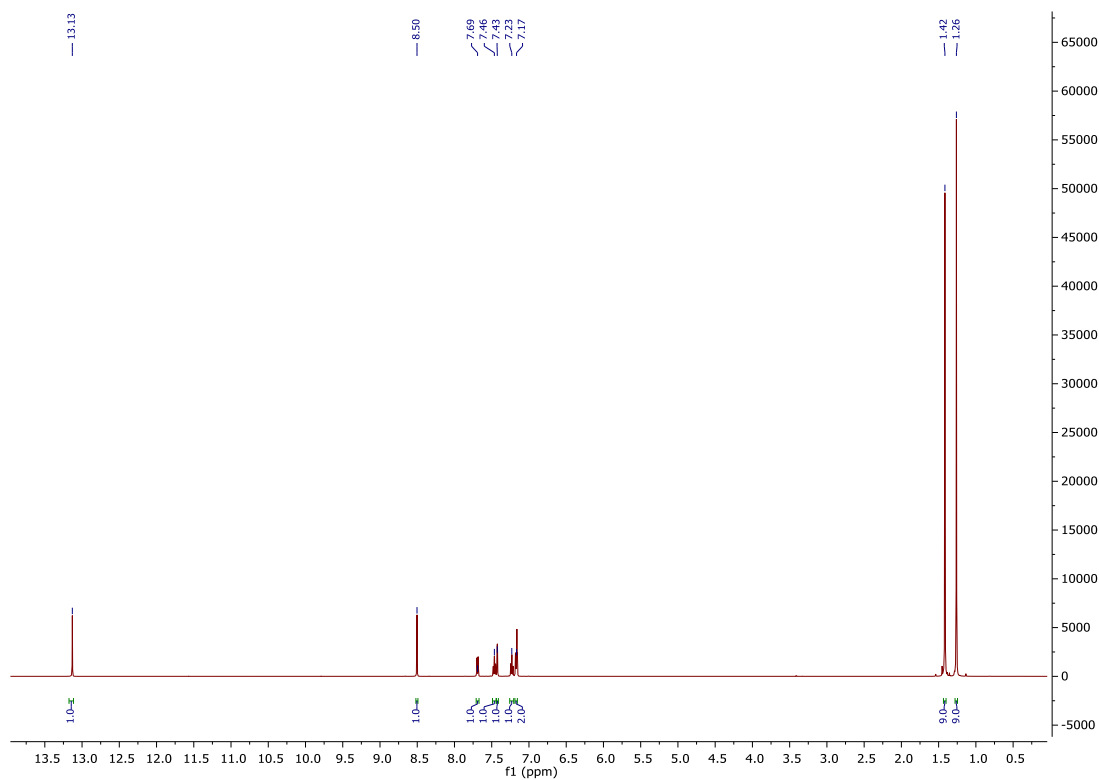


Figure 5.44: ^1H NMR (500 MHz, CDCl_3) of LH.

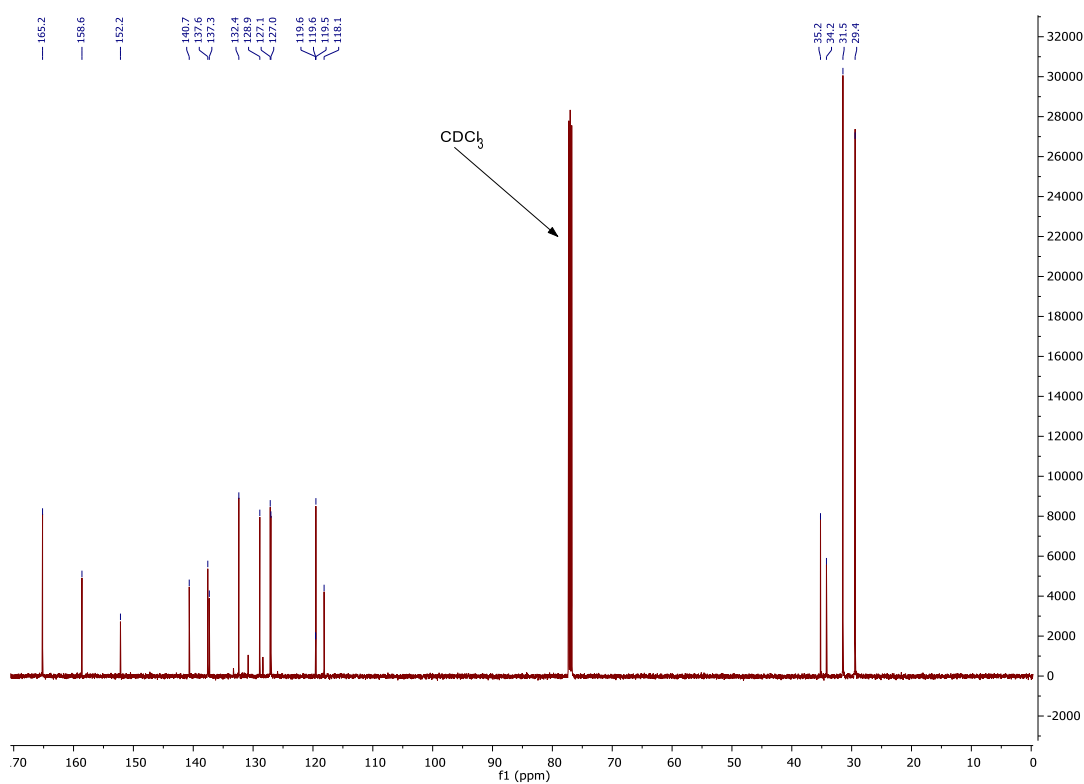
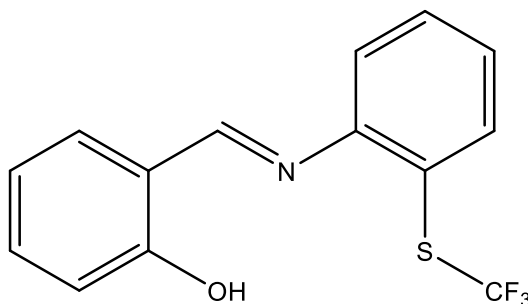


Figure 5.45: $^{13}\text{C}\{^1\text{H}\}$ NMR (126 MHz, CDCl_3) of LH.



MH A solution of salicylaldehyde (1.22 g, 1.04 mL, 10.0 mmol) and 2-(trifluoromethylthio) aniline (1.93 g, 10.0 mmol) in methanol (30 mL) was stirred at room temperature for two hours. The solvent was removed *in vacuo* to give a pale-yellow oil. The crude product was washed with methanol (0.80 g, 22%).

^1H NMR (500 MHz, CDCl_3) δ 8.51 (s, 1H, CH), 7.71 (dd, $J = 7.8, 1.4$ Hz, 1H, Ar-H), 7.49 (td, $J = 7.7, 1.5$ Hz, 1H, Ar-H), 7.37 – 7.32 (m, 2H, Ar-H), 7.26 (td, $J = 7.6, 1.3$ Hz, 1H, Ar-H), 7.21 (dd, $J = 8.1, 1.3$ Hz, 1H, Ar-H), 6.99 (dd, $J = 8.7, 1.0$ Hz, 1H, Ar-H), 6.88 (td, $J = 7.5, 1.1$ Hz, 1H, Ar-H).

$^{13}\text{C}\{^1\text{H}\}$ NMR (126 MHz, CDCl_3) δ 163.9 (C=N), 161.4, 151.6, 138.0, 134.02, 132.7, 132.6, 127.5, 119.7, 119.3, 119.2, 118.0, 117.6 (Ar).

m/z calc. $[\text{C}_{14}\text{H}_{11}\text{F}_3\text{NOS}]^+$ (acetonitrile) = 298.0508, found = 298.0505.

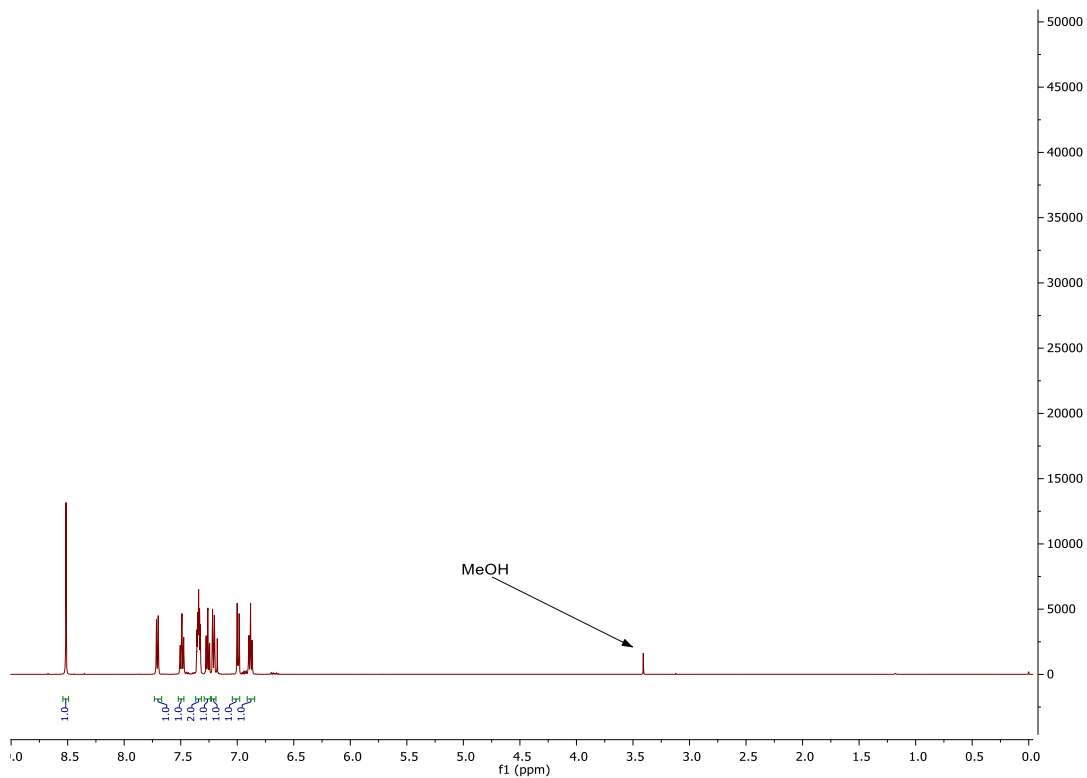


Figure 5.46: ^1H NMR (500 MHz, CDCl_3) of MH.

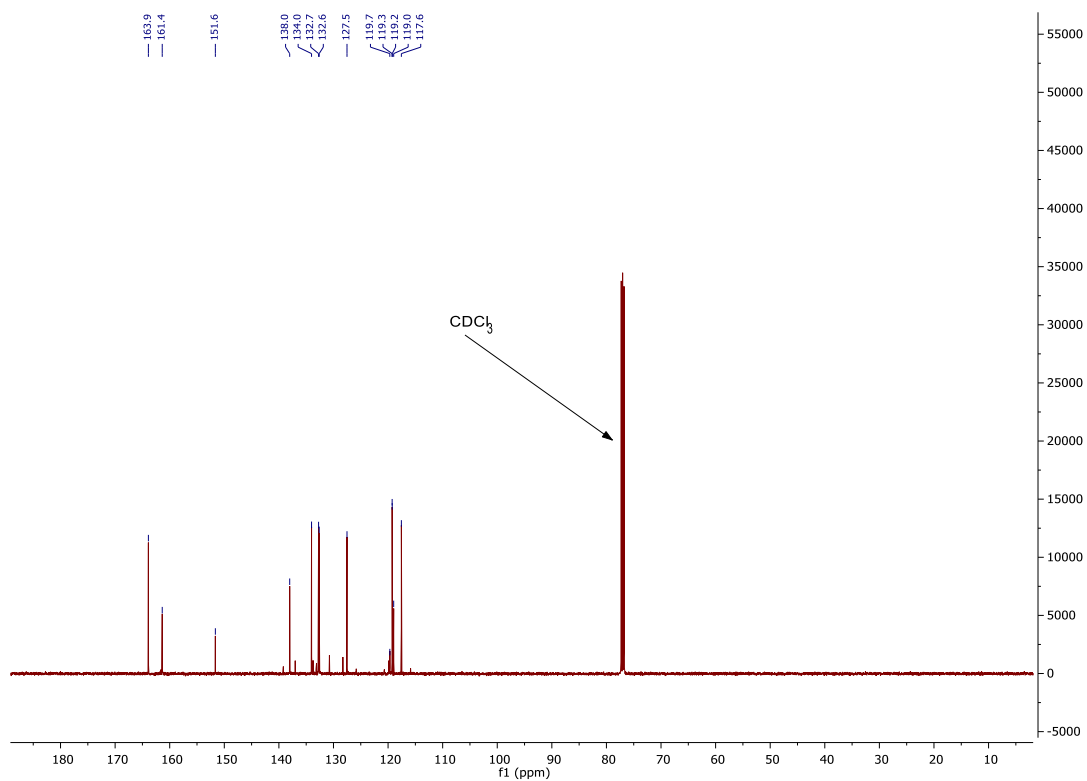
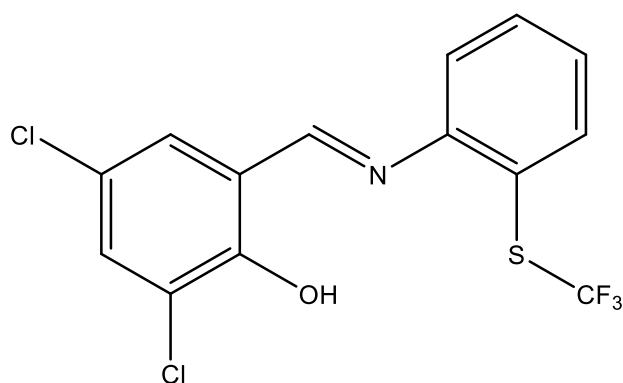


Figure 5.47: $^{13}\text{C}\{^1\text{H}\}$ NMR (126 MHz, CDCl_3) of MH.



NH A solution of 3,5-dichloro-2-hydroxybenzaldehyde (1.91 g, 10.0 mmol) and 2-(trifluoromethylthio) aniline (1.93 g, 10.0 mmol) in methanol (30 mL) was stirred at room temperature for two hours until a precipitate formed. The crude product was collected and recrystallised from methanol to give a yellow powder (2.72 g, 74%).

^1H NMR (500 MHz, CDCl_3) δ 8.45 (s, 1H, CH), 7.73 (dd, $J = 7.8, 1.3$ Hz, 1H, Ar-H), 7.52 (td, $J = 7.8, 1.5$ Hz, 1H, Ar-H), 7.42 (d, $J = 2.5$ Hz, 1H, Ar-H), 7.32 (td, $J = 7.6, 1.3$ Hz, 1H, Ar-H), 7.25 (d, $J = 2.5$ Hz, 1H, Ar-H), 7.21 (dd, $J = 7.9, 1.3$ Hz, 1H, Ar-H).

$^{13}\text{C}\{^1\text{H}\}$ NMR (126 MHz, CDCl_3) δ 162.0 (CH), 155.83, 150.7, 138.3, 133.4, 132.8, 130.2, 128.4, 123.7, 123.1, 120.2, 120.0, 119.2 (Ar).

m/z calc. $[\text{C}_{14}\text{H}_9\text{F}_3\text{Cl}_2\text{NOS}]^+$ (acetonitrile) = 365.9729, found = 365.9737.

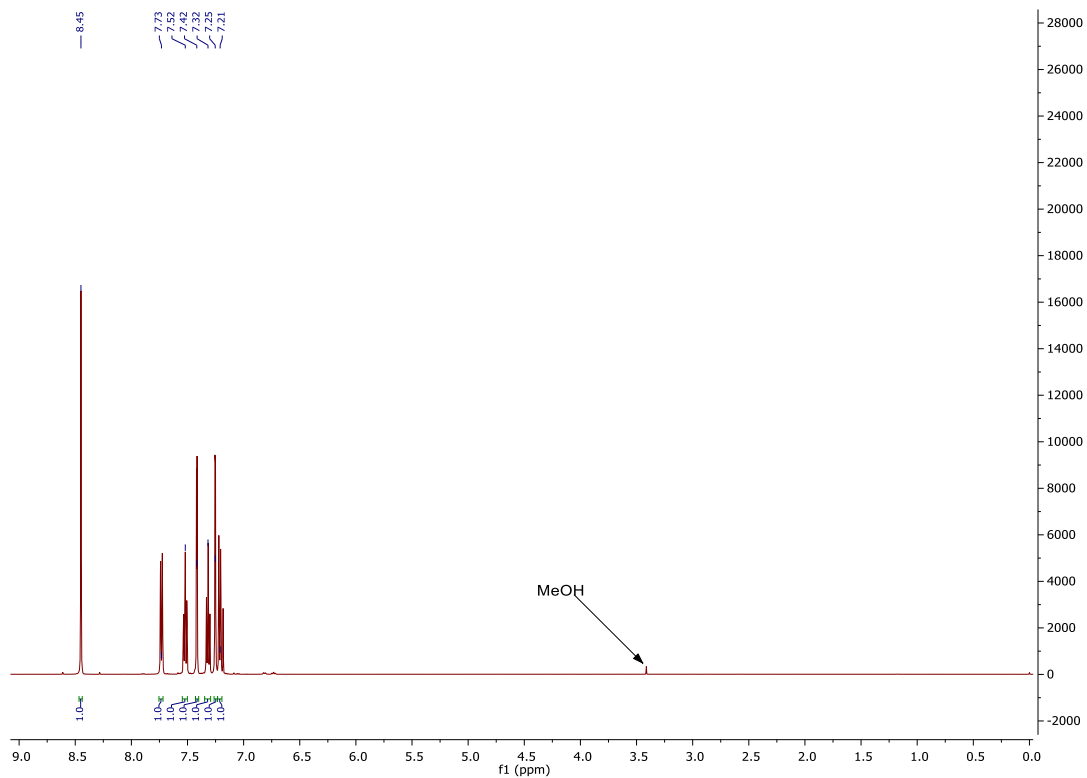


Figure 5.48: ^1H NMR (500 MHz, CDCl_3) of NH.

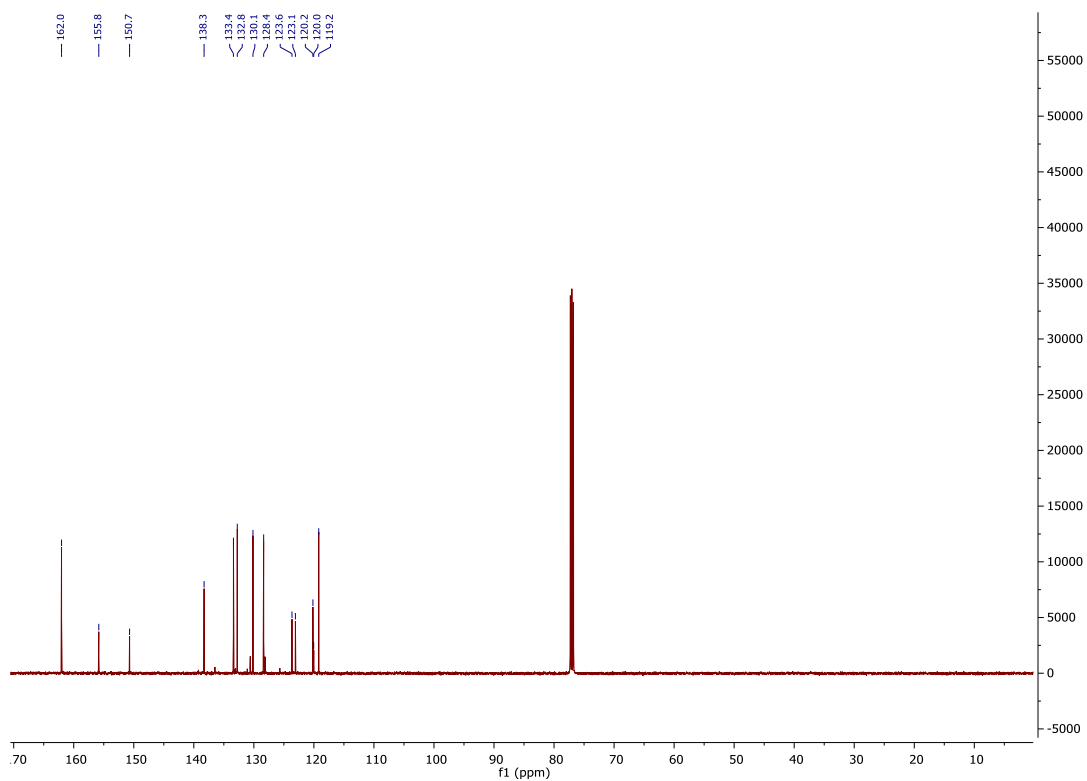


Figure 5.49: $^{13}\text{C}\{^1\text{H}\}$ NMR (126 MHz, CDCl_3) of NH.

5.3.2 Synthesis and characterisation of zinc {ONS} complexes

Zn(F)₂ Ligand FH (2 mmol, 0.62 g) was dissolved in toluene (10 mL). ZnEt₂ (1 mmol, 1 mL, 1.0 M) was added dropwise and the solution stirred for two hours. The product crystallised from toluene as a pale-yellow solid (0.15 g, 22%).

¹H NMR (400 MHz, C₆D₆) δ 7.68 (d, *J* = 2.7 Hz, 1H, Ar-H), 7.62 (s, 1H, CH), 6.85 (d, *J* = 2.6 Hz, 1H, Ar-H), 3.32 (m, 2H, CH₂), 2.67 – 2.27 (m, 2H, CH₂), 1.70 (s, 9H, C(CH₃)₃), 1.57 (s, 3H, CH₃), 1.36 (s, 9H, C(CH₃)₃).

¹³C{¹H} NMR (101 MHz, C₆D₆) δ 172.6 (CH), 169.3, 141.7, 135.5, 130.0, 125.5, 117.5 (Ar), 59.6, 35.9 (CH₂), 34.7, 33.9 (CH), 31.6, 29.8 (CH₃), 15.1 (S-CH₃).

Elemental analysis (C₃₆H₅₆N₂O₂S₂Zn) Calcd in %: C, 63.75; H, 8.32; N, 4.13. Found: C, 61.56; H, 8.39; N, 3.87.

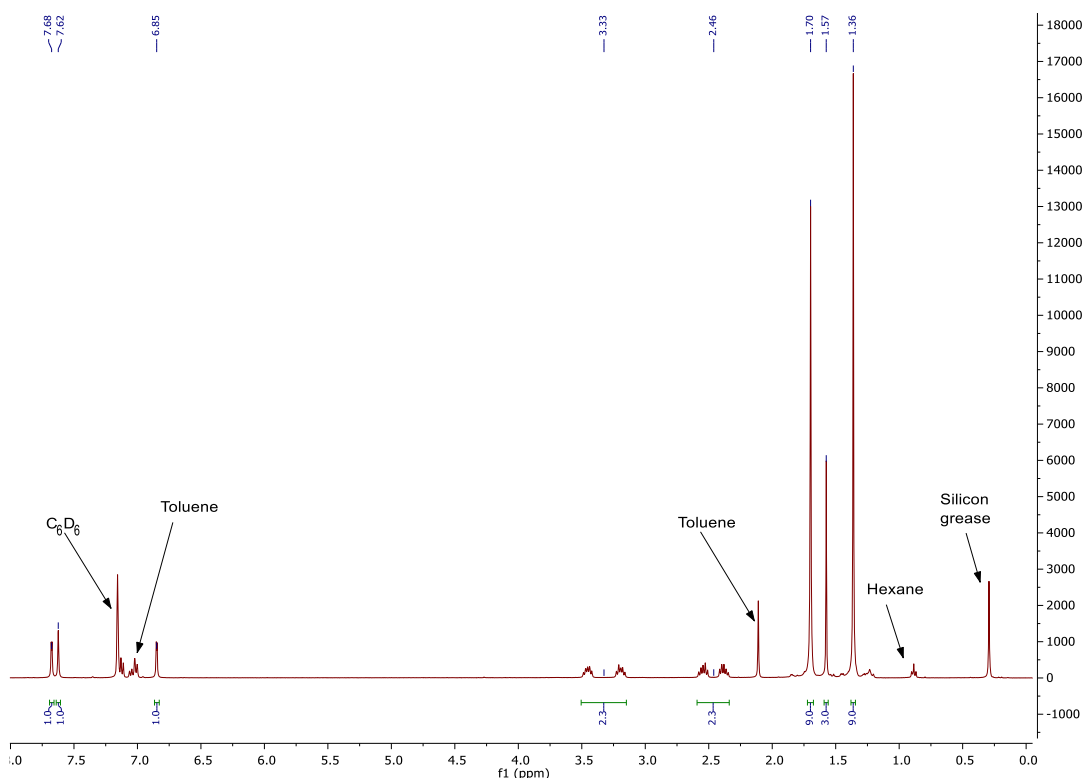


Figure 5.50: ¹H NMR (400 MHz, C₆D₆) of Zn(F)₂.

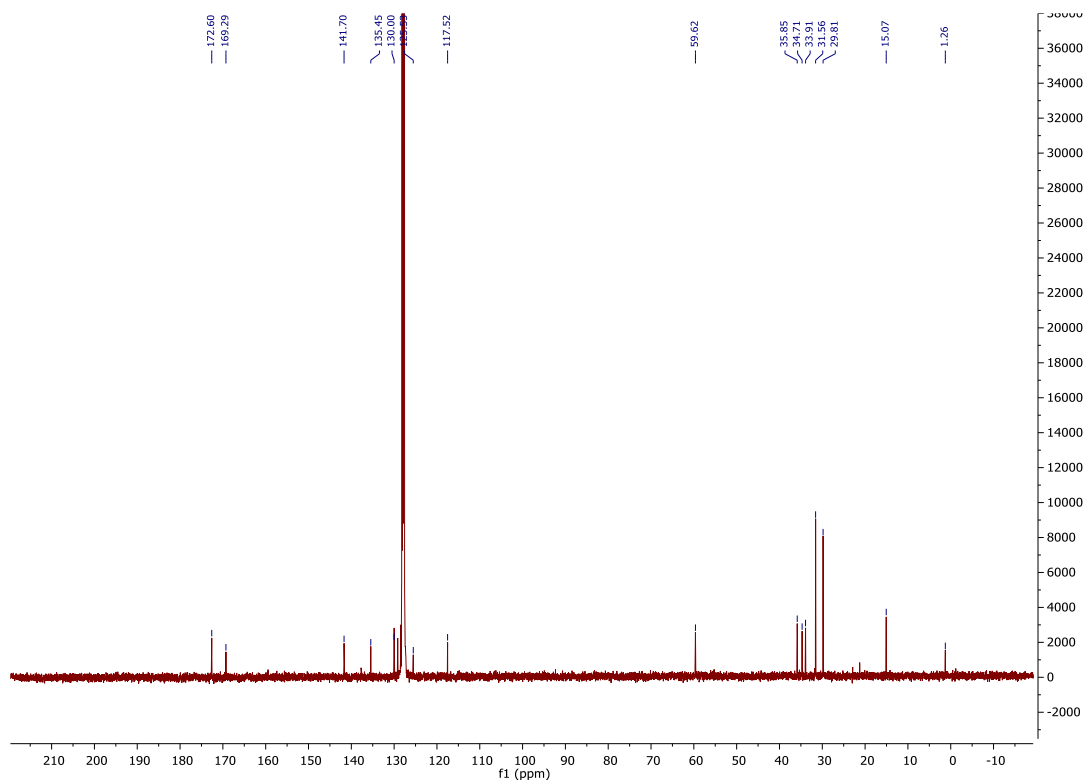


Figure 5.51: $^{13}\text{C}\{^1\text{H}\}$ NMR (101 MHz, C_6D_6) of $\text{Zn}(\text{F})_2$.

$\text{Zn}(\text{G})_2$ Ligand **GH** (2 mmol, 0.39 g) was dissolved in toluene (10 mL). ZnEt_2 (1 mmol, 1 mL, 1.0 M) was added dropwise and the solution stirred for two hours. The product crystallised from toluene as an off-white solid (0.37 g, 82%).

^1H NMR (500 MHz, CDCl_3) δ 8.12 (s, 1H, CH), 7.23 (ddd, $J = 8.7, 7.0, 1.9$ Hz, 1H, Ar), 7.05 (dd, $J = 7.8, 1.9$ Hz, 1H, Ar), 6.77 (d, $J = 8.5$ Hz, 1H, Ar), 6.53 (ddd, $J = 8.0, 7.0, 1.2$ Hz, 1H, Ar), 3.69 (t, $J = 6.7$ Hz, 2H, CH_2), 2.68 (t, $J = 6.7$ Hz, 2H, CH_2), 1.90 (s, 3H, CH_3).

$^{13}\text{C}\{^1\text{H}\}$ NMR (126 MHz, CDCl_3) δ 171.9 (CH), 170.7, 135.8, 135.2, 123.2, 117.9, 114.6 (Ar), 59.5, 34.7 (CH_2), 15.5 (S- CH_3).

Elemental analysis ($\text{C}_{20}\text{H}_{24}\text{N}_2\text{O}_2\text{S}_2\text{Zn}$) Calcd in %: C, 52.92; H, 5.33; N, 6.17. Found: C, 53.12; H, 5.33; N, 6.17.

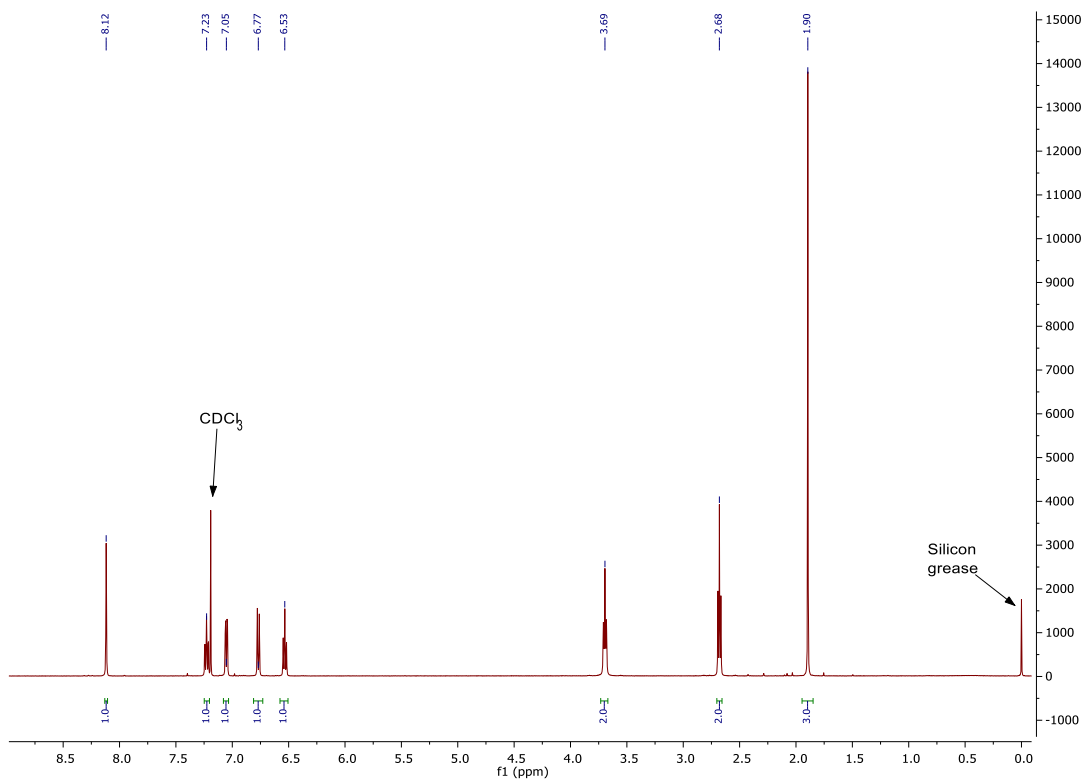


Figure 5.52: ^1H NMR (500 MHz, CDCl_3) of $\text{Zn}(\text{G})_2$.

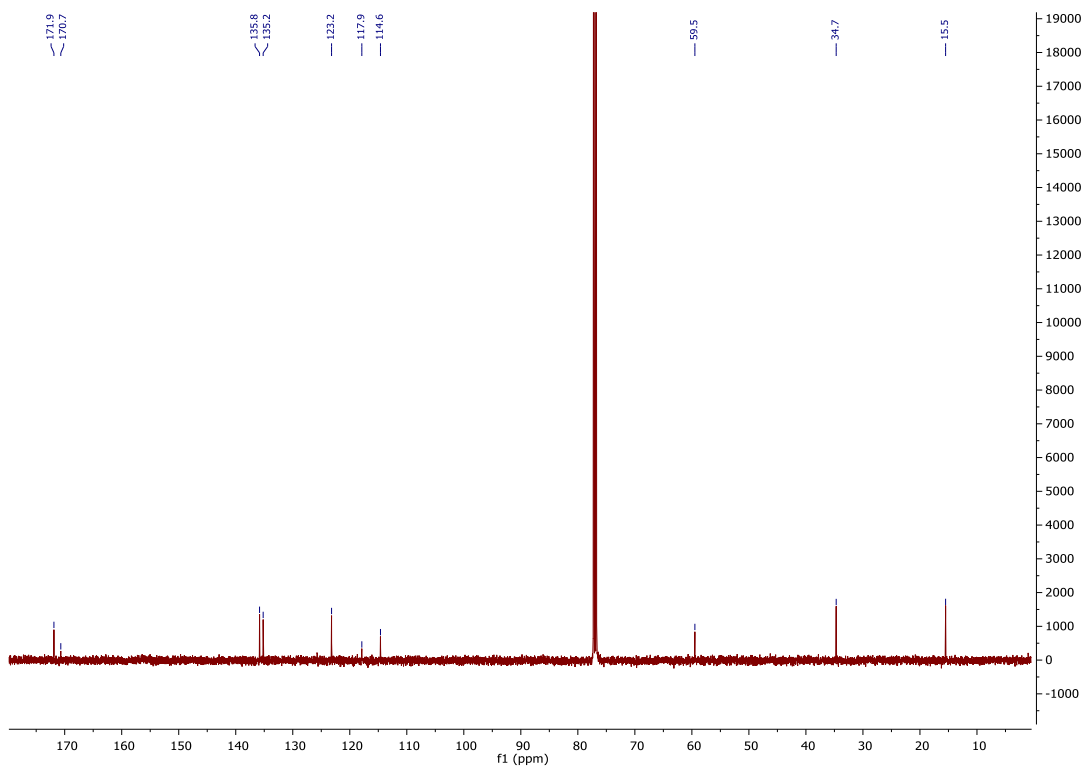


Figure 5.53: $^{13}\text{C}\{^1\text{H}\}$ NMR (126 MHz, CDCl_3) of $\text{Zn}(\text{G})_2$.

Zn(H)₂ Ligand HH (2 mmol, 0.53 g) was dissolved in toluene (10 mL). ZnEt₂ (1 mmol, 1 mL, 1.0 M) was added dropwise and the solution stirred for two hours. The product crystallised from toluene as a bright yellow solid (0.44 g, 74%).

¹H NMR (500 MHz, CDCl₃) δ 8.08 (s, 1H, CH), 7.36 (d, *J* = 2.8 Hz, 1H, Ar), 6.97 (d, *J* = 2.8 Hz, 1H, Ar), 3.81 (t, *J* = 6.0 Hz, 2H, CH₂), 2.71 (t, *J* = 6.0 Hz, 2H, CH₂), 1.83 (s, 3H, CH₃).

¹³C{¹H} NMR (126 MHz, CDCl₃) δ 169.8 (CH), 164.1, 133.9, 132.7, 127.7, 118.8, 117.3 (Ar), 58.4, 35.1 (CH₂), 15.2 (S-CH₃).

Elemental analysis (C₂₀H₂₀N₂O₂S₂Cl₄Zn) Calcd in %: C, 40.60; H, 3.41; N, 4.73. Found: C, 40.57; H, 3.41; N, 4.64.

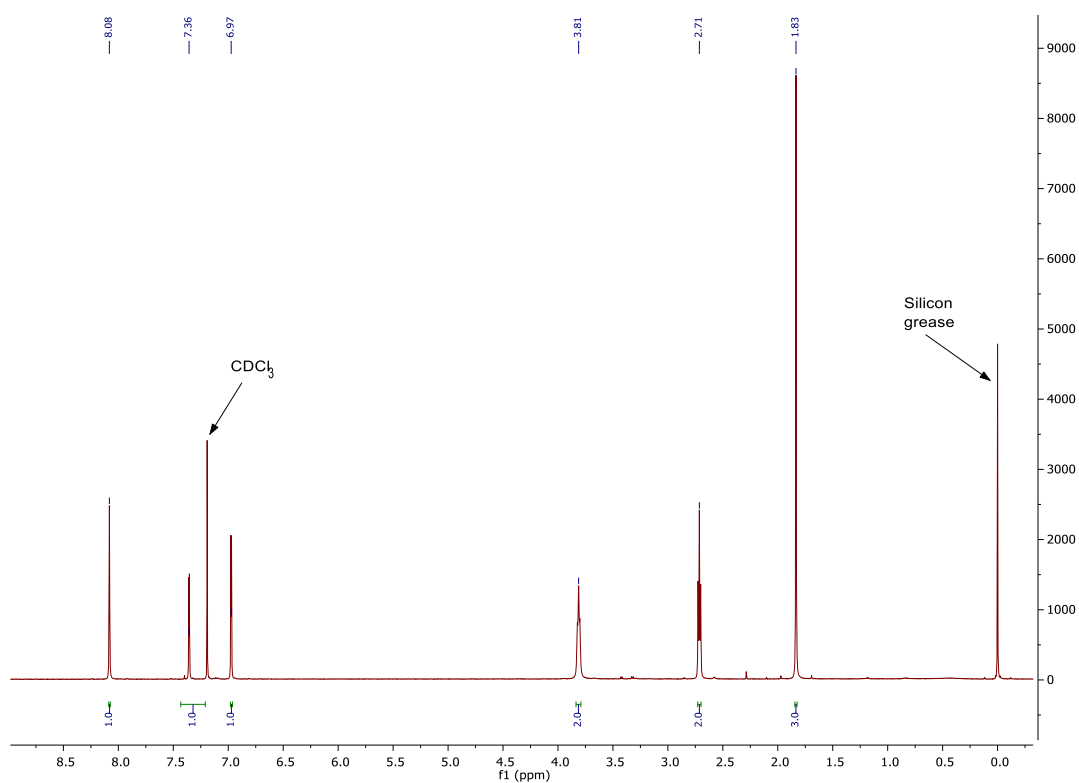


Figure 5.54: ¹H NMR (500 MHz, CDCl₃) of Zn(H)₂.

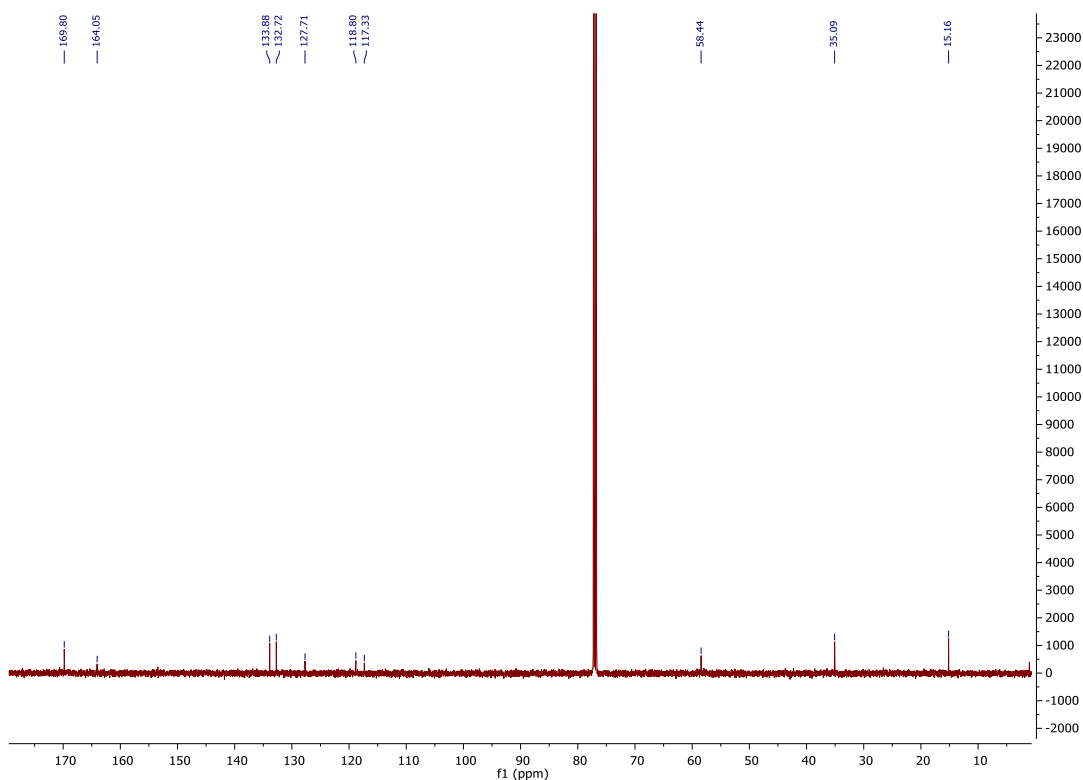


Figure 5.55: ^{13}C NMR (126 MHz, CDCl_3) of $\text{Zn}(\text{H})_2$.

$\text{Zn}(\text{I})_2$ Ligand **1H** (2 mmol, 0.71 g) was dissolved in toluene (10 mL). ZnEt_2 (1 mmol, 1 mL, 1.0 M) was added dropwise and the solution stirred for two hours. The product crystallised from a mixture of toluene and hexane as a yellow solid (0.31 g, 40%).

^1H NMR (400 MHz, CDCl_3) δ 8.15 (s, 1H, CH), 7.44 (d, $J = 2.6$ Hz, 1H, Ar), 7.20 – 7.04 (m, 2H, Ar), 7.03 – 6.91 (m, 1H, Ar), 6.90 (d, $J = 2.6$ Hz, 1H, Ar), 6.53 (d, $J = 7.8$ Hz, 1H, Ar), 2.04 (s, 3H, CH_3), 1.38 (s, 9H, $\text{C}(\text{CH}_3)_3$), 1.30 (s, 9H, $\text{C}(\text{CH}_3)_3$).

$^{13}\text{C}\{^1\text{H}\}$ NMR (101 MHz, CDCl_3) δ 170.9 (CH), 170.8, 148.5, 142.1, 134.7, 131.8, 130.5, 129.4, 127.1, 126.5, 126.0, 121.9, 117.7 (Ar), 35.5, 33.8 (CH), 31.3, 29.3 (CH_3), 16.8 (S- CH_3).

Elemental analysis ($\text{C}_{44}\text{H}_{56}\text{N}_2\text{O}_2\text{S}_2\text{Zn}$) Calcd in %: C, 68.24; H, 7.29; N, 3.62. Found: C, 65.08; H, 7.25; N, 3.41.

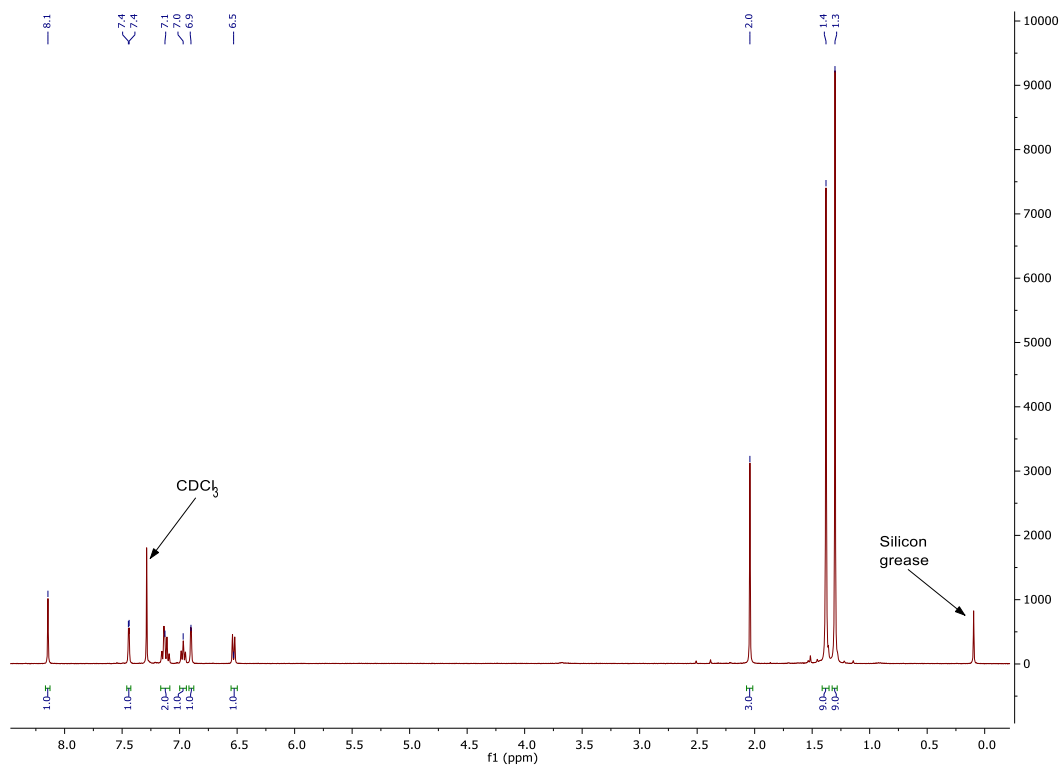


Figure 5.56: ^1H NMR (400 MHz, CDCl_3) of $\text{Zn}(\text{I})_2$.

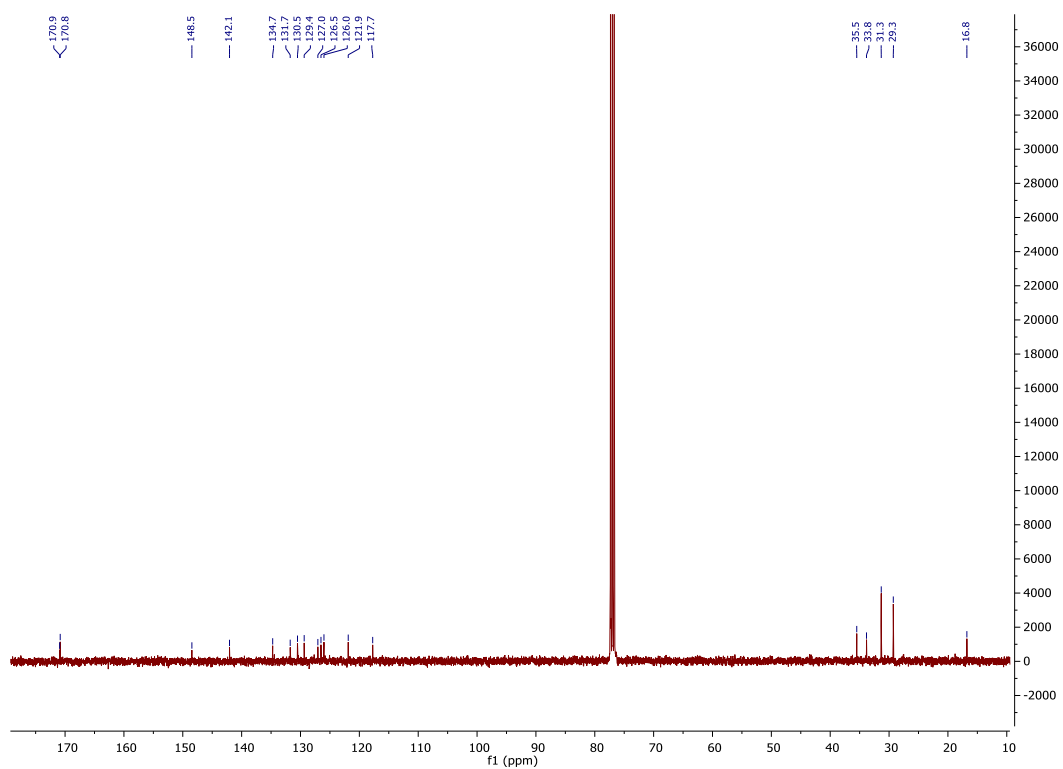


Figure 5.57: $^{13}\text{C}\{^1\text{H}\}$ NMR (101 MHz, CDCl_3) of $\text{Zn}(\text{I})_2$.

Zn(J)₂ Ligand JH (2 mmol, 0.48 g) was dissolved in toluene (10 mL). ZnEt₂ (1 mmol, 1 mL, 1.0 M) was added dropwise and the solution stirred for two hours. The product crystallised from a mixture of toluene and hexane as a pale-yellow solid (0.28 g, 50%).

¹H NMR (400 MHz, CDCl₃) δ 8.13 (s, 1H, CH), 7.34 (ddd, *J* = 8.8, 6.9, 2.0 Hz, 1H, Ar), 7.31 – 7.24 (m, 1H, Ar), 7.25 – 7.18 (m, 1H, Ar), 7.10 (dd, *J* = 7.9, 2.0 Hz, 1H, Ar), 7.04 – 6.90 (m, 2H, Ar), 6.66 – 6.53 (m, 1H, Ar), 6.48 (d, *J* = 7.6 Hz, 1H, Ar), 2.11 (s, 3H, CH₃).

¹³C{¹H} NMR (101 MHz, CDCl₃) δ 172.0 (CH), 169.2, 146.6, 134.9, 130.4, 128.0, 127.2, 126.4, 125.8, 125.5, 123.1, 120.4, 117.8, 113.1 (Ar), 16.1 (S-CH₃). Signals corresponding to toluene are also present.

Elemental analysis (C₂₈H₂₄N₂O₂S₂Zn) Calcd in %: C, 61.15; H, 4.40; N, 5.09. Found: C, 61.67; H, 4.73; N, 4.75.

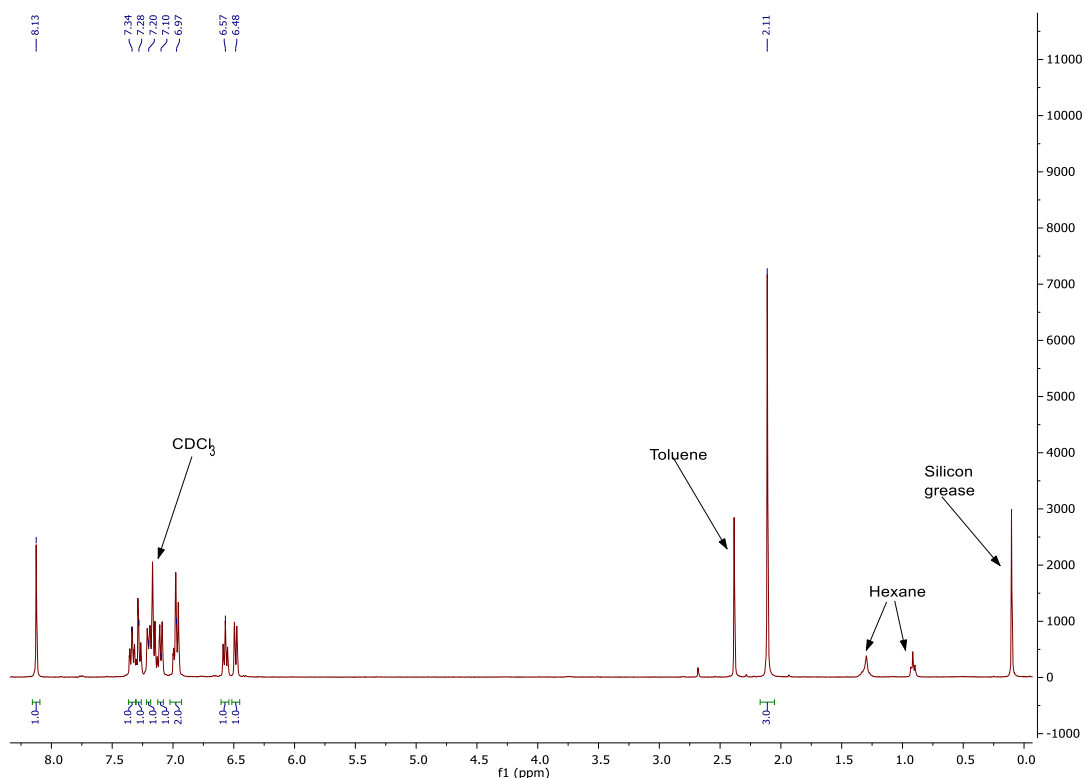


Figure 5.58: ¹H NMR (400 MHz, CDCl₃) of Zn(J)₂.

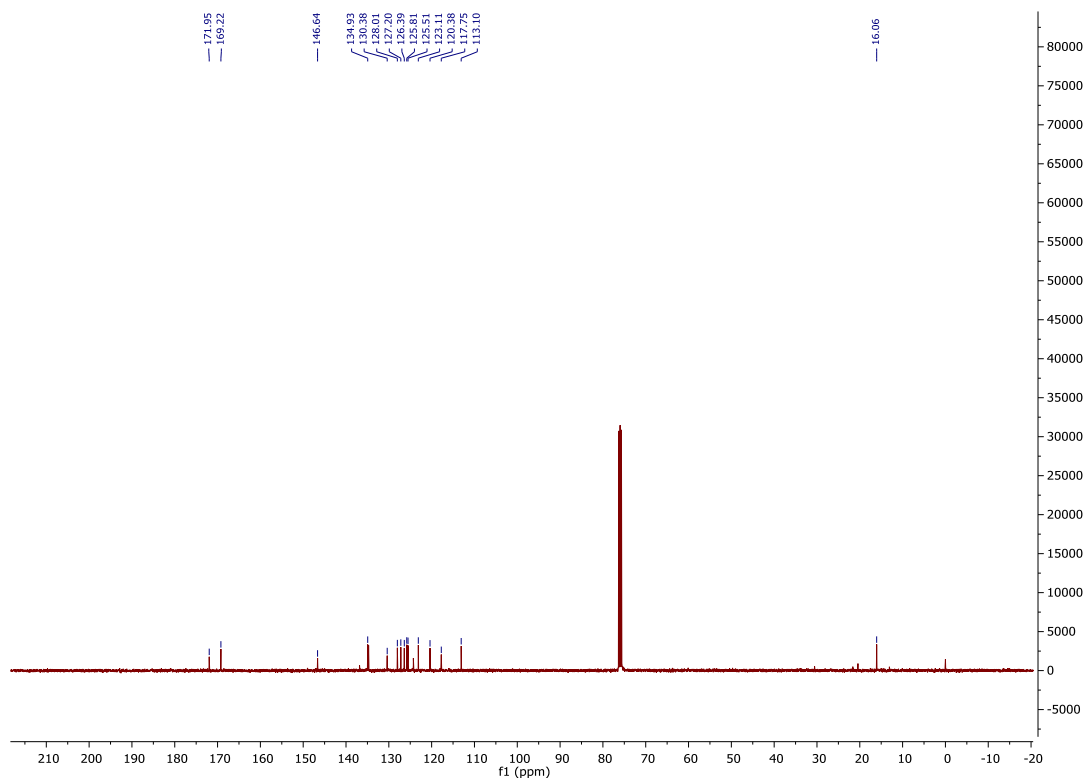


Figure 5.59: $^{13}\text{C}\{^1\text{H}\}$ NMR (101 MHz, CDCl_3) of $\text{Zn}(\text{J})_2$.

$\text{Zn}(\text{K})_2$ Ligand **KH** (2 mmol, 0.62 g) was dissolved in toluene (10 mL). ZnEt_2 (1 mmol, 1 mL, 1.0 M) was added dropwise and the solution stirred for two hours. The product crystallised from a mixture of toluene and hexane as a yellow solid (0.55 g, 80%).

^1H NMR (400 MHz, CDCl_3) δ 8.20 (s, 1H, CH), 7.42 (d, $J = 2.7$ Hz, 1H, Ar), 7.37 – 7.25 (m, 3H, Ar), 7.07 (d, $J = 2.8$ Hz, 1H, Ar), 6.92 (d, $J = 8.0$ Hz, 1H, Ar), 2.13 (s, 3H, CH_3).

$^{13}\text{C}\{^1\text{H}\}$ NMR (101 MHz, CDCl_3) δ 167.3 (CH), 164.5, 145.9, 133.4, 131.6, 127.3, 127.2, 126.8, 126.6, 124.3, 120.7, 118.5, 116.1 (Ar), 16.4 (S- CH_3). Signals corresponding to toluene are also present.

Elemental analysis ($\text{C}_{28}\text{H}_{20}\text{N}_2\text{O}_2\text{S}_2\text{Cl}_4\text{Zn} + \text{C}_7\text{H}_8$) Calcd in %: C, 53.88; H, 3.61; N, 3.59. Found: C, 52.22; H, 3.60; N, 3.54.

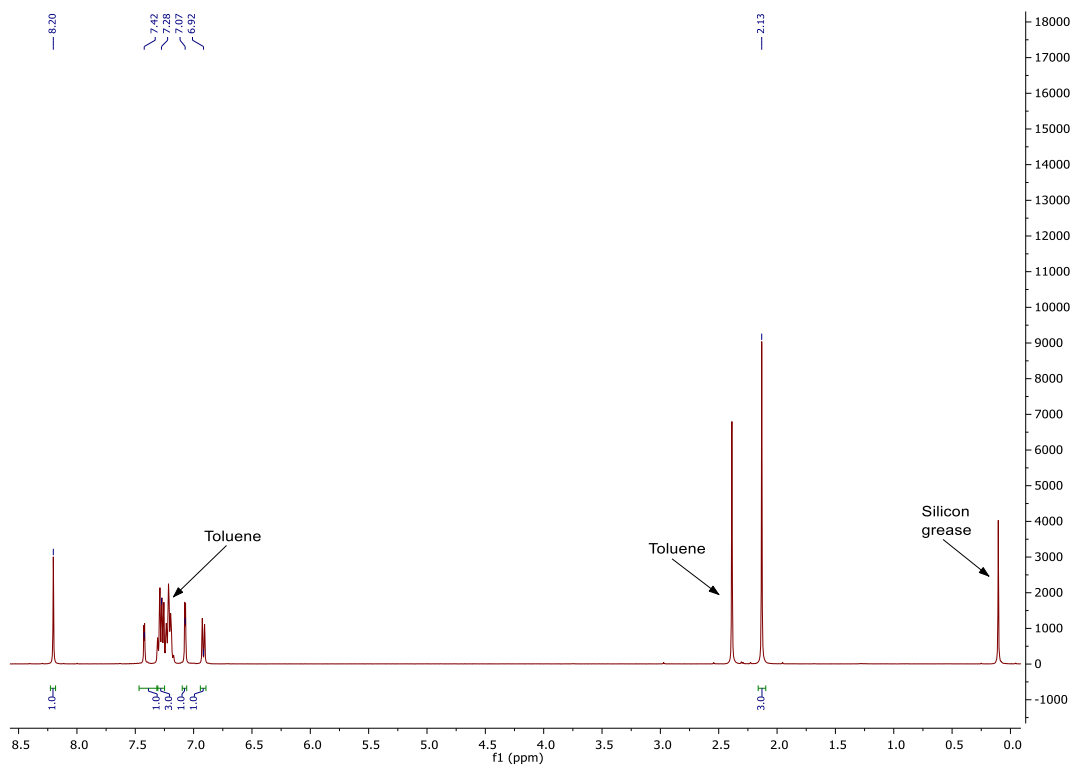


Figure 5.60: ^1H NMR (400 MHz, CDCl_3) of $\text{Zn}(\text{K})_2$.

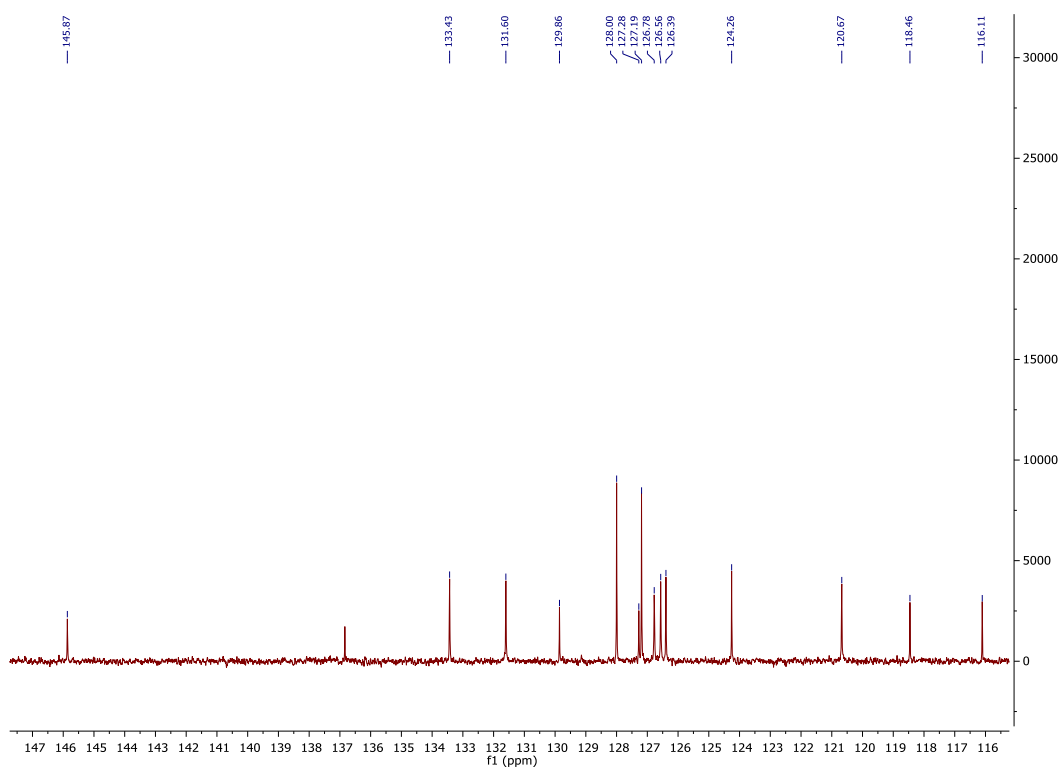


Figure 5.61: $^{13}\text{C}\{^1\text{H}\}$ NMR (101 MHz, CDCl_3) of $\text{Zn}(\text{K})_2$.

Zn(L)₂ Ligand LH (2 mmol, 0.82 g) was dissolved in toluene (10 mL). ZnEt₂ (1 mmol, 1 mL, 1.0 M) was added dropwise and the solution stirred for two hours. The product crystallised from hexane as a yellow solid (0.21 g, 24%).

¹H NMR (500 MHz, CDCl₃) δ 8.01 (s, 1H, CH), 7.51 (d, *J* = 7.0 Hz, 1H, Ar), 7.46 (d, *J* = 2.7 Hz, 1H, Ar), 7.12 (m, 2H, Ar), 6.82 (d, *J* = 2.6 Hz, 1H, Ar), 6.53 (dd, *J* = 7.2, 2.1 Hz, 1H, Ar), 1.36 (s, 9H, C(CH₃)), 1.23 (s, 9H, C(CH₃)).

¹³C{¹H} NMR (101 MHz, CDCl₃) δ 173.4 (CH), 170.7, 153.5, 142.5, 137.9, 135.7, 132.5, 131.8, 129.9, 126.6, 124.2, 117.0, 110.9 (Ar), 35.5, 33.9 (CH), 31.2, 29.4 (CH₃).

Elemental analysis (C₄₄H₅₀N₂O₂S₂F₆Zn) Calcd in %: C, 59.89; H, 5.71; N, 3.17. Found: C, 58.71; H, 5.84; N, 3.08.

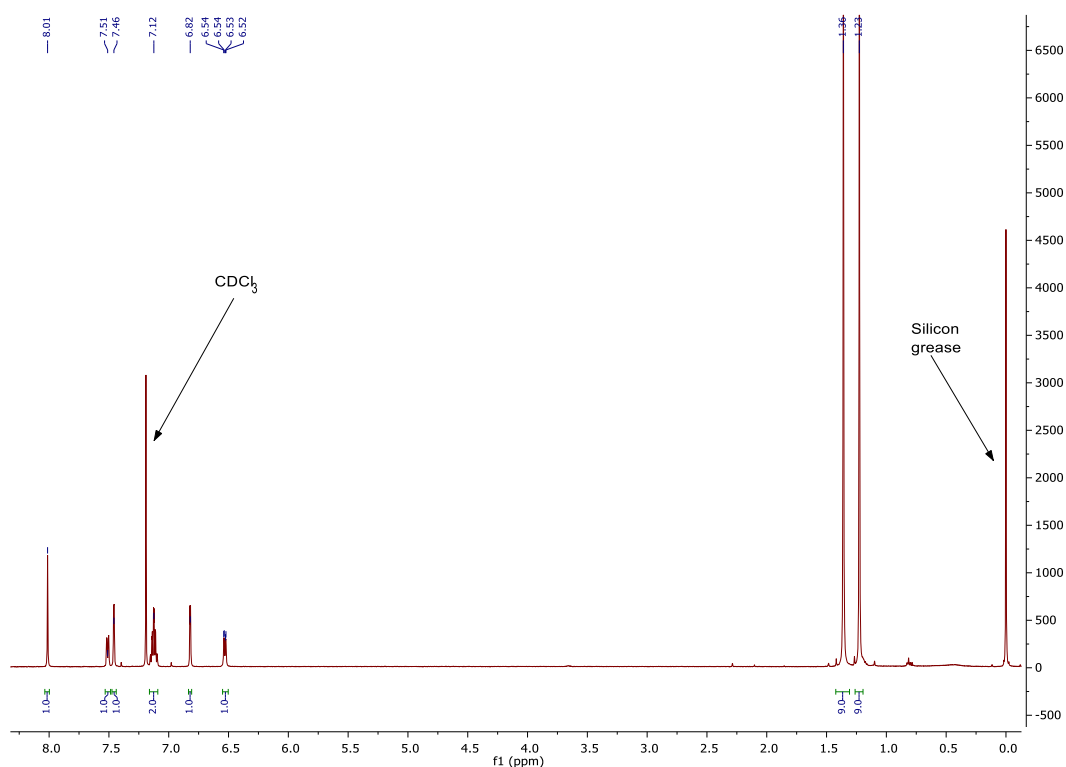


Figure 5.62: ¹H NMR (500 MHz, CDCl₃) of Zn(L)₂.

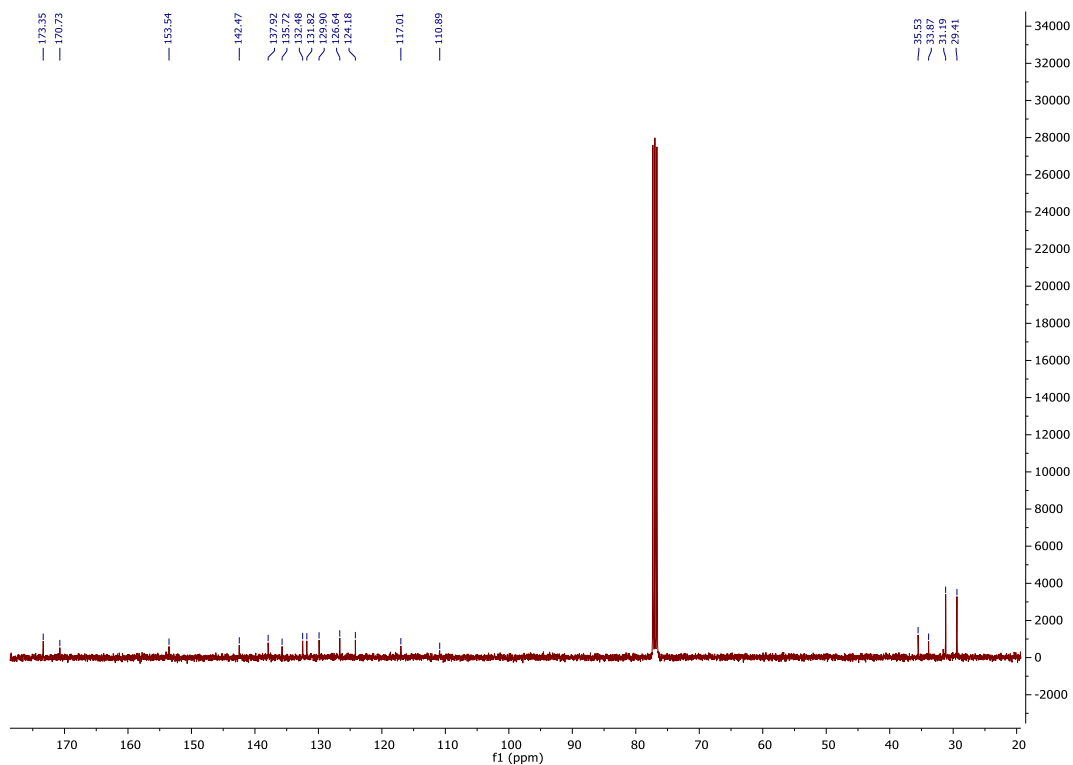


Figure 5.63: $^{13}\text{C}\{^1\text{H}\}$ NMR (101 MHz, CDCl_3) of $\text{Zn}(\text{L})_2$.

$\text{Zn}(\text{M})_2$ Ligand **MH** (2 mmol, 0.59 g) was dissolved in toluene (10 mL). ZnEt_2 (1 mmol, 1 mL, 1.0 M) was added dropwise and the solution stirred for two hours. The product crystallised from a mixture of toluene and hexane as a yellow solid (0.33 g, 50%).

^1H NMR (400 MHz, CDCl_3) δ 8.11 (s, 1H, CH), 7.66 (d, $J = 7.7$ Hz, 1H, Ar), 7.40 (ddd, $J = 8.9, 6.9, 1.9$ Hz, 1H, Ar), 7.38 – 7.33 (m, 1H, Ar), 7.31 – 7.25 (m, 1H, Ar), 7.12 (dd, $J = 8.0, 1.8$ Hz, 1H, Ar), 6.95 (d, $J = 8.7$ Hz, 1H, Ar), 6.90 – 6.78 (m, 1H, Ar), 6.64 (ddd, $J = 7.8, 6.9, 1.1$ Hz, 1H, Ar).

$^{13}\text{C}\{^1\text{H}\}$ NMR (101 MHz, CDCl_3) δ 173.1 (CH), 172.3, 152.6, 138.1, 136.8, 136.6, 132.6, 127.3, 124.1, 124.0, 118.0, 115.5, 115.1 (Ar).

Elemental analysis ($\text{C}_{28}\text{H}_{18}\text{N}_2\text{O}_2\text{S}_2\text{F}_6\text{Zn}$) Calcd in %: C, 51.11; H, 2.76; N, 4.26. Found: C, 50.36; H, 2.99; N, 4.10.

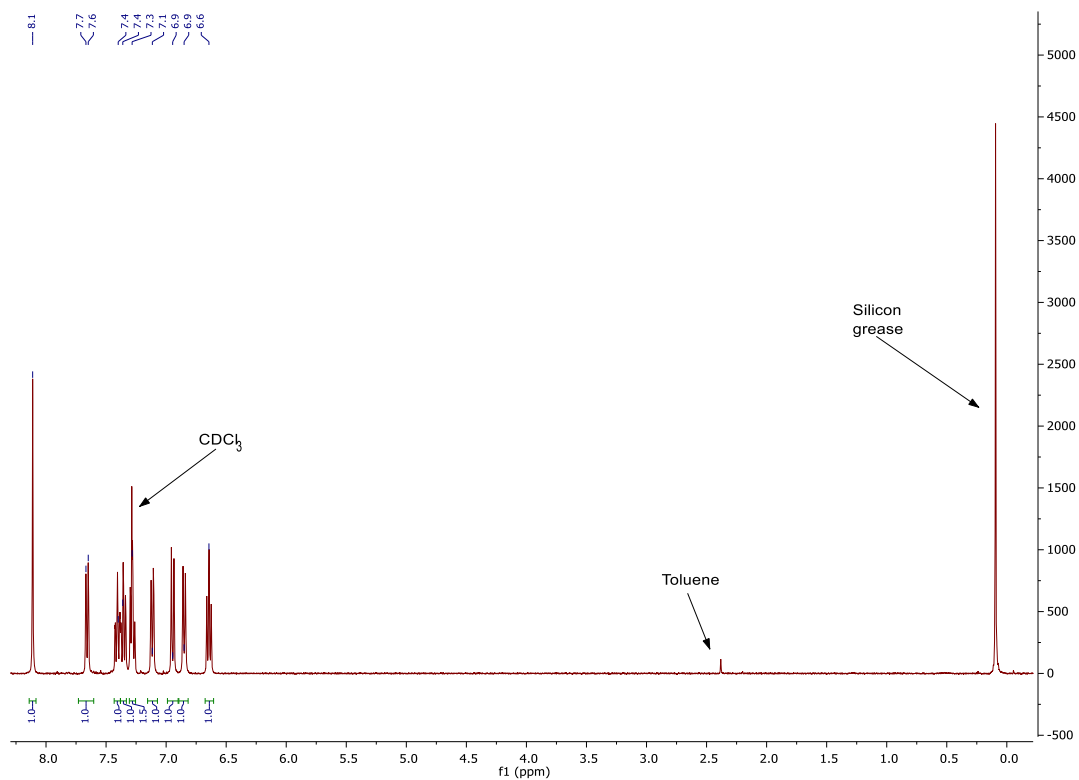


Figure 5.64: ^1H NMR (400 MHz, CDCl_3) of $\text{Zn}(\text{M})_2$.

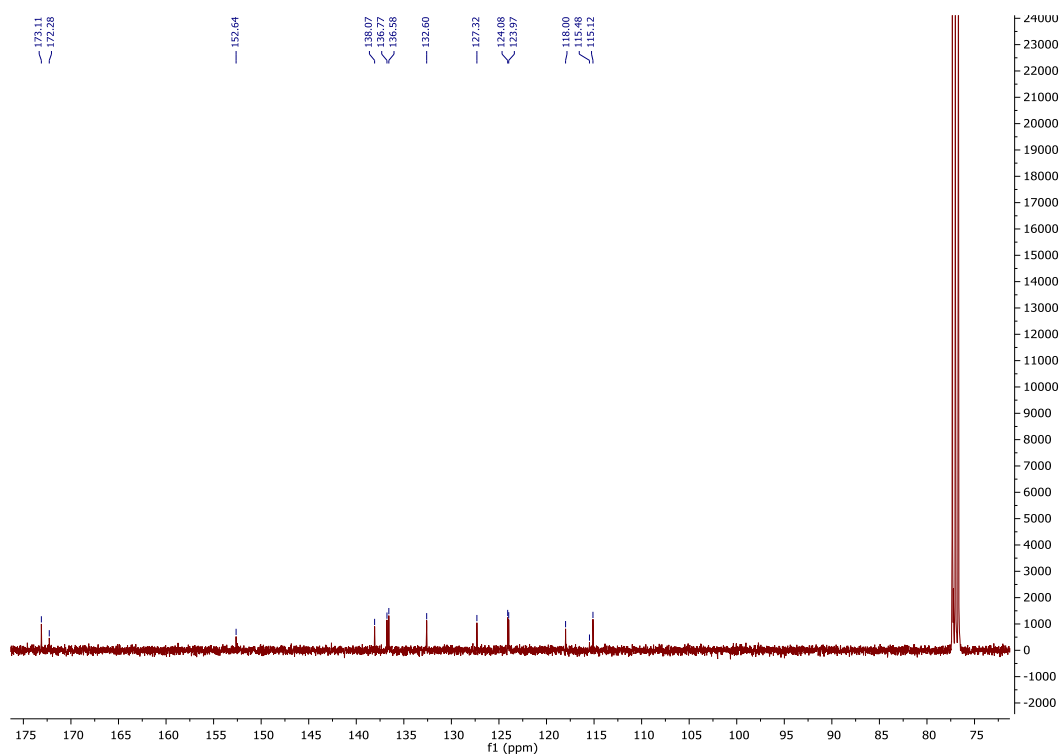


Figure 5.65: $^{13}\text{C}\{^1\text{H}\}$ NMR (101 MHz, CDCl_3) of $\text{Zn}(\text{M})_2$.

Zn(N)₂ Ligand NH (2 mmol, 0.73 g) was dissolved in toluene (10 mL). ZnEt₂ (1 mmol, 1 mL, 1.0 M) was added dropwise and the solution stirred for two hours. The product crystallised from a mixture of toluene and hexane as a yellow solid (0.54 g, 68%).

¹H NMR (400 MHz, CDCl₃) δ 8.10 (s, 1H, CH), 7.68 (d, *J* = 7.8 Hz, 1H, Ar), 7.47 (t, *J* = 7.7 Hz, 1H, Ar), 7.43 – 7.39 (m, 1H, Ar), 7.33 (t, *J* = 7.7 Hz, 1H, Ar), 7.11 (d, *J* = 7.9 Hz, 1H, Ar), 7.04 (d, *J* = 2.7 Hz, 1H, Ar).

¹³C{¹H} NMR (101 MHz, CDCl₃) δ 171.7 (CH), 138.5, 135.2, 133.0, 132.8, 130.5, 129.0, 128.6, 128.2, 128.1, 125.9, 124.0, 118.7 (Ar).

Elemental analysis (C₂₈H₁₄N₂O₂S₂F₆Cl₄Zn) Calcd in %: C, 42.26; H, 1.77; N, 3.52. Found: C, 44.22; H, 2.27; N, 3.32.

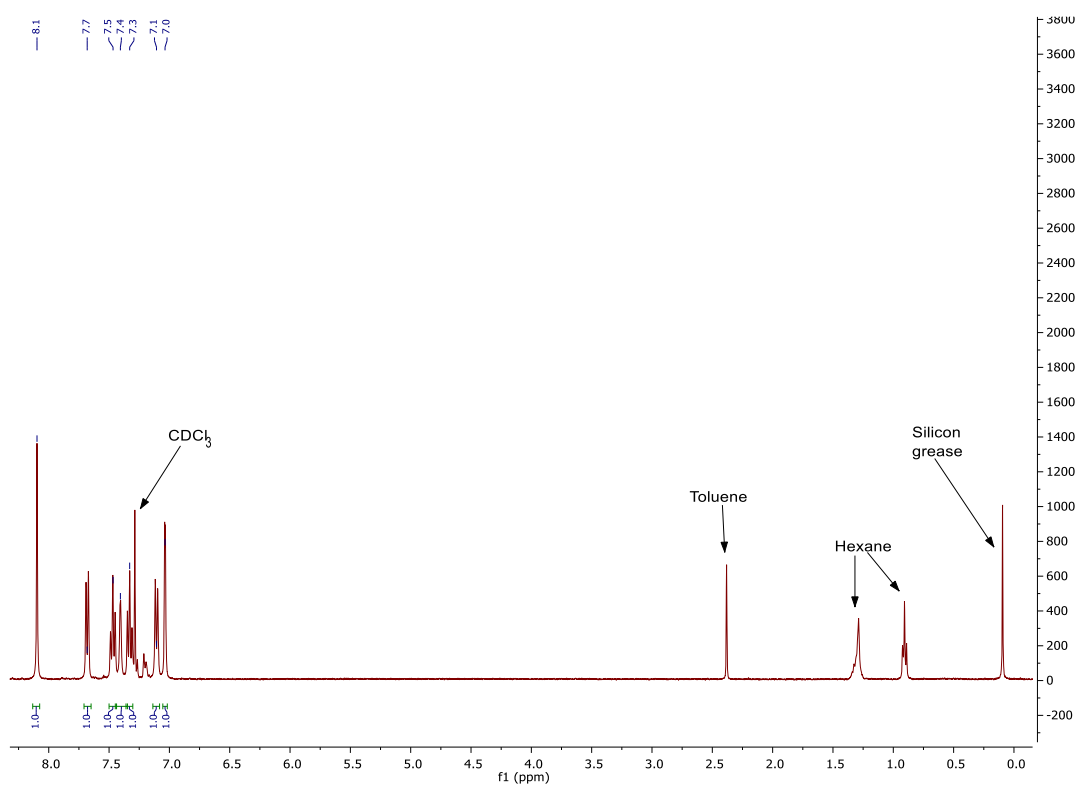


Figure 5.66: ¹H NMR (400 MHz, CDCl₃) of Zn(N)₂.

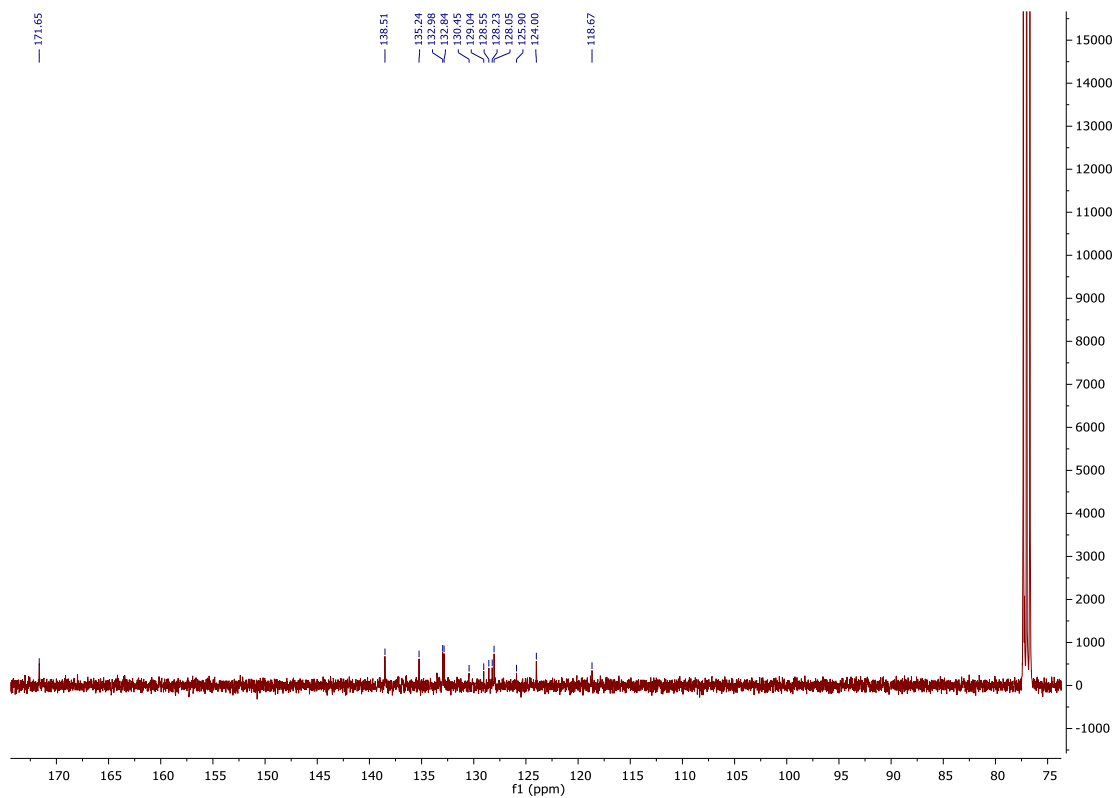


Figure 5.67: $^{13}\text{C}\{^1\text{H}\}$ NMR (101 MHz, CDCl_3) of $\text{Zn}(\text{N})_2$.

5.3.3 Example GPC spectra

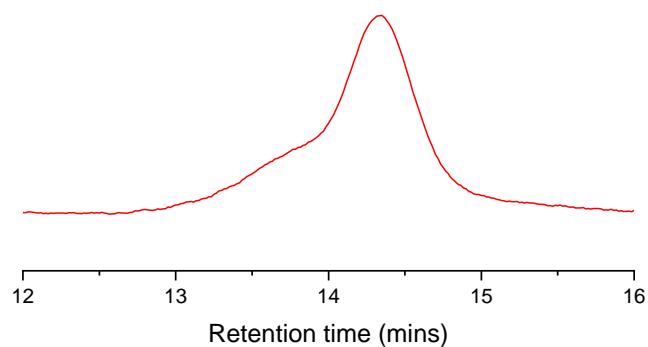


Figure 5.68: GPC trace of PLA initiated by $\text{Zn}(\text{G})_2$ (130 °C, 30 mins) at a ratio of 3000:1:10 ([LA]:[I]:[BnOH]) in the melt. M_n (GPC) = 19200 gmol^{-1} , $\text{Đ} = 1.14$, M_n (theo.) = 31650 gmol^{-1} .

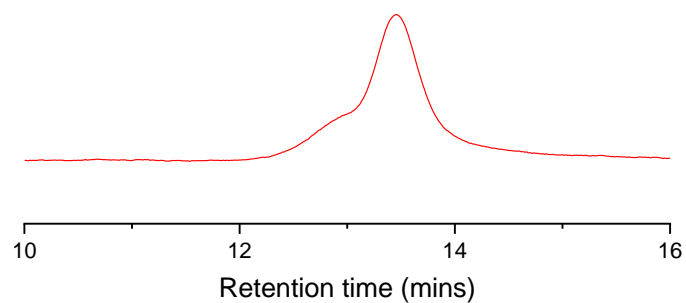


Figure 5.69: GPC trace of PLA initiated by $Zn(K)_2$ (180 °C, 40 mins) at a ratio of 3000:1:10 ([LA]:[I]:[BnOH]) in the melt. M_n (GPC) = 38400 $gmol^{-1}$, \bar{D} = 1.16, M_n (theo.) = 23050 $gmol^{-1}$.

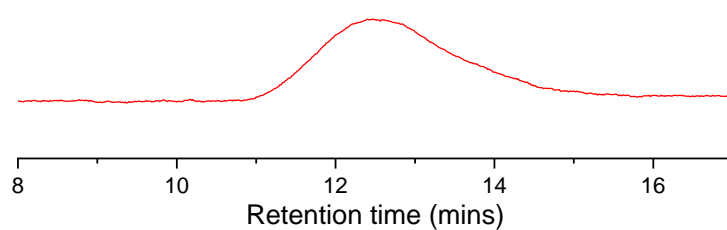


Figure 5.70: GPC trace of PLA initiated by $Zn(9)_2$ (180 °C, 12 mins) at a ratio of 10000:1:30 ([LA]:[I]:[BnOH]) in the melt. M_n (GPC) = 42050 $gmol^{-1}$, \bar{D} = 1.68, M_n (theo.) = 31400 $gmol^{-1}$.

5.3.4 Example $^1\text{H}\{^1\text{H}\}$ NMR spectra

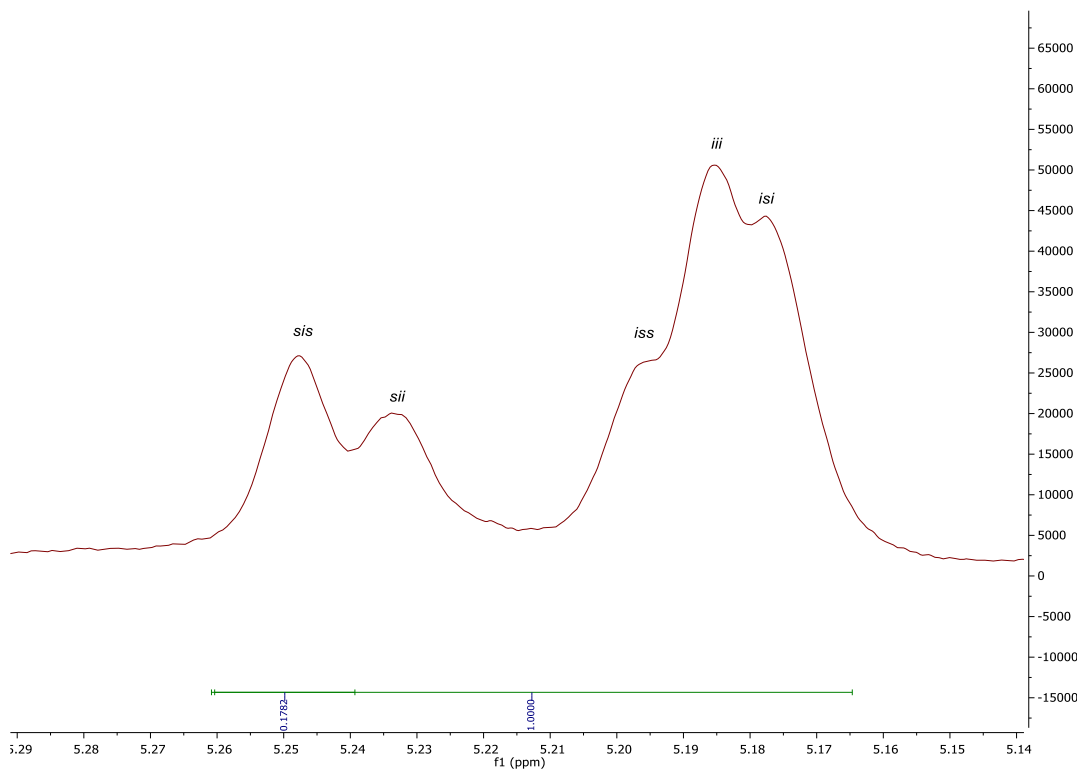


Figure 5.71: $^1\text{H}\{^1\text{H}\}$ NMR spectrum of atactic PLA from $\text{Zn}(\text{K})_2$. $P_m = 0.61$.

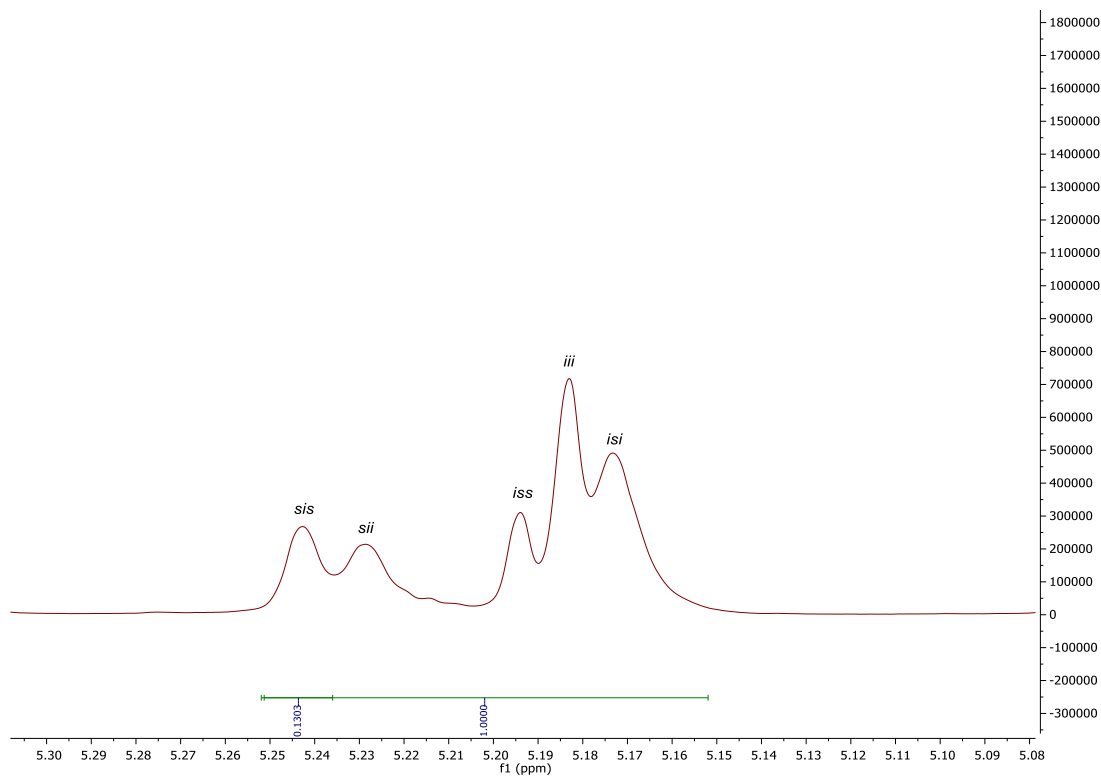


Figure 5.72: $^1\text{H}\{^1\text{H}\}$ NMR spectrum of atactic PLA from $\text{Zn}(\text{M})_2$. $P_m = 0.51$.

5.3.5 Characterisation of aluminium {ONS} complexes

Al(I)Me₂ Ligand IH (2 mmol, 0.71 g) was dissolved in toluene (10 mL). AlMe₃ (1 mmol, 0.5 mL, 2.0 M) was added dropwise and the solution stirred for two hours. The product crystallised from a mixture of toluene and hexane as a yellow solid (0.43 g, 57%).

¹H NMR (500 MHz, Tol) δ 7.97 (d, *J* = 2.6 Hz, 1H, Ar), 7.93 (s, 1H, CH), 7.36 (d, *J* = 7.7 Hz, 1H, Ar), 7.23 – 7.19 (m, 2H, Ar), 7.17 – 7.11 (m, 1H, Ar), 7.06 (d, *J* = 2.6 Hz, 1H, Ar), 2.06 (s, 3H, Ar), 1.86 (s, 9H, C(CH₃)₃), 1.54 (s, 9H, C(CH₃)₃), 0.00 (s, 6H, Al-CH₃).

¹³C NMR (126 MHz, Tol) δ 174.6 (CH), 163.2, 144.8, 140.8, 138.8, 137.1, 133.3, 132.9, 129.3, 127.6, 125.4, 124.1, 118.4 (Ar), 35.3, 33.8 (CH), 31.0, 29.3 (CH₃), 15.21 (S-CH₃), -9.10 (Al-CH₃).

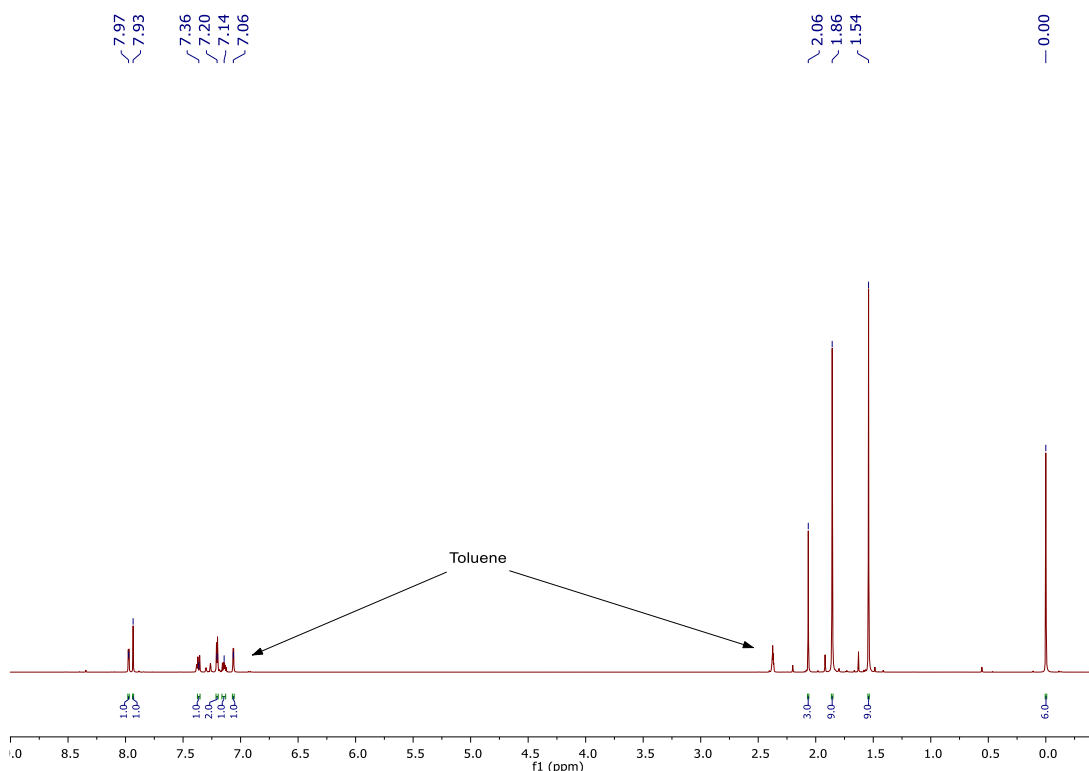


Figure 5.73: ¹H NMR spectrum (500 MHz, Tol) of Al(I)Me₂

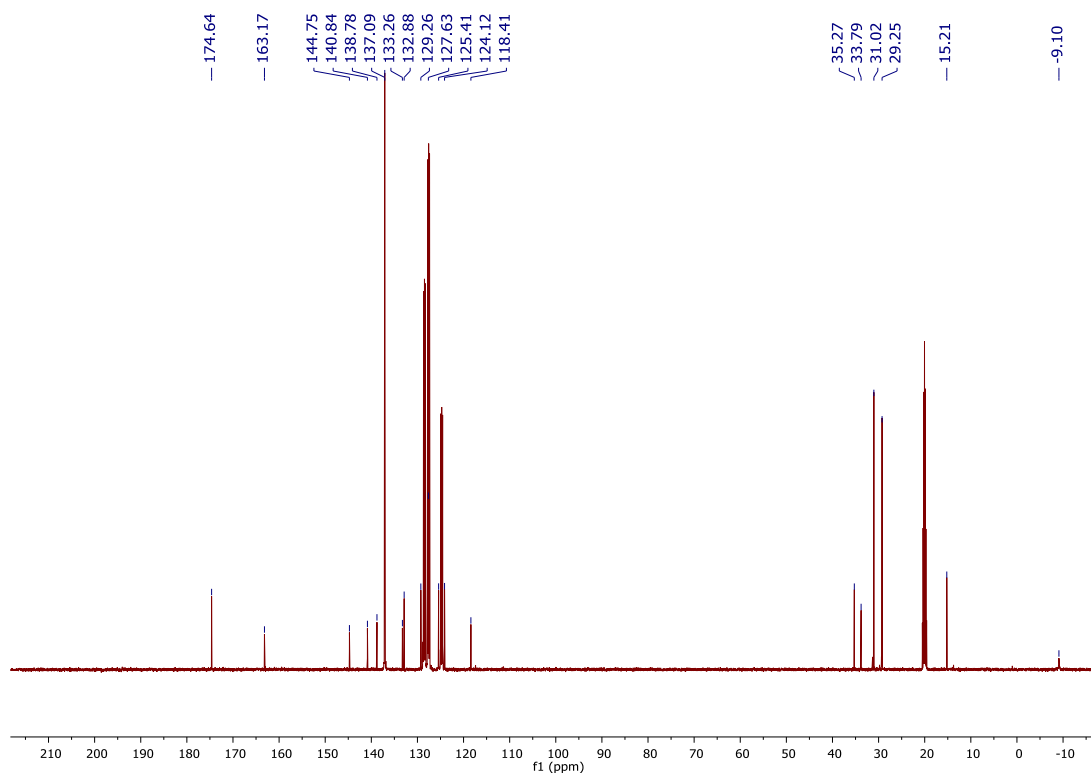


Figure 5.74: ^{13}C NMR spectrum (126 MHz, Tol) of Al(I)Me_2 .

$\text{Al(K)}_2\text{Me}$ Ligand KH (2 mmol, 0.62 g) was dissolved in toluene (10 mL). AlMe_3 (1 mmol, 0.5 mL, 2.0 M) was added dropwise and the solution stirred for two hours. The product crystallised from a mixture of toluene and hexane as a yellow solid (0.39 g, 60%).

^1H NMR (500 MHz, C_6D_6) δ 8.62 (d, $J = 7.9$ Hz, 2H, Ar), 7.52 (s, 2H, CH), 7.15 (d, $J = 2.6$ Hz, 2H, Ar), 7.05 – 6.92 (m, 6H, Ar), 6.62 (d, $J = 2.6$ Hz, 2H, Ar), 1.80 (d, $J = 2.4$ Hz, 6H, CH_3), -0.68 (s, 3H, Al- CH_3).

^{13}C NMR (126 MHz, C_6D_6) δ 169.2 (CH), 157.8, 148.6, 137.5, 137.2, 134.5, 131.8, 131.8, 128.9, 128.1, 127.9, 127.1, 126.4, 125.7, 125.3, 121.3, 120.5 (Ar), 15.7 (CH_3).

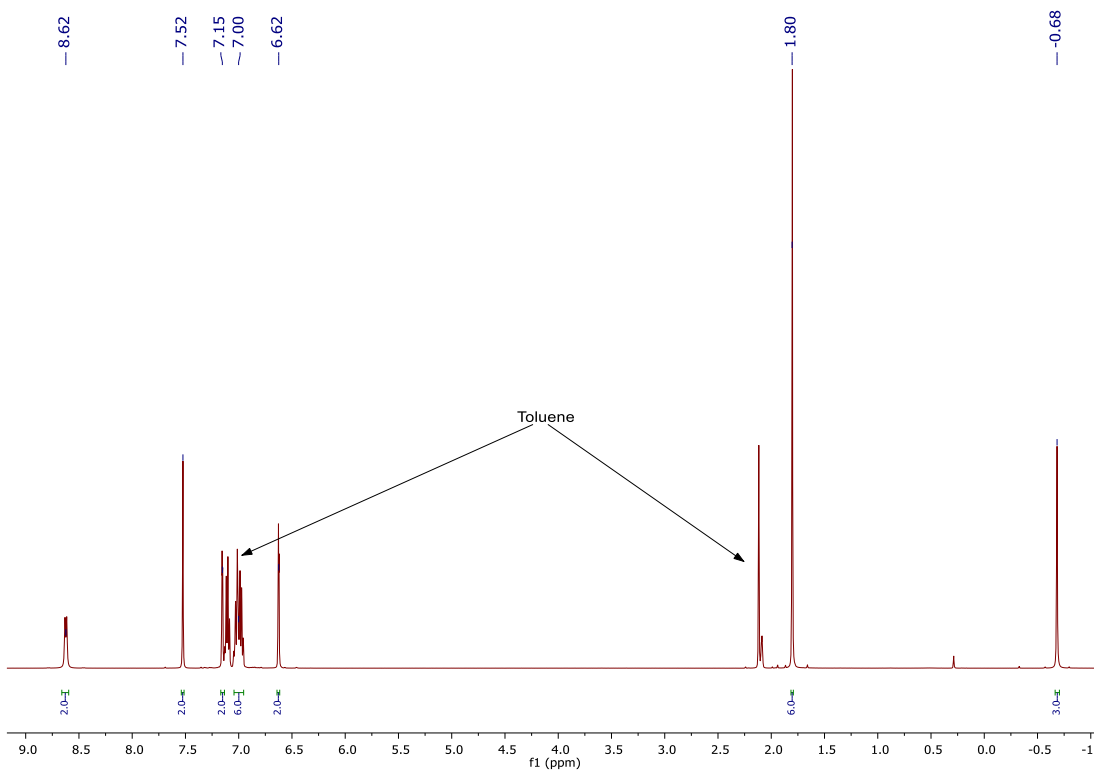


Figure 5.75: ^1H NMR spectrum (500 MHz, C_6D_6) of $\text{Al}(\text{K})_2\text{Me}$.

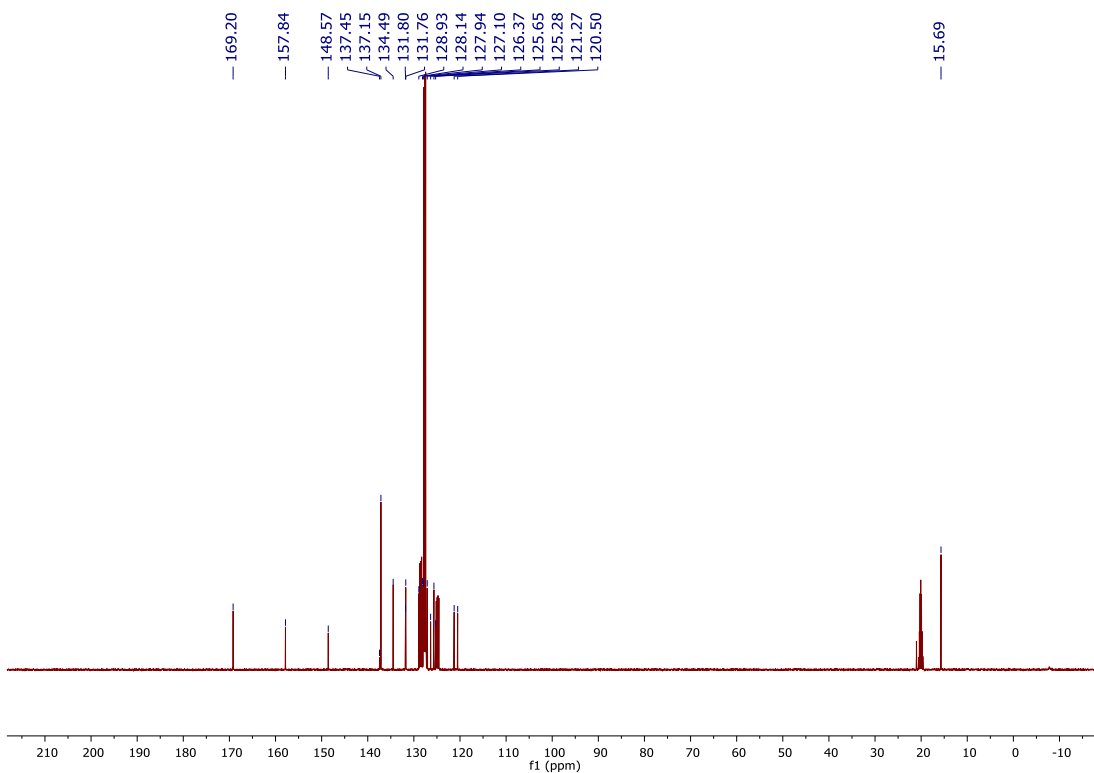


Figure 5.76: ^{13}C NMR spectrum (126 MHz, C_6D_6) of $\text{Al}(\text{K})_2\text{Me}$.

Al(L)₂Me Ligand LH (2 mmol, 0.82 g) was dissolved in toluene (10 mL). AlMe₃ (1 mmol, 0.5 mL, 2.0 M) was added dropwise and the solution stirred for two hours. The product crystallised from a mixture of toluene and hexane as a yellow solid (0.56 g, 66%).

¹H NMR (500 MHz, Tol) δ 8.09 (d, *J* = 8.4 Hz, 2H, Ar), 7.75 (s, 2H, CH), 7.46 – 7.35 (m, 4H, Ar), 6.98 – 6.86 (m, 2H, Ar), 6.83 (d, *J* = 2.5 Hz, 2H, Ar), 6.69 – 6.57 (m, 2H, Ar), 1.26 (s, 18H, C(CH₃)), 1.02 (s, 18H, C(CH₃)), -1.06 (s, 3H, Al-CH₃).

¹³C NMR (126 MHz, Tol) δ 171.9 (CH), 161.1, 153.7, 139.1, 138.3, 137.5, 136.4, 130.6, 130.2, 128.6, 126.0, 125.9, 119.2, 117.8 (Ar), 34.2, 33.0 (CH), 30.4, 29.1 (CH₃).

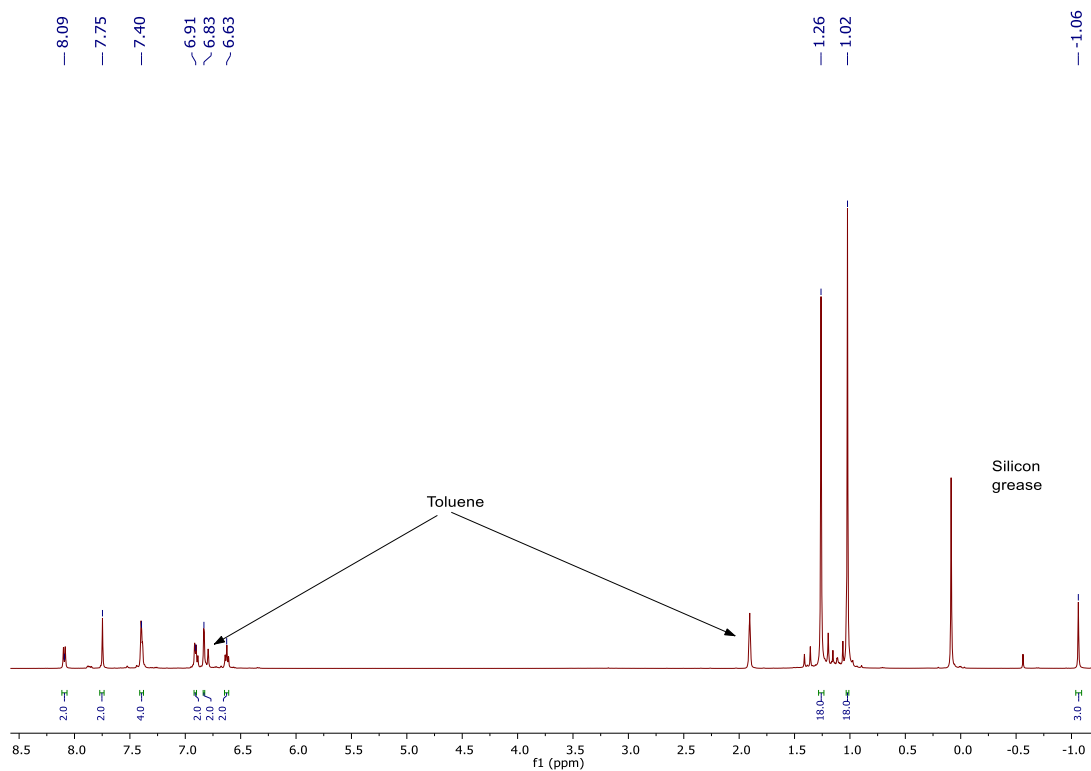


Figure 5.77: ¹H NMR spectrum (500 MHz, Tol) of Al(L)₂Me.

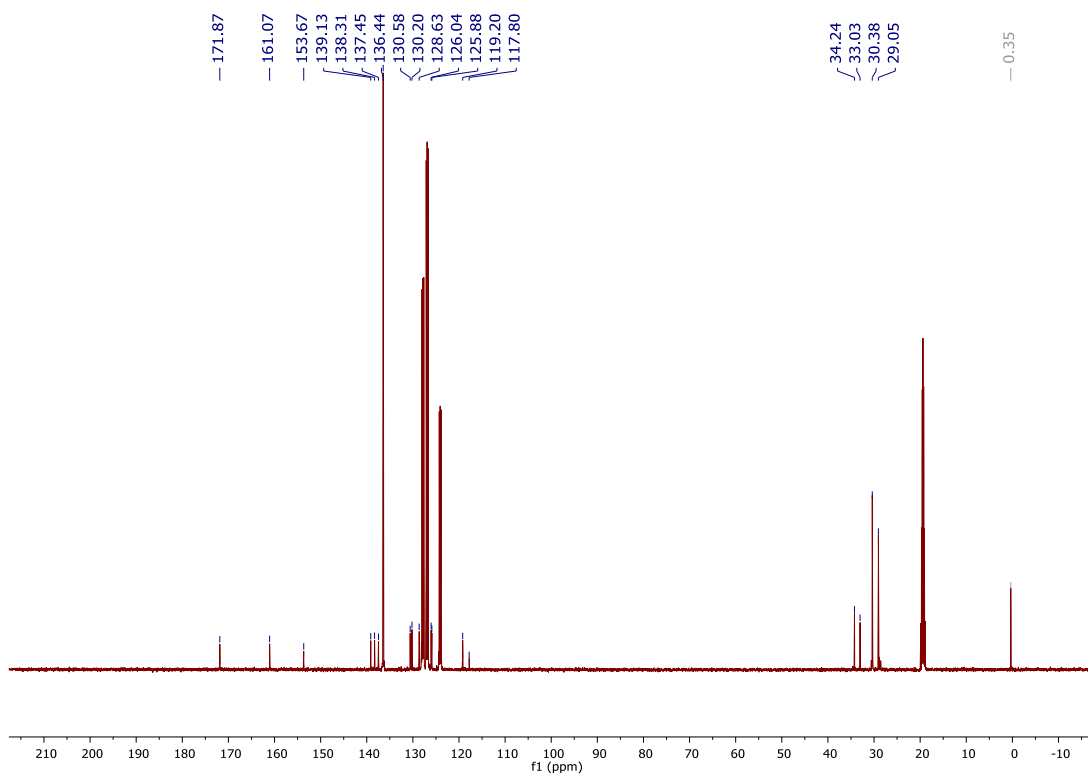


Figure 5.78: ^{13}C NMR spectrum (126 MHz, Tol) of $\text{Al}(\text{L})_2\text{Me}$.

$\text{Al}(\mathbf{M})_2\text{Me}$ Ligand \mathbf{MH} (2 mmol, 0.59 g) was dissolved in toluene (10 mL). AlMe_3 (1 mmol, 0.5 mL, 2.0 M) was added dropwise and the solution stirred for two hours. The product crystallised from a mixture of toluene and hexane as a yellow solid (0.32 g, 50%).

^1H NMR (500 MHz, Tol) δ 7.62 (s, 2H, CH), 7.50 (d, $J = 7.8$ Hz, 2H, Ar), 6.95 – 6.90 (m, 2H, Ar), 6.86 – 6.83 (m, 2H, Ar), 6.72 – 6.63 (m, 4H, Ar), 6.32 (t, $J = 7.2$ Hz, 2H, Ar), - 0.84 (s, 3H, Al- CH_3).

^{13}C NMR (126 MHz, Tol) δ 163.9 (CH), 153.3, 136.4, 135.2, 133.5, 130.3, 128.1, 127.21, 126.1, 120.5, 118.6, 116.8 (Ar), 0.4 (CF_3).

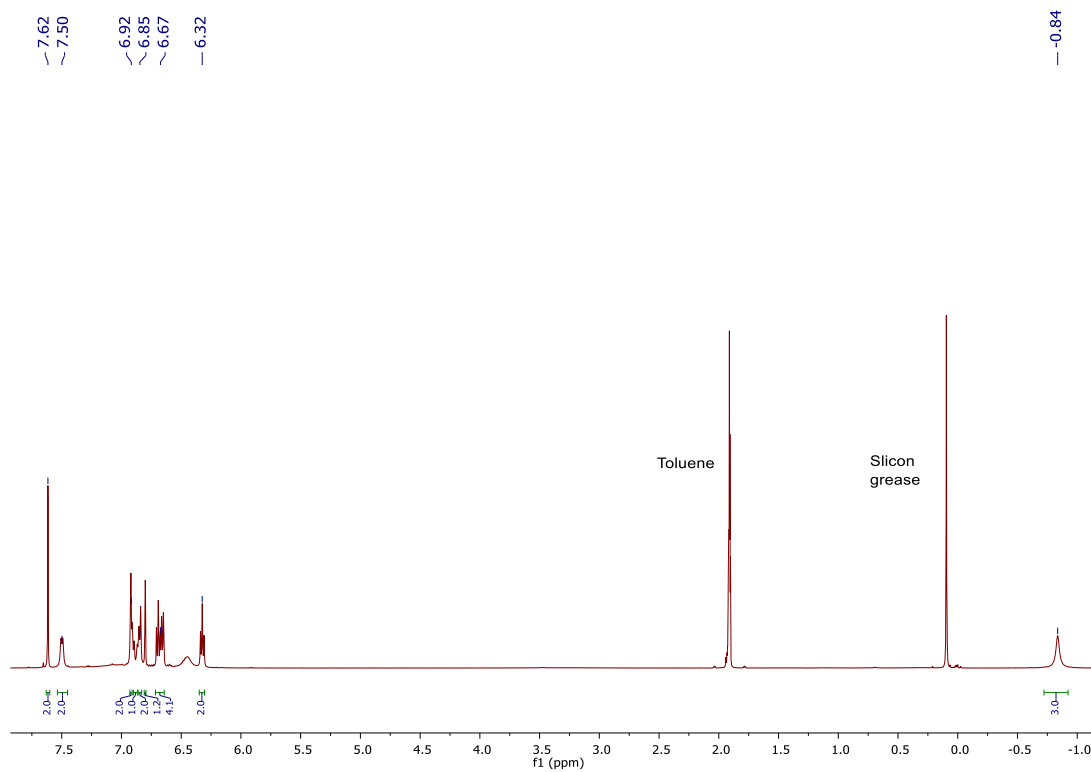


Figure 5.79: ^1H NMR spectrum (500 MHz, Toluene- d_8) of $\text{Al}(\text{N})_2\text{Me}$.

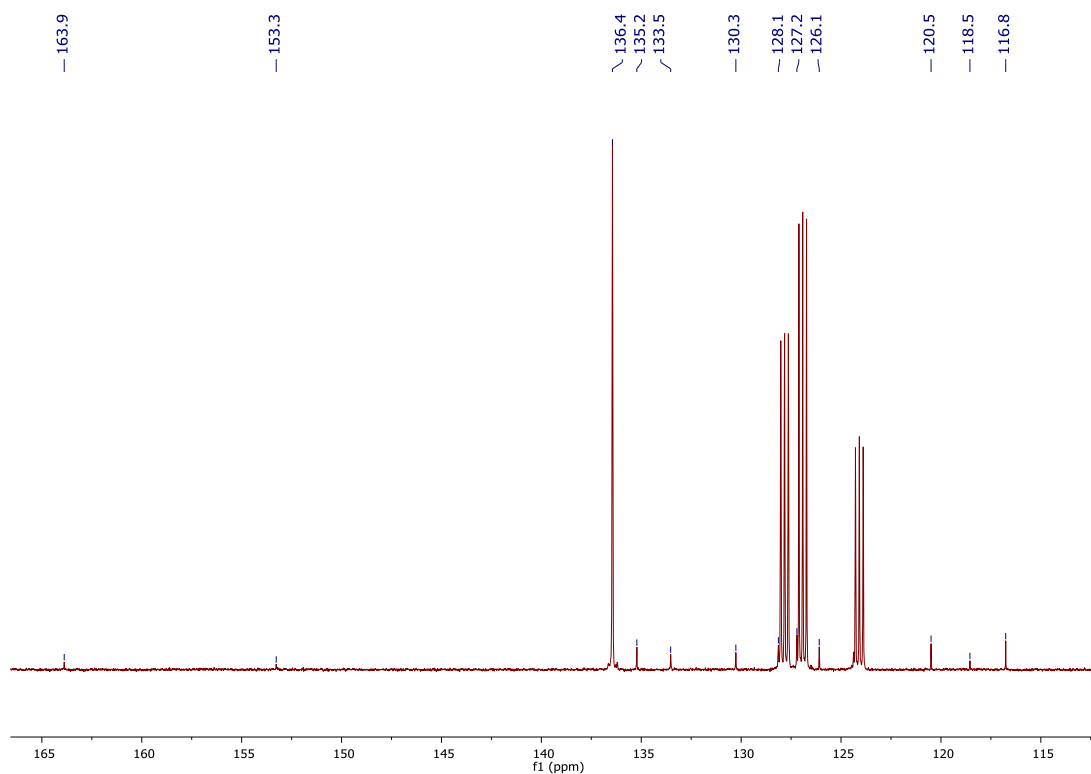
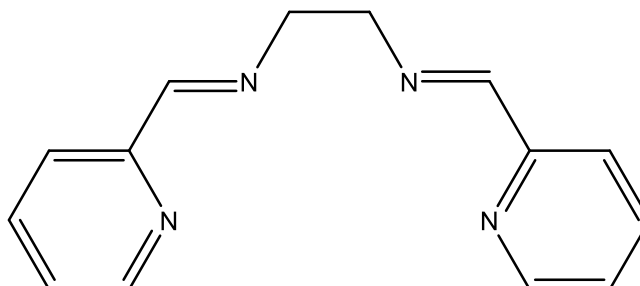


Figure 5.80: ^{13}C NMR spectrum (126 MHz, Tol) of $\text{Al}(\text{N})_2\text{Me}$.

5.4 Electrochemically switchable initiators

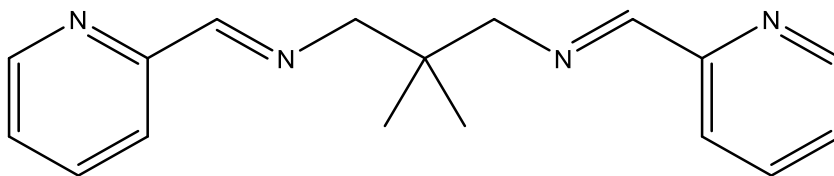
5.4.1 Synthesis and characterisation of neutral {NNNN} ligands



● A solution of 2-formylpyridine (1.90 mL, 20 mmol) and 1,2 ethylene diamine (0.67 mL, 10mmol) in methanol (30 mL) was stirred under reflux for one hour. The solvent was removed under vacuum to give a pale yellow solid (2.10 g, 8.8 mmol, 88%).

m/z calc. $[C_{14}N_4H_{15}]^+ = 239.1291$, found 239.1291

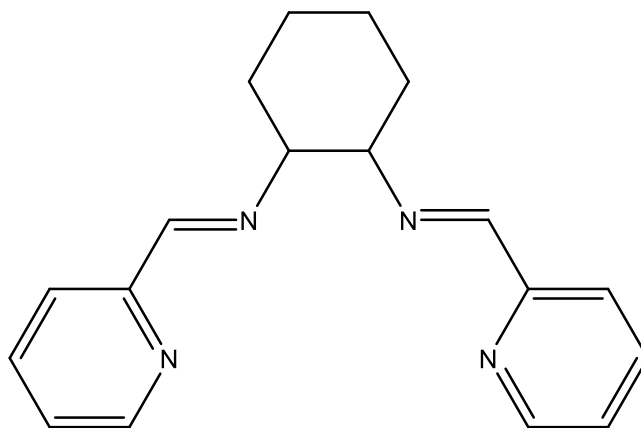
1H NMR (400 MHz, $CDCl_3$) δ 8.64 (ddd, $J = 4.9, 1.8, 1.0$ Hz, 2H, Ar-H), 8.44 (s, 2H, CH), 8.00 (dt, $J = 7.9, 1.1$ Hz, 2H, Ar-H), 7.74 (m, 2H, Ar-H), 7.32 (ddd, $J = 7.5, 4.9, 1.2$ Hz, 2H, Ar-H), 4.09 (d, $J = 0.7$ Hz, 4H, CH_2).



P A solution of 2-formylpyridine (1.90mL, 20mmol) and 2,2-dimethylpropane-1,3-diamine (1.20mL, 10mmol) in methanol (30mL) was stirred under reflux for one hour. The solvent was removed under vacuum to give a pale yellow solid (2.22g, 7.92mmol, 79%).

m/z calc. $[C_{17}N_4H_{21}]^+ = 281.1761$, found 281.1761

1H NMR (400 MHz, $CDCl_3$) δ 8.59 (m, 2H, Ar), 8.36 (s, 2H, CH), 8.03 (m, 2H, Ar), 7.69 (m, 2H, Ar), 7.27 (m, 2H, Ar), 3.57 (s, 4H, CH_2), 1.03 (s, 6H, $C(CH_3)_2$).



Q A solution of 2-formylpyridine (1.90mL, 20mmol) and (trans)-cyclohexane-1,2-diamine (1.20mL, 10mmol) in methanol (30mL) was stirred under reflux for 2 hours. The solvent was removed under vacuum to give a pale orange solid (2.21g, 7.57mmol, 75%).

m/z calc. $[C_{18}N_4H_{21}]^+ = 293.1778$, found 293.1778

1H NMR (400 MHz, $CDCl_3$) 8.55 (m, 2H, Ar), 8.32 (s, 2H, CH), 7.90 (dt, $J = 7.9, 1.1$ Hz, 2H, Ar), δ 7.66 (td, $J = 7.7, 1.7$ Hz, 2H, Ar), 7.24 (ddd, $J = 7.5, 4.9, 1.3$ Hz, 2H, Ar), 3.55 (s, 4H, CH_2), 1.85 (m, 10H, CH_2, CH_2, CH).

5.4.2 Synthesis and characterisation of iron (II) {NNNN} complexes

Fe(O)Cl₂: Ligand **O** (0.48g, 2mmol) was added to a Schlenk flask and dried under vacuum for one hour. Dry toluene (10mL) was added under an inert argon atmosphere, followed by FeCl₂ (0.25g, 2mmol), resulting in a dark blue solution and precipitate. The mixture was stirred at room temperature for one hour, and then at 50°C for 2 hours. The solid product was then isolated by cannula filtration and dried under vacuum to give a blue powder (0.27g, 0.74mmol, 37%).

m/z calc. [C₁₄N₄H₁₄FeCl]⁺ = 329.0256, found 339.0491

Elemental analysis (C₁₄N₄H₁₄FeCl₂) Calcd in %: C, 46.06; H, 3.87, N, 15.35. Found: C, 45.73; H, 4.01; N, 14.93.

Fe(P)Cl₂ Ligand **P** (0.57g, 2mmol) was added to a Schlenk flask and dried under vacuum for one hour. Dry acetonitrile (10mL) was added under an inert argon atmosphere, followed by FeCl₂ (0.25g, 2mmol), resulting in a dark purple solution and precipitate. The mixture was stirred at room temperature for one hour. The solid product was then isolated by cannula filtration and dried under vacuum to give a purple powder (0.22g, 0.54 mmol, 27%).

m/z calc. [C₁₇N₄H₂₀FeCl]⁺ = 371.0725, found 371.0736.

Elemental analysis (C₁₇N₄H₂₀FeCl₂) Calcd in %: C, 50.15; H, 4.95; N, 13.76. Found: C, 50.00; H, 4.88; N, 13.95.

Fe(Q)Cl₂: Ligand **Q** (0.29 g, 1 mmol) was added to a Schlenk flask and dried under vacuum for one hour. Dry acetonitrile (5 mL) was added under an inert argon atmosphere, followed by FeCl₂ (0.13 g, 1 mmol), resulting in a dark blue solution and precipitate. The mixture was stirred at room temperature for one hour. The solid product was then isolated by cannula filtration and dried under vacuum to give a dark blue powder (0.11 g, 0.26 mmol, 26%).

m/z calc. [C₁₈N₄H₂₁FeCl]⁺ = 383.0726, found 383.0735

Elemental analysis ($C_{14}N_4H_{14}FeCl_2$) Calcd in %: C, 51.58; H, 4.81; N, 13.37. Found: C, 51.54; H, 4.61; N, 13.81.

5.5 References

- [1] X. Wang, A. Thevenon, J. L. Brosmer, I. Yu, S. I. Khan, P. Mehrkhodavandi, P. L. Diaconescu, *J. Am. Chem. Soc.* **2014**, *136*, 11264–11267.